STUDY OF BIO OIL PRODUCTION WITH RICE HUSK AND PLASTIC WASTES

BY USING PYROLYSIS TECHNIQUE

Thesis Submitted for the Award of the Degree of

DOCTOR OF PHILOSOPHY

in

Physics

By

Divya Bisen

Registration Number: 11919639

Supervised By

Dr. Ashish Pratap Singh Chouhan

(17466)

Physics (Associate professor)

School of Chemical Engineering and Physical Sciences

LOVELY PROFESSIONAL UNIVERSITY, PUNJAB

2024

DECLARATION

I, hereby declared that the presented work in the thesis entitled "**Study of bio oil production with rice husk and plastic wastes by using co-pyrolysis technique**" in fulfilment of degree of Doctor of Philosophy (Ph. D.) is an outcome of research work carried out by me under the supervision of **Dr Ashish Pratap Singh Chouhan** working as Associate professor in the Department of Physics, School of Chemical Engineering and Physical Sciences of Lovely Professional University, Punjab, India. In keeping with general practice of reporting scientific observations, due acknowledgments have been made whenever work described here has been based on the findings of another investigator. This work has not been submitted in part or full to any other University or Institute for the award of any degree.

(Signature of Scholar)

Name of the scholar: DIVYA BISEN

Registration No.: 11919639

Department: PHYSICS

Lovely Professional University, Jalandhar-Delhi,

G.T. Road (NH-1), Phagwara Punjab (INDIA) -144411

CERTIFICATE

This is to certify that the work reported in the Ph. D. thesis entitled "**Study of bio oil production with rice husk and plastic wastes by using co-pyrolysis technique**" submitted in fulfillment of the requirement for the award of degree of **Doctor of Philosophy (Ph.D.)** in the Department of Physics, School of Chemical Engineering and Physical Sciences is a research work carried out by Miss Divya Bisen (11919639) is bonafide record of her original work carried out under my supervision and that no part of thesis has been submitted for any other degree, diploma or equivalent course.

(Signature of Supervisor)

Name of supervisor**:** Dr Ashish Pratap Singh Chouhan

Designation: Associate Professor

Department: Physics

Lovely Professional University, Jalandhar-Delhi,

G.T. Road (NH-1), Phagwara Punjab (INDIA) -144411

ACKNOWLEDGEMENTS

I want to take this opportunity to express my heartfelt gratitude to them, whose contributions have made this thesis possible.

In particular, the foremost appreciation goes to my supervisor **Dr Ashish Pratap Singh Chouhan** for his valuable guidance throughout the research work. I thank him for his encouragement, guidance, and moral support, which enabled me to pursue my academic skills under his precious guidance and expertise. I also want to acknowledge my sincere gratitude to **Dr. Sankar Chakma**, professor (IISERB) for their insightful advice and suggestions throughout the research work. My sincere thanks to **Dr. Kailash Chandra Juglan** Professor and Head of School of Chemical Engineering and Physical Sciences, Lovely Professional University for his suggestions and support. My sincere thanks to Dr. Rajesh Kumar, Head of the research lab for providing the necessary facilities to carry out the research work at Lab. I acknowledge **Mr**. **Nitin Kumar Yadav**, Assistant Superintendent, for helping me with all the equipment in the research lab. I owe my sincere thanks to all the staff members of the Central Instrumentation Facility (CIF), Division of Research and Development, Lovely Professional University for providing modern analytical instruments facilities to accelerate fundamental and advanced research. I feel incredibly blessed to have the good company of friends **Yugesh Singh Thakur and Amisha Rathi** for their continuous moral support and unconditional friendship. Last but not least, I express my deepest sense of gratitude to my parents, their support and motivation given by my father B.R Bisen, and mother Asha Bisen, elder sister Poorva Rahangdale and my brother-in-law Manish Rahangdale and my younger brother Parag Bisen for motivation and friendly support and lovely niece Pakhi Rahangdale. For their patience, endless support, and inspiration towards the completion of my Ph.D. thesis. I extend my sincere thanks to all my relatives and dear friends who had consistently supported and encouraged me, without which this work would have never been completed. My sincere apology goes to those whom I forgot to mention but who helped me with any part of the research work.

Thank you all! **DIVYA BISEN**

Abstract

The increasing demand for utilizing plastic trash and biomass as sustainable energy sources is highlighted in the present research. Pyrolysis is a fundamental step in all thermochemical [gasification, torrefaction, combustion] conversion processes. In this process, three main products are produced: liquid bio-oil, solid biochar, and gasses (pyrogas). The feedstock biomass and organic materials are cooked in an inert atmosphere without oxygen. Both operational and non-operating variables have a major impact on the pyrolysis process.

The temperature, type of reactor, heating rate, vapour residence time, and feedstock particle size all have a significant impact on the pyrolysis products' yield and composition. Biomass and plastic pyrolysis appeared to be a multi-phase process involving a number of concurrent chemical and physical reactions. To effectively model, build, and construct a biomass conversion system for pyrolysis, a thorough understanding of the physicochemical properties and pyrolysis kinetics of biomass is therefore essential. The kinetic parameters of pyrolysis must be determined to forecast reaction behavior and optimize process parameters for the intended product distribution.

The potential of biomass which includes rice husk and polymers, including low-density polyethylene (LDPE) and high-density polyethylene (HDPE), for the synthesis of biofuels is the particular emphasis of this work. The physiochemical examination of the selected biomass and plastics aimed to comprehend their compositional and structural characteristics. Proximate analysis, Ultimate analysis, and heating value of selected feedstock have been investigated to understand their suitability to use as feedstock for pyrolysis.

The kinetics of RH, plastic waste (PET, LDPE, and HDPE), and their mixtures at various ratios under non-isothermal conditions and at variable heating rates of 10°C/min, 20°C/min, 30°C/min, and 40°C/min were assessed using a TGA analyser. Friedman model (FM), Tang Method (TM), Ozawa-Flynn-Wall model (OFW), Kissinger-Akahira-Sunose model (KAS), and Starink method (SM) were the five model-free techniques utilize to calculate the kinetic and, thermodynamics parameters.

Rice husk (RH), low-density polyethylene (LDPE), and high-density polyethylene (HDPE) were among the feedstocks that were thermally co-pyrolyzed. Particle size of 2-3 mm, heating rate of 10 °C min-1, sweeping nitrogen gas flow rate of 200 mL min-1, and individual and blended ratios of RH and plastic (LDPE and HDPE) at 50:50, 20:80, and 65:35 were all used in this semi-batch reactor in a nitrogen atmosphere at 500 °C for the co-pyrolysis process. ZSM-5 and calcined dolomite powder were used to catalytically co-pyrolyze rice husk and plastic waste (LDPE, HDPE) at optimal temperatures (500°C, 10°C/min).

FTIR analysis, GC-MS analysis, NMR, and other fuel properties like density, viscosity, specific gravity, cloud point, and pour point of the generated pyro-oil were among the analytical techniques used to characterize the thermal oil to evaluate its potential for use as an energy source by comparing it to commercial diesel. The outcomes of the ultimate and proximate analysis showed reduced levels of ash and nitrogen, a rise in carbon content, and a greater volatile matter content. Moreover, the content of sulphur was found to be nearly negligible across all blended samples.

The TG analysis shows that during the active pyrolytic zone (second phase), the mass loss thermographs showed the greatest breakdown. Furthermore, the TGA curves moved towards regions of greater temperature as the heating rates rose. The activation energy mean value was computed and found to vary with conversion values, reflecting the diverse composition of biomass and plastic. The sample's thermodynamic analysis verified that variations in enthalpy and activation energy promoted the creation of products. Furthermore, the samples' increased calorific value and Gibbs free energy suggested their potential for the generation of fuel and energy.

The co-pyrolysis experiment shows that the amount produced of pyrolytic products was shown to be highly impacted by temperature, heating rate, & size of particles and the weight composition ratio of biomass and plastics. The optimized conditions were found to maximize the liquid yield. The findings showed that at different individual and blended ratios of RH and plastic (LDPE and HDPE) at 50:50, 20:80, and 65:35, co-pyrolysis of RH and plastic increased the formation of pyrolytic liquid.

The thermal oil was characterized and found to have a greater heating value, lower acidity, higher viscosity, and higher oxygen concentration. While GC-MS analysis revealed more oxygenated chemicals, FTIR examination revealed the existence of phenol, alcohol, aromatics, alkane, ether, ester, acid, and aldehyde. These findings harmed the pyrolytic oil's usability as a fuel for transportation. The maximum liquid yield was achieved under optimal conditions, and the results showed that adding plastic waste to biomass at these conditions increased the liquid yield. On the other hand, when the biomass concentration grew, the liquid production decreased, and char formation increased. GC analysis showed that while carbon dioxide creation reduced with higher temperatures, the synthesis of hydrogen and hydrocarbons rose dramatically.

However, the moment a catalyst was introduced, the yield of liquid dropped, and the output of gas increased. The characterization's results demonstrated that the catalysts' addition improved the pyrolytic oil's properties, as evidenced by the oil's increased heating value and decreased viscosity, density, and oxygen content. GC-MS research revealed that the addition of catalysts significantly increased the number of hydrocarbons, alcohols, and aldehydes while drastically reducing the amount of oxygenated compounds.

The NMR investigation indicated that there was a significant amount of paraffin and aromatics present. Pyrolytic oil is a more desirable fuel for transportation because it contains more alcohols and aldehydes and less oxygenated molecules and acids, as demonstrated by GC-MS study of thermal co-pyrolysis and catalytic co-pyrolysis.

Keywords: Rice husk, Plastic waste (LDPE, HDPE), Co-pyrolysis, Kinetics, Activation energy, Pyro oil upgradation, Catalytic cracking, Dolomite, ZSM Catalyst

CHAPTER 1: INTRODUCTION

CHAPTER 2: LITERATURE REVIEW, RESEARCH GAPS AND OBJECTIVES

LIST OF FIGURES

LIST OF TABLES

List of Abbreviations

Symbol	Abbreviation
RH	Rice husk
LDPE	low-density polyethylene
PET	polyethylene terephthalate
HDPE	High-density polyethylene
FTIR	Fourier transform infrared spectroscopy
GC-MS	Gas chromatography – Mass spectroscopy
^{13}C NMR	Carbon Nuclear magnetic resonance
^{1}H NMR	Proton Nuclear Magnetic resonance
SEM	Scanning electron microscopy
EDS	Energy Dispersive Xray Spectroscopy
BET	Brunauer-Emmet-Teller
XRD	X-ray Diffraction
DLS	Dynamic light Scattering
KAS	Kissinger-Akahira-Sunose
FWO	Flyn-Wall-Ozawa
FM	Friedman
CHNSO	Carbon hydrogen nitrogen sulphur oxygen
TGA	Thermogravimetric analysis
DTG	Derivative thermogravimetry
DSC	Differential Scanning Calorimetry
HHV	Higher heating value
PO	pyrolysis oil
CV	Calorific value
AP	Aniline point
MC	Moisture content
VM	Volatile matter
AC	Ash content
FC	Fixed carbon
CR	Carbon Residue
NC	Non-catalytic
ZSM-5	Zeolite Socony Mobil–5
DOL	Dolomite
DOLZSM	Dolomite with ZSM-5
ASTM	American Standard for Testing Material

NOMENCLATURE

Symbols	Nomenclature
Ea	Activation Energy
A	Pre-exponential Factor
R	Universal gas constant
α	Conversion
t	Time (sec)
T	Temperature (°C)
T_0	Initial temperature (°C)
T_m	Peak Temperature (°C)
W_i	The initial mass of the sample
W_t	Sample mass at time 't'
W_f	The final mass of the sample
N	Order of the reaction
k	Rate constant
cSt	Centistokes
MJ/kg	Megajoule per kilogram
°C	Degree centigrade

CHAPTER – 1
INTRODUCTION

1.1 Introduction

Primarily derived from fossil fuels, about 80% of global energy consumption comes from these sources (BP, 2020). Using fossil fuels has led to several significant issues, including resource depletion, environmental degradation, and geopolitical instability. Burning fossil fuels is the primary source of greenhouse gas emissions that contribute to climate change and global warming. Furthermore, using and extracting fossil fuels harms ecosystems, water supplies, and air quality, which results in health problems and a decline in biodiversity (IEA, 2019) [1].

There is an urgent need to switch to renewable energy sources to address these problems. One sustainable substitute for fossil fuels is renewable energy, like solar, wind, and biomass. The capacity of biomass to transform organic material into energy makes it stand out among them, addressing waste management as well as energy generation. A versatile and abundant resource, biomass may be transformed into a range of energy sources through thermochemical and biochemical processes. Anaerobic digestion and fermentation are examples of biochemical methods, whereas pyrolysis, gasification, and combustion are examples of thermochemical routes [2].

Pyrolysis offers several advantages for biomass conversion. The byproducts of a thermochemical process that breaks down organic materials at high temperatures without oxygen include biochar, syngas, and bio-oil. The process of pyrolysis is very adaptable, capable of handling a wide range of feedstocks, including plastic waste, forestry debris, and residual agricultural materials. Biochar may be added to soil to increase fertility and absorb carbon, but it can also be modified such that the bio-oil produced during pyrolysis can serve as a sustainable liquid fuel [3]. Moreover, pyrolysis processes can be optimized for energy efficiency and product yield through careful control of parameters including temperature, heating rate, gas flow rate, and residence time.

Research on technology for producing bio-oil, especially by co-pyrolysis of plastic waste and rice husk, is crucial given the worldwide movement towards sustainable

energy systems. A byproduct of milling rice, rice husk presents disposal issues and is widely accessible in rice-producing nations. Similarly, because plastic garbage doesn't biodegrade, it poses a serious threat to the ecosystem. By using these materials' synergies, co-pyrolysis increases bio-oil output and quality while lowering dependency on fossil fuels and promoting a circular economy [4].

A novel process called pyrolysis involves heating biomass at various temperatures in the absence of air or oxygen to create charcoal, non-condensable gases, and liquid bio-oil. Nevertheless, the bio-oil generated during pyrolysis contains significant quantities of oxygenated chemicals and water, rendering it inappropriate for immediate use as a biofuel. Furthermore, bio-oil is inherently unstable, meaning its qualities might change as time passes. This means that upgrading procedures are required to improve its stability, calorific value, and other fuel properties. To enhance the qualities and stability of biomass pyrolysis oil, researchers have employed the co-pyrolysis of plastics with biomass as a unique technique to generate liquid biofuels. Through this process, waste biomass and polymer waste may be effectively used to create a variety of useful products [5].

Plastic trash creation has significantly increased in recent years due to the spike in the manufacturing and consumption of plastic products. As of 2024, approximately 220 million tons of plastic were produced worldwide annually, a figure that continues to rise due to the versatile applications and durability of plastics. However, managing this vast amount of plastic waste remains a critical challenge. Recycled content is still only around 9% of total plastic garbage generated, despite global efforts to improve recycling. Because plastic is not biodegradable, the bulk of garbage (79%), winds up in landfills where it can remain for hundreds of years. Additionally, a considerable amount of plastic waste, approximately 12%, is incinerated, often releasing harmful pollutants into the atmosphere.

There are serious risks associated with the environmental buildup of plastic garbage, including the contamination of soil and water bodies, harm to marine and terrestrial wildlife, and potential human health risks due to the ingestion of microplastics and exposure to toxic chemicals released during degradation and incineration processes [6].

Based on its content and structure, biomass, a diversified source of renewable energy, may be roughly divided into two categories: non-lignocellulosic biomass and lignocellulosic biomass. The structural components of plant cell walls, cellulose, hemicellulose, and lignin, make up the majority of lignocellulosic biomass. Materials of this category include wood from pine and oak trees, agricultural wastes like maize stover and wheat straw, and forestry residues such as wood chips and branches. These materials are abundant and widely used for bioenergy production through processes like biochemical conversion and thermochemical processes. In contrast, non-lignocellulosic biomass encompasses a broader array of organic materials that may or may not contain significant amounts of cellulose, hemicellulose, and lignin. Examples include starch-based biomass like corn and potatoes, sugar-rich biomass such as sugarcane and sugar beet, oil-rich biomass from soybeans and palm, and algae, which can accumulate lipids or carbohydrates suitable for biofuels. Each type of biomass offers distinct advantages and challenges, influencing their applications in biofuel production, bioproducts, and sustainable energy solutions [7].

Plastics like PP, PE, and HDPE may be co-pyrolyzed with different biomass systems to produce bio-oils that are higher in quality and quantity. Compared to bio-oils formed from pure biomass pyrolysis, those produced by co-pyrolysis are more stable and have lower concentrations of oxygenated chemicals and water. Plastics work in concert with biomass to promote thermal breakdown and increase pyrolytic oil production. By removing the requirement for catalytic pyrolysis, which raises the process's overall operating costs, co-pyrolysis also lowers output costs. Various polymer types can interact with biomass in different ways to produce bio-oils with different properties and amounts. The precise processes by which plastics and biomass interact are currently unclear and need more research [8].

In order to produce useful chemicals, several combinations of biomass waste and plastic polymers have been studied in recent co-pyrolysis research. One such research yielded the maximum oil production of 52.75% at a 1:1 ratio when sugarcane bagasse and low-density polyethylene (LDPE) were co-pyrolyzed. This process also significantly reduced oxygenated compounds by up to 50%, improving the oil's quality. The largest concentrations of aromatic compounds and olefins were found in the liquid products of a different investigation that involved co-pyrolyzing paper biomass with different

mixes of polypropylene (PP), high-density polyethylene (HDPE), and polyethylene terephthalate (PET) in a 1:5 ratio. Co-pyrolysis is a useful method for raising the output and quality of biofuel overall. However, several limitations remain in converting it into biofuels and value-added chemicals, necessitating further research for its successful application across various sectors [9].

Research has also looked into enhancing bio-oil properties by adding polystyrene (plastic). Oil production from co-pyrolysis of biomass and polymers has advanced, especially with the introduction of zeolite catalysts. Zhang et al. investigated the catalytic co-pyrolysis of polymers and lignocellulosic biomass and discovered that this method leads to less catalyst coke production and oil with a greater concentration of aromatic chemicals, particularly mono-aromatics. In a similar manner, Xue et al. investigated the co-pyrolysis of polyethylene with model biomass materials using a HZSM-5 zeolite catalyst. They discovered that there was a rise in the synthesis of aromatic hydrocarbons and a decrease in the creation of coke, in comparison to the catalytic pyrolysis of plastic and biomass separately [11]. Catalytic co-pyrolysis of biomass and polymers was investigated by Uzoejinwa et al. to enhance the quality of bio-oil. Their findings demonstrated increased process efficiency since catalytic co-pyrolysis required less activation energy and temperature and produced more aromatic chemicals [12]. Using a ZSM-5 zeolite catalyst, Li et al. investigated the catalytic co-pyrolysis of biomass and waste polymers, including polyethylene, polypropylene, and polystyrene. The co-pyrolysis of polyethylene and cellulose/wood was shown to have the most significant synergistic effect, indicated by a greater aromatic content [13].
Using dolomite ($CaMg(CO_3)_2$) as the catalyst, Conesa and Domene performed pyrolysis of grass and municipal solid waste to create syngas (H_2 + CO) [14]. Dolomite was found to lower the sulfur concentration in coal pyrolysis, according to Gao et al. (2019). Additionally, other studies indicated that dolomite reduced tar production during pyrolysis [15]. This study investigated the production of bio-oil from biomass (rice husk) using thermal and catalytic cracking in the presence of dolomite catalyst and zeolite Socony Mobil-5 (ZSM-5) at room pressure and nitrogen atmosphere. A variety of plastics were used, including low-density polyethylene (LDPE) and high-density polyethylene (HDPE) [16].

1.2 Renewable sources of energy

The majority of people on the earth reside in countries that import fossil fuels [17]. Six billion people are at risk from geopolitical crises and disruptions due to their reliance on imported fossil fuels [18]. Conversely, although they are widely accessible, renewable energy sources have not yet realized their full potential. The International Renewable Energy Agency (IRENA) projects that renewable energy sources will account for 90% of global energy consumption by 2050. Furthermore, by producing a large amount of greenhouse gases, the excessive use of fossil fuels and non-renewable energy sources adds to global warming. To counteract climate change, greenhouse gas emissions from the production and consumption of energy must be reduced [19].

Hydropower, solar, biomass, wind, geothermal, hydropower, and tidal energy are the main sources of renewable energy. By reducing carbon emissions to relatively low levels, renewable energy helps to lessen the impact of climate change brought on by the combustion of fossil fuels. Since it lowers carbon dioxide emissions, energy generation from the burning of biomass is regarded as a renewable energy source that has gained popularity recently [20]. Because the CO2 released during burning is nearly equal to the CO2 absorbed by plants during growth, biomass, which is made of organic matter, is regarded as a carbon-neutral fuel source because it has little effect on atmospheric CO_2 levels. Use of biomass to generate biofuels would reduce fossil fuel dependency which contributes to greenhouse gases [21,22]. Just 4% of the total energy consumed is accounted for by biomass energy. It is not possible to fully comprehend the "Waste to Wealth" notion. This promotes the use of the pyrolysis process to turn biomass into energy. The energy distribution from different renewable energy sources is shown in Figure 1.4. The field of biomass valuation study has a lot of untapped potential. Energy conversion and a sustainable environment will be the two main outcomes of this.

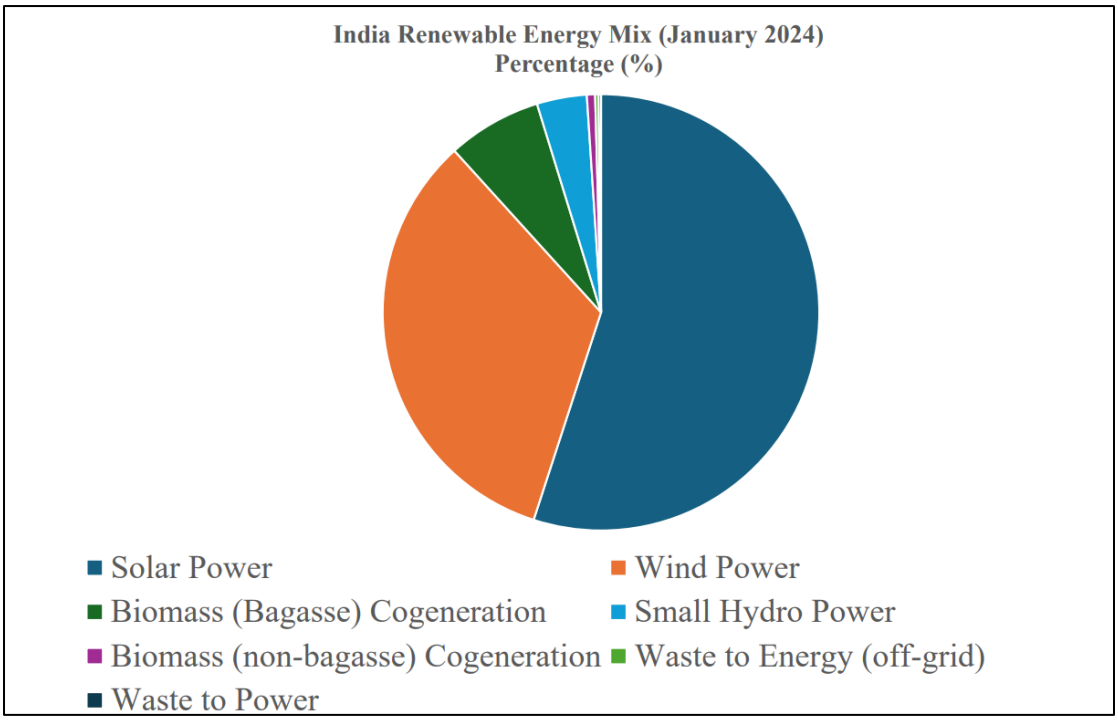

Figure 1.1 The energy distribution from different renewable energy sources

1.3 Conversion Technologies

Thermochemical conversion processes are employed to produce energy such as oils, producer gas or methanol under controlled temperature and oxygen conditions instead of directly generating energy. The products obtained from thermochemical routes have convenient combustion characteristics and more density, reducing the cost of transportation. These processes include pyrolysis, carbonization, gasification, and catalytic liquefaction. Pyrolysis is one of these processes that often yields biofuel with high fuel-to-biomass ratios. Pyrolysis has garnered more interest in recent times as an enhanced method for converting biomass into biofuel [23]. The pyrolysis process aims to generate superior bio-oil capable of rivalling and supplanting traditional fossil fuels. The cost breakdown for different thermochemical treatments concerning biofuel production and reforming operations across various solid waste types is illustrated in **Fig. 1.2**

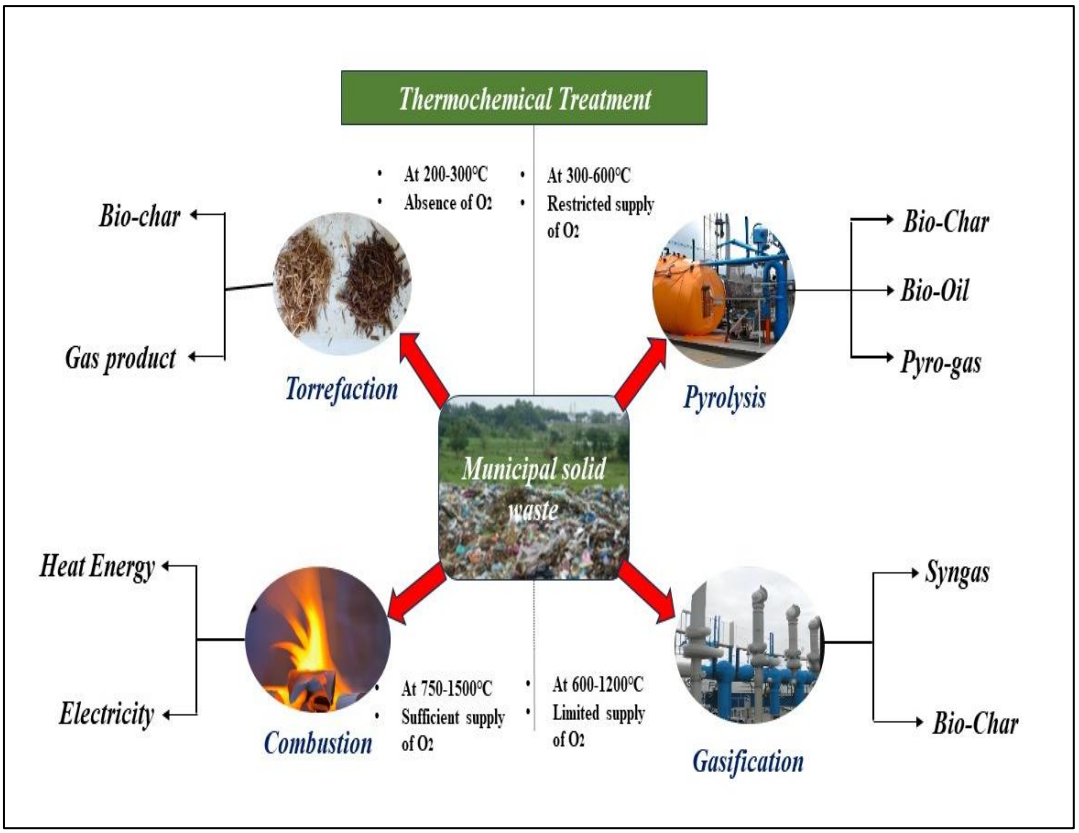

Figure 1.2 The classification of thermochemical treatment methods for solid waste energy production.

1.3.1 Thermo-chemical conversion technologies

Biomass is a sustainable, clean, and green resource that can be used to make fuels to meet energy demands. Yet, there are many drawbacks to using biomass directly as biofuels, including low calorific value, unfavourable moisture content, anomalous composition, and characteristics. By enhancing the operating conditions, thermochemical techniques provide methods that significantly reduce undesirable by-products and mitigate these drawbacks. Thermochemical processes help to produce biofuels from both lignocellulosic and non-lignocellulosic materials [24].

1.3.1.1 Torrefaction Process

Torrefaction stands out as an intriguing thermochemical method frequently employed as a preliminary heat treatment for biomass resources [25]. Torrefaction enhances the effectiveness of thermochemical transformation methods like pyrolysis, and liquefaction, along with gasification by removing moisture and partially breaking down the biomass [26]. By lowering oxygen levels and elevating carbon content, Torrefaction

enhances the biomass's capacity to generate heat. The purpose of Torrefaction is to create materials with high hydrophobicity and solid fuel as an alternative to coal [27]. Torrefaction involves subjecting the biomass to a heat treatment in an oxygen-depleted setting, typically within temperatures spanning from 200 to 300°C. Within this category, it is divided into three severities: mild (235-275°C), and severe (275-300°C) temperatures Torrefaction [28]. Due to its capacity to increase biomass's energy content, stability, and handling qualities, torrefaction is essential to thermochemical conversion. It helps solve issues related to the unpredictability of biomass feedstocks in various conversion processes and promotes the effective use of biomass resources for the generation of sustainable energy.

1.3.1.2 Pyrolysis Process

Biomass may be pyrolyzed at high temperatures to produce charcoal, bio-oil, non-condensable gases (H_2, CH_4, CO, and CO_2), and charcoal. Both organic and aqueous components are included in bio-oil. Its organic part contains tar and dense hydrocarbon molecules, which, when refined, can yield more refined transportation fuels. The enhancement of bio-oil requires both processes, catalytic and non-catalytic, to remove oxygen, nitrogen, and sulfur compounds. In the absence of these substances, the fuel's heating value may be reduced, and NOx and SOx may be released during combustion [29]. Three major classes of current pyrolysis techniques may be distinguished: flash pyrolysis, fast pyrolysis, and slow pyrolysis. Furthermore, cutting-edge technologies such as hydrous pyrolysis, hydro-pyrolysis, catalytic hydro-pyrolysis, microwave pyrolysis, and hydro-pyrolysis improve and diversify the pyrolysis processes even further [30].

1.3.1.3 Gasification Process

By carefully oxidizing biomass, a process known as gasification, a gas rich in CO, H_2, CH_4, and CO_2 is produced. This gas, after purification, can directly power engines or can be transformed into liquid fuels or chemical feedstocks through biological fermentation. Managing the condensation of heavier molecular weight volatiles into tars presents a challenge within the gasification process; these tars not only cause fouling issues but also present potential long-term environmental hazards, such as polycyclic aromatic hydrocarbons [31]. Moreover, by modifying factors like

temperature, pressure, reaction duration, medium, concentration of feedstock, equivalence ratio, and catalyst quantity in the gasification procedure, it's possible to enhance both efficiency and the rate of carbon conversion to hydrogen. This adjustment can also affect the selectivity of the produced hydrogen and the calorific value of the resulting syngas.

1.3.1.4 Combustion process

Heat is the primary product of combustion technology, and yield is affected by factors like feedstock, gasifier, and temperatures ranging from 750 to 1500°C. It's a versatile method applicable to remediate nearly all solid waste. Apart from energy production, industries employ combustion for tasks like drying and pre-heating along with steam generation. While carbon-rich resources like coal are extensively used for energy generation, they release substantial CO_2 emissions [32]. Full combustion, converting the carbon and hydrogen-abundant biomass into CO_2 and H_2O, generates heat. Coal contributes about 44% of CO_2 emissions, ranging from 0.34 to 0.39 $kgCO_2/kWh$, according to the International Energy Agency. Utilizing biomass alongside coal could serve as a feasible strategy to reduce total CO_2 emissions [33]. More than 70% of all heat production comes from the burning of volatile gases. It occurs above the fuel bed, and yellow flames are typically present to indicate it. Little blue flames are indicative of char combustion in the fuel bed [34].

Table 1.1 Advantages and disadvantages of thermochemical conversion [35]

Technology	Advantages	Disadvantages	Opportunities
Torrefaction	• It can be applied to both biomass conversion and pretreatment. • A high amount of energy per volume. • Increases the biomass's calorific value. • Torrefied biomass may be transported across long distances more easily when it is pelletized. • Lowers the amount of	• Torrefaction reactor optimization is crucial to meet end-use financial requirements and attain uniform product quality for market purposes. • Reduced overall efficiency.	Torrefaction serves a dual purpose: as a direct fuel and as a means to enhance various properties of feedstock. • Catalyst is not necessary.

	moisture. Low energy requirement. • Lower operational expenses		
pyrolysis	High performance. • Potential uses for chemicals produced (e.g., tar, bio-oil, and char). • Reduces waste sent to landfills and greenhouse gas emissions. • Lowered energy input is needed for slow pyrolysis. • Demands more energy input for pyrolysis that occurs quickly.	High CO concentrations make it difficult to release product gases into the atmosphere without treatment.	• Wide-ranging experience • Growth of the pyrolysis liquid and char products market
Gasification	• Syngas can be used directly as a fuel or to create products with additional value such as synthetic natural gas, chemicals, hydrogen, kerosene, and naphtha.	• Expensive maintenance and running costs. • Problems with homogenous and carbon-based catalysts' capacity to be recycled.	• There's a chance for large-scale activities. • Significant untapped potential.
Combustion	• The heat loss is very small, and the thermal efficiency is higher. • Fuel consumption is very low	• Incomplete combustion of hydrocarbon also results in carbon monoxide.	• High greenhouse gas reduction potential using renewable methane. • Fast transition to cleaner renewable transport.

1.4 Future Energy Demand

It demonstrates a positive trend toward switching to renewable energy sources from fossil fuels. By 2040, the usage of coal has practically reached its peak while the use of oil and natural gas has drastically declined. Figure 1.3 illustrates the current trends in renewable energy sources, which include solar, wind, hydropower, and biofuels. The

Indian government has put in place a number of energy-related policies, such as subsidies and increasing public awareness of the need of using a wide range of renewable energy sources.

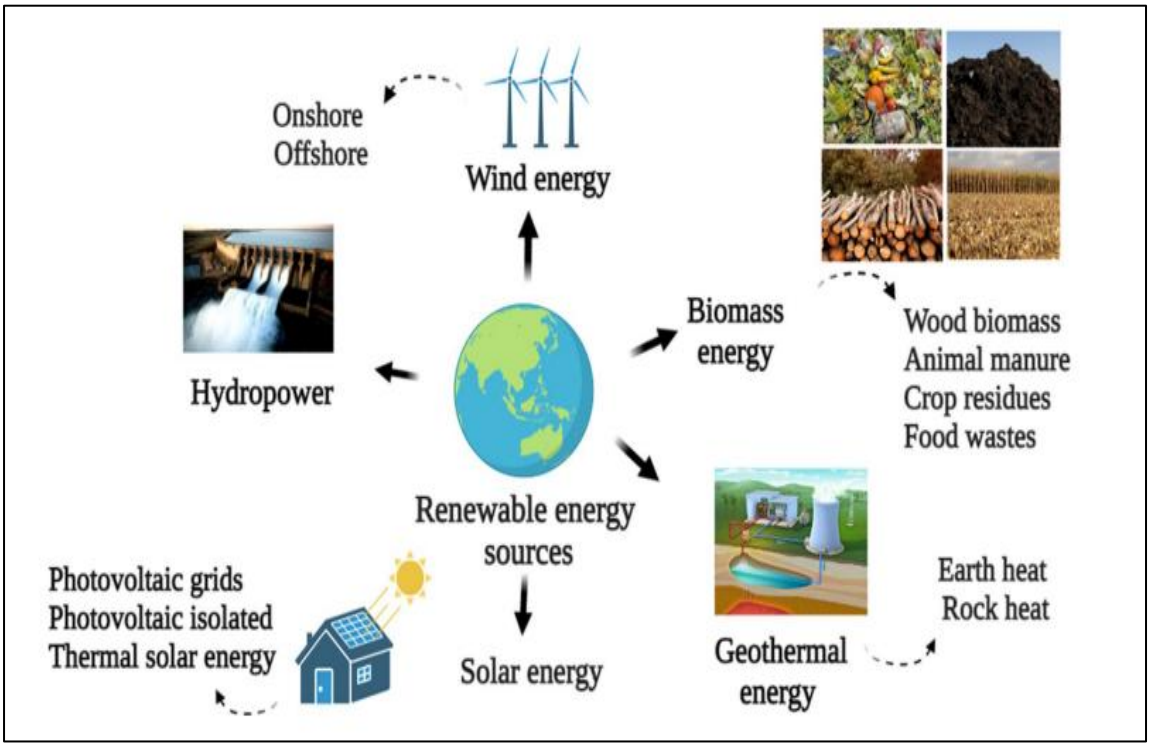

Figure 1.3 Renewable energy sources. Fossil fuels may be replaced by renewable energy sources, which will slow down climate change. Solar, wind, geothermal, hydropower, and biomass are the main energy sources. [36]

1.5 Classification of feedstock for thermal treatment

Thermochemical treatment utilizes heat to transform various feedstocks, including waste materials, into valuable products like energy, fuels, or chemicals. The classification of different feedstocks for thermochemical treatment depends on their composition, characteristics, and potential for conversion.

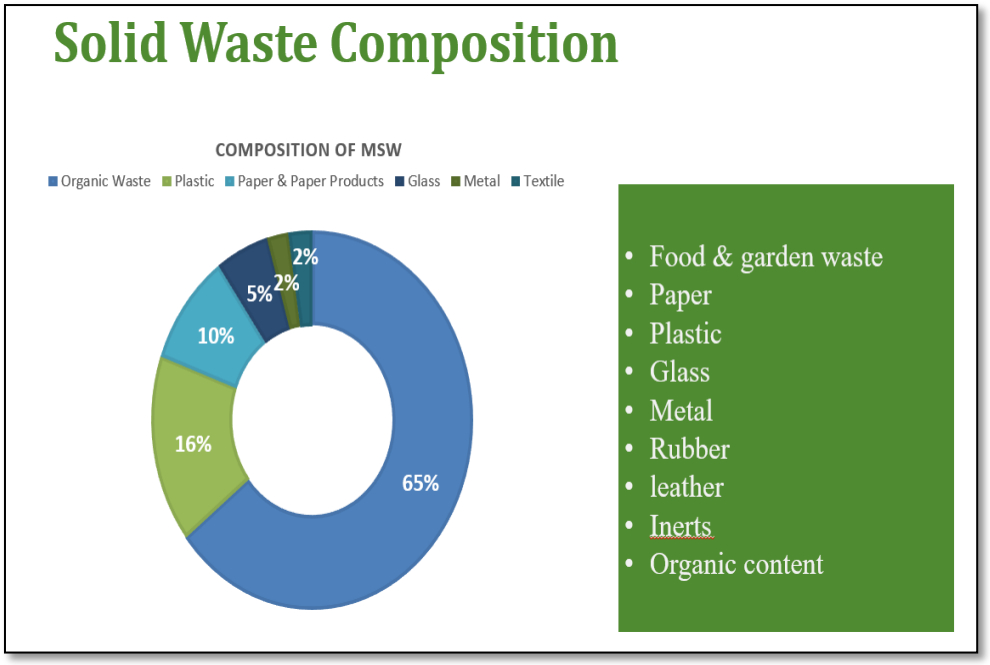

Figure 1.4 Composition of Municipal Solid Waste.

Table 1.2 summarizes the classification of feedstocks based on their origin and properties.

Category	Feedstock Type	Origin	properties	References
Lignocellulosic Biomass	Wood Residues	Forests, sawmills	High lignin concentration, mild moisture, and consistent structure.	37
	Agricultural Residues	Crop harvesting	High cellulose and hemicellulose, low lignin, and variable moisture.	38
		Dedicated plantations	High yield, suited for energy generation; constant quality.	38
Aquatic Biomass	Algae	Freshwater, marine sources	High lipid content, fast growth, high moisture	39
	Seaweed	Coastal areas	High carbohydrate content, moderate protein, high moisture	40

Organic Waste	Municipal solid waste	Urban areas	Heterogeneous composition, variable moisture, and contaminants	41
	Food Waste	Households, food industry	High organic content, high moisture, and biodegradable	42
Industrial waste	Spent Grain	Breweries, distilleries	High fiber and protein, moderate moisture	43
	Black Liquor	The pulp and paper industry	High lignin content, caustic chemicals	44
Animal waste	Manure	Livestock farms	High nitrogen content, variable moisture, and biodegradable	45
Fossil biomass		Peatlands	Moderate moisture, high carbon content, partially decomposed	46
Dedicated Energy Crops	Switchgrass	Marginal lands, plantations	High cellulose, low lignin, drought-resistant	47
	Miscanthus	Agricultural lands	High yield, high fibre content, low moisture	47

1.6 Selection of Feedstock

1.6.1 Biomass waste

Among the more than 140 billion tonnes of biomass waste generated annually by agriculture, only 40% are put to utilized [36]. The yearly production of lignocellulosic biomass from forestry and agricultural wastes is used in just 4.5% of cases [48]. The yearly production of biomass is predicted to be 181.5 billion tonnes. In addition to forestry and agriculture, human-produced organic waste is a significant source of biomass. Global issues stem from the increasing volume of solid waste produced by a growing global population. With its yearly renewable energy sources, biomass has a lot of potential for application in next-generation energy systems. Municipal solid waste,

wood and forestry trash, and agricultural waste are all widely available in India. Among the carbohydrates in biomass are cellulose, hemicellulose, and lignin, all of which are necessary for the pyrolysis process. The production of bio-oil, often referred to as pyrolytic fuel oil, is dependent on several factors, including the suitability of the feedstock, the temperature at which pyrolysis occurs, the rate of heating, and the flow rate of the sweep gas, which is usually nitrogen. The economic viability of bio-oil production is influenced by the feedstock's compatibility, which can expedite the process. Rice husk was used for the study since it is the main crop grown in India (Table 1.1 & 1.2).

1.6.2 Plastic Waste

Recent years have seen a sharp increase in plastic waste because of rising manufacturing and low recycling rates. Globally, approximately 55% of plastic trash is landfilled or thrown in nature [49]. Approximately 255 million tonnes of plastic garbage are generated annually. Plastics, derived from petroleum refineries, have witnessed a surge in usage since 1990. According to estimations, the half-lives of plastics in the environment range from 58 years for bottles to 1200 years for pipes [50]. By 2050, 12,000 million tonnes of plastic garbage are expected to be in landfills and the environment, if current trends continue [51]. Reaching circularity and making the most of plastic goods requires putting energy conversion or recycling into practice as a plastic waste management strategy. A synthetic polymer that can be moulded with pressure or heat is called plastic. It is made up of repeating molecular chains made of nitrogen, hydrogen, carbon (in single and double bonds), and either Sulphur or chlorine. Because they lack functional groups, are hydrophobic and have a large molecular weight, plastics are frequently chemically and physiologically inert. Because of their refractory nature, plastics resist breaking down quickly [52]. Recycling plastic garbage is crucial due to its massive production each year. Polyethylene terephthalate (PET), polycarbonate (PC), polypropylene (PP), polystyrene (PS), high-density and low-density polyethylene (HDPE and LDPE), and other polymers are among those found in plastic waste. These polymers have different compositions of carbon, oxygen, and hydrogen, but they all have distinct chemical structures and high volatile, viscous, and heating values along with very low moisture and ash contents [51].

Table 1.3 Biomass and Plastic Waste Availability in India in the Last 10 year.

Production of biomass and plastic in India. (Million Tons)		
Year	**Rice husk**	**Plastic waste**
2010-2011	95.98	262
2011-2012	105.30	279
2012-2013	105.24	288
2013-2014	106.65	299
2014-2015	105.48	311
2015-2016	104.41	322
2016-2017	109.70	335
2017-2018	112.91	348
2018-2019	116.48	365.3
2019-2020	118.87	374.8
2020-2021	124.37	375.3
2021-2022	130.29	390.7

Table 1.4 Biomass and plastic waste production in Punjab. (Million Tons) in the last 5 years.

Production of rice husk and plastic waste in Punjab. (Million Tons)		
Year	**Rice husk**	**Plastic waste**
2017-2018	13.38	142
2018-2019	12.82	129
2019-2020	11.78	187
2020-2021	12.78	243
2021-2022	12.89	298

Source - Website of Food & Agriculture Organization of the United Nations , World Bank MSW report, 2018

Source- plastic production worldwide (Statista), Punjab Pollution Control Board.

1.7 Types of Pyrolysis Process

Table 1.5 demonstrates the many types of pyrolysis processes, which are divided according to temperature and residence duration.

Table 1.5 Common operational parameters for pyrolysis methods and their typical outcomes [54]

Pyrolysis Type	**Temperature Range (°C)**	**Residence Time**	**Heating rate**	**Typical outcomes**	**Application**
Slow pyrolysis	300-600	Hours to days	Low(<10°C/min)	High char yield (30-50%) Moderate liquid yield (20-40%) Low gas yield (10-30%)	Production of biochar for soil amendment and carbon sequestration
Fast Pyrolysis	400-600	seconds	High (10-200°C/s)	High liquid yield (60-75%) Low char yield (10-15%) Moderate gas yield (10-20%)	Bio-oil production for biofuel and chemical feedstock, heat, and power generation
Flash Pyrolysis	450-900	< 1 second	Very High (> 1000°C/s)	Very high liquid yield (> 75%) Very low char yield (< 10%) Low gas yield (< 15%)	Bio-oil production for high-value chemicals
Intermediate Pyrolysis	400-600	Minutes	Medium(10-50°C/min)	Balanced yields: liquid (30-50%), char (25-35%), gas (15-25%)	Combined heat and power (CHP) systems, biofuel production

Hydro pyrolysis	300-500	Seconds to minutes	Medium to high	- High-quality liquid fuels (less oxygenated)	Production of high-quality liquid fuels and chemical feedstocks
Catalytic Pyrolysis	400-600	Seconds to minutes	Medium to high	Enhanced liquid quality (lower oxygen content) lower char yield Varies based on the catalyst used	Upgraded bio-oil production, production of chemicals, and fuels

1.8 Environmental impact

Burning rice husks outside has a detrimental effect on the environment, raising air pollution, greenhouse gas emissions, and health hazards. During the process, humans may be exposed to dangerous gases such as carbon monoxide, carbon dioxide, methane, and particulate matter, which can cause respiratory and cardiovascular problems. Global warming and climate change are also caused by emissions of carbon dioxide and methane. Burning rice husk releases ash that is devoid of important minerals, reducing soil fertility and impacting crop growth. Open burning lowers air quality due to smoke and particle matter, which results in smog and poor visibility, harming the ecosystem of environment and the health of humans. The release of toxic substances during burning can harm local flora and fauna, reducing photosynthesis and affecting wildlife. Moreover, the ash can be washed into nearby water bodies, leading to water contamination and affecting aquatic life [55]. These pollutants can exacerbate respiratory conditions such as asthma and bronchitis, posing significant public health risks, especially to vulnerable populations like children and the elderly. The sulfur and nitrogen compounds released can also contribute to acid rain, harming ecosystems, buildings, and water sources. To mitigate these negative effects, alternative methods of

managing rice husk, such as energy production through controlled combustion or converting it into bio-oil via pyrolysis, are being explored [56]. An overview of the lifecycle of plastics, categorizing them into polyvinyl chloride (PVC–U), polystyrene or Styrofoam (PS), polypropylene (PP), high-density polyethylene (HDPE), polyethylene terephthalate (PETE), and other types. Additionally, the discussion encompasses the issues arising from insufficient plastic waste processing and explores potential solutions to promote a healthier environment. Packaging stands out as a crucial and frequently encountered use of plastic materials, with approximately 40% of global plastic production dedicated to storing and packaging various manufactured goods. Plastics play a vital role in establishing a sustainable, proper, hygienic, cost-effective, energy-efficient, and eco-friendly packaging system, contributing to environmental cleanliness [57]. The adaptability of plastics has proven effective in ensuring hygienic and economical packaging for a range of food products such as wheat flour, liquids, bread, rice, snacks, milk, and spices, confectioneries, and diverse pharmaceutical products. However, there is a big environmental problem because of the significant buildup of post-consumer trash caused by the widespread usage of these items.

Figure 1.5 illustrates the comparative CO_2-equivalent emissions associated with the treatment of LDPE and rice husk through landfilling, incineration, and pyrolysis. Landfilling and incineration of LDPE result in substantial greenhouse gas emissions, estimated at 3.0 and 2.5 tons of CO_2 per ton of waste, respectively. In contrast, pyrolysis significantly reduces emissions to 0.2 tons CO_2-eq. For rice husk, pyrolysis offers an even greater environmental advantage, showing a negative emission value of –1.2 tons CO_2-eq due to carbon sequestration via biochar. These results emphasize the environmental benefits of adopting pyrolysis over conventional waste disposal methods [58,59].

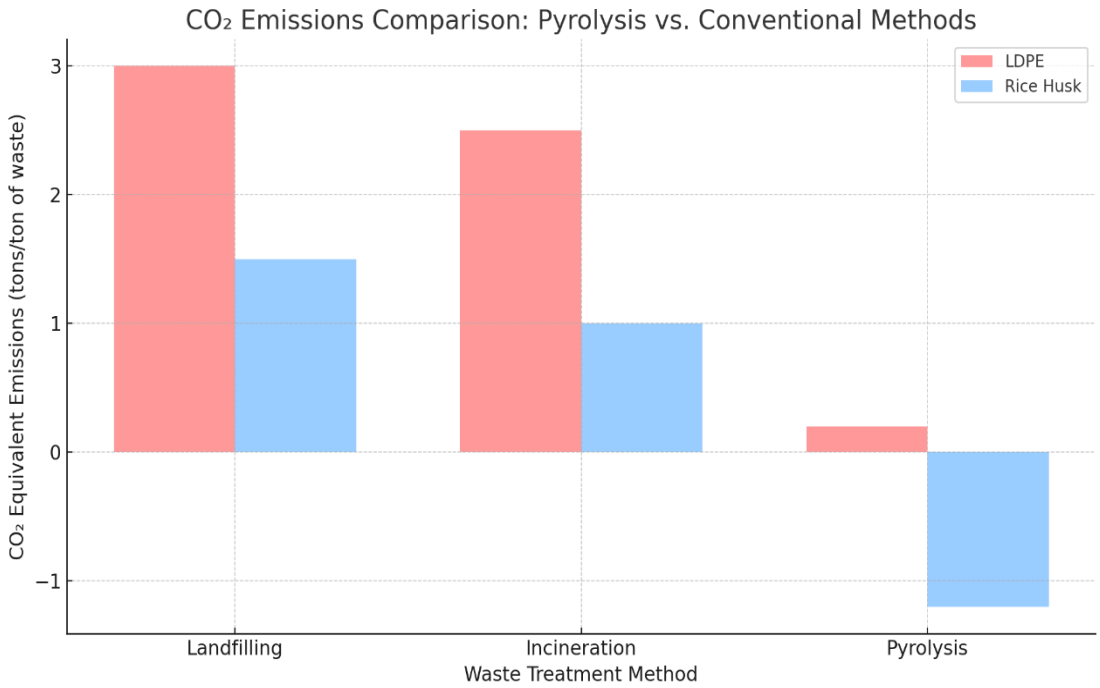

Figure 1.5: Comparison of CO_2-equivalent emissions per ton of LDPE and rice husk treated via landfilling, incineration, and pyrolysis. Pyrolysis significantly reduces emissions and enables carbon sequestration for biomass

1.9 Motivation of the work

The necessity of addressing the two problems of waste management and sustainable energy generation is what motivates this study. Effective utilization solutions are urgently needed due to the growing amounts of forestry waste, urban solid waste, and agricultural waste, especially in areas like India. Simultaneously, the environmental and economic impacts of plastic waste necessitate innovative approaches to recycling and reusing these materials. Co-pyrolysis of plastic and biomass provides a viable way to reduce pollution in the environment and contribute to renewable energy sources by turning these wastes into useful bio-oil, biochar, and syngas. To improve the yield and efficiency of bio-oil production, this research will look at ideal parameters such as temperature, heating rate, blending ratio, residence time, and feedstock selection**.** Moreover, the quality of the bio-oil may be raised, making it a more attractive substitute for fossil fuels, by comprehending the chemical interactions and streamlining the process using catalysts. The overall goal of this effort is to further the field of waste-to-

energy conversion by offering long-term, financially feasible solutions for energy generation and trash management [60–62]. The co-pyrolysis approach yields more oil than standalone biomass pyrolysis, as several studies have shown. The interactions between the hydrocarbon polymers during the process are the reason for this.

1.10 Application of Pyro-oil in Compression Ignition Engines

The pyrolysis process takes place in an inert atmosphere, resulting in the production of liquid fuel and biochar as its end products. The pyro-oil that is produced can be used directly in boilers and turbines, or it can be combined with diesel to be used in diesel engines [63]. But because the pyro-oil produced by pyrolysis has a greater self-ignition temperature, it must be blended with methanol or diesel or upgraded [64]. Pyro-oil's stoichiometric air-fuel ratio indicates that it has a reduced calorific value because of its increased oxygen content. Diesel and pyro-oil together result in lower emissions of hydrocarbons, carbon monoxide, and particulate matter but higher emissions of NOX. It is essential to remember that the type of feedstock utilized affects the engine's emission characteristics [65].

1.11 Organizations of the thesis

Chapter 1: Highlights the importance of bio-oil and its numerous uses in a variety of industries as it introduces the current study. In addition, this chapter addresses the drawbacks of bio-oil and examines methods for improving it.

Chapter 2: Discusses the literature review of all thermochemical conversion and its challenges.

Chapter 3: Addresses the collection and preparation of raw materials, the setup of experimental procedures, and the analysis of the resulting products through different experimental methods. This section also outlines the extent of the experiment.

Chapter 4: Describes the thermal dynamics of plastic, biomass, and their combination using a variety of analytical models.

Chapter 5: Focusses on the thermal pyrolysis of rice husk and plastic waste (LDPE, HDPE), as well as the thermal pyrolysis of these materials. This chapter contains comprehensive physical and chemical characterizations of the bio-oil that is produced during the pyrolysis of various source materials. The chapter also compares thermal

pyrolysis and co-pyrolysis and discusses the differences in their results.

Chapter 6: describes how to catalytically pyrolyse rice husk and plastic waste (LDPE, HDPE) in an 80:20 ratio using dolomite and ZSM catalysts. The pyrolysis oil's chemical and physical characteristics are thoroughly examined in this chapter.

Chapter 7: Conclusion and Future Aspects.

1.12 References

1. Abnisa, F., and Daud, W. M. A. W. (2014). A review on co-pyrolysis of biomass: an optional technique to obtain a high-grade pyrolysis oil. *Energy Conversion and Management*, *87*, 71-85.
2. Demirbas, A. (2011). Waste management, waste resource facilities and waste conversion processes. *Energy Conversion and Management*, *52*(2), 1280-1287.
3. Bridgwater, A. V. (2012). Review of fast pyrolysis of biomass and product upgrading. *Biomass and bioenergy*, *38*, 68-94.
4. Wang, G., Dai, Y., Yang, H., Xiong, Q., Wang, K., Zhou, J., and Wang, S. (2020). A review of recent advances in biomass pyrolysis. *Energy & fuels*, *34*(12), 15557-15578.
5. Bhatnagar, A., Singhal, A., Tolvanen, H., Valtonen, K., Joronen, T., and Konttinen, J. (2022). Effect of pretreatment and biomass blending on bio-oil and biochar quality from two-step slow pyrolysis of rice straw. *Waste Management*, *138*, 298-307.
6. Arif, M., Li, Y., El-Dalatony, M. M., Zhang, C., Li, X., and Salama, E. S. (2021). A complete characterization of microalgal biomass through FTIR/TGA/CHNS analysis: An approach for biofuel generation and nutrients removal. *Renewable Energy*, *163*, 1973-1982.
7. Song, Y., Tahmasebi, A., and Yu, J. (2014). Co-pyrolysis of pine sawdust and lignite in a thermogravimetric analyzer and a fixed-bed reactor. *Bioresource Technology*, *174*, 204-211.
8. Shadangi, K. P., and Mohanty, K. (2015). Co-pyrolysis of Karanja and Niger seeds with waste polystyrene to produce liquid fuel. *Fuel*, *153*, 492-498.
9. Chaturvedi, E., Roy, P., Upadhyay, R., and Chowdhury, P. (2024). Enhanced yield and production of aromatics-rich fractions in bio-oil through co-pyrolysis of waste biomass and plastics. *Journal of Analytical and Applied Pyrolysis*, *178*, 106379.
10. Zhang, X., Lei, H., Chen, S., and Wu, J. (2016). Catalytic co-pyrolysis of lignocellulosic biomass with polymers: a critical review. *Green Chemistry*, *18*(15), 4145-4169.

11. Xue, X., Pan, Z., Zhang, C., Wang, D., Xie, Y., and Zhang, R. (2018). Segmented catalytic co-pyrolysis of biomass and high-density polyethylene for aromatics production with MgCl2 and HZSM-5. *Journal of Analytical and Applied Pyrolysis*, *134*, 209-217.
12. Uzoejinwa, B. B., Cao, B., Wang, S., Hu, X., Hu, Y., Pan, C., and He, Z. (2022). Catalytic co-pyrolysis of macroalgal components with lignocellulosic biomass for enhanced biofuels and high-valued chemicals. *International Journal of Energy Research*, *46*(3), 2674-2697.
13. Li, X., Li, J., Zhou, G., Feng, Y., Wang, Y., Yu, G., and Wang, B. (2014). Enhancing the production of renewable petrochemicals by co-feeding of biomass with plastics in catalytic fast pyrolysis with ZSM-5 zeolites. *Applied Catalysis A: General*, *481*, 173-182.
14. Conesa, J. A., and Domene, A. (2015). Gasification and pyrolysis of Posidonia oceanica in the presence of dolomite. *Journal of Analytical and Applied Pyrolysis*, *113*, 680-689.
15. Gao, J., Zhang, Y., Meng, D., Jiao, T., Qin, X., Bai, G., and Liang, P. (2019). Effect of ash and dolomite on the migration of sulfur from coal pyrolysis volatiles. *Journal of Analytical and Applied Pyrolysis*, *140*, 349-354.
16. Tan, R. S., Abdullah, T. A. T., Mahmud, S. A., Zin, R. M., and Isa, K. M. (2019). Catalytic steam reforming of complex gasified biomass tar model toward hydrogen over dolomite promoted nickel catalysts. *International Journal of Hydrogen Energy*, *44*(39), 21303-21314.
17. IRENAd (2022) Energy Transition Holds Key to Tackle Global Energy and Climate Crisis. https://www.irena.org/newsroom/pressreleases/2022/Mar/Energy-Transition-Holds-Key-to-Tackle-GlobalEnergy-and-Climate-Crisis. Accessed 16 Aug 2022.
18. Ala'a, H., Osman, A. I., Kumar, P. S. M., Jamil, F., Al-Haj, L., Al Nabhani, A., and Rooney, D. W. (2021). Circular economy approach of enhanced bifunctional catalytic system of CaO/CeO2 for biodiesel production from waste loquat seed oil with life cycle assessment study. *Energy Conversion and Management*, *236*, 114040.

19. Chen, L., Msigwa, G., Yang, M., Osman, A. I., Fawzy, S., Rooney, D. W., & Yap, P. S. (2022). Strategies to achieve a carbon neutral society: a review. *Environmental Chemistry Letters*, *20*(4), 2277-2310.
20. Guo, J. X., & Zhu, K. (2022). Operation management of hybrid biomass power plant considering environmental constraints. *Sustainable Production and Consumption*, *29*, 1-13.
21. Spiru, P., and Lizica-Simona, P. (2018). Technical and economical analysis of a PV/wind/diesel hybrid power system for a remote area. *Energy Procedia*, *147*, 343-350.
22. Furubayashi, T., and Nakata, T. (2021). Analysis of woody biomass utilization for heat, electricity, and CHP in a regional city of Japan. *Journal of Cleaner Production*, *290*, 125665.
23. Demirbaş, A. (2002). Partly chemical analysis of a liquid fraction of flash pyrolysis products from biomass in the presence of sodium carbonate. *Energy Conversion and Management*, *43*(14), 1801-1809.
24. Tortosa-Masiá AA, Buhre BJP, Gupta RP, Wall TF. (2007). Characterizing ash of biomass and waste. Fuel Processing Technology, 88, 1071–1081.
25. Ong, H. C., Chen, W. H., Singh, Y., Gan, Y. Y., Chen, C. Y., and Show, P. L. (2020). A state-of-the-art review on thermochemical conversion of biomass for biofuel production: A TG-FTIR approach. *Energy Conversion and Management*, *209*, 112634.
26. Sarker, T. R., Nanda, S., Dalai, A. K., and Meda, V. (2021). A review of torrefaction technology for upgrading lignocellulosic biomass to solid biofuels. BioEnergy Research, 14, 645–669.
27. Christoforou, E., and Fokaides, P. (2018). Recent Advancements in Torrefaction of Solid Biomass. Current Sustainable/Renewable Energy Reports, 5(2), 163–171.
28. Basu, P., Sadhukhan, A. K., Gupta, P., Rao, S., Dhungana, A., and Acharya, B. (2014). An experimental and theoretical investigation on torrefaction of a large wet wood particle. Bioresource Technology, 159, 215–222.
29. Chen WH, Lin BJ, Lin YY, Chu YS, Ubando AT, and Show PL, (2021). Progress in biomass torrefaction: principles, applications and challenges. Progress in

Energy and Combustion Science, 82, 100887. https://doi.org/10.1016/j.pecs.2020.100887

30. Chen WH, Lin BJ, Huang MY, and Chang JS. (2015). Thermochemical Conversion of microalgal biomass into biofuels: A review. Bioresource Technology, 184, 314–327.
31. Chen, W. H., Lin, B. J., Lin, Y. Y., Chu, Y. S., Ubando, A. T., Show, P. L., and Pétrissans, M. (2021). Progress in biomass torrefaction: principles, applications, and challenges. Progress in Energy and Combustion Science, 82, 100887.
32. Osman, A. I., Abdelkader, A., Johnston, C. R., Morgan, K., and Rooney, D. W. (2017). Thermal investigation and kinetic modeling of lignocellulosic biomass combustion for energy production and other applications. Industrial & Engineering Chemistry Research, 56(42), 12119–12130.
33. Fan, J.-L., Xu, M., Wei, S., Shen, S., Diao, Y., and Zhang, X. (2021). Carbon reduction potential of China's coal-fired power plants based on a CCUS source-sink matching model. Resources, Conservation & Recycling, 168, 105320.
34. Shahbaz, M., Al-Ansari, T., Aslam, M., Khan, Z., Inayat, A., Athar, M., and McKay, G. (2020). A state-of-the-art review on biomass processing and conversion technologies to produce hydrogen and its recovery via membrane separation. International Journal of Hydrogen Energy, 45(30), 15166–15195.
35. Pahnila, M., Koskela, A., Sulasalmi, P., and Fabritius, T. (2023). A review of pyrolysis technologies and the effect of process parameters on biocarbon properties. *Energies*, *16*(19), 6936
36. Osman, A. I., Chen, L., Yang, M., Msigwa, G., Farghali, M., Fawzy, S., and Yap, P. S. (2023). Cost, environmental impact, and resilience of renewable energy under a changing climate: a review. *Environmental chemistry letters*, *21*(2), 741-764.
37. Bridgwater, A. V. (2012). Review of fast pyrolysis of biomass and product upgrading. *Biomass and Bioenergy*, 38, 68-94. DOI: 10.1016/j.biombioe.2011.01.048.
38. Menon, V., and Rao, M. (2012). Trends in bioconversion of lignocellulose: Biofuels, platform chemicals & biorefinery concept. *Progress in Energy and Combustion Science*, 38(4), 522-550. DOI: 10.1016/j.pecs.2012.02.002

39. Milledge, J. J., and Heaven, S. (2013). A review of the harvesting of micro-algae for biofuel production. *Reviews in Environmental Science and Bio/Technology*, 12, 165-178. DOI: 10.1007/s11157-012-9301-z.
40. Ghadiryanfar, M., Rosentrater, K. A., Keyhani, A., and Omid, M. (2016). A review of macroalgae production, with potential applications in biofuels and bioenergy. *Renewable and Sustainable Energy Reviews*, 54, 473-481. DOI: 10.1016/j.rser.2015.10.022.
41. Tan, S. L., Lim, J. W., Ho, W. S., Lim, P. E., and Hashim, H. (2019). Energy, economic and environmental (3E) analysis of waste-to-energy (WTE) strategies for municipal solid waste (MSW) management in Malaysia. *Science of The Total Environment*, 652, 257-275. DOI: 10.1016/j.scitotenv.2018.10.200.
42. Lin, C. S. K., Pfaltzgraff, L. A., Herrero-Davila, L., Mubofu, E. B., Abderrahim, S., Clark, J. H., and Luque, R. (2013). Food waste as a valuable resource for the production of chemicals, materials and fuels. *Energy & Environmental Science*, 6(2), 426-464. DOI: 10.1039/C2EE23440H.
43. Mussatto, S. I., Dragone, G., and Roberto, I. C. (2006). Brewers' spent grain: generation, characteristics and potential applications. *Journal of Cereal Science*, 43(1), 1-14. DOI: 10.1016/j.jcs.2005.06.001.
44. Bajpai, P. (2016). Pulp and Paper Industry: Chemicals Recovery. In *Biermann's Handbook of Pulp and Paper* (pp. 339-372). Elsevier. DOI: 10.1016/B978-0-12-409570-2.00011-0.
45. Bernal, M. P., Alburquerque, J. A., and Moral, R. (2009). Composting of animal manures and chemical criteria for compost maturity assessment. *A review. Bioresource Technology*, 100(22), 5444-5453. DOI: 10.1016/j.biortech.2008.11.027.
46. Sjöström, E. (1993). Wood Chemistry: Fundamentals and Applications. Academic Press.
47. Heaton, E. A., Flavell, R. B., Mascia, P. N., Thomas, S. R., Dohleman, F. G., and Long, S. P. (2008). Herbaceous energy crop development: recent progress and future prospects. *Current Opinion in Biotechnology*, 19(3), 202-209. https://doi.org/10.1016/j.copbio.2008.05.001

48. Tripathi, N., Hills, C. D., Singh, R. S., & Atkinson, C. J. (2019). Biomass waste utilisation in low-carbon products: harnessing a major potential resource. *NPJ climate and atmospheric science*, *2*(1), 35.
49. Dahmen, N., Lewandowski, I., Zibek, S., & Weidtmann, A. (2019). Integrated lignocellulosic value chains in a growing bioeconomy: Status quo and perspectives. *Gcb Bioenergy*, *11*(1), 107-117.
50. Shotyk, W., & Le Roux, G. (2005). Biogeochemistry and cycling of lead. *Metal Ions in Biological Systems, Volume 43-Biogeochemical Cycles of Elements*, 239-275.
51. Chamas, A., Moon, H., Zheng, J., Qiu, Y., Tabassum, T., Jang, J. H., ... & Suh, S. (2020). Degradation rates of plastics in the environment. *ACS Sustainable Chemistry & Engineering*, *8*(9), 3494-3511.
52. Geyer, R., Jambeck, J. R., and Law, K. L. (2017). Production, use, and fate of all plastics ever made. *Science advances*, *3*(7), e1700782.
53. Önal, E., Uzun, B. B., and Pütün, A. E. (2014). Bio-oil production via co-pyrolysis of almond shell as biomass and high density polyethylene. *Energy conversion and management*, *78*, 704-710.
54. Kumar, R., and Strezov, V. (2021). Thermochemical production of bio-oil: A review of downstream processing technologies for bio-oil upgrading, production of hydrogen and high value-added products.
55. Bansal, A. (2022). Management of Crop-Residue to Control Environmental Hazards. *The Scientific Temper*, *13*(02), 146-152.
56. Gupta, S., Sood, N., Rath, R., and Saxena, R. (2022). Crop residue burning in northern India: environmental challenges and strategies for mitigating the environmental impact of biomass burning–a review. *Journal of Experimental Zoology India*, *25*(2).
57. Jain, N., Sehgal, V. K., Pathak, H., Kumar, O., and Dhakar, R. (2021). Greenhouse gas and particulate matter Emissions from Rice residue burning in Punjab and Haryana states of India. In *Biomass Burning in South and Southeast Asia* (pp. 171-190). CRC Press.
58. Akimowicz, M., Del Corso, J. P., Gallai, N., & Képhaliacos, C. (2021). Adopt to adapt? Farmers' varietal innovation adoption in a context of climate change.

The case of sunflower hybrids in France. *Journal of Cleaner Production*, *279*, 123654.

59. Hopewell, J., Dvorak, R., & Kosior, E. (2009). Plastics recycling: challenges and opportunities. *Philosophical Transactions of the Royal Society B: Biological Sciences*, *364*(1526), 2115-2126.
60. Miandad, R., Barakat, M. A., Aburiazaiza, A. S., Rehan, M., Ismail, I. M. I., & Nizami, A. S. (2017). Effect of plastic waste types on pyrolysis liquid oil. *International biodeterioration & biodegradation*, *119*, 239-252.
61. Zhang, X., Lei, H., Chen, S., and Wu, J. (2016). Catalytic co-pyrolysis of lignocellulosic biomass with polymers: a critical review. *Green Chemistry*, *18*(15), 4145-4169.
62. Jin, X., Lee, J. H., and Choi, J. W. (2022). Catalytic co-pyrolysis of woody biomass with waste plastics: effects of HZSM-5 and pyrolysis temperature on producing high-value pyrolytic products and reducing wax formation. *Energy*, *239*, 121739.
63. Alagu, R. M., and Sundaram, E. G. (2018). Preparation and characterization of pyrolytic oil through pyrolysis of neem seed and study of performance, combustion and emission characteristics in CI engine. *Journal of the Energy Institute*, *91*(1), 100-109.
64. Chintala, V., Kumar, S., and Pandey, J. K. (2018). A technical review on waste heat recovery from compression ignition engines using organic Rankine.

CHAPTER - 2

Literature Review, Research Gaps and Objectives

2.1 Importance of Pyrolysis

By breaking down biomass at a high temperature, pyrolysis produces charcoal, bio-oil, and oxygen-free non-condensable gases (H2, CH4, CO, and CO2). Bio-oil contains both organic and aqueous components. Its organic part contains tar and dense hydrocarbon molecules, which, when refined, can yield more refined transportation fuels. The enhancement of bio-oil requires both processes, catalytic and non-catalytic, to remove oxygen, nitrogen, and sulfur compounds. Otherwise, these substances may lower the heating value of the fuel and cause NOx and SOx to be released during combustion [1].

According to **Chen et al. (2015)**, Flash pyrolysis, quick pyrolysis, and slow pyrolysis are the three main kinds of pyrolysis methods now in use. Modern technologies including hydrous pyrolysis, hydro-pyrolysis, catalytic hydro-pyrolysis, microwave pyrolysis, and hydro-pyrolysis also contribute to the improvement and diversification of pyrolysis processes [2].

Kumar et al. 2021 investigated the fast pyrolysis, operating within seconds to minutes of residence time, is ideal for generating pyrolysis oil. On the other hand, slow pyrolysis, which has residence periods ranging from minutes to days, is designed to yield an uneven surface [3].

Zaman et al. 2017 concentrated on refining process variables like temperature, heating speed, and oxidation environment. Additionally, efforts are directed towards upgrading the products through catalytic and thermal processes. The ultimate goal is to produce liquid transportation fuels that are compatible with the existing infrastructure. The process of common pyrolysis techniques and the variations in the composition of their unique outputs are covered in depth in the next sections [4]. The organic material breaks down into vapours and chars during fast pyrolysis because it heats up quickly and oxygen-free.

Chouhan et al. 2013 investigate that condensing these vapors produces a dark brown liquid known as bio-oil. Fast pyrolysis, a precisely controllable advanced method, aims to maximize liquid product output. Reported outcomes typically show around 60 to 75% bio-oil, 15-25% charcoal, and 10-20% pyro gases from fast pyrolysis.

The solid fuels bio-oil and char are used to generate energy, and the pyro gases may be recycled back into the reactor [5].

Babu et al. 2008 assessed the slow pyrolysis process, which requires heating at a rate of 5–10°C/min and a temperature of 500–600°C. Bio-oil, charcoal, and pyro gases are all formed during the pyrolysis process; however, using this approach will provide a higher concentration of pyro-gas and charcoal and less bio-oil. Creating bio-oil by pyrolysis, a process that converts biomass into chemicals and liquid fuels, is one possible method. Bio-oil, recognized as pyrolysis oil or bio-crude, is the result of heating biomass like wood, agricultural residues, or algae without oxygen. This method decomposes the biomass into a blend of liquid compounds. The feasibility of bio-oil production through pyrolysis depends on various factors, including energy regeneration, economic considerations, and environmental sustainability [6].

Figure 2.1 depicts a standard process flow diagram demonstrating pyrolysis, a thermal breakdown technique applied to biomass at temperatures ranging from 300 to 700ºC without oxygen. This technique produces bio-oil, biochar, and non-condensable gases (like H_2, CH_4, CO, and CO_2). Bio-oil has both organic-phase and aqueous-phase. The organic part contains tar and heavier hydrocarbon compounds, which can be refined through upgrading techniques to create cleaner transportation fuels. This enhancement process involves both catalytic and non-catalytic methods to eliminate oxygen, nitrogen, and sulfur elements or constituents. This removal is crucial to maintain the fuel's heating value and prevent potential emissions of NOx and SOx during combustion [7]. Also, Table 2 shows the range of operational parameters for slow, intermediate and fast pyrolysis [8].

Table 2.1 A comparative analysis of process yields with different feedstocks.

Thermo-chemical treatment method	Feedstock	Temperature	Yield	Ref.
	Waste cereals and peanut	750-800 C	The mixture comprises 61 volume percent of bio-oil and 66 volume percent of hydrogen	9

	crisps		(H_2)	
Pyrolysis	Plastic waste	500±30 C	Without the use of any catalyst, 24% liquid fraction is obtained, while in the presence of a catalyst, the liquid fraction ranges from 16% to 22%.	10
	Polypropylene waste	450-600 C	Under both atmospheric and vacuum conditions, the liquid product constitutes a range of 81% to 93% by weight.	11
	Pinewood	310-450 C	The composition includes a variable range, with bio-oil ranging from 5% to 90%, solid products from 3% to 31%, and gaseous products from 7% to 91%.	12
	Wildland fire	500-765 C	At a temperature of 765°C, the composition comprises 53% to 62% by weight of tar, 17% to 24% by weight of gas, and 17% to 23% by weight of biochar.	13
	solid waste and paper factory sludge	110-900 C	The attained average activation energies for the additives were 237.42 kJ/mol in the case of 5% MgO and 239.44 kJ/mol for 5% activated carbon.	14

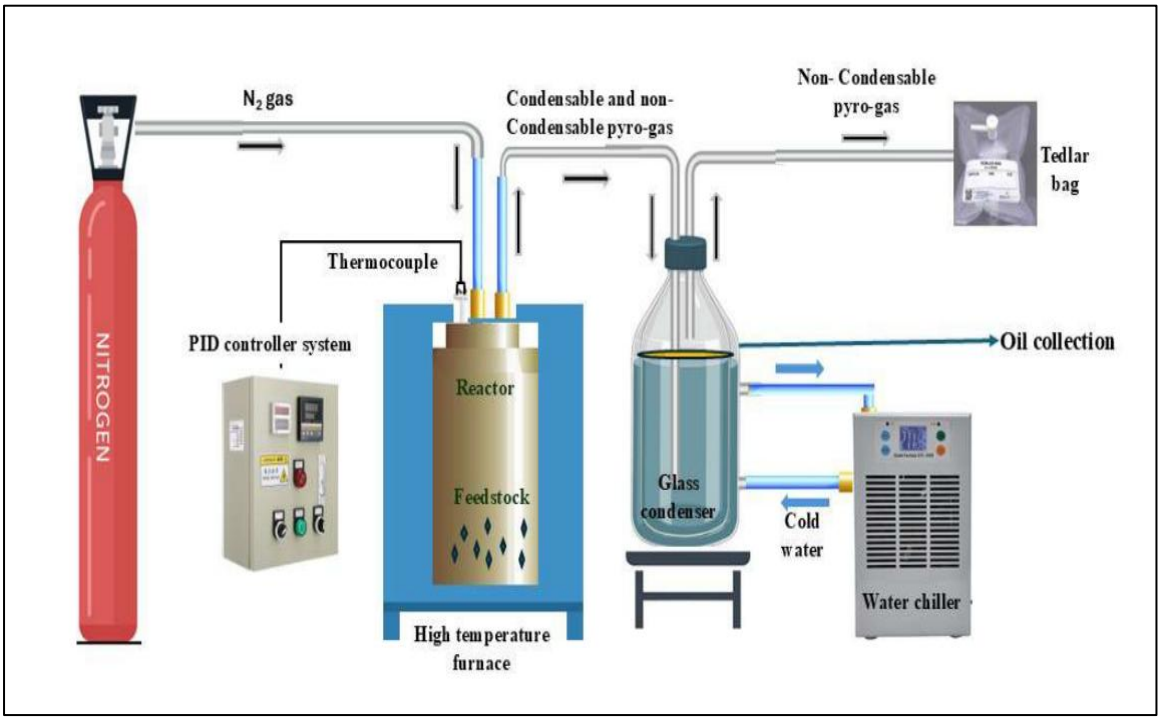

Figure 2.1. Flow chart of waste processing through pyrolysis and its benefits.

2.2 Physicochemical properties of raw materials

The proximate analysis categorizes biomass into four crucial components for thermal conversion: moisture, volatile matter (encompassing gases and vapours liberated in pyrolysis), fixed carbon (representing non-volatile carbon), and ash (the inorganic residue that remains after combustion). This analysis serves as an indicative measure

of the thermochemical conversion performance, the ultimate analysis of a raw sample provides valuable insights into its elemental composition, enabling a comprehensive understanding of its properties and potential applications. This analytical approach is widely employed across diverse industries, ranging from energy and environmental monitoring to materials science and agriculture. The content and yields of solid, liquid, and gaseous products produced by the pyrolysis and gasification processes are directly influenced by the fixed carbon and volatile matter ratio connections. The calorific value, sometimes referred to as the heating value, is an essential indicator of the quality of a given feedstock.

Shrivastava et al. 2021, this value represents the energy content within the feedstock, calculated based on the heat generated from the full combustion into CO_2 and H_2O (whether as gas for lower heating value or liquid for higher heating value), along with secondary byproducts such as N_2 and ash.

Various types of biomasses are commonly employed in thermochemical conversion processes, with the selection influenced by factors like regional availability, cost, energy content, and the desired final products. Here are some examples of biomass frequently employed in thermochemical conversion [15].

Table 2.2. Compositional properties of various biomass feedstocks

Feedstock	Proximate Analysis			Ultimate Analysis					HHV MJ/Kg	Ref.
	VM	FC	Ash	C	H	N	O	S		
Pistachio soft shell	67.85	8.69	14.21	45.53	5.56	1.74	47.17	–	18.57	16
Coconut shell	77.19	22.1	0.71	50.22	5.70	43.37	–	–	20.50	17
Wheat straw	82.12	10.98	6.90	42.95	5.35	–	46.99	–	17.99	18
Olive stones	78.30	19.5	2.20	49.00	6.10	0.80	42.00	–	20.23	18
Almond shell	80.50	18.4	1.10	48.80	5.90	0.50	43.70	–	19.92	18
Sunflower seed shell	84.70	11.7	3.60	51.70	6.20	1.00	41.10	–	17.60	19
Esparto plant	80.50	16.8	2.20	46.94	6.44	0.86	43.56	–	19.10	20
Shea meal	66.30	28.7	5.00	48.56	5.86	2.88	37.70	–	19.80	21
Dried grains	82.50	12.84	3.89	50.24	6.89	4.79	33.42	0.7	21.75	22
Coffee husk	78.50	19.10	2.40	47.50	6.40	–	43.70	–	19.80	23
Oil palm fruit	78.20	16.46	4.53	45.90	5.80	1.20	40.10	–	16.96	23
Forest residue	79.80	20.00	0.20	53.16	6.25	0.30	40.00	0.09	19.50	24

Willow wood	82.22	16.07	1.71	49.90	5.90	0.61	41.80	0.07	19.59	25
Oakwood	77.45	18.50	4.05	48.76	6.35	2.81	42.08	–	19.20	26
Corn straw	73.15	19.19	7.65	44.73	5.87	0.60	40.44	0.07	17.68	27

NOTE: VM – volatile matter, FC – fixed carbon, HHV – high heating value

2.3 Co-pyrolysis technology

One of the most significant commercial polyesters is polyethylene terephthalate (PET), which accounts for 7-9% of the world's plastic use [28,29].

Kuczenski et al. 2010, explore that PET is not biodegradable, it has a similar oxygen content to the bulk of another solid biomass and a comparable H/C_{eff}. Although some PET wastes were used to make engineering resins [30], their extensive usage with other plastic wastes significantly reduced their rate of recycling to less than 10% in the United States [31]. A variety of solid biomass sources, such as paulownia wood [32], cotton stalks, hazelnut shells, leftovers from sunflowers [33], municipal solid wastes, nut shells [34], and samanea saman seeds, were investigated for co-pyrolysis with solid wastes and PET.

Sajdak et al. 2015 investigated how adding PP raised the heating value of the char while lowering the amounts of oxygen and sulphur in the solid portion. But the gaseous fraction, which contained reduced amounts of CO2, CH4, and H2, suffered from co-pyrolysis. Additionally, mixing biomass with a tiny quantity of PP helped keep the autothermal state throughout the process, especially when working with raw biomass that had a high moisture content. This was so that the co-pyrolysis process could be optimized, and the heating value emitted by the PP could fully meet the energy requirements [34].

Erdogan et al. 2020 explore the oil produced by pyrolyzing plastic has several advantageous qualities, such as a high heating value (HHV) and a high hydrocarbon content, which are comparable to those of regular petrol. However, the pyrolysis of plastic results in significant volumes of ash, and the oil is very caustic and viscous with high oxygen and moisture content [35].

Han et al. 2014 investigation, adding organic material from biomass feedstock to the co-pyrolysis process may reduce these unfavourable properties. According to research findings, co-pyrolyzing any biomass with plastic effectively increased the amount and quality of biofuels produced without having any negative effects. As an alternative to

high-pressure hydrogenation treatment, co-pyrolysis is thought to be a simple and safe way to create superior biofuels [36].

Kuppens et al. 2010 have demonstrated that co-pyrolysis is more advantageous than typical biomass pyrolysis in producing higher-quality bio-oil and accelerating commercial expansion [37].

Yaman et al. 2021, examined the potential to recover critical molecules and lessen reliance on fossil fuels is another benefit of co-pyrolysis. When fossil fuels are fractionally distilled, co-pyrolysis processes yield less carbon dioxide. This is such that there is no need for solvents, co-pyrolysis can proceed with or without catalysts, and hydro-treating crude bio-oil will need less hydrogen [38]. Similar to petro-diesel, the biodiesel produced through co-pyrolysis has qualities that make it useful for a variety of purposes and enhance combustion efficiency.

Table 2.3. Process parameter range for co-pyrolysis of different feedstocks

Sample	**Reactor**	**Temp. (°C)**	**Heating rate**	**Gas flow**	**Bio-oil yield** (wt%)	**Biochar** (wt%)	**Ref.**
RH and LDPE (1:1)	pyrolytic reactor	400	17.5°C/min	He flow rate of 1 ml/min	36.47	38.68	39
		450			40.92	32.49	
		500			43.55	25.63	
		550			47.74	21.26	
		600			51.26	17.58	
Solid tire waste and rice husk	fixed-bed LPG heating pyrolysis system	450	10°C /min	He at a flow rate of 100 ml/min	52	33	40
Lignin and low-density polyethylene	microwave pyrolysis apparatus	500	15°C/min.	N_2 flowing at the rate of 50 ml/min	21.87	51.27	41
Oil shale and High-density polyethylene	stainless steel autoclave reactor	500–525	10°C/min	N_2 flowing at the rate of 20 ml/min	52.3	-	42

Corn Stover and Polypropylene 1:1	Tube Furnace	550	-	N_2 and CO_2	41.8	12.6	43
50:50 (w/w) pine wood/PS	auger-fed reactor	450	10°C/min	N_2	64.9	12.1	44
HDPE/pine	-	525	-	-	38.9	25.9	
PP/Pine		450	-	-	46	32.2	
Juliflora biomass with low-density polyethylene	Auger reactor	600	10°C/min	-	32	37	45
Waste tire addition on wheat straw	fixed bed reactor	500	20°C/min	N_2 flowing at the rate of 50 ml/min	44	37.60	46
Polystyrene and waste nitrile gloves	semi-batch reactor	550	80 ◦C/min	100 ml/min N_2 flow rate	45.89	-	47
Corn stalk and Polypropylene (1:1)	Tube Furnace Pyrolysis	500	10°C/min	(N_2 and CO_2) gas flowing at the rate of 150 mL/min	41.8	12.6	48

2.4 Design and performance of the pyrolysis reactor

A key element that allows for the accurate breakdown of raw materials at high temperatures, variable pressures, airless environments, and the presence of inert or fluidised gas is the pyrolysis reactor. Multiple reactors are utilized in this method to create the optimal conditions for maximizing specific outputs like oil, char, or gas. These reactors are categorized based on how the feedstock moves within them. In certain cases, the feedstock remains stationary, while in other cases, it can be moved using additional force. Numerous researchers have explored a range of reactor types for producing biodiesel. There are some reactor types which is generally used for the

pyrolysis process [49].

2.4.1 Fixed bed reactor

Chopra et al. 2007 discussed the fixed-bed pyrolysis system, which consists of a reactor along with a gas cooling and cleaning system. The fixed bed reactor's integrated technology is well recognised for its uncomplicated nature, dependability, and shown efficacy. As such, it is especially appropriate for fuels with consistent particle size and little fine content [49].

Leung et al. 2004, this concept involves solid materials moving downhill in a vertical shaft and coming into contact with an upward-flowing product gas stream. Among other essential components, a standard fixed bed reactor comprises a fuel feeding unit, an ash removal unit, a gas outlet, and is constructed of steel, concrete, or firebricks [50]. Such reactors are under consideration for small-scale electricity and heating uses. Wet scrubbers, dry filters, and cyclones are some of the filtering techniques used in the gas cleaning process and cooling system [51,52].

Pathak et al. 2005 looked at the removal of tar as the main issue with fixed-bed reactors. Nonetheless, new developments in the thermal and catalytic reduction of tar have made practical methods for tar removal feasible [53].

2.4.2 Fluidized bed reactor

Lv et al. 2004 examined that in a fluidized-bed reactor, fluid and solid materials blend, imitating fluid-like properties usually attained by introducing pressurized fluid through solid particles. These reactors are preferred for rapid pyrolysis because they have a large surface area per unit bed volume, allow for extensive fluid-solid contact, provide fine control over pyrolysis reactions and vapour residence time, and permit rapid heat transfer. They also maintain a significant relative speed difference between the fluid and solid phases and aid in efficient heat transmission throughout the system [54].

2.4.3 Circulating fluidized bed reactor

Li et al. 2004 study on circulating fluidised beds found that while they are similar to bubbling fluidized-bed reactors, their residence durations for chars and vapours are shorter. When compared to bubbling fluidised bed reactors, this causes higher gas velocity and char content levels in the bio-oil. Despite their more intricate hydrodynamics, circulating fluidized-bed reactors offer a notable advantage due to their suitability for handling very large throughputs [55].

2.4.4 Auger reactor

Mohan et al. 2006 reveal that augers help drive biomass feedstock through a heated, cylindrical tube devoid of oxygen in this kind of reactor. The feedstock goes through devolatilization and gasification as it passes down the tube and reaches the appropriate pyrolysis temperature, which is typically between 400°C and 800°C. The process yields char, the gases it creates condense into bio-oil, and the non-condensable vapour is collected as biogas. Crucially, this design offers the flexibility to modify vapor residence time by adjusting the section of the heated zone through which vapor travels before reaching the condenser train [56].

Table 2.4 Types of reactors used for the pyrolysis process reported in various investigation

Biomass sample	Reactor type	Temperature	Dimension	Biomass material used	Ref.
Woodchips from eucalyptus (EU) and oak (OAK)	downdraft fixed-bed stainless steel reactor	500°C	16 mm dia. and 400 mm length	5 g	57
Cotton stalk	fast pyrolysis bench-scale	350-400°C	100 mm and height of 750 mm	2kg	58
Rice straw and polypropylene (PP)	fixed bed drop-type pyrolyzer	600°C	53mm d and 166mm height	10g	59
Plastic waste (HDPE)	fixed bed pyrolysis batch reactor	475°C	38 cm and 15 cm,	-	60
Plastic waste	bench-scale pyrolysis	500 °C	(Diameter 35 cm, length 60 cm	maximum capacity 5 kg	61
Cassava plants	fluidized-bed reactor	475–510°C	diameter of 3.81 cm and a height of 30 cm	100 g.	62
Beechwood	drop tube	800°C	2.3 m long,	-	63

	reactor (DTR)		0.075 m dia.		
rice husk with underutilized biomass	fixed bed reactor	600 °C	(115 cm length, 5 cm inner diameter	100 g	64
Rice husks	fluidized bed pyrolyze reactor	600 °C	50 mm and 350 mm	20 g	65
Kitchen Waste pellets	batch pyrolysis reactor	400 - 600 °C.	(Length: 520 mm; d.: 44 mm	24g	66
waste polythene and rice straw	fixed-bed LPG heating pyrolysis system.	450-500°C.	10mm in diameter, 300 mm in length	-	67
Stem Wood	cyclone pyrolyzer	750 °C	diameter of 0.39 m, inner wall area of 1.54 m^2,	37 kg/h	68
Rice husk	fluidized bed reactor	450°C	thickness of 35mm, height of 470 mm	200 gm	69
switch grass	semi-pilot scale auger pyrolyzer	500°C.	20 cm in diameter and 100 cm long	8.5 kg/h	70
Poultry wastes	Bench-scale fast pyrolysis reactor	500°C	6cm in diameter and 21cm high	50g	71
Biomass	bubbling fluidized bed regenerator	500°C	5.33 m tall with a 45.7 cm diameter	45 kg/h	72
sawdust and giant Miscanthus	circulating fluidized bed reactor	400 to 600°C	-	42 kg/ h	73
Switchgrass	Bench-Scale Fluidized-Bed	480°C	7.8 cm nominal diameter and 52 cm in length	20 kg/h	74

Aladin et al. 2017 [75] explore that Pyrolysis reactors have specific requirements

regarding feedstock size to ensure optimal heat transfer and operational efficiency. Fluidized bed pyrolysis reactors generally perform optimally when utilizing particle sizes within the range of 2 to 6 mm. This often necessitates preparatory steps for biomass, like cutting and grinding, to achieve the desired particle size. Furthermore, unless naturally dry materials like straw are being used, it is imperative to dry biomass resources to reduce moisture content to below 10 weight percent. The process of drying is essential for preventing problems with water that might affect the pyrolysis product's stability, viscosity, pH, corrosiveness, and other liquid qualities. Nevertheless, whereas raw material drying and grinding might raise liquid yields, they also raise production costs. Here are some examples of reactors.

2.5 Experimental apparatus for pyrolysis

Dayton et al. 2015 represent the rapid pyrolysis system made use of a circulating fluidised bed (CFB) reactor that could feed 42 kg of biomass per hour. A comprehensive schematic of the pyrolysis system is shown in Figure 2.6, with a focus on key parts of the CFB reactor. The system includes an enclosed heating chamber with an electrical furnace, a biomass hopper, a screw feeder, a fluidized bed reactor, a cyclone, two condensers, and an electrostatic precipitator. Inside the CFB reactor, three distinct processes unfold: (i) rapid pyrolysis reactions, (ii) the swift condensation of generated gas to extract oil, and (iii) the recycling of gas and controlled incineration of excess gas. This entails reusing non-condensed gas and managing surplus gas through controlled combustion [72].

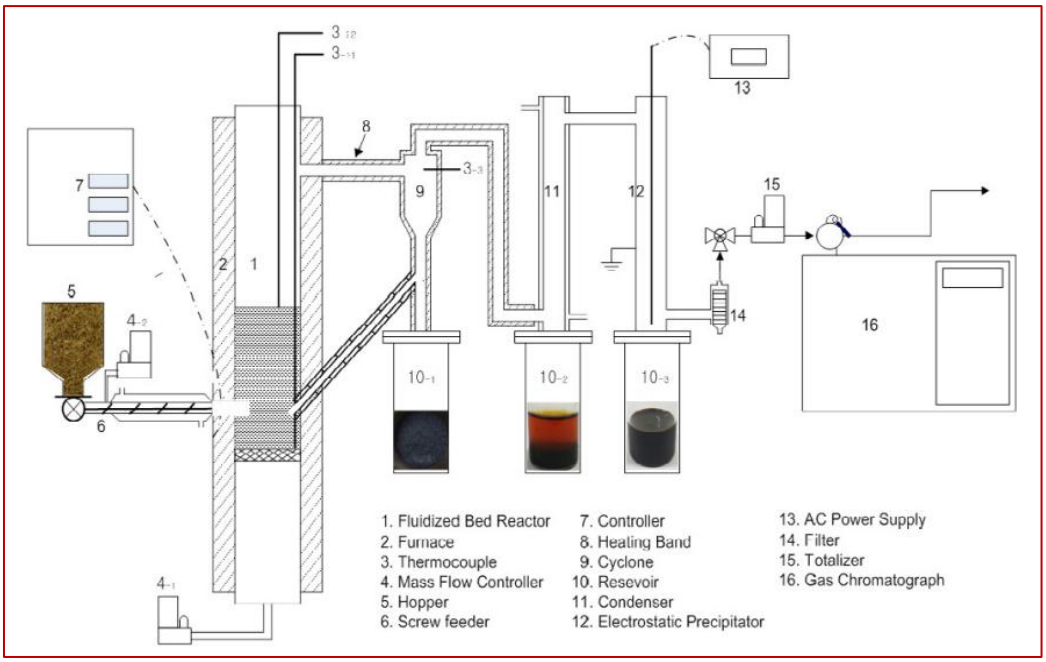

Figure 2.2: Schematic diagram of the experimental pilot-scale circulating fluidized bed (CFB) reactor setup used for the biomass fast-pyrolysis experiments [72].

Ali et al. 2014 discusses the complete apparatus of the fast pyrolysis method involved in transporting controlled biomass material into a fluidized bed reactor via a screw feeder. The reactor's bottom sand bed was made more fluid by using inert nitrogen gas that had been preheated to between 350 and 400°C. Charcoal and pyrolysed volatiles came out of the reactor's top. Using cyclone separators, the solid char particles were extracted from the gas. The pyrolysis gas was first condensed in a dry ice condenser and then in a water-cooled condenser to produce pyrolysis liquid. Every fifteen minutes, samples were obtained for examination and the non-condensable gas was filtered to eliminate minute particles. The reactor has a fluidised bed and measures 750 mm in height by 100 mm in diameter. It was constructed out of stainless steel (SS 316 L). The reactor was indirectly heated using carbamate heating rods to keep the pyrolysis reaction temperature constant [76].

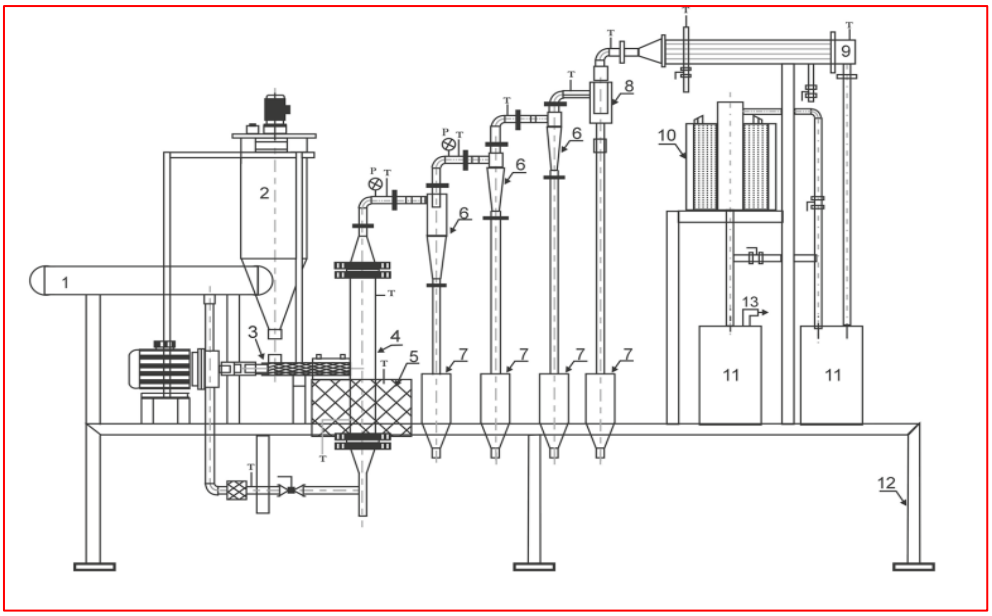

Figure 2.3: Pyrolysis setup components: (1) Nitrogen header, (2) Feed hopper, (3) Biomass feeder, (4) Fluidized bed reactor, (5) Reactor heater, (6) Cyclones, (7) Char collector, (8) Strainer, (9) Water condenser, (10) Dry ice condenser, (11) Pyrolysis liquid collector, (12) Frame, (13) Vent gas [76]

Izzatie et al. 2016 examined the rice straw and PP plastics are co-pyrolyzed in a drop-type fixed-bed pyrolyzer. The pyrolyzer's schematic diagram is seen in **Figure 2.8**. The apparatus was a cylindrical reactor made of stainless steel, measuring 166 mm in height and 53 mm in internal diameter. Within an electrical heater with a water jacket and insulation, the pyrolyzer was positioned to enable a robust heating reaction up to 600°C in the reactor. Nitrogen gas can be purgeable through nitrogen and vacuum lines to provide inert conditions inside the pyrolyzer. The co-pyrolysis temperature in the reactor was controlled by a K-type thermocouple installed within the pyrolyzer. Two condensers immersed in a bath of cooled ethylene glycol were connected to the reactor to be connected to the pyrolysis vapour at a temperature vapour low of -10°C. A 3 litre gas sample bag was connected to the vapour trap's output in order to collect the non-condensable gases [59].

To pyrolyse herbaceous energy crops, the Agricultural Research Service (ARS) of the United States Department of Agriculture has developed a bench-scale fluidized-bed reactor (USDA). The objective was to overcome obstacles related to the pyrolysis oil production from energy crops through experimentation. Obstacles may include reactor

performance difficulties, including energy balancing, optimal yields, and feeding and conversion efficiency. Efficiency is affected by a number of elements, including high rates of heating and heat transfer, a regulated temperature of around 500 °C, and the quick cooling of the vapours generated. As a result, system component design and operation may be crucial, as illustrated in **Figure 2.9.** [73].

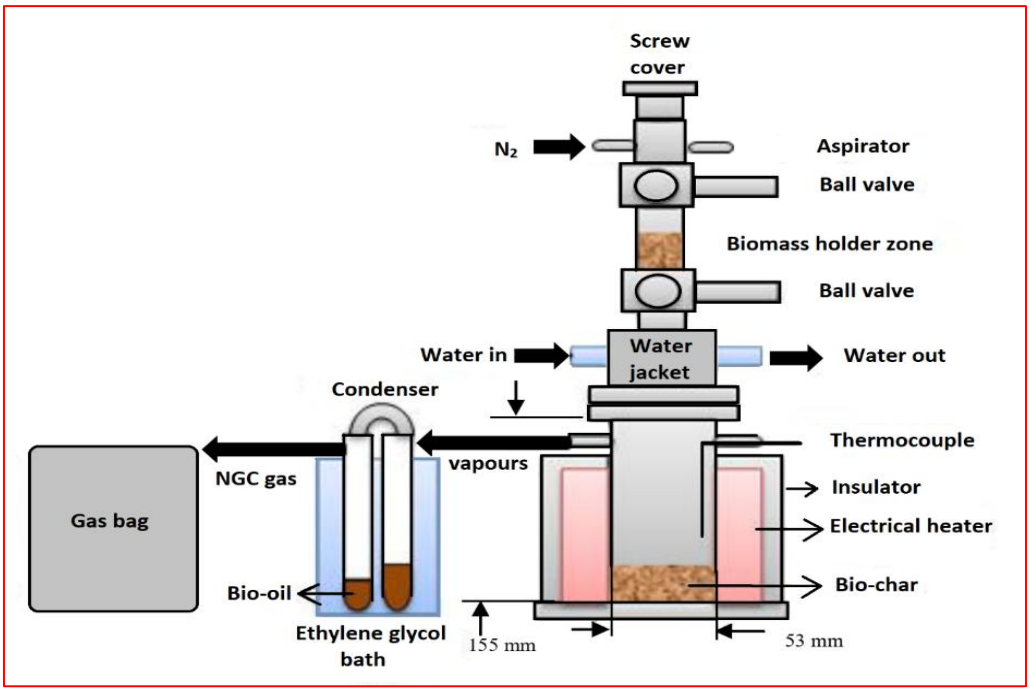

Figure 2.4: The schematic diagram of the fixed bed pyrolysis system [59]

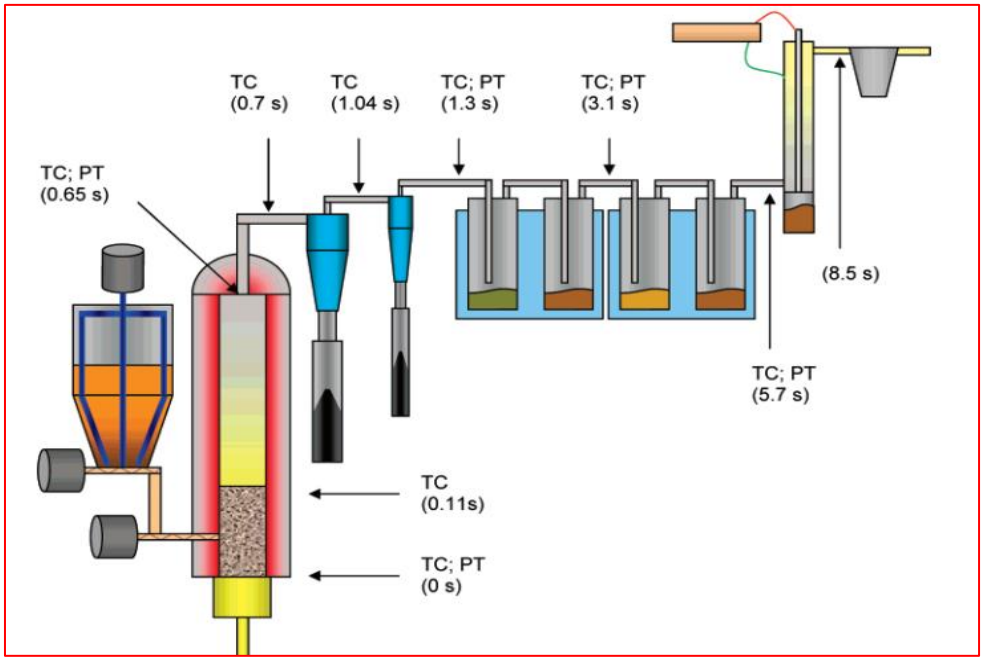

Figure 2.5: Schematic representation of experimental setup (TC) thermocouple; PT -

pressure tap. [73].

The University of the Punjab's Institute of Chemical Engineering and Technology developed, constructed, and ran a bench-scale facility dedicated to fast pyrolysis, detailed in Figure 2.10.

The feed capacity handled by this plant is 2 kg/h. It includes the following main components: a system for feeding biomass, a reactor with a fluidised bed, a heating setup, a system for separating gas and particulates, a system for condensing pyrolysis vapours, and an extensive instrumentation and control system. A well calibrated screw feeder is used in the rapid pyrolysis process to supply predetermined volumes of biomass feedstock into the fluidised bed reactor. This reactor is supplied with preheated inert gas nitrogen, maintained around the range of 350-400°C, and introduced from the reactor's bottom to facilitate fluidization within the sand bed [60].

Khan et al. 2016, Pyrolysis is an endothermic process that may be done at 250 to 600°C in an oxygen-free atmosphere, depending on the feedstock's characteristics and the desired output that maximises the solid, liquid, or gaseous fraction. Heat must be introduced into the reactor during pyrolysis to cause the feedstock to thermally break down into products.

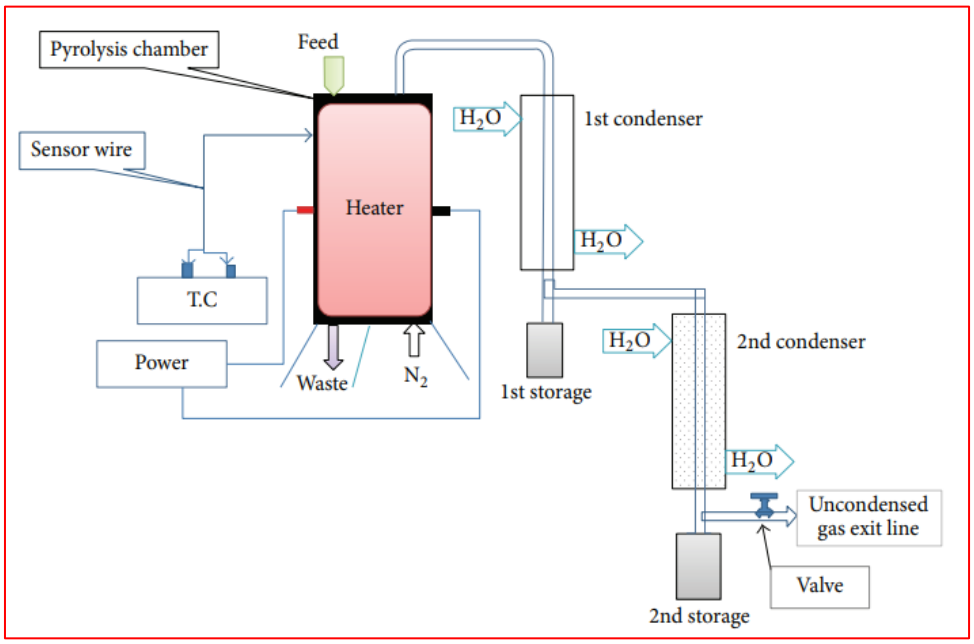

Figure 2.6: Schematic diagram of bench scale pyrolysis unit used for investigation. [60]

2.6 Techniques for energy conversion and upgradation

Ali et al. 2014, [76] investigate that catalysts are pivotal in boosting process efficiency by enabling targeted reactions and lowering processing temperature and time. They wield control over the chemical composition and distribution of pyrolysis products. Rahman et al. 2018 [77] Catalytic pyrolysis shows promise in transforming oxygenated compounds within bio-oil mixtures, leading to an enhancement in bio-oil quality. Various approaches have been utilized to incorporate catalysts into the bio-oil upgrading process.

Liu et al. 2020 [79] examine that customizing catalyst synthesis is crucial to meet precise specifications for the end product. Customization depends significantly on understanding the reaction mechanisms involved in catalytic pyrolysis to enhance bio-oil quality. The pathways in catalytic pyrolysis hinge on the catalytic system's reactions and the unique compositions of biomass. The complex biomass structure, hurdles in mass transfer, and catalyst immobilization pose challenges in fully grasping catalytic pyrolysis mechanisms.

Mihalcik et al. 2011 [80] examined that Catalytic pyrolysis involves several primary routes: deoxygenation, ketonization, cracking, Aldol condensation, and aromatization (equations 1-5) [81].

Valle et al. 2010 concluded that among these, hydrodeoxygenation (HDO) stands out as a favorable method for enhancing bio-oil quality. HDO involves removing oxygenated compounds like CO, CO_2, and H_2O using hydrogen and a catalyst [82]. Through this process, primary renewable fuel products like gasoline and diesel hydrocarbons are obtained.

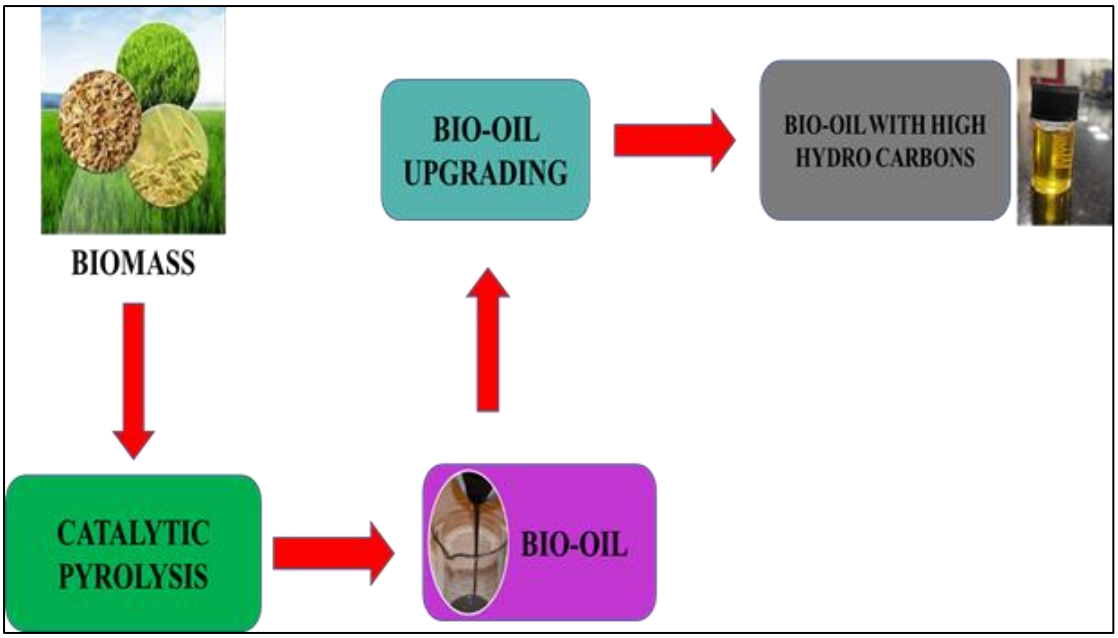

Figure 2.7: Upgradation routes of bio-oil from biomass

2.6.1 Thermo-catalytic upgradation using zeolite

Wang et al. 2017 [83] investigate the Zeolite catalysts have garnered significant interest for their cost-effectiveness, wide availability, and potential to generate premium bio-oil. Among these, ZSM-5, renowned for its strong acidity and optimal pore size, stands out for its remarkable efficacy in bio-oil enhancement. It leads to bio-oil with reduced viscosity, lower acidity, and heightened energy content.

Wang et al. 2018 [68] concluded that ZSM-5 also increases the amount of organic materials, gaseous compounds, and aromatic hydrocarbons in bio-oil through processes including decarbonization, aromatization, and cracking reactions. The bio-oil that was extracted from the reactor had a 25% decrease in oxygenated compounds and a high heating value (HHV) of 34.6 MJ/kg, which was comparable to that of diesel and heavy fuel oil. Researchers have altered the acidity of ZSM-5 using a variety of transition metals, including iron, nickel, cobalt, cerium, and gallium, to improve bio-oil yields and prevent coke formation on catalysts [80,81].

Nie et al. 2014 explore that zeolite supports are widely favored for upholding metal-based catalysts because they necessitate both metals and acidic sites to activate H2 and O-containing compounds. Zeolite supports characterized by heightened Lewis and Bronsted acid site density tend to stimulate robust dehydration reactions [84]. Zeolites, specifically aluminosilicate crystalline solids characterized by intricate pore structures,

find widespread and effective applications in catalytic pyrolysis processes for biomasses.

Iliopoulou et al. 2012 identified that these catalysts are essential for promoting the processes that lead to cracking, dehydration, and deoxygenation, which mostly produce monoaromatic components. Zeolite catalysts have specific size and shape preferences for various components present in bio-oil due to its unique pore structure, which functions as a specialized filter [85-87].

Kumar et al. 2019 investigated that these catalysts are categorized by pore size: small (<0.5 nm), examples being SAPO and A; medium (0.5-0.6 nm), like ZSM-5 and ZSM-11; and large (0.6–0.8 nm), including Y, Beta, and mordenite [88].

ZSM-5 zeolite distinguishes itself with elliptical pores, micro and microporosity, high crystallinity, and adaptable acidity regarding density, strength, along type. These traits make ZSM-5 zeolite a promising catalyst for deoxygenation reactions and for generating both aliphatic and aromatic hydrocarbons [89-92].

Crucially, ZSM-5's pore size matches well with the sizes of benzene, toluene, and xylene, making it a catalyst that selectively produces monoaromatic components [93].

Mishra and Mohanty (2020) investigated the co-pyrolysis of mahua seeds (a non-edible biomass) with polystyrene and waste nitrile gloves in a semi-batch reactor at 550 °C. Their findings revealed that blending plastics (at 20 wt%) significantly increased liquid yield compared to biomass-only pyrolysis. The co-pyrolytic oils exhibited improved properties, such as reduced oxygen content and viscosity, higher heating value, and enhanced aromatic content, as confirmed by FTIR, NMR, and GC–MS analyses. The study demonstrates strong synergistic interactions between biomass and plastics, resulting in more hydrocarbon-rich, energy-dense fuels suitable for further upgrading or direct use [47].

Seah et al. (2023) presented a comprehensive review of co-pyrolysis as a sustainable strategy to valorize biomass and plastic wastes into high-value biofuels. The study emphasized the circular bioeconomy approach, where synergistic interactions between biomass and plastic during co-pyrolysis enhance the yield and quality of bio-oil and syngas while reducing biochar production. The review highlights the influence of parameters like feedstock type, blending ratio, pyrolysis temperature, and heating rate on product distribution. Mechanistic insights revealed that hydrogen transfer from

plastics to biomass radicals promotes deoxygenation and hydrocarbon formation. The study concludes that co-pyrolysis not only addresses waste management challenges but also offers a feasible pathway for renewable energy production [95].

Harith et al. (2022) investigated the catalytic co-pyrolysis of high-density polyethylene (HDPE) and empty fruit bunch (EFB) biomass using modified Malaysian dolomite doped with metal oxides (Ni, Fe, Ca) to enhance bio-oil yield and quality. The study demonstrated that NiO/CMD900 catalyst achieved the highest hydrocarbon yield (85.32%) with significantly reduced oxygenated compounds (14.68%), outperforming even commercial NiO/ZSM-5. The synergistic interaction between biomass and plastic, facilitated by bi-functional acid–base catalytic properties and mesoporous structure, promoted deoxygenation and hydrocarbon formation. This work highlights the potential of low-cost, modified dolomite catalysts in upgrading pyrolysis oil for renewable energy applications [96].

Table 2.5 An analysis of diverse feedstocks employing various catalysts to optimize and enhance the quality of fuel [94-103]

Feedstock	Catalyst	Temp.	Carrier Gas	Analysis	Remarks	Ref.
Sugarcane bagasse	HZSM-5	400-550°C	Helium	Without the use of a catalyst, sugarcane bagasse pith was pyrolysed to produce bio-oil, which is mostly composed of phenolic and carboxylic acids.	The quality of bio-oil was enhanced over the HZSM-5 catalyst with the inclusion of aromatic compounds like benzene, toluene, as well as xylene (BTX).	97
Chlorella vulgaris Biomass	HZSM-5	550°C	Nitrogen	Aromatic hydrocarbon yields were highest at biomass-to-catalyst ratios of 1:4 and 1:9, which were calculated to be 44.9 and 50.8%, respectively.	Pyrolyzing algae catalytically using HZSM-5 resulted in 52.7% bio-oil, 25.7% bio-char, and 21.6% syngas.	98
Xylan	HZSM-5 CaO	450-700°C	Helium	CaO and HZSM-5 have shown two different functions in terms of improving the produced bio-oil. CaO catalyst lowered the yield of acids to 2.74%, a decrease from 10.60% observed without the catalyst. On the other hand, HZSM-5 exhibited greater selectivity towards aromatic hydrocarbons.	Employing the HZSM-5 catalyst boosted the yield of aromatic hydrocarbons from 0% (without catalyst) to 26.91%. Pyrolysis using dual catalyst beds of CaO and HZSM-5 resulted in the highest production of aromatic hydrocarbons (31.66%).	99
Hemicellulose, cellulose, and lignin	HZSM-5 Mo2/HZSM-5	700°C	Helium	Under helium presence, pyrolyzing hemicellulose, cellulose, and lignin with HZSM-5 has generated bio-oil with fewer oxygenated compounds	Cellulose: 35% aromatics, 0.78% oxygenates. Hemicellulose: 19.48% aromatics, 0.31% oxygenates. Lignin: 12.80% aromatics, 1.40% oxygenates.	100

				and elevated levels of aromatic hydrocarbons.		
Used cooking oil and fatty acids	Activated Carbons Alumina HZSM-5 MgO	500°C	-	Activated carbons proved to be the most suitable for yielding hydrocarbons (23%) from used cooking oil at 4h WHSV.	The production of hydrocarbons increased to 35% at 2.5 WHSV. The production of hydrocarbons for fatty acids rose to 40%.	101
Bamboo sawdust	HZSM-5 ZrO2/γ-Al2O3 CeO2/γ-Al2O3 ZrO2–CeO2/ γ-Al2O3	600°C	Helium	Bio-oil from fast pyrolysis of bamboo sawdust without catalysts and with catalysts primarily consists of ketones, acids, phenol, alkylphenols, heavy phenols, monoaromatic hydrocarbons, and mono-functional furans.	ZrO_2–CeO_2/ γ-Al_2O_3 exhibited a threefold increase in monoaromatic hydrocarbon yield compared to the other two catalysts and had the lowest acidity level. Combining ZrO_2–CeO_2/ γ-Al2O3 and HZSM-5 in a dual catalytic bed further elevated the yield of aromatic hydrocarbons.	102
tire waste	HZSM-5 TiO2 $CaCo_3$ CaO ZnO	500°C	Nitrogen	ZnO exhibited the highest selectivity, at 22.55% for hydrocarbons, in comparison to CaO, which had a selectivity of 20%.	Using catalytic pyrolysis, layered catalysts (made up of ZnO and HZSM-5 layers) showed a high yield of 30.23% for hydrocarbons.	103
Posidonia Oceanica	HZSM-5 CeO_2 NiCe/HZSM-5 Ni/HZSM-5 Ni/CeO_2 Ni/Al_2O_3 Dolomite	500°C	Nitrogen	With a hydrocarbon yield of 40%, the HZSM-5 catalyst produced the greatest results. Utilising the Ni/HZSM-5 catalyst, 80.81% of the biomass was converted overall.	CeO_2 demonstrated the highest bio-oil yield and the lowest oxygen content, measuring 51.15 wt% and 6.87 wt%, respectively.	104

Table 2.6 Upgradation of bio-oil through zeolite-based catalysts with different biomass

Catalyst	Biomass	Bio-oil yield	Aromatic	Result	Ref.
HZSM-5	rice husk	3.4-7.2%	2.24%	Among the tested catalysts, HZSM-5 demonstrated the highest efficiency in producing aromatics.	105
HZSM -5 H-USY. H-BETA	sunflower stalk, cedar, knotweed, apple stem	27-36%	56-100%	HZSM-5 continuously generated greater concentrations of some aromatic hydrocarbons, such as naphthalene, p-xylene, and toluene, across all biomass feedstocks.	106
Cu/HZSM-5	Sunflower stalk	30%	73.20%	The Cu/HZSM-5 catalyst, featuring a low loading of Cu, demonstrated the superior catalytic performance in generating relative quantities of aromatic hydrocarbons.	107
Co/HZSM-5	Beech wood	44%	54%	The synthesis of aromatics and phenols was enhanced using Co/HZSM-5 catalysts.	108
Fe/ZSM-5	Rice husk	28%	-	The introduction of 4%Fe/ZSM-5 not only increased hydrocarbon production but also heightened selectivity towards BTX.	109
Fe/ZSM-5	Beech sawdust	25%	21%	The Fe/ZSM-5 catalyst improved the synthesis of desirable products such phenolics and aromatic compounds while reducing the presence of oxygenated molecules.	110
Zn/HZSM-5	Douglas fir	33%	50.70%	Zn/ZSM-5 catalysts were used, and while the gas production increased, the bio-oil and coke yields decreased.	111
Ga/HZSM-5	Pine sawdust	45.9% (including water)	43%	Ga/HZSM-5 demonstrated outstanding selectivity for very valuable aromatics, such as BTX.	112

pd/HZSM-5 Ga/HZSM-5 Co/HZSM-5 Ni/HZSM5	Jatropha waste	-	91-97%	The catalyst consists of metal/HZSM-5 enhancing the selectivity towards aromatics.	113
Mg/HZSM-5, Cu/HZSM-5 Zn/HSM-5 Ga/HZSM-5 Ni/HZSM-5 Co/HZSM-5	Yunnan pine particle	15% 14% 23% 26% 20% 22%	-	The concentration of single-ring aromatic hydrocarbons, such as C7 and C8, was impacted by the addition of HZSM-5 catalysts loaded with metal components. More specifically, Ni/ZSM-5 created more polycyclic aromatic hydrocarbons, whereas Zn/ZSM-5 produced the highest concentration of single-ring aromatics.	114

2.7 Research Gaps Identification

So, far throughout the study of the literature some problems were identified and selected for the study, it is mentioned below:

1. During the co-pyrolysis process, which mixed rice husk and plastic waste, more bio-oil was generated than during the pyrolysis of raw rice husk. As a result of co-pyrolysis, more bio-oil will be generated.

2. Limited understanding of how different catalysts impact the co-pyrolysis process and their specific mechanisms. There is a need for optimization of catalysts to enhance bio-oil yield and quality, and to study how catalysts decompose or deactivate over time.

3. Incomplete analysis of the complex composition of bio-oil and by-products, including potential toxicities and environmental impacts. More detailed

characterization is needed to ensure the safety and usability of the bio-oil produced.

2.8 Conclusion

This chapter highlights the research objectives and identifies the research gaps based on the literature survey. It also provides an overview of various types of reactors and their working principles, and discusses the key parameters that influence the enhancement of bio-oil production.

2.9 Research Objectives

1. 1. To investigate the kinetics and physicochemical characteristics (proximate, ultimate, heating value, and density) of rice husk with and without plastic wastes using the TGA/DTG analyser.

2. To design the lab-scale pyrolysis reactor for the bio-oil production by using rice husk with and without plastic wastes.

3. To determine the Physicochemical properties of the bio-oil produced from the co-pyrolysis process by using rice husk and plastic wastes.

4. To upgrade the properties of the bio-oil produced with and without plastic waste using suitable upgrade techniques.

2.10 Scope of the study

In the current study, rice husk and plastic waste are co-pyrolyzed utilising pyrolysis technology to create bio-oil, an environmentally and economically friendly fuel. There is an abundance of rice produced in the Punjab region, which may be utilised to create clean energy fuel and is easily accessible. Plastic waste is harmful to the ecology because it cannot biodegrade. This study strongly encourages the utilisation of biomass from rice husks and plastic waste to reduce greenhouse gas emissions in the environment. It is possible to co-pyrolyze plastic waste and rice husk to increase the fuel's chemical

composition, thermal value, and efficiency of combustion. This study will yield encouraging results for industry and the scientific community.

2.11 References

1. Chen WH, Lin BJ, Lin YY, Chu YS, Ubando AT, and Show PL, (2021). Progress in biomass torrefaction: principles, applications and challenges. Progress in Energy and Combustion Science, 82, 100887. https://doi.org/10.1016/j.pecs.2020.100887
2. Chen WH, Lin BJ, Huang MY, and Chang JS. (2015). Thermochemical Conversion of microalgal biomass into biofuels: A review. Bioresource Technology, 184, 314–327.
3. Kumar, R., and Strezov, V. (2021). Thermochemical production of bio-oil: A review of downstream processing technologies for bio-oil upgrading, production of hydrogen and high value-added products.
4. Zaman, C. Z., Pal, K., Yehye, W. A., Sagadevan, S., Shah, S. T., Adebisi, G. A., and Hossain, A. (2017). Pyrolysis: a sustainable way to generate energy from waste. Croatia: IntechOpen Rijeka.
5. Chouhan, P. S., and Sarma, A. K. (2013). Critical analysis of process parameters for bio-oil production via pyrolysis of biomass: A review. Recent Patents on Engineering, 7(2), 98-114.
6. Babu, B. V. (2008). Biomass pyrolysis: a state-of-the-art review. Biofuels Bioproducts Biorefining, 2, 393–414. doi: 10.1002/bbb.92
7. Uzoejinwa, B. B., He, X., Wang, S., Abomohra, A. E. F., Hu, Y., and Wang, Q. (2018). Co-pyrolysis of biomass and waste plastics as a thermochemical conversion technology for high-grade biofuel production: recent progress and future directions worldwide. Energy Conversion and Management, 163, 468–492. doi:10.1016/j.enconman.2018.02.004.
8. Demirbas, A. (2007). Progress and recent trends in biofuels. Progress in Energy and Combustion Science, 33, 1–18. doi:10.1016/j.pecs.2006.06.001.

9. Grycová, B., Koutník, I., and Pryszcz, A. (2016). Pyrolysis process for the treatment of food waste. Bioresource Technology, 218, 1203–1207. doi:10.1016/j.biortech.2016.07.064.
10. Singh, T. S., Verma, T. N., and Singh, H. N. (2020). A lab-scale waste to energy conversion study for pyrolysis of plastic with and without catalyst: engine emissions testing study. Fuel, 277, 118176. doi:10.1016/j.fuel.2020.118176.
11. Parku, G. K., Collard, F. X., and Görgens, J. F. (2020). Pyrolysis of waste polypropylene plastics for energy recovery: influence of heating rate and vacuum conditions on composition of fuel product. Fuel Processing Technology, 209, 106522. doi:10.1016/j.fuproc.2020.106522.
12. Remón, J., Arcelus-Arrillaga, P., García, L., and Arauzo, J. (2016). Production of gaseous and liquid bio-fuels from the upgrading of lignocellulosic bio-oil in sub-and supercritical water: effect of operating conditions on the process. Energy Conversion and Management, 119, 14–36. doi:10.1016/j.enconman.2016.04.010.
13. Safdari, M. S., Amini, E., Weise, D. R., and Fletcher, T. H. (2019). Heating rate and temperature effects on pyrolysis products from live wildland fuels. Fuel, 242, 295–304. doi:10.1016/j.fuel.2019.01.040.
14. Fang, S., Yu, Z., Ma, X., Lin, Y., Chen, L., Fan, Y., and Liao, Y. (2017). Co-pyrolysis characters between combustible solid waste and paper mill sludge by TG-FTIR and Py-GC/MS. Energy Conversion and Management, 144, 114–122. doi:10.1016/j.enconman.2017.04.046.
15. Shrivastava, P., Kumar, A., Tekasakul, P., Lam, S. S., and Palamanit, A. (2021). Comparative investigation of yield and quality of bio-oil and biochar from pyrolysis of woody and non-woody biomasses. Energies, 14(4), 1092.
16. Demiral I, Atilgan NG, and Sensöz S. (2009). Production of biofuel from soft shell of pistachio (Pistacia vera L.). Chemical Engineering Communications, 196, 104–115.
17. Channiwala SA, and Parikh PP. (2002). A unified correlation for estimating HHV of solid, liquid and gaseous fuels. Fuel, 81, 1051–1064.

18. Cordero T, Marquez F, Rodriguez-Mirasol J, and Rodriguez J. (2001). Predicting heating values of lignocellulosic and carbonaceous materials from proximate analysis. Fuel, 80, 1567–1571.

19. Haykiri-Acma H, Yaman S. (2009). Effect of biomass on burnouts of Turkish lignites during co-firing. Energy Conversion and Management, 50, 2422–2427.

20. Debdoubi A, El-Amarti A, Colacio E. (2005). Production of fuel briquettes from esparto partially pyrolyzed. Energy Conversion and Management, 46, 1877–1884.

21. Munir S, Daood SS, Nimmo W, Cunliffe AM, Gibbs BM. (2009). Thermal analysis and devolatilization kinetics of cotton stalk, sugar cane bagasse and shea meal under nitrogen and air atmospheres. Bioresource Technology, 100, 1413–1418.

22. Morey RV, Hatfield DL, Sears R, Haak D, Tiffany DG, Kaliyan N. (2009). Fuel properties of biomass feed streams at ethanol plants. Applied Engineering in Agriculture, 25(1), 57–64.

23. Suárez JA, Luengo CA, Felfli FF, Bezzon G, Beatón PA. (2000). Thermochemical properties of Cuban biomass. Energy Sources, 22, 851–857.

24. Sugumaran P, Seshadri S. (2009). Evaluation of selected biomass for charcoal production. Journal of Scientific and Industrial Research, 68, 719–723.

25. Vamvuka D, Kakaras E, Kastanaki E, Grammelis P. (2003). Pyrolysis characteristics and kinetics of biomass residuals mixtures with lignite. Fuel, 82, 1949–1961.

26. Jenkins BM, Baxter LL, Miles Jr TR, Miles TR. (1998). Combustion properties of biomass. Fuel Processing Technology, 54, 17–46.

27. Miranda MT, Arranz JI, Rojas S, Montero I. (2009). Energetic characterization of densified residues from Pyrenean oak forest. Fuel, 88, 2106–2112

28. Chemical Retrieval on the Web Polymer properties database: most common thermoplastics;2019.http://polymerdatabase.com/polymer%20classes/Thermoplastics.html. Accessed December 4.

29. Koshti, R., Mehta, L., and Samarth, N. (2018). Biological recycling of polyethylene terephthalate: a mini-review. Journal of Polymers and the Environment, 26, 3520–3529. doi:10.1007/s10924-018-1214-7.
30. Kuczenski, B., and Geyer, R. (2010). Material flow analysis of polyethylene terephthalate in the US, 1996–2007. Resources, Conservation and Recycling, 54, 1161–1169. doi:10.1016/j.resconrec.2010.03.013.
31. Çepeliogullar, Ö., and Pütün, A. E. (2014). Product characterization study of slow pyrolysis of biomass-plastic mixtures in a fixed-bed reactor. Journal of Analytical and Applied Pyrolysis, 110, 363–374. doi:10.1016/j.jaap.2014.10.002.
32. Ko, K-H., Rawal, A., and Sahajwalla, V. (2014). Analysis of thermal degradation kinetics and carbon structure changes of co-pyrolysis between macadamia nut shell and PET using thermogravimetric analysis and 13C solid state nuclear magnetic resonance. Energy Conversion and Management, 86, 154–164. doi:10.1016/j.enconman.2014.04.060.
33. Sajdak, M., and Słowik, K. (2014). Use of plastic waste as a fuel in the co-pyrolysis of biomass: Part II. Variance analysis of the co-pyrolysis process. Journal of Analytical and Applied Pyrolysis, 109, 152–158. doi:10.1016/j.jaap.2014.07.001.
34. Sajdak, M., Muzyka, R., Hrabak, J., and Słowik, K. (2015). Use of plastic waste as a fuel in the co-pyrolysis of biomass: part III: optimization of the co-pyrolysis process. Journal of Analytical and Applied Pyrolysis, 112, 298–305. doi:10.1016/j.jaap.2015.01.008.
35. Erdogan, S. (2020). Recycling of waste plastics into pyrolytic fuels and their use in IC engines. In Sustainable Mobility. doi:10.5772/intechopen.90639.
36. Han, B., Chen, Y., Wu, Y., Hua, D., Chen, Z., Feng, W., and Xie, Q. (2014). Co-pyrolysis behaviors and kinetics of plastics-biomass blends through thermogravimetric analysis. Journal of Thermal Analysis and Calorimetry, 115(1), 227–235. doi:10.1007/s10973-013-3228-7.
37. Kuppens, T., Cornelissen, T., Carleer, R., Yperman, J., Schreurs, S., Jans, M., and Thewys, T. (2010). Economic assessment of flash co-pyrolysis of short rotation coppice

and biopolymer waste streams. Journal of Environmental Management, 91, 2736–2747.

38. Yaman, E., Ulusal, A., and Uzun, B. B. (2021). Co-pyrolysis of lignite and rapeseed cake: a comparative study on the thermal decomposition behavior and pyrolysis kinetics. SN Applied Sciences, 3. doi:10.1007/s42452-020-04040-y.
39. Binnal, P., Kumar, D. J., Sasalu Parameshwaraiah, M., and Patil, J. (2022). Upgrading rice husk biochar characteristics through microwave-assisted phosphoric acid pretreatment followed by co-pyrolysis with LDPE. Biofuels, Bioproducts and Biorefining, 16(5), 1254-1273.
40. Hossain, M. S., Islam, M. R., Rahman, M. S., Kader, M. A., and Haniu, H. (2017). Biofuel from co-pyrolysis of solid tire waste and rice husk. Energy Procedia, 110, 453-458.
41. Morgan Jr, H. M., Liang, J., Chen, K., Yan, L., Wang, K., Mao, H., and Bu, Q. (2018). Bio-oil production via catalytic microwave co-pyrolysis of lignin and low-density polyethylene using zinc-modified lignin-based char as a catalyst. Journal of Analytical and Applied Pyrolysis, 133, 107-116.
42. Aboulkas, A., Makayssi, T., Bilali, L., Nadifiyine, M., and Benchanaa, M. (2012). Co-pyrolysis of oil shale and high density polyethylene: structural characterization of the oil. Fuel processing technology, 96, 203-208.
43. Wu, F., Ben, H., Yang, Y., Jia, H., Wang, R., and Han, G. (2020). Effects of different conditions on co-pyrolysis behavior of corn stover and polypropylene. Polymers, 12(4), 973.
44. Bhattacharya, P., Steele, P. H., El Barbary, M. H., Mitchell, B., Ingram, L., and Pittman Jr, C. U. (2009). Wood/plastic co-pyrolysis in an auger reactor: Chemical and physical analysis of the products. Fuel, 88(7), 1251-1260.
45. Kothandaraman, M. P., and Somasundaram, M. (2021). Non-isothermal kinetic study on co-pyrolysis of Juliflora and low-density polyethylene. Biomass Conversion and Biorefinery, 11(5), 2147-2155.

46. Farooq, M. Z., Zeeshan, M., Iqbal, S., Ahmed, N., and Shah, S. A. Y. (2018). Influence of waste tire addition on wheat straw pyrolysis yield and oil quality. Energy, 144, 200-206.
47. Mishra, R. K., and Mohanty, K. (2020). Co-pyrolysis of waste biomass and waste plastics (polystyrene and waste nitrile gloves) into renewable fuel and value-added chemicals. Carbon Resources Conversion, 3, 145-155.
48. Wu, F., Ben, H., Yang, Y., Jia, H., Wang, R., and Han, G. (2020). Effects of different conditions on co-pyrolysis behavior of corn stover and polypropylene. Polymers, 12(4), 973.
49. Chopra, S., and Jain, A. (2007). A review of fixed bed gasification systems for biomass. Agric. Eng. Int. 2007, 5, 1–23.
50. Altafini, C.R., Wander, P.R., and Barreto, R.M. (2003). Prediction of the working parameters of a wood waste gasifier through an equilibrium model. Energy Conversion and Management, 44, 2763–2777.
51. Leung, D.Y.C., Yin, X.L., and Wu, C.Z. (2004). A review on the development and commercialization of biomass gasification technologies in China. Renewable and Sustainable Energy Reviews, 8, 565–580.
52. Barker, S.N. (1996). Gasification and pyrolysis-routes to competitive electricity production in the UK. Energy Conversion and Management, 37, 861–866.
53. Pathak, B.S. (2005). Biomass to power rural development. In B.S. Pathak (Ed.), Proceedings of National Seminar on Biomass Based Decentralized Power Generation (pp. 1–6). Vallabh Vidyanagar, India: Sardar Patel Renewable Energy Research Institute.
54. Lv, P.M., Xiong, Z.H., Chang, J., Wu, C.Z., Chen, Y., and Zhu, J.X. (2004). An experimental study on biomass air–steam gasification in a fluidized bed. Bioresource Technology, 95, 95–101.
55. Li, X.T., Grace, R., Lim, C.J., Watkinson, A.P., Chen, H.P., and Kim, J.R. (2004). Biomass gasification in a circulating fluidized bed. Biomass and Bioenergy, 26, 171–193.

56. Mohan, D., Pittman, C.U., and Steele, P.H. (2006). Pyrolysis of wood/biomass for bio-oil: A critical review. Energy & Fuels, 20, 848–889.
57. Fermoso, J., Hernando, H., Jiménez-Sánchez, S., Lappas, A.A., Heracleous, E., Pizarro, P., and Serrano, D.P. (2017). Bio-oil production by lignocellulose fast-pyrolysis: Isolating and comparing the effects of indigenous versus external catalysts. Fuel Processing Technology, 167, 563–574.
58. Ali, N., Saleem, M., Shahzad, K., and Chughtai, A. (2015). Bio-Oil Production from Fast Pyrolysis of Cotton Stalk in Fluidized Bed Reactor. https://doi.org/10.1007/s13369-015-1801-z.
59. Izzatie, N.I., Basha, M.H., Uemura, Y., Mazlan, M.A., Hashim, M.S.M., Amin, N.A.M., and Hamid, M.F. (2016). Co-pyrolysis of rice straw and polypropylene using fixed-bed pyrolyzer. IOP Conference Series: Materials Science and Engineering, 160(1).
60. Khan, M.Z.H., Sultana, M., Al-Mamun, M.R., and Hasan, M.R. (2016). Pyrolytic Waste Plastic Oil and Its Diesel Blend: Fuel Characterization. Journal of Environmental and Public Health, 2016.
61. Budsaereechai, S., Hunt, A.J., and Ngernyen, Y. (2019). Catalytic pyrolysis of plastic waste for the production of liquid fuels for engines. RSC Advances, 9(10), 5844-5857.
62. Pattiya, A. (2011). Bio-oil production via fast pyrolysis of biomass residues from cassava plants in a fluidized-bed reactor. Bioresource Technology, 102, 1959–1967.
63. Guizani, C., Valin, S., Billaud, J., Peyrot, M., and Salvador, S. (2017). Biomass fast pyrolysis in a drop tube reactor for bio oil production: Experiments and modeling. Fuel, 207, 71–84.
64. Mohammed, I.Y., Lim, C.H., Kazi, F.K., Yusup, S., Lam, H.L., and Abakr, Y.A. (2017). Co-pyrolysis of Rice Husk with Underutilized Biomass Species: A Sustainable Route for Production of Precursors for Fuels and Valuable Chemicals. Waste and Biomass Valorization, 8(3), 911–921.
65. Hsu, C.P., Huang, A.N., and Kuo, H.P. (2015). Analysis of the rice husk pyrolysis products from a fluidized bed reactor. Procedia Engineering, 102, 1183–1186.

66. Kumar, M., Srivastava, N., Upadhyay, S.N., and Mishra, P.K. (2021). Thermal degradation of dry kitchen waste: kinetics and pyrolysis products. Biomass Conversion and Biorefinery.
67. Hossain, M.S., Ferdous, J., Islam, M.S., Islam, M.R., Mustafi, N.N., and Haniu, H. (2019). Production of liquid fuel from co-pyrolysis of polythene waste and rice straw. Energy Procedia, 160(2018), 116–122.
68. Wiinikka, H., Carlsson, P., Johansson, A.C., Gullberg, M., Ylipää, C., Lundgren, M., and Sandström, L. (2015). Fast pyrolysis of stem wood in a pilot-scale cyclone reactor. Energy & Fuels, 29(5), 3158-3167.
69. Wang, W.C., and Jan, J.J. (2018). From laboratory to pilot: design concept and techno-economic analyses of the fluidized bed fast pyrolysis of biomass. Energy, 155, 139-151.
70. Ren, S., Ye, X.P., Borole, A.P., Kim, P., and Labbé, N. (2016). Analysis of switchgrass-derived bio-oil and associated aqueous phase generated in a semi-pilot scale auger pyrolyzer. Journal of Analytical and Applied Pyrolysis, 119, 97-103.
71. Kantarli, I.C., Stefanidis, S.D., Kalogiannis, K.G., and Lappas, A.A. (2019). Utilization of poultry industry wastes for liquid biofuel production via thermal and catalytic fast pyrolysis. Waste Management & Research, 37(2), 157-167.
72. Dayton, D.C., Carpenter, J.R., Kataria, A., Peters, J.E., Barbee, D., Mante, O.D., and Gupta, R. (2015). Design and operation of a pilot-scale catalytic biomass pyrolysis unit. Green Chemistry, 17(9), 4680-4689.
73. Park, J.Y., Kim, J.K., Oh, C.H., Park, J.W., and Kwon, E.E. (2019). Production of bio-oil from fast pyrolysis of biomass using a pilot-scale circulating fluidized bed reactor and its characterization. Journal of Environmental Management, 234, 138-144.
74. Boateng, A.A., Daugaard, D.E., Goldberg, N.M., and Hicks, K.B. (2007). Bench-scale fluidized-bed pyrolysis of switchgrass for bio-oil production. Industrial & Engineering Chemistry Research, 46(7), 1891-1897.

75. Aladin, A., Alwi, R.S., and Syarif, T. (2017, May). Design of pyrolysis reactor for production of bio-oil and bio-char simultaneously. AIP Conference Proceedings, 1840(1).
76. Ali, N., Saleem, M., Shahzad, K., Chughtai, A., and Khan, W.A. (2014). Fast pyrolysis of Pakistani cotton stalks in fluidized bed reactor: design and preliminary results. Life Science Journal, 11(7), 137-144.
77. Rahman, M.M., Liu, R., and Cai, J. (2018). Catalytic fast pyrolysis of biomass over zeolites for high quality bio-oil: a review. Fuel Processing Technology, 180, 32–46.
78. Nie, L., de Souza, P. M., Noronha, F. B., An, W., Sooknoi, T., and Resasco, D. E. (2014). Selective conversion of m-cresol to toluene over bimetallic Ni–Fe catalysts. *Journal of Molecular Catalysis A: Chemical*, *388*, 47-55.
79. Liu, R., Rahman, M. M., Sarker, M., Chai, M., Li, C., and Cai, J. (2020). A review on the catalytic pyrolysis of biomass for the bio-oil production with ZSM-5: Focus on structure. *Fuel processing technology*, *199*, 106301.
80. Mihalcik, D. J., Mullen, C. A., and Boateng, A. A. (2011). Screening acidic zeolites for catalytic fast pyrolysis of biomass and its components. Journal of Analytical and Applied Pyrolysis, 92(1), 224–232.
81. French, R., and Czernik, S. (2010). Catalytic pyrolysis of biomass for biofuel production. Fuel Processing Technology, 91(1), 25–32.
82. Valle, B., Gayubo, A. G., Aguayo, A. T., Olazar, M., and Bilbao, J. (2010). Selective production of aromatics by crude bio-oil valorization with a nickel-modified HZSM-5 zeolite catalyst. *Energy & Fuels*, *24*(3), 2060-2070.
83. Wang, S., Dai, G., Yang, H., and Luo, Z. (2017). Lignocellulosic biomass pyrolysis mechanism: A state-of-the-art review. *Progress in energy and combustion science*, *62*, 33-86.
84. Nie, L., de Souza, P. M., Noronha, F. B., An, W., Sooknoi, T., and Resasco, D. E. (2014). Selective conversion of m-cresol to toluene over bimetallic Ni–Fe catalysts. *Journal of Molecular Catalysis A: Chemical*, *388*, 47-55.

85. Valle, B., Gayubo, A. G., Aguayo, A. T., Olazar, M., and Bilbao, J. (2010). Selective production of aromatics by crude bio-oil valorization with a nickel-modified HZSM-5 zeolite catalyst. *Energy & Fuels*, *24*(3), 2060-2070.
86. Zhang, H., Xiao, R., Huang, H., and Xiao, G. (2009). Comparison of non-catalytic and catalytic fast pyrolysis of corncob in a fluidized bed reactor. *Bioresource technology*, *100*(3), 1428-1434.
87. Iliopoulou, E. F., Stefanidis, S. D., Kalogiannis, K. G., Delimitis, A., Lappas, A. A., and Triantafyllidis, K. S. (2012). Catalytic upgrading of biomass pyrolysis vapors using transition metal-modified ZSM-5 zeolite. *Applied Catalysis B: Environmental*, *127*, 281-290.
88. Kumar, R., Strezov, V., Lovell, E., Kan, T., Weldekidan, H., He, J., and Scott, J. (2019). Enhanced bio-oil deoxygenation activity by Cu/zeolite and Ni/zeolite catalysts in combined in-situ and ex-situ biomass pyrolysis. *Journal of analytical and applied pyrolysis*, *140*, 148-160.
89. Paula, A., Dias, S., Rego, F., Fonseca, F., Casquilho, M., and Rodrigues, A. (2019). Catalyzed pyrolysis of SRC poplar biomass. Alkaline carbonates and zeolites catalysts. Energy, 183, 1114–1122.
90. Wang, J., Zhang, B., Zhong, Z., Ding, K., Xie, Q., and Wang, J. (2016). Catalytic fast co-pyrolysis of mushroom waste and waste oil to promote the formation of aromatics. Clean Technology and Environmental Policy, 18, 2701–2708.
91. Li, X., Li, G., Li, J., Yu, Y., Feng, Y., Chen, Q., Komarneni, S., and Wang, Y. (2016). Producing petrochemicals from catalytic fast pyrolysis of corn fermentation residual byproducts generated from citric acid production. Renewable Energy, 89, 331–338.
92. Jae, J., Tompsett, G. A., Foster, A. J., Hammond, K. D., Auerbach, S. M., and Lobo, R. F. (2011). Investigation into the shape selectivity of zeolite catalysts for biomass conversion. Journal of Catalysis, 279, 257–268. https://doi.org/10.1016/j.jcat.2011.01.019.

93. Mishra, R. K., and Mohanty, K. (2022). Pyrolysis of Cascabela thevetia seeds over ZSM-5 catalysts: fuel properties and compositional analysis. *Biomass Conversion and Biorefinery*, *12*(5), 1449-1464.
94. Bhoi, P. R., Ouedraogo, A. S., Soloiu, V., and Quirino, R. (2020). Recent advances on catalysts for improving hydrocarbon compounds in bio-oil of biomass catalytic pyrolysis. *Renewable and Sustainable Energy Reviews*, *121*, 109676.
95. Seah, C. C., Tan, C. H., Arifin, N. A., Hafriz, R. S. R. M., Salmiaton, A., Nomanbhay, S., & Shamsuddin, A. H. (2023). Co-pyrolysis of biomass and plastic: Circularity of wastes and comprehensive review of synergistic mechanism. *Results in engineering*, *17*, 100989.
96. Harith, N., Hafriz, R. S. R. M., Arifin, N. A., Tan, E. S., Salmiaton, A., & Shamsuddin, A. H. (2022). Catalytic co-pyrolysis of blended biomass–plastic mixture using synthesized metal oxide (MO)-dolomite-based catalyst. *Journal of Analytical and Applied Pyrolysis*, *168*, 105776.
97. Ghorbannezhad, P., Dehghani Firouzabadi, M., and Ghasemian, A. (2018). Catalytic fast pyrolysis of sugarcane bagasse pith with HZSM-5 catalyst using tandem micro-reactor-GCMS. Energy Sources, 40, 15–21.
98. Qu, W., Wei, L., and Julson, J. (2013). An exploration of improving the properties of heavy biooil. Energy & Fuels, 27, 4717–22.
99. Ding, K., Zhong, Z., Wang, J., Zhang, B., Fan, L., Liu, S., and Ruan, R. (2018). Improving hydrocarbon yield from catalytic fast co-pyrolysis of hemicellulose and plastic in the dual-catalyst bed of CaO and HZSM-5. *Bioresource technology*, *261*, 86-92.
100. Yang, Z., Kumar, A., and Apblett, A. (2016). Integration of biomass catalytic pyrolysis and methane aromatization over Mo/HZSM-5 catalysts. Journal of Analytical and Applied Pyrolysis, 120, 484–92.
101. Ding, K., Zhong, Z., Wang, J., Zhang, B., Addy, M., and Ruan, R. (2017). Effects of alkali-treated hierarchical HZSM-5 zeolites on the production of aromatic

hydrocarbons from catalytic fast pyrolysis of waste cardboard. Journal of Analytical and Applied Pyrolysis, 125, 153–6.

102. Wang, J., Xu, C., Zhong, Z., Deng, A., Hao, N., Li, M., and Ragauskas, A. J. (2018). Catalytic conversion of bamboo sawdust over ZrO2–CeO2/γ-Al2O3 to produce ketonic hydrocarbon precursors and furans. *ACS Sustainable Chemistry & Engineering*, *6*(11), 13797-13806.

103. Thangalazhy-Gopakumar, S., Adhikari, S., Chattanathan, S. A., and Gupta, R. B. (2012). Catalytic pyrolysis of green algae for hydrocarbon production using H+ ZSM-5 catalyst. Bioresource Technology, 118, 150–7.

104. Zhang, G., Sun, Y., Shi, Y., Jia, Y., Xu, Y., Zhao, P., and Zhang, Y. (2016). Characteristic and kinetics of corn stalk pyrolysis in a high-pressure reactor and steam gasification of its char. *Journal of analytical and applied pyrolysis*, *122*, 249-257.

105. Bakar, M. S. A., & Titiloye, J. O. (2013). Catalytic pyrolysis of rice husk for bio-oil production. *Journal of analytical and applied pyrolysis*, *103*, 362-368.

106. Chaihad, N., Karnjanakom, S., Kurnia, I., Yoshida, A., Abudula, A., Reubroycharoen, P., & Guan, G. (2019). Catalytic upgrading of bio-oils over high alumina zeolites. Renewable Energy, 136, 1304-1310.

107. Chaihad, N., Anniwaer, A., Karnjanakom, S., Kasai, Y., Kongparakul, S., Samart, C., Reubroycharoen, P., Abudula, A., and Guan, G. (2021). In-situ catalytic upgrading of bio-oil derived from fast pyrolysis of sunflower stalk to aromatic hydrocarbons over bifunctional Cu-loaded HZSM-5. Journal of Analytical and Applied Pyrolysis, 155, 105079.

108. Iliopoulou, E. F., Stefanidis, S., Kalogiannis, K., Psarras, A. C., Delimitis, A., Triantafyllidis, K. S., and Lappas, A. A. (2014). Pilot-scale validation of Co-ZSM-5 catalyst performance in the catalytic upgrading of biomass pyrolysis vapours. Green Chemistry, 16(2), 662-674.

109. Zhang, S., Zhang, H., Liu, X., Zhu, S., Hu, L., and Zhang, Q. (2018). Upgrading of bio-oil from catalytic pyrolysis of pretreated rice husk over Fe-modified ZSM-5 zeolite catalyst. Fuel Processing Technology, 175, 17-25.

110. Saraçoğlu, E., Uzun, B. B., & Apaydın-Varol, E. (2017). Upgrading of fast pyrolysis bio-oil over Fe modified ZSM-5 catalyst to enhance the formation of phenolic compounds. International Journal of Hydrogen Energy, 42(32), 21476-21486.

111. Wang, L., Lei, H., Bu, Q., Ren, S., Wei, Y., Zhu, L., and Tang, J. (2014). Aromatic hydrocarbons production from ex-situ catalysis of pyrolysis vapor over zinc-modified ZSM-5 in a packed-bed catalysis coupled with microwave pyrolysis reactor. Fuel, 129, 78-85.

112. Park, H. J., Heo, H. S., Jeon, J. K., Kim, J., Ryoo, R., Jeong, K. E., and Park, Y. K. (2010). Highly valuable chemicals production from catalytic upgrading of radiata pine sawdust-derived pyrolytic vapors over mesoporous MFI zeolites. Applied Catalysis B: Environmental, 95(3-4), 365-373.

113. Vichaphund, S., Aht-ong, D., Sricharoenchaikul, V., and Atong, D. (2014). Catalytic upgrading pyrolysis vapors of Jatropha waste using metal promoted ZSM-5 catalysts: An analytical PY-GC/MS. Renewable Energy, 65, 70-77.

114. Zheng, Y., Wang, F., Yang, X., Huang, Y., Liu, C., Zheng, Z., and Gu, J. (2017). Study on aromatics production via the catalytic pyrolysis vapor upgrading of biomass using metal-loaded modified H-ZSM-5. Journal of Analytical and Applied Pyrolysis, 126, 169-179.

Chapter -3

Materials and Methods

3.1 Introduction

This chapter covers the different feedstocks' collecting and processing methods. Using ASTM standards, the chosen feedstock samples were examined for proximate, elemental, and calorific values. The thermogravimetric analyzer was used to examine the feedstock's thermal deterioration behavior. The operation and experimental methodology of the batch reactor are described. FT-IR, NMR, and GC-MS analysis were used to identify the functional groups and chemicals in the oil produced during pyrolysis and co-pyrolysis. The physical properties of the oil, including its calorific value (CV), density, kinematic viscosity, cloud/pour point, aniline point, API gravity, and flash/fire point, were determined using recognized methods.

3.2 Collection and preparation of the feedstock for the pyrolysis experiment

3.2.1 Raw Sample Preparation

The rice husk was collected from Jalandhar and plastic waste (LDPE, HDPE, and PET) will be collected from the local market and local regions in Punjab. After being washed with regular water, the feedstock—which consisted of rice husks (RH) and plastic waste (HDPE-02, LDPE-04, and PET-01—was sun-dried for five days to remove any remaining moisture. The sun-dry feedstock was crushed to create tiny, uniform RH particle sizes, which were further sieved via a BSS standard sieve to generate an average particle size of 2.8 μm. This procedure was done in order to decrease the volume of the processed plastic garbage. Then, in a hot air oven, the dehydrated RH and plastic waste were baked for eight hours and two hours, respectively, at 120 °C and 110 °C. The processed feedstock was stored in an airtight bag for the analysis of physicochemical characteristics like proximate and ultimate analysis, calorific value, and thermogravimetric analysis for pyrolysis experiments. Before pyrolysis, the powdered rice husk and plastic waste (LDPE and HDPE) samples were mixed for further analysis.

Figure 3.1 Photographic image of all the selected raw and crushed samples.

3.2.2 Preparation of calcined dolomite (DOL), ZSM-5, and DOLZSM catalysts

The catalyst preparation involved the use of dolomite powder from SPECTROCHEM and ZSM-5 from Alfa Aesar. The ZSM-5 powder was subjected to 6 hours of drying in a hot air oven to eliminate any moisture content. After undergoing further calcination, the

dolomite (DOL) catalyst was dried in a hot air oven until the moisture content dropped to 80 °C. This involved gradually increasing the temperature until it reached 900 °C, or 5 °C every minute, to ensure full calcination of the dolomite. The next step was a two-hour holding period. The DOLZSM catalyst was made by mixing equal quantities (50:50) of ZSM-5 with calcined dolomite in a mortar and pestle. The resulting mixture, known as ZSMDOL, was employed in the catalytic co-pyrolysis process. During the catalytic pyrolysis tests, a catalyst-to-feed ratio of 1:20 was maintained for both types of material, calcined dolomite (DOL) and DOLZSM. This ratio ensured an optimal balance between catalyst concentration and feedstock volume, facilitating efficient catalytic conversion during the co-pyrolysis process.

Figure 3.2 Pictorial representation of catalyst in powder form.

3.3 Physicochemical characterization of biomass and plastic waste.

Biomass and plastic waste samples were characterized by using the different ASTM (American Standard Methods). The characterization methods are discussed below.

3.3.1 Proximate analysis

Estimating the raw feedstocks' capability for thermochemical conversion required careful consideration of their characterization. Highly volatile raw materials with low ash and sulfur concentrations are necessary for efficient thermal pyrolysis. To get ready for more testing and pyrolysis, the raw ingredients were dried in an oven. ASTM D 3172-07a was used for the proximate examination of RH, LDPE, HDPE, PET, and their mixes. This is the first stage of the characterization methodology that presents the concept that Moisture (MC), volatile matter (VM), fixed carbon (FC), and ash content (AC) will be examined by utilizing this method.

3.3.1.1 Analysis of Moisture Content

A weighted sample was dried in a crucible and heated to between 100 and 120 °C for eight hours, or until the weight was constant, to determine the moisture content (MC). The moisture in the sample is represented by the difference between the beginning and end weights of the sample. Equation (1) is used to determine the percentage composition of the moisture content in feedstock.

$$\text{Moisture content \%} = \frac{B-C}{C-A} \times 100 \qquad [1]$$

Where A = The mass of the empty crucible was measured. B = The mass of the crucible with the sample was measured. C =This value represents the weight of the sample after moisture removal.

3.3.1.2 Analysis of Volatile Matter

An alumina crucible with a cover was filled with a sample that had been preweighed and dried off. Two drops of phenol were applied to displace the ambient air. After that, the sample was heated for ten minutes at 700 °C. Following heating, the sample was cooled, and its ultimate weight was noted. The weight loss was divided by the sample's initial weight, and then multiplied by 100 to get the percentage of volatile matter (VM).

$$\text{Volatile Matter \%} = \frac{B-C}{B-A} \times 100 \qquad [2]$$

Where A = The mass of the empty crucible was measured. B = The mass of the crucible with the sample was measured. C = This value indicates the sample's weight following the elimination of moisture.

3.3.1.3 Analysis of Ash Content

An alumina crucible containing a known weight of moisture-removed material was heated in a furnace for two hours at around 500 °C. The ash content (AC) on a dry basis is calculated by dividing the weight of the residue that remains in the crucible by the starting weight of the feedstock.

$$\% \text{ Ash Content} = \frac{C-A}{B-A} \times 100 \qquad [3]$$

Where A = The mass of the empty crucible was measured. B = The mass of the crucible with the sample was measured. C = This value represents the weight of the sample after volatile matter exclusion.

3.3.1.4 Analysis of Fixed Carbon

The fixed carbon (FC) in the liquid fuel is a representation of its non-volatile component. In the context of liquid production by pyrolysis, the fixed carbon content is an important parameter since it influences the heating value and the efficiency of the process. The following formula for the material balance may be used to get the fixed carbon:

Fixed Carbon (FC) = 100% − [(MC) + (VM) + (AC)] [4]

3.3.2 Ultimate Analysis of Feedstocks

A CHNS elemental analyzer (ELEMENTARY Vario EL III) was used to do the ultimate or elemental analysis of the feedstocks on 2 to 4 mg of sample. The elemental composition was obtained from this analysis, which showed the proportions of "carbon (C), hydrogen (H), nitrogen (N), and sulfur (S)." The percentage of oxygen was calculated using the difference.

3.3.3 Analysis of the Higher Heating Value (HHV) of Feedstocks

Using a bomb calorimeter (Toshniwal Company), the greater heating values of raw materials and liquid fuels were ascertained. Prior to use, the bomb calorimeter was calibrated by burning fuel with a known calorific value, specifically benzoic acid. To create a homogenous sample, a dry sample of biomass and plastic garbage were crushed together. After that, a pelletizer was used to palletized it. A weighted amount sample (less than 1g) was burnt in oxygen in the bomb calorimeter. With the weight of cotton thread and nichrome wire measured in advance, the heat value of the solid-to-liquid fuel was calculated.

Figure 3.3 (a) Bomb calorimeter

3.3.4 Analysis of low heating value (LHV)

The LHV of the feedstocks is calculated using the standard formula that accounts for the latent heat of vaporization of the moisture and hydrogen content. The following relation was used:

LHV= HHV-0.09* H*2.24 [5]

where **H** is the hydrogen content (%) of the sample, and **Moisture** is the moisture percentage. The LHV values have now been added alongside the HHV data in the results section and summarized in **Table 4.3**.

Dulong's Formula

HHV Dulong = 0.388C+1.428(H-O/8)+0.095S [6]

Channiwala and Parikh's Formula

$\mathbf{HHV_{Channiwala}}$=0.3491C+1.1783H+0.1005S−0.1034O−0.0151N−0.0211A [7]

Where:

While C, H, O, N, S, A = wt% of Carbon, Hydrogen, Oxygen, Nitrogen, Sulfur, Ash and Units in MJ/kg.

3.3.5 Particle size of feedstocks

Particle size plays a significant role in the pyrolysis process and determines how much bio-oil is produced from plastic waste (LDPE and HDPE) and biomass (RH). For feed uniformity, the solid material was thoroughly blended and ground before being sieved to produce particles smaller than 2.6 mm. A U.S. standard sieve No. 7,8, shown in the Figure, achieves the desired particle size.

Heat transport is hampered by larger particle sizes, which can have an impact on product production. Larger particles may provide higher solid char and gas yields but may also result in lower bio-oil yields. Smaller particles have a better potential for producing bio-oil.

3.3.6 Analysis using Fourier Transform Infrared Spectroscopy (FTIR)

FTIR with Diamond ATR (Perkin Elmer Spectrum 2) for estimating chemical structures and chemical compounds from rice husk and plastic waste (LDPE, HDPE) and their blends. The FTIR instrument operates based on the vibrational and rotational modes of molecular motion. When compared to the absorption outlines of all other compounds, an organic compound's infrared band gives a distinct appearance that may be shown.

3.4 Catalyst characterization technique

3.4.1 XRD Analysis

X-ray diffraction (XRD) analysis was conducted to evaluate the crystallinity and phase structure of ZSM-5 and dolomite catalyst samples. The measurements were carried out at

the Materials Characterization Laboratory, IISER Bhopal, using a Rigaku Miniflex 600 diffractometer equipped with Cu Kα radiation (λ = 1.5406 Å). The instrument operated at 40 kV and 15 mA, with data collected over a 2θ range of 10°–80° at a step size of 0.02° and a scan rate of 2°/min. In a complementary setup, a single-crystal X-ray diffractometer was also employed to record XRD patterns at low temperature using Cu-Kα radiation (9.0 kW, 250 mA) over a 2θ range of 5°–70°, to further assess the crystal structure at room temperature. Powdered samples were evenly spread on a flat sample holder without binders to prevent interference. The crystallinity index (CI) of the catalysts was calculated using the Scherrer equation.

3.4.2 BET Analysis

The analysis was conducted using a surface area and porosity analyzer. Before analysis, the samples were degassed at 200 °C for 6 hours under a vacuum to remove moisture and volatile impurities. The measurements were carried out at the Materials Characterization Laboratory, IISER Bhopal to find the surface area was determined using the Brunauer–Emmett–Teller (BET) method**,** while the Barrett–Joyner–Halenda (BJH) method was applied for the calculation of pore size distribution from the desorption isotherms. All measurements were conducted using nitrogen gas at 77 K. These technical specifications have now been incorporated into the Experimental section of the manuscript. We thank the reviewer for highlighting this important aspect and helping improve the methodological clarity and reproducibility of our study.

3.4.3 DLS Analysis

The measurements were carried out at the Materials Characterization Laboratory, IISER Bhopal, by using a particle size analyzer, and the particle size of the catalyst ZSM-5 and dolomite samples was ascertained. Studies involving transient absorption and fluorescence upconversion can be performed using the Ultrafast Laser system. Five centimeters of material were placed into the cuvette. The material was illuminated with a HeNe laser (780-120 nm wavelength), which caused oscillations in the scattered light's intensity. For

particles that moved more swiftly and smaller in size, the variance was absorbed more slowly.

3.4.4 FE-SEM and EDX Analysis

The catalyst's surface morphology, particle size, and internal micro-structure were observed using field emission scanning electron microscopy (FE-SEM) equipped with an energy-dispersive X-ray spectrometer (EDX) at the Central Instrumentation Facility, IISER Bhopal. The catalyst particles' high porosity, as seen by the FE-SEM, suggests a large specific surface area. This increases the catalyst's activity since there are more active sites accessible for catalytic reactions, which facilitates effective mass transport and reactant molecule diffusion. To avoid sample charging, the oven-dried catalyst samples were placed on carbon tape and coated with a thin layer of gold. High vacuum conditions were maintained while the FE-SEM was operated at acceleration voltages between 5 and 20 kV. The EDX results were used qualitatively to identify the elemental composition of the samples; quantitative analysis was not performed due to the semi-quantitative nature of EDX under these conditions.

3.5 Instrumentation for thermal analysis

Thermogravimetric analysis (TGA) was performed to study the pyrolysis behavior of the samples under non-isothermal conditions. The experiments were conducted in IISER Bhopal using both a TGA 4000 (PerkinElmer) and a TA Instruments SDT Q600 analyzer for cross-validation of results. Approximately 10 ± 0.5 mg of each sample was placed in Al_2O_3 crucibles and heated from ambient temperature up to 600 °C. The analysis was conducted under a high-purity nitrogen atmosphere (99.999%) to ensure an inert environment, with flow rates of 20 mL/min (PerkinElmer) and 100 mL/min (TA Instruments), respectively. Heating rates of 10, 20, 30, and 40 °C/min were applied to observe the effect of temperature ramp on thermal degradation. Baseline correction was carried out using an empty reference pan under identical thermal conditions, and the

instruments were calibrated for both temperature and weight using standard reference materials to ensure data accuracy.

3.5.1 Instrumentation, control, and limitations

By monitoring mass changes as a function of temperature, thermogravimetric analysis (TGA) is a vital method for determining the thermal stability, composition, and breakdown kinetics of materials. The highly sensitive balance, the precise temperature-controlling furnace, the temperature-measuring thermocouples, the gas flow system for maintaining an inert atmosphere, and the data collection system for real-time monitoring and analysis make up the TGA setup. Despite its efficiency, TGA has limitations, including the ability to handle only small sample sizes, the major influence of heating rates on findings, and the requirement for high-purity inert gases to prevent oxidation. Furthermore, data interpretation might be complicated owing to overlapping thermal events, and establishing homogeneous heating can be difficult. Long-term instrument drift, as well as possible interactions between the sample and holder materials, make reliable observations difficult. To address these constraints, precise control of experimental conditions and regular calibration are required to achieve consistent findings.

3.5.2 Kinetic analysis

Using a different approach, the kinetic analysis of the thermal decomposition of biomass waste

The reaction rate $\frac{d\alpha}{dt}$ of the pyrolysis of biomass (RH) and plastic samples (LDPE and PET) can be expressed as follows [11]

$$\frac{d\alpha}{dt} = K(T) \times F(\alpha) \qquad [8]$$

$$\alpha = \frac{wi - wt}{wi - wf} \qquad [9]$$

Where A is a pre-exponential factor (s^{-1}). α is the reaction conversion, t is the time (min), and k is the reaction rate constant (K^{-1}),. Ea is the activation energy (kJ/mol), and R is the

universal gas constant (8.314 J $mol^{-1}.K^{-1}$), W_i is the starting weight of the sample used in the experiment; T is the temperature in Kelvin.

W_t: is the sample's current weight in milligrams. W_f: The remaining weight of the sample after the experiment. For non-isothermal pyrolysis, the heating rate (β) can be defined as$\beta = \frac{dT}{dt}$, and the equation can be simplified as:

$$\beta \frac{d\alpha}{dT} = A\, exp\left(-\frac{Ea}{RT}\right) \times F(\alpha) \qquad [10]$$

Accurately obtaining kinetic parameters is required for the creation of a highly effective kinetic model that can explain the pyrolysis procedure. Utilizing TGA data at various heating rates, the activation energy can be determined using iso-conversional (model-free) models like the KAS Equation (11), FWO Equation (12), Freidman Equation (13), Starink Equation (14), and Tang Equation (15). These five models were included in this study since they are some of the most widely used models.

3.5.3 Iso-conversional methods

The iso-conversional techniques are predicated on the notion that the degree of conversion is constant and that the rate constant (k) for a reaction depends solely on temperature. Methods for iso-conversion might be either differential or integral [12]. In this research, five iso-conversational techniques, including the Friedman, Tang, Starink, FWO, and KAS approaches, are used in this study to calculate the activation energy. All these methods have been discussed below.

3.5.3.1 Kissinger Akahira Sunose model

$$ln\left[\frac{\beta}{T^2}\right] = ln\left(\frac{AE_\alpha}{Rg(\alpha)}\right) - \frac{E_\alpha}{RT} \qquad [11]$$

The value of kinetic parameters for each conversion is represented by the slope of the figure ln β /T^2 vs. 1/T [13].

3.5.3.2 Flynn Wall Ozawa model

$$log(\beta) = log\left(\frac{AE_\alpha}{Rg(\alpha)}\right) - 2.315 - 0.457\frac{E_\alpha}{RT} \quad [12]$$

The value of kinetic parameters for each conversion is represented by the slope of the linear plot between log (β) and 1/T [14].

3.5.3.3 Starink model

$$log(\frac{\beta}{T^{1.92}}) = \text{constant} - 1.0008\frac{E_\alpha}{RT} \quad [13]$$

The value of kinetic parameters at each conversion is given by the slope of the graph between

ln β /$T^{1.92}$ and 1/T [15].

3.5.3.4 Friedman method

The Friedman equation is represented as follows:

$$ln\left(\frac{dx}{dt}\right) = ln\, f\,(x) + ln\, A - \frac{Ea}{RT} \quad [14]$$

The kinetic parameters can be calculated using this equation. A straight line carrying the activation energy is produced by plotting the ln(dx/dt) and 1/T curves [16].

3.5.3.5 Tang model

$$ln(\frac{\beta}{T^{1.894661}}) = C_1 - 1.001450\frac{E_\alpha}{RT} \quad [15]$$

The value of kinetic parameters at each conversion is given by the slope of the graph between

$ln(\frac{\beta}{T^{1.894661}})$ and 1/T [17].

3.5.3.6 Thermodynamic parameter

The FWO method and KAS method were employed to estimate the thermodynamic triplets like ΔH, ΔG, and ΔS using the relations below

$$\Delta H = Ea - RT \quad [16]$$

$$\Delta G = E + RT\ln\left(\frac{KT}{hA}\right) \quad [17]$$

$$\Delta S = \left(\frac{\Delta H - \Delta G}{T} \right) \qquad [18]$$

Here, K is the Boltzmann constant (1.381×10^{-23} J/K) and h represents Planck's constant (6.626×10^{-34} J-s).

3.6 Comprehensive pyrolysis index

The following comprehensive pyrolysis index (CPI) was used to quantify pyrolysis performance:

$$CPI = \frac{-(R_a \times R_m) \times M_f}{T_i \times T_p \times \Delta T_{1/2}} \qquad [19]$$

The following parameters can be used to assess biomass and plastic waste pyrolysis performance

T_i –initial devolatilization time, T_p- DTG maximum peak time, $\Delta T_{1/2}$ - half-peak width range, M_f – final weight loss, R_a - Average decomposition rate, R_m- maximum decomposition rate, CPI- comprehensive pyrolysis index.

3.7 Experiment Setup for pyrolysis and co-pyrolysis experiments

3.7.1 The experimental procedure for a tubular reactor

The tubular pyrolysis reactor was designed to ensure efficient and homogeneous heat transfer for the thermal decomposition of biomass and plastic samples. The external dimensions of the reactor are 100 cm in length and 34 cm in width, with the holding vessel having a diameter of 14 cm. The internal chamber measures 41 cm in length and 30 cm in width, with a holding capacity of up to 500 g of feedstock. A mesh sample container was placed inside the reactor, constructed from a 1 mm-thick stainless-steel sheet welded into a cylindrical pipe. The inner and outer diameters of the pipe are 6 cm and 7 cm, respectively, and the mesh height is maintained at 34 cm to store biomass and charcoal both before and after pyrolysis. The reactor operates within an optimal temperature range of 500–800 °C, with heating rates adjustable from 10 to 50 °C/min. A nitrogen gas flow

rate of 50–200 mL/min. is supplied to maintain an inert atmosphere during the process. The system's temperature is precisely regulated using a PID temperature controller, which modulates the power supply to the heating elements based on feedback from a centrally placed K-type thermocouple. The setup allows for accurate control of temperatures from ambient up to 800 °C, with a control precision of ±1 °C.

Figure 3.4 Design and development of the experimental setup

Figure 3.5 Real Image view of pyrolysis reactor for bio-oil production.

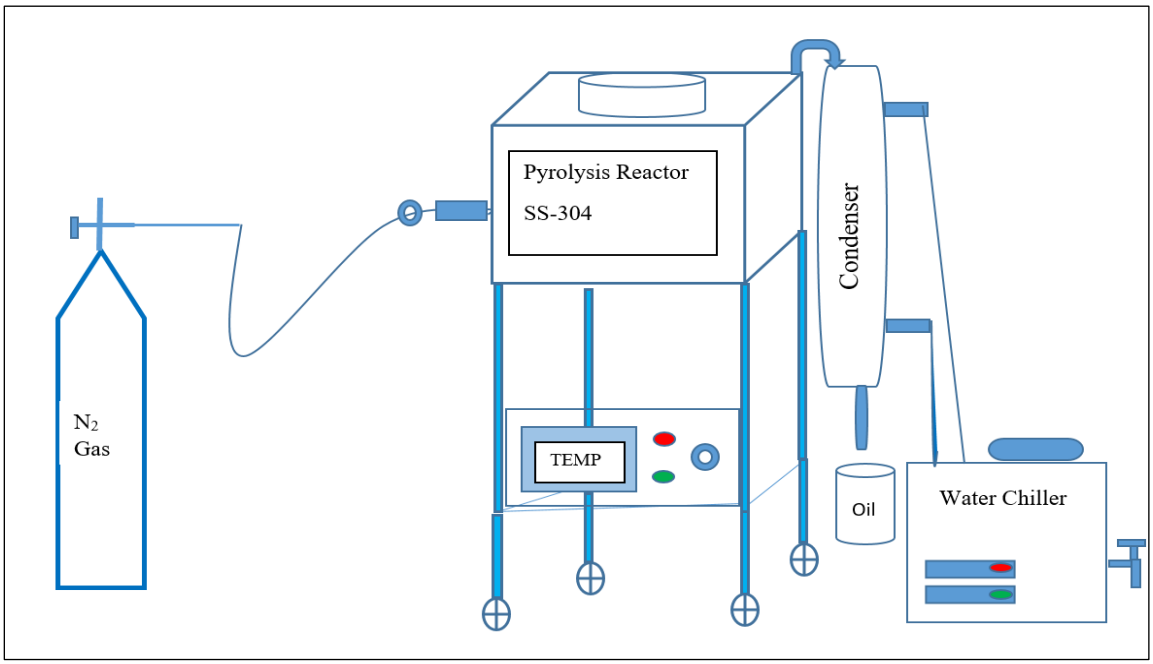

Figure 3.6 Schematic diagram of batch-type pyrolysis reactor

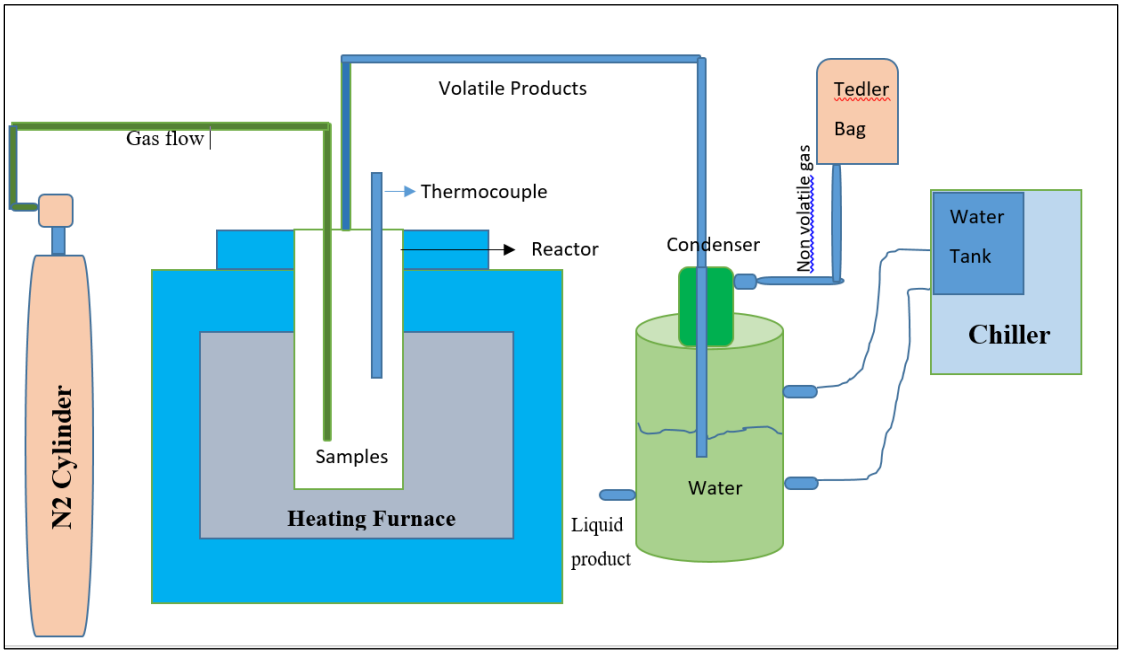

Figure 3.7 Schematic representation of the experimental arrangement for the pyrolysis of waste materials, illustrating the different components involved.

3.7.2 Experimental reactor for co-pyrolysis technique

The plastic waste (LDPE, HDPE) and biomass (RH) materials underwent thermochemical conversion in a fabricated furnace that can operate up to 1100℃ temperatures. The furnace consists of a tube-shaped reactor, a proportional-integral-derivative (PID) controller based on relays, a thermocouple, coil-type heating elements, and an insulator made of cerawool to avoid heat loss. Additionally, to condense the gases, a cooling water circulator (Model-R134a, Coal-Parmer) was connected to the sample collection system. The flow rate of N_2 gas was 200 ml/min during the experiments. A second thermocouple was also inserted into the SS-316 reactor (dimension: 20 cm length x 10 cm ID) to record the reactor's inside temperature in real time. The complete setup for the pyrolysis of waste material is illustrated in **Fig. 3.9** A typical experiment involved feeding 200 grams of feedstock and heating it to 500 ℃ at a heating rate of 10 °C per minute and holding it at that temperature for another 50 minutes. Subsequently, we determined the pyrolysis process yield by estimating the mass percentage of liquid product, gas product, and solid char product. Further characterization of the liquid sample was conducted to evaluate the influence of the feedstock composition.

Characterization of pyrolysis products

$$O_Y\ (\%) = \frac{W_O}{W_F} \times 100\% \qquad [20]$$

$$C_Y\ (\%) = \frac{W_C}{W_F} \times 100\% \qquad [21]$$

$$Gy\ (\%) = 100\% - (Oy + Cy)\% \qquad [22]$$

Where the $O_{Y,}$ $C_{Y,}$ and G_Y represent product yields (%) of pyro-oil (liquid product), solid-char (residue product), and pyro-gas (gaseous products), respectively. Additionally, W_O, $W_{C,}$ and W_F represent the weight of pyro-oil (liquid product), solid-char (residue product), and raw material feedstock in grams.

3.7.3 Experimental reactor for catalytic pyrolysis technique

In a similar tabular reactor described in section 3.2, catalytic pyrolysis was also carried out using a variety of samples, including plastic waste (HDPE and LDPE) with biomass (RH) at 80:20. Two distinct catalysts were used, and the catalyst-to-feed ratio was found to be 1:20 during the catalytic pyrolysis process. A PID controller was installed in the reactor to track the internal reaction temperature at 500 °C, which was ramping up to 10°C every minute. Nitrogen gas was utilised in each experiment, provided in an inert environment at a rate of 200 millilitres per minute. The reactor was filled with a catalyst and a predetermined amount of feedstock (200 g) before the thermal cracking process began. Measuring the products was the last stage in obtaining the yield, which was then stated as a weight proportion of gas, liquid, and solid residue. Further study was performed on the liquid product, often referred to as pyro-oil, to ascertain the makeup of the feedstock and the effects of different catalysts.

3.8 Physio-chemical characterization of liquid sample

Physio-chemical characterization of bio-oil for the determination of different fuel parameters. Produced bio-oil properties will be analyzed by the different ASTM methods which are discussed below.

3.8.1 Density of bio-oil

The analysis will be conducted using an ASTM-D1217-based density meter. The relative density can be measured with a 25 ml capacity relative density bottle. After the bottle has been oven-dried, its initial weight should be noted. The bottle will then be filled with bio-oil, and to make sure there are no air bubbles within, a capillary stopper will be carefully fitted on the neck of the bottle. The combined weight of the oil and the relative density bottle will be recorded. The density will be calculated using the following equation:

$d = (W_2-W_1)/ 25$ [23]

d = density of oil samples in g/ml

Where W_2 = Weight of the relative density bottle with liquid fuels gram (g) W_1 = Weight of the empty relative density bottle (in grams).

A thermometer will be inserted into the density bottle to measure the impact of temperature on the density of bio-oil. The density of the liquid sample at the designated temperature will next be determined by following the previously mentioned protocol. Measurements were conducted in **triplicate**, and the average density value was reported along with the **standard deviation** to reflect measurement reproducibility. The mass measurements were taken using a calibrated analytical balance with an accuracy of ±0.1 mg.

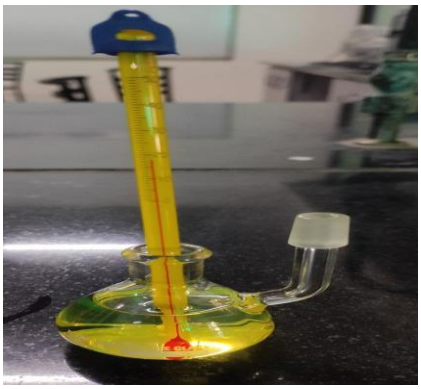

Figure 3.8 Pycnometer for density analysis of bio-oil

3.8.2Analysis of Flash and Fire Point of Bio-oil

Flash-point is a property of the fuel where flames ignite the vaporized fuel mixer with air and continuously increased temperature repeat the ignition and becomes continuous burning of the fuel is known as fire point of the fuel. The pyro-oil's flash and fire points were determined through the utilization of Abel's Apparatus in a closed-cup setup, following the principle outlined in IP-170 (ISO 13736:2008). This testing technique is commonly applied to ascertain the flash point of flammable liquid fuels temperature within the range of 70 °C to -30 °C.

Figure 3.9 Real-view image of flash/fire point instrument

3.8.3 Analysis of Aniline point of bio-oil

Using an aniline point instrument, the U-tube method described in IP-2 was used to determine the aniline point (AP) of the liquid fuel samples. To determine the number of aromatics in bio-oil, utilize the aniline point method.

Figure 3.10 Image view of aniline point apparatus.

3.8.4 Analysis of Cloud and Pour Point of Bio-oil

The cloud point and pour point of the samples were ascertained using the ASTM D-2500 and ASTM D-97 protocols. The pour point is the lowest temperature at which oil will flow under typical test settings.

Figure 3.11 Cloud and pour point instrument

3.8.5 The higher heating value of bio-oil

An automated bomb calorimeter can be used to analyze higher heating values (HHV). The higher heating value (HHV), commonly referred to as the gross calorific value, is an essential characteristic of solid, liquid, and gaseous fuels. It may be expressed in a number of ways, including Kcal/Kg, Joules/gram, KJ/Kg, and MJ/Kg.

Procedure: The primary use of the bomb calorimeter is standardized by the combustion of a fuel with a known calorific value, such as benzoic acid. The solid sample is oven-dried, crushed, and converted into a powder form, then pelletized using a pelletizer. Within the bomb calorimeter, a weighted sample weighing less than one gram is burnt in oxygen. The heat value of the solid or liquid sample is taken into consideration when the weight and heat value of the cotton thread and nichrome wire, which are measured beforehand, are known. A gelatin capsule is utilized to hold liquid bio-oil while it is being measured. The following expression is used to determine the sample's heating value, whether it is solid or liquid: The following formula is used to determine the total amount of heat released:

Total heat liberated = Water equivalent × Modified temperature rise of water

To determine the heat released by the solid fuel, the heat generated by the thread and nichrome wire is deducted from the total heat radiated. The solid fuel's actual heat emitted is then divided by its weight in kilograms to get its calorific value:

Figure 3.12 Bomb calorimeter for measuring calorific value.

3.8.6 Analysis of Carbon Residue of bio-oil

A Ramsbottom carbon residue instrument was used to analyze the propensity for carbonaceous deposition, which is assessed as carbon residue (CR) in weight percent (wt.%), following the ASTM D-524 technique. After weighing a known amount of the sample in a crucible and subjecting it to destructive distillation, the carbon residue was ascertained. Throughout a predetermined amount of severe heating, the residue goes through thermal cracking and coking processes. The crucible containing the carbonaceous residue is heated and then cooled in a desiccator until it is ready to weigh.

3.8.7 Analysis of Viscosity of Bio-oil

Viscosity will be measured by an ASTM D-445 method-based viscometer. Kinematics viscosities will be determined at 25 ^{o}C to 60 ^{o}C temperatures using the standard technique ASTM D445. A kinematic viscometer will be used for the measurement of the kinematics

viscosity of the liquid sample. The kinematic viscosity of the pyro-oil sample was assessed using the Cannon-Fenske apparatus (Model: Hamco 50-259) with a viscosity range of 0.8 – 4 cSt by introducing an 8 ml liquid oil sample in it. The kinematic viscosity, measured in centistokes (cSt). Before testing, the viscometer was cleaned and calibrated using certified viscosity reference oils with known kinematic viscosity values traceable to national standards. The calibration ensured that the instrument provided accurate flow times within the expected viscosity range of the samples. Each measurement was conducted in triplicate to ensure reproducibility, and the average value was reported along with the standard deviation.

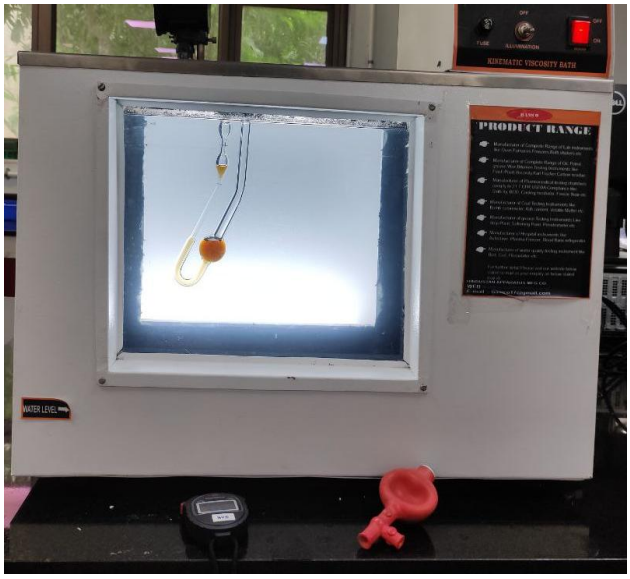

Figure 3.13 Image view of the kinematic Viscometer

3.8.8 Analysis of pH measurement:

The pH of the bio-oil is a key parameter that indicates its acidic or basic nature. To assess this, pH measurements were conducted using a digital pH meter (Model: pH Tutor, Eutech Instruments). The pH meter was calibrated before use with standard buffer solutions of pH 4.00, 7.00, and 10.00 at room temperature to ensure accuracy across the full pH range.

During calibration and measurement, the electrode was thoroughly rinsed with distilled water between each buffer and sample to prevent cross-contamination. Approximately 1–

2 mL of the bio-oil sample was used for each measurement. All measurements were performed in triplicate, and the average value was reported as the final pH of the bio-oil.

3.8.9 Analysis of API gravity

The ◦API, an estimate of liquid fuel density compared to water at 60°F (15.6 °C), was determined using the following scientific method.

$$API = \frac{141.5}{SG_{15.6^0C}} - 131.5 \qquad [24]$$

Diesel Index = Aniline point (°F) × °API gravity.

In contrast, the cetane index (CI) of the liquid sample produced by pyrolyzing separate and combined plastic waste with rice husk was determined using the formula Cetane Index = 0.72 × D.I. + 10. Additionally, the table provides comprehensive analytical methods for the items' characterization.

Table 3.1: Physicochemical Characteristics of Pyro-Oil by Using Analytical Techniques

SI. No.	Parameter	Analytical Techniques	Instrument's name
1.	Pour and Cloud point	ASTMD-2500, ASTM D-97	Pour and cloud point apparatus
2.	Fire and Flashpoint	IP-170	Abel's apparatus
3.	Density (at 30 °C)	ASTM D-1217	Bingham Pycnometer
4.	Specific Gravity	ASTM D-1298	Hydrometer
5.	Kinematic viscosity (40 °C)	ASTM D-445	Cannon-Fenske method
6.	Calorific value (CV)	IP-12	Bomb calorimeter Apparatus
7.	Carbon residue (CR)	ASTM D-524	Ramsbottom carbon residue Instrument

8.	pH value	direct measurement with calibrated pH meter	PH Tutor (Eutech Instrument)

3.9 Elemental Analysis of Liquid Sample

The oil samples were analysed with a CHNS analyser (Model: Elementar; Vario EL-cube) to determine the composition of the original samples and the pyro-oil that was produced by co-pyrolyzing of rice husk, plastic trash, and their combinations. The final analysis gives a precise breakdown of the elements that make up bio-oil, including how much carbon, hydrogen, nitrogen, and sulphur there are. Using the following formula, deduct the total quantity of other components from the total amount to find the oxygen content:

[Oxygen% = 100 - (Carbon content% + Hydrogen content% +Nitrogen content%+ Sulfur content%]. The study follows the ASTM standard procedure D3176-74. The CHNS/O analyzer is used to estimate these elements as a percentage.

3.10 Characterization of composition

The analysis of pyro-oil involved two techniques: gas chromatography (GC) & nuclear magnetic resonance (NMR). For GC analysis, we utilized Agilent-7890A gas chromatography with a 5975C MS (mass spectrometer) and a dual detector. This analysis performed at material characterization instrument facility (CIF), IISER Bhopal, Madhya Pradesh. The gas chromatography system had an HP-5 capillary column (30 meters long, 0.25 millimeters in diameter, and 0.25 micrometers in thickness). Helium served as the carrier gas, and it was pumped at a rate of 1.1971 milliliters per minute at a pressure of 14.36 psi. The temperature schedule called for an initial 5-minute interval at 50°C, followed by 5 minutes at 280°C and a progressive ascent from 50°C to 280°C at a rate of 5 °C per minute. The split ratio was one to 10. The analysis took fifty-six minutes to finish. As previously indicated, a temperature of 300 °C was maintained for the detector. Electron ionization (EI) was utilized to detect mass over the mass-to-charge ratio (m/z) range of 0 to 700 atomic mass units, with an ionization energy of 70 eV.

3.10.2 NMR Analysis

The pyrolysis liquid products were subjected to ^{1}H and ^{13}C NMR analysis, which was conducted using a Bruker NMR spectrometer (AVANCE-III 500 MHz FT). NMR analysis performed at the Material Characterization Instrument Facility (CIF), IISER Bhopal, Madhya Pradesh. For this analysis, samples were prepared using $CDCl_3$ at a 1:20 ratio, and the data were analyzed using MestreNova software to estimate the proportions of paraffin content, olefin content, and aromatics content based on the proton and carbon atom compositions within the liquid fuel. For the estimation of various hydrocarbons, the correlations mentioned below have been utilized.

$$N_a = 0.7216H_a + 1.3323H_\alpha - 0.1400H_d + 10.692 \quad [25]$$

$$N_0 = -0.4980H_a + 3.5374H_0 + 0.5267H_{c1} + 6.9846 \quad [26]$$

$$N_p = -4.2327H_0 - 1.2499H_a + 0.4106H_d + 62.576 \quad [27]$$

$$D = \frac{H_d}{H_{C2}} \quad [28]$$

Where N_a indicates the aromatic content, N_o indicates the olefin content, and N_p signifies the paraffin content in the fuel. While the variable 'D' signifies the degree of branching in the hydrocarbons. Additionally, the aromatics content, olefins content, and paraffin content (volume fraction) in the liquid fuels derived from plastic waste with rice husk and their combinations at different ratios were also estimated. The detailed calculation for the identification of hydrocarbon types can be found elsewhere.

3.10.3 FTIR investigation of liquid oil

Fourier Transform Infrared (FTIR) spectroscopy using a Perkin-Elmer instrument was employed to analyze the functional groups present in the liquid pyro-oil samples. This test was analysed at material characterization instrument facility (CIF), IISER Bhopal, Madhya Pradesh. The analysis was conducted over the spectral range of 4000–400 cm^{-1} with a resolution of 4 cm^{-1}. The samples were analyzed directly without any dilution or preprocessing, as the Attenuated Total Reflectance (ATR) mode allows for direct scanning of liquid samples. Each spectrum was obtained by averaging 42 scans to improve the

signal-to-noise ratio. The pyro-oil samples were placed in the liquid cell window, and spectral data were processed using Perkin-Elmer Spectrum software, which included baseline correction and spectral normalization to ensure accurate peak identification and comparison.

3.11 Distillation unit

Figure 3.14 Process of bio-oil filtration through the distillation unit.

Distillation of oil is a process vital to refining crude oil into its various components, including pyro-oil. This method involves heating the crude oil in a distillation unit, typically a tall column with multiple trays or plates. As the crude oil is heated, its various components vaporize at different temperatures ranging from 100 to 300 ℃. The sample of crude oil is placed into the heating mantle, where it undergoes intense heating. As the temperature rises, lighter hydrocarbons such as gases and gasoline vaporize first, rising the column. These vapors then condense at different heights depending on their boiling points and are collected separately. The heavier components, like pyro-oil, which have higher boiling points, remain in liquid form at the bottom of the column. Through this process, impurities are separated, and the desired components, including pure distilled oil like pyro-oil, are obtained.

Chapter - 4

Thermal parameters of Rice husk, plastic waste and Kinetics of individual Feedstocks

4.1 Introduction

The use of alternative energy methods, including pyrolysis, gasification, fermentation, and liquefaction, can help India overcome its energy issue by lowering its reliance on fossil fuels. A sizable amount of the nation's energy needs might potentially come from biomass. In addition to reducing greenhouse gas emissions, creating jobs, promoting rural development, and protecting the environment, biomass-based energy production techniques offer a sustainable energy source. Designing and refining a modern pyrolysis reactor requires a deep understanding of the thermal behaviour and kinetic characteristics of feedstocks, such as rice husk, low-density polyethylene, and polyethylene terephthalate. To encourage the use of alternative energy sources in India, a comprehensive strategy including the public, corporate sector, and government is required [1-2].

To effectively use this extra biomass and reduce dependency on fossil fuels, India is focusing on exploiting it through a range of energy conversion techniques, such as pyrolysis, gasification, fermentation, and liquefaction. Biomass may be used using these methods to produce heat, power, and biofuel. Using rice husk as a feedstock for energy generation is one of India's main priorities. Because of the vast amount of rice produced in India, rice husk, a byproduct of rice manufacturing, is easily accessible there [3]. Rice husk has a high energy content and may be pyrolysed to provide energy that is useful. Research and development in biomass conversion technologies must be stepped up to further boost the viability of using biomass as an alternative energy source in India [4]. Kinetic studies on Solar hemp, an Indian fibrous plant-based product, utilizing different model-free techniques revealed activation energies between 93.3 and 104.8 kJ/mol [5]. The activation energies of the biochar gasification and pyrolysis processes on maize straw were 239.43,

232.82 kJ/mol and 180.82, 180.42 kJ/mol, respectively [6]. By modelling the breakdown of biomass using the reaction rate correlation and addressing it with several models for variable heating rates and reaction temperatures, large-scale pyrolytic reactors can be developed, and their optimal reactor process parameters may be determined [7]. One of the most popular and useful methods for researching the kinetic and thermogravimetric analysis (TGA) properties is to examine biomass pyrolysis [8]. TGA is used to continuously measure the growth or loss of biomass mass as the reaction temperature rises. Using TGA data for various heating rates, kinetic parameters are calculated [9].

The present work uses thermogravimetric analysis to perform a thermal and kinetic examination of plastic trash (LDPE and PET) and rice husk. By examining the materials at ambient to 600oC and with different heating rates, the goal is to learn more about the pyrolysis conditions and thermal stability of the materials. The paper also explores thermal decomposition kinetics to characterise the pyrolysis process and assesses several methods for evaluating non-isothermal solid-state kinetic data. The activation energy of the samples is determined using thermo-gravimetric analysis with five different methods such as Friedman, Starink, Tang, Flynn-Wall-Ozawa, and Kissinger-Akahira-Sunose methods. The research also compares the utility of the samples as an energy feedstock by comparing the activation energy of rice husk and plastic waste. This research aims to provide better clarity of the pyrolysis process and to identify the most efficient and effective methods for converting these materials into clean energy. Furthermore, a detailed investigation was conducted into the impact of thermodynamic parameters on the pyrolysis behaviour of RH, LDPE, and PET, as well as the pyrolysis performance index. These factors included change in enthalpy (ΔH), change in entropy (ΔS), and change in Gibbs free energy (ΔG) fluctuation.

4.2 Physio-chemical characterization of feedstock's

The proximate and elemental content of the chosen feedstock, rice husk (RH), and plastic waste (LDPE, HDPE, and PET; Low-Density Polyethylene, High-Density Polyethylene, and Polyethylene Terephthalate), as well as its mixes, are listed in Table 1.

4.2.1 Proximate Analysis

The present samples had a notable moisture content of 0.6% in LDPE, 0.02% in PET, and 6.75 percent in RH. Less than 10% moisture content biomasses are typically preferred for the pyrolysis process. The result indicated that RH represented low volatile matter (61.8 %) but PET and LDPE represented a high number of volatile matters 87.5 and 98 wt.% because of high polymeric contents. High volatile matter content is advantageous for thermal breakdown through pyrolysis because it is highly reactive, devolatizes easily, and yields a significant amount of bio-oil. High organic content also favours the higher heating value and good combustible properties as solid fuel. RH has a high ash level (16.8 weight percent), however PET and LDPE have lower ash contents (1.8 and 0.1 weight percent). By using elemental analysis, the carbon and hydrogen contents in RH, PET, and LDPE were determined to be 35.84 weight percent, 6.14 weight percent, 63.02 weight percent, 7.92 weight percent, 71.71 weight percent, and 15.26 weight percent, respectively. PET and LDPE were found suitable sources for the pyrolysis process due to their high bio-oil yield and high heating value. The higher heating values observed in PET and LDPE were 18.05 and 21.2 MJ/Kg.

Table 4.1- Proximate Properties of RH, LDPE, HDPE, PET and its mixture.

Feedstocks	Moisture (%)	Volatile matter (%)	Ash content (%)	Fixed carbon (%)
RH: LDPE (100:0)	6.75	61.8	16.8	14.65
RH: LDPE (0:100)	0.6	98	0.1	1.3
RH: LDPE (75:25)	3.4	71	13.6	11.2
RH: LDPE (25:75)	0.9	88	5.7	5.1
RH: LDPE (50:50)	2.7	80	11.3	5.5
RH: PET (0:100)	0.02	87.5	1.8	10.68
RH: PET (25:75)	1	70	12.3	13.7
RH: PET (75:25)	1.6	81.8	7.3	9.1

RH: PET (50:50)	1.3	74.7	9.6	12.9
RH: HDPE (0:100)	0	99	0.7	0.3
RH: HDPE (20:80)	1.4	98.2	0.2	0.2
RH: HDPE (35:65)	1.8	96.7	0.4	1.1
RH: HDPE (50:50)	2.1	95.2	1.0	1.7

4.2.2 Ultimate analysis

The CHNS analyser will be used to investigate this test and assess the samples' carbon, hydrogen, nitrogen, and sulphur levels. This research will determine the elemental purity of the samples. The "Dumas method," which involves "flash combustion," or the total and instantaneous oxidation of the material, is how the analyser worked. The organic molecules C, H, N, O, and S were found by the thermal conductivity detector after the combustion products were separated using a chromatographic column. An output signal that was proportionate to each component's concentration in the combination was the end result.

Table 4.2 Elemental analysis of all the raw samples **-**

Feedstocks	**Carbon (%)**	**Nitrogen (%)**	**Oxygen (%)**	**Hydrogen (%)**	**Sulfur (%)**
RH: LDPE (100:0)	35.84	0.44	57.57	6.14	0
RH: LDPE (0:100)	71.71	0.09	12.03	15.26	0.92
LDPE: RH (50:50)	47.2	0.29	46.83	10.68	0
LDPE: RH (25:75)	44.71	0.37	45.84	8.77	0.32
LDPE: RH (75:25)	56.78	0.2	29.62	12.16	1.23
PET: RH (100:0)	63.02	0.09	31.97	4.92	0
PET: RH (50:50)	52.54	0.27	35.74	10.43	1.02
PET: RH (25:75)	38.21	0.47	56.55	5.78	0

PET: RH (75:25)	57.43	0.04	50.07	0.46	0
HDPE: RH (100:0)	81.71	0	3.03	15.26	0
HDPE: RH (50:50)	50.3	0.27	39.4	10.4	0
HDPE: RH (80:20)	75.24	0.11	11.45	13.4	0
HDPE: RH (65:35)	64.3	0.19	24.72	11.6	0

4.2.3 Higher heating value

The automated bomb calorimeter will be used to calculate the greater heating value. A greater heating value will indicate the solid fuel's heat quality. It will analyse the heating value in KJ/Kg. Greater heating value (HHV) is a crucial factor in the planning and execution of energy systems powered by biomass. The automated adiabatic bomb calorimeter was used to calculate the calorific value (CV).

Table 4.3 Experimental and theoretical Heating values of all the samples

Sample	HHV(MJ/KG) (EXP)	HHV (DULONGS) (MJ/KG)	HHV(CHANNIWALA) (MJ/KG)	LHV (MJ/kg)
RH: LDPE (100:0)	14.81	13.59	14.62	13.46
RH: LDPE (0:100)	21.2	20.34	20.63	17.85
LDPE: RH (50:50)	17.34	16.71	16.33	14.99
LDPE: RH (25:75)	16.91	17.54	16.92	14.98
LDPE: RH (75:25)	20.63	21.54	19.48	17.96
PET: RH (100:0)	20.75	22.65	19.40	19.67
PET: RH (50:50)	16.76	16.48	16.53	14.47
PET: RH (25:75)	15.72	14.72	15.66	14.45

PET: RH (75:25)	17.64	18.34	17.91	17.54
RH: HDPE (0:100)	30.2	29.7	29.2	26.85
RH: HDPE (20:80)	28.5	29.1	28.4	26.22
RH: HDPE (35:65)	25.5	24.8	26.2	22.95
RH: HDPE (50:50)	23.1	23.7	22.5	20.16

4.3 Thermal Analysis by TGA and DTG Method

The RH, LDPE, HDPE, and PET degradation processes for all three samples are shown in the data. But at this moment, the baseline weight of each sample had only been lowered by 0.2% to 5.40%. The weight loss during the second stage of the volatile area degradation process, which takes place at higher temperatures between 200 and 500°C, ranges from 43% to 82%. The third stage, which happens at temperatures between 500 and 600°C, results in weight loss between 1 and 10% at the conclusion of the thermal process. The following tables (4.4, 4.5, 4.6, and 4.7) for RH, LDPE, PET, and HDPE describe thermal characterization.

Table 4.4 Thermal stages of rice husk (RH) in TGA analysis.

	First level			**Second level**			**Third level**		
β (°C min^{-1})	Start	End	Weight Loss (%)	Start	End	Weight Loss (%)	Start	End	Weight Loss (%)
10	30.2	91.2	4	243.7	383.3	48	402	793	14
20	31.8	92.1	5.5	248	385	45	393	604	10
30	30.15	99	5	266	397	44	401	592	9.4
40	30.19	105	3.7	273	402	43	415	600	8

Start is the temperature at which the specified breakdown process begins. End describes the temperature at which the specified breakdown stage comes to an end.

Table 4.5 Thermal stages of low-density polyethylene (LDPE) in TGA analysis

	First level			Second level			Third level		
β	Start	End	Weight	Start	End	Weight	Start	End	Weight
(°C min^{-1})			Loss (%)			Loss (%)			Loss (%)
10	30.8	100	0.2	412	493	82.4	510	796	2.3
20	31.7	82.8	0.6	437	503	53	513	605	1.3
30	31.7	108	1	439	515	54	521	600	1.1
40	31.7	130	1.2	431	522	65	529	601	1

The temperature at which the specified breakdown process begins is referred to as "start." End is a term used to describe the temperature at which a certain decomposition stage ends.

Table 4.6 Thermal stages of polyethylene terephthalate (PET) in TGA analysis.

	First level			Second level			Third level		
β	Start	End	Weight	Start	End	Weight	Start	End	Weight
(°C min^{-1})			Loss (%)			Loss (%)			Loss (%)
10	30.1	97	1	390	467	80.2	491	798	3.5
20	30.2	91.3	0.2	438	506	63	513	597	1.5
30	30.4	99	0.4	414	486	78.1	492	606	3
40	30.12	97	0.3	418	493	81.8	507	599	2.6

Start refers to the temperature at the start of the stated decomposition process. End refers to the temperature at the end of the stated decomposition stage

Table 4.7 Thermal stages of High-density polyethylene (HDPE) in TGA analysis.

	First level			Second level			Third level		
β	Start	End	Weight	Start	End	Weight	Start	End	Weight
(°C min^{-1})			Loss (%)			Loss (%)			Loss (%)
10	31.1	99	0.3	398	460	82.2	500	608	2.5
20	31.5	95.3	0.4	420	506	72.1	530	597	1.3
30	31.7	100	0.3	434	497	80.1	504	606	2,8
40	31.6	102	0.2	440	513	78.8	510	599	2.2

Start refers to the temperature at the start of the stated decomposition process. End refers to the temperature at the end of the stated decomposition stage

4.3.1 Weight loss analysis of feedstocks

The DTG curve's first and second absorption peaks corresponded to the weight loss peaks of the hemicellulose and cellulose decompositions. **Figure 4.1 (a-f)** displays the temperature-dependent DTG analysis of RH, LDPE, and PET at four distinct heating

speeds (10, 20, 30, and 40 °C/min). At lower temperatures, the rate of mass loss is quite modest; nevertheless, it increases during the second stage of the process. Due to char production at 500 °C, the mass loss rate is once again modest. The DTG peaks are visible in the RH sample at 356, 369,376 and 381°C at heating rates of 10, 20, 30 and 40 °C/min in the second stage of degradation and LDPE at temperature peak at 480, 492,498 and 505 °C and polyethylene terephthalate at a peak temperature of 440, 454, 466 and 469°C respectively. The DTG peak's location and size are influenced by the pace of heating. Degradation requires a higher temperature, as fig. 4.1 (a–f) illustrates. A greater heating rate leads the peak to move towards a higher temperature because the reaction time is shorter [19]. The TGA and DTG curves of common biomasses as sawdust, seaweed, almond fruit, and garlic husk have been seen to exhibit comparable observational tendencies [20, 21]. Peak decomposition temperatures are 307°C, 314.54°C, 320.81°C, and 330.86°C for the heating rates of 5°C, 10°C, 15°C, and 20°C/min, respectively. The breakdown processes of RH, LDPE, and PET appear to follow a multi-step kinetic reaction mechanism with several inflection points, according to the TG and DTG graphs. Raising the heating rate did not appear to have any influence on the mass and loss quantities or the form of DTG profiles, based on the little increase in peak temperatures [20]. This increase in maximum decomposition temperature with increasing heating rate might be attributable to increased heat transport constraints. A high heating rate indicates that the biomass is heated unevenly across its volume due to the short period it is maintained at a given temperature. As a result, higher heating rates and a higher temperature are needed to complete the degradation of the same amount of biomass [22].

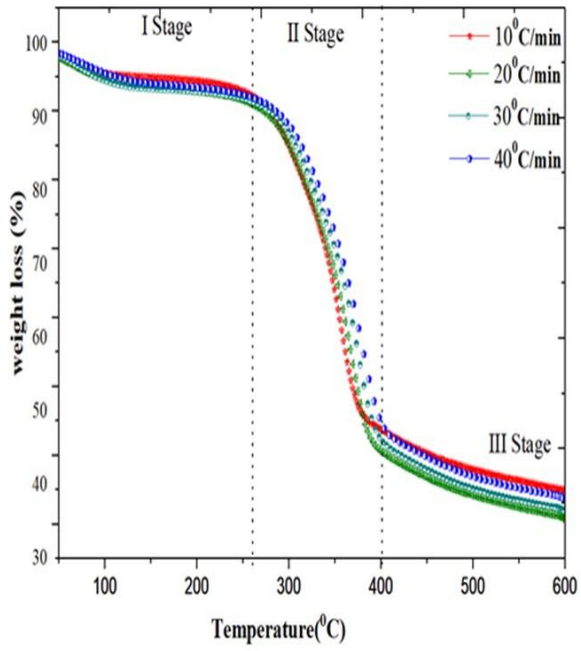
I Stage
II Stage
III Stage
10⁰C/min
20⁰C/min
30⁰C/min
40⁰C/min
weight loss (%)
Temperature(⁰C)

(a)

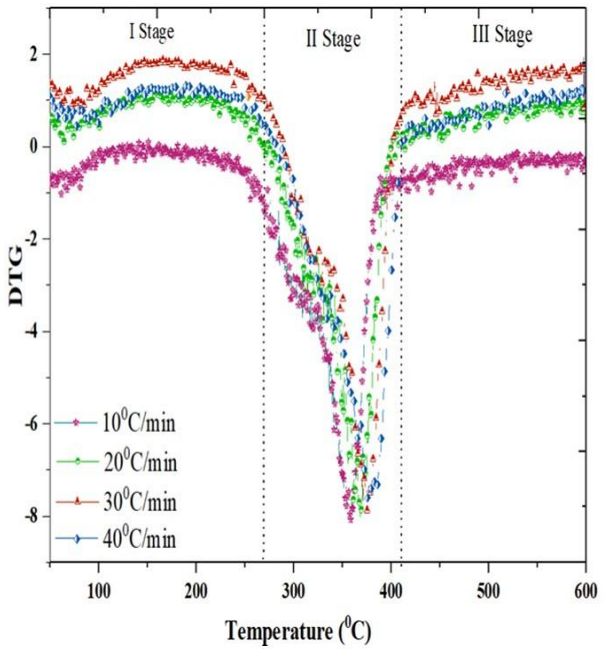
I Stage
II Stage
III Stage
10⁰C/min
20⁰C/min
30⁰C/min
40⁰C/min
DTG
Temperature (⁰C)

(b)

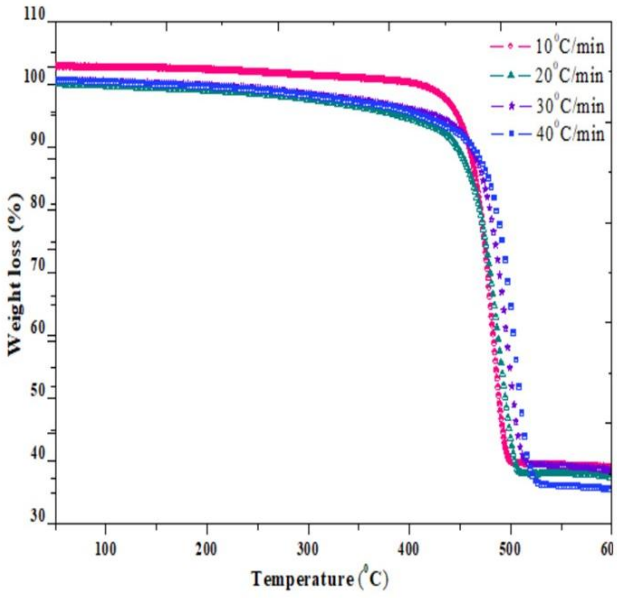
10°C/min
20°C/min
30°C/min
40°C/min
Weight loss (%)
Temperature (°C)

(c)

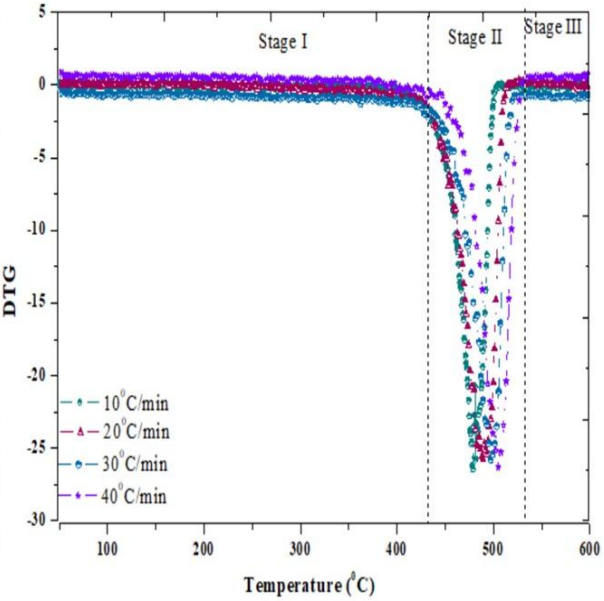
Stage I
Stage II
Stage III
10°C/min
20°C/min
30°C/min
40°C/min
DTG
Temperature (°C)

(d)

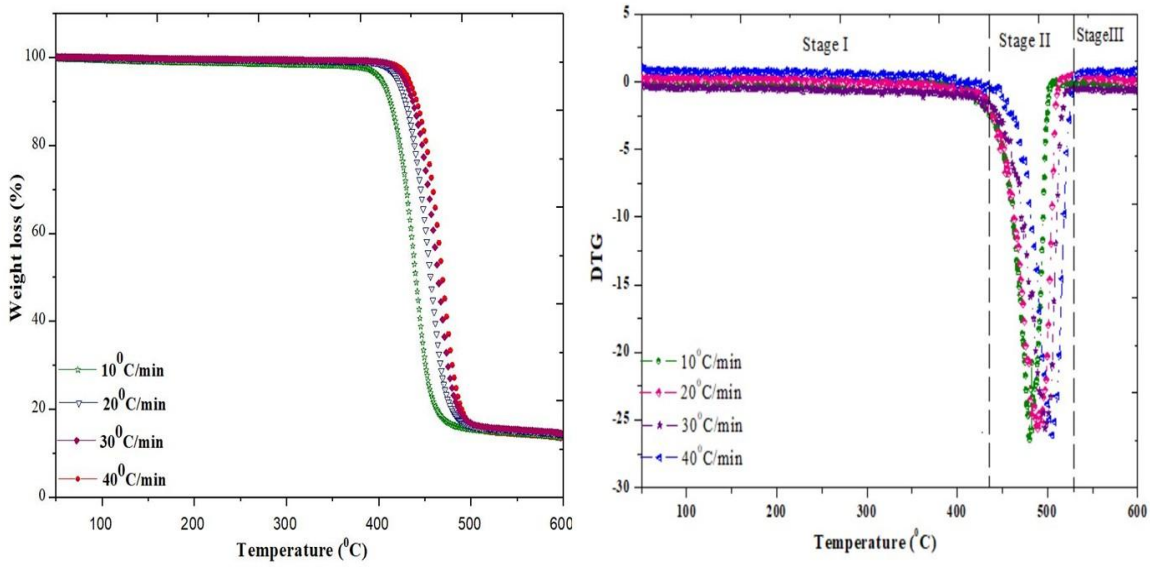

(e) **(f)**

Figure 4.1 (a) TGA and (b) DTG graph of Rice husk at 10, 20, 30 and 40℃/min.(c) TGA and (d) DTG graph of LDPE at 10, 20, 30 and 40℃/min. (e) TGA and (f) DTG graph of PET at 10, 20, 30 and 40℃/min

4.4 Kinetic analysis

The kinetics analysis used to determine activation energy is shown in Figs. 4.2, 4.3, and 4.5 below. The thermal behaviour of RH, LDPE, and PET was investigated kinetically using iso-conversional techniques. The Flynn wall Ozawa, Kissinger Akahira Sunose, Friedman, Starink, and Tang iso-conversional models were used to analyse the TGA data at different heating rates between 10 and 40 °C/min. These methods were applied to examine the effects of different kinetic variables on the variation in activation energy levels. Equations (7), (8), (9) (10) and (11) were used to calculate the slopes of the plots against (1/T, weight loss) to get the kinetic parameter in the conversion range of 0.2 to 0.8. Tables 4.8, 4.9, and 4.10 provide the activation energy values for each conversion level as well as the associated average values for each of the five models [11].

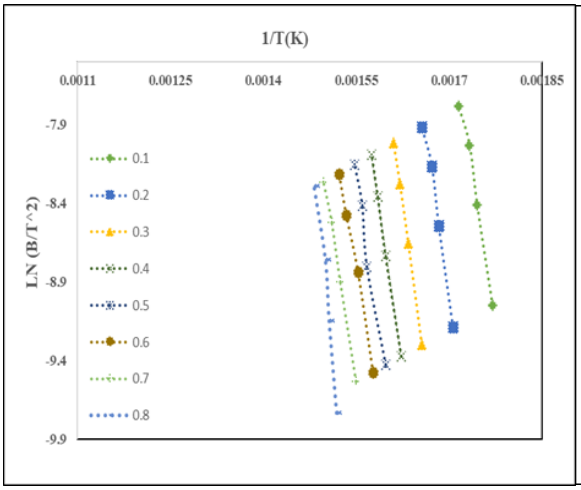

(a) KAS Method

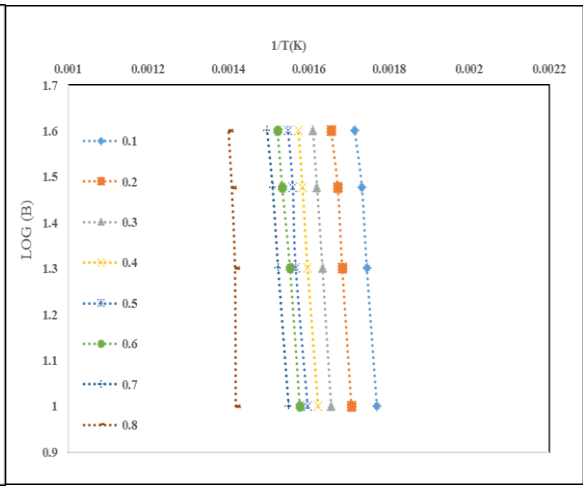

(b) FWO Method

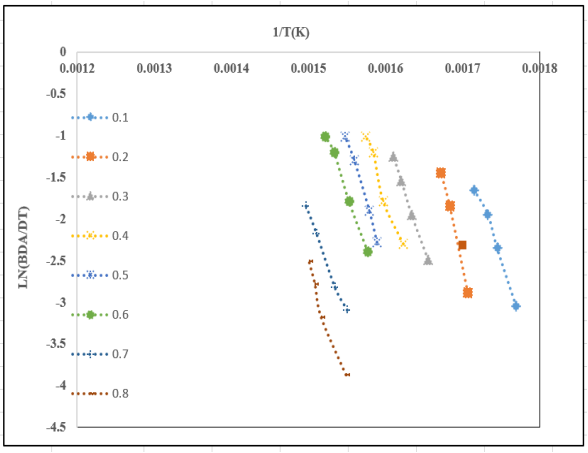

(c) FM Method

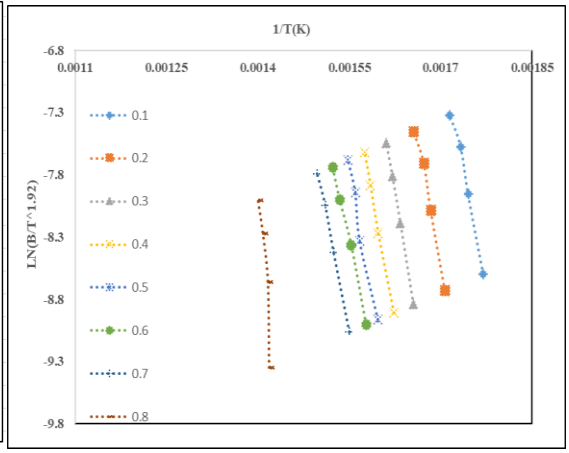

(d) Starink Method

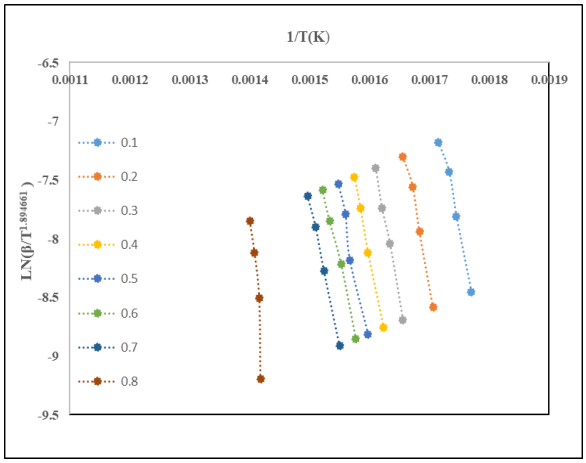

(e) Tang Method

Figure 4.2 Kinetics graph of RH with 5 different methods

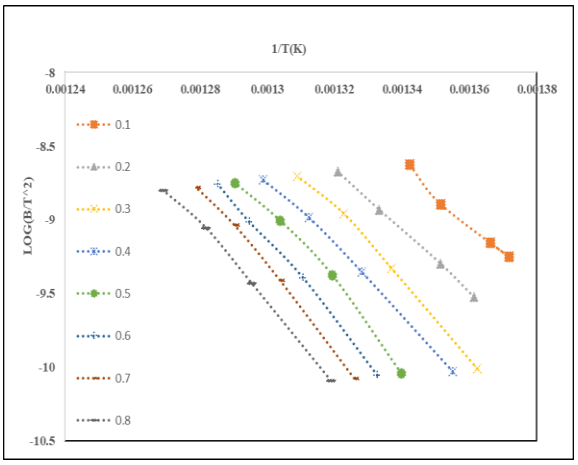

(a) KAS Method

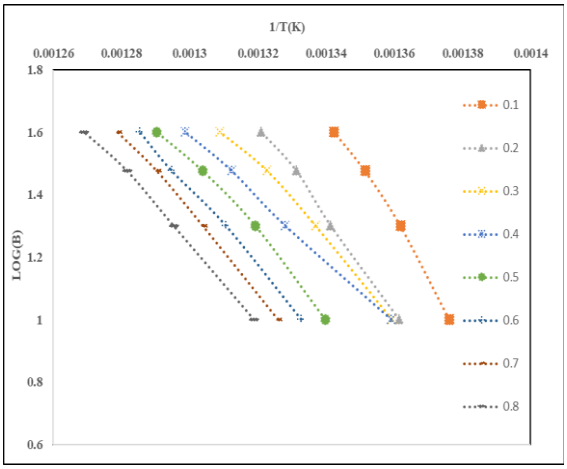

(b) FWO Method

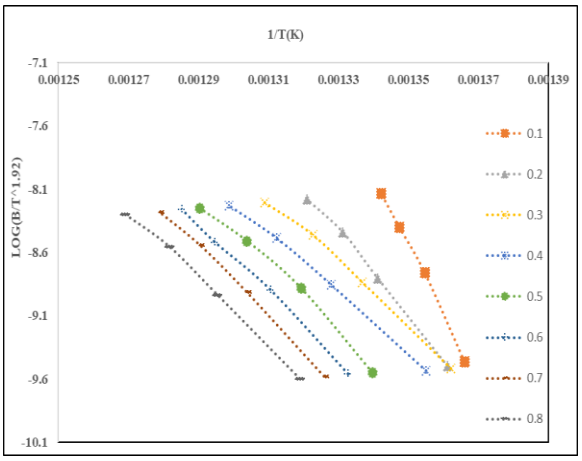

(c) FM Method

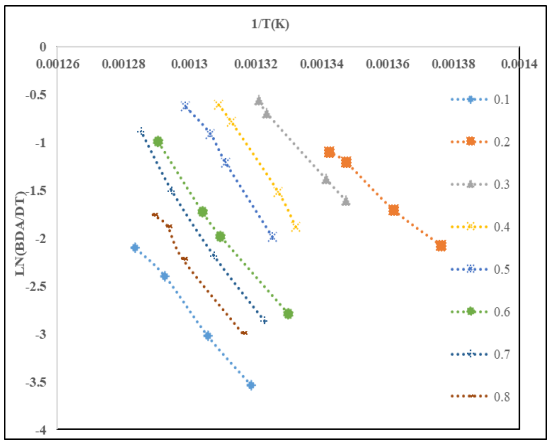

(d) Starink Method

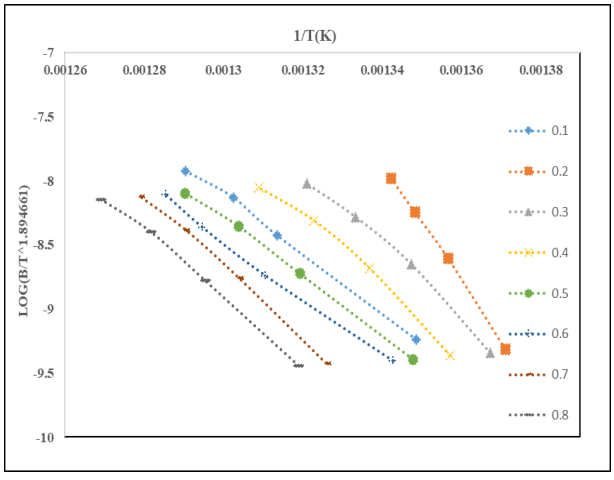

(e) Tang Method

Figure 4.3 Kinetics graph of LDPE with 5 different methods

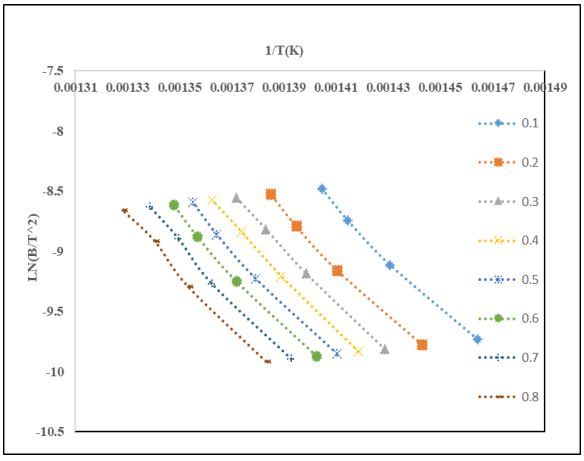

(a) KAS Method

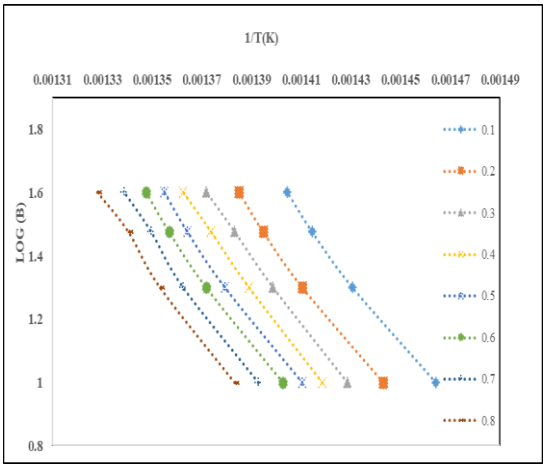

(b) FWO Method

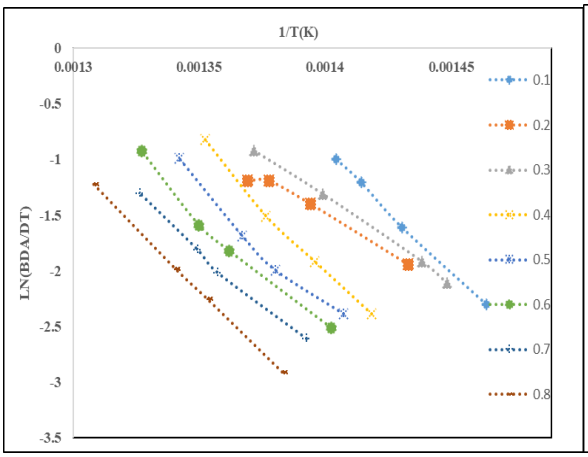

(c) FM Method

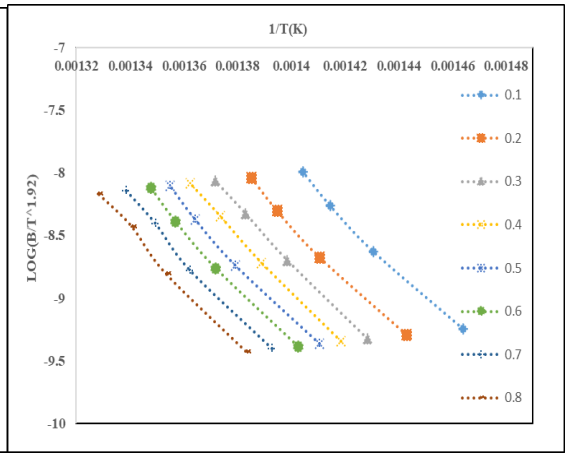

(d) Starink Method

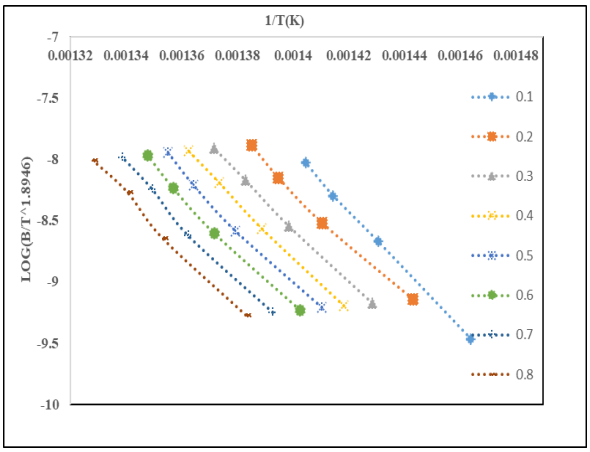

(e) Tang Method

Figure 4.4 Kinetics graph of PET with 5 different methods

Table 4.8 Thermal degradation kinetics analysis of RH using iso-conversional methods

	Differential method						Integral method			
Conversion	FWO		Friedman		KAS		Starink		Tang	
	E_a (kJ mol^{-1})	R^2	E_a (kJ mol^{-1})	R^2	E_a (kJ mol^{-1})	R^2	E_a (kJ mol^{-1})	R^2	E_a (Kj mol^{-1})	R^2
0.1	106	0.99	118	0.99	116	0.99	107	0.98	119	0 .99
0.2	118	0.99	119	0.99	117	0.99	110	0.99	113	0.99
0.3	113	0.99	122	0.98	121	0.99	112	0.99	118	0.99
0.4	112	0.99	124	0.99	112	0.99	110	0.99	119	0.99
0.5	117	0.99	127	0.99	118	0.99	108	0.98	118	0.99
0.6	111	0.99	130	0.97	117	0.97	107	0.99	119	0.99
0.7	108	0.99	131	0.98	110	0.98	108	0.99	117	0.99
0.8	119	0.99	133	0.98	122	0.98	119	0.96	113	0.99
Average	113	0.98	123	0.98	120	0.98	117	0.97	121	0.99

Table 4.9 Thermal degradation kinetics analysis of low-density polyethylene using iso-conversional methods.

	Differential method						Integral method			
Conversion	FWO		Friedman		KAS		Starink		Tang	
	E_a (kJ mol^{-1})	R^2	E_a (kJ mol^{-1})	R^2	E_a (kJ mol^{-1})	R^2	E_a (kJ mol^{-1})	R^2	E_a (kJ mol^{-1})	R^2
0.1	102	0.99	103	0.99	106	0.99	104	0.98	109	0.99
0.2	110	0.99	105	0.99	108	0.99	103	0.99	103	0.99
0.3	112	0.99	106	0.98	105	0.99	110	0.99	106	0.99
0.4	110	0.99	104	0.99	104	0.99	105	0.99	107	0.99
0.5	108	0.99	101	0.99	107	0.99	106	0.98	108	0.99
0.6	107	0.99	105	0.97	101	0.97	107	0.99	104	0.99
0.7	114	0.99	110	0.98	108	0.98	108	0.99	109	0.99
80.8	113	0.99	103	0.98	101	0.98	109	0.96	107	0.99
Average	109	0.98	103	0.98	105	0.99	106	0.97	101	0.98

Table 4.10 Thermal degradation kinetics analysis of polyethylene terephthalate using iso-conversional methods.

	Differential method				Integral method					
Conversion	FWO		Friedman		KAS		Starink		Tang	
	E_a (kJ mol^{-1})	R^2	E_a (kJ mol^{-1})	R^2	E_a (kJ mol^{-1})	R^2	E_a (kJ mol^{-1})	R^2	E_a (kJ mol^{-1})	R^2
0.1	115	0.99	108	0.99	119	0.99	119	0.99	117	0.99
0.2	117	0.99	103	0.99	120	0.99	117	0.99	113	0.99
0.3	112	0.99	102	0.99	123	0.99	110	0.99	114	0.99
0.4	111	0.99	101	0.99	116	0.99	112	0.99	117	0.99
0.5	115	0.99	105	0.99	117	0.99	114	0.99	116	0.99
0.6	117	0.99	110	0.97	118	0.97	116	0.99	119	0.99
0.7	102	0.99	109	0.98	110	0.98	118	0.99	119	0.99
0.8	100	0.99	108	0.98	119	0.98	110	0.99	115	0.99
Average	111	0.98	105	0.98	117	0.98	114`	0.99	115	0.98

A detailed explanation of Tables 4.8, 4.9, and 4.10 and Figures 4.2,4.3, and 4.4 shows that activation energy values are obtained using both differential and integral-based methods. In addition to differential-based approaches like the Friedman method and the FWO (Flynn-Wall-Ozawa) method, this inquiry employed integral-based techniques, including the KAS (Kissinger-Akahira-Sunose), Starink, and Tang methods. The average activation energy values of polyethylene terephthalate, low-density polyethylene, and rice husk were determined using the FWO approach. The results showed that the values were, in order, 113 kJ/mol, 109 kJ/mol, and 111 kJ/mol. These findings suggest that because LDPE and PET require less activation energy during the pyrolysis process, they are better choices as feedstock. The Friedman technique was also used to compute the activation energy values, which came out to be 123 kJ/mol, 103 kJ/mol, and 105 kJ/mol, respectively. 120 kJ/mol, 105 kJ/mol, and 117 kJ/mol were the results of the KAS technique; 117 kJ/mol, 106 kJ/mol, and 114 kJ/mol were the results of the Starink method. The activation energy values of 121 kJ/mol, 101 kJ/mol, and 115 kJ/mol were obtained using the Tang technique. These findings offer a thorough comprehension of the kinetic characteristics and thermal behaviour of RH, LDPE, and PET during pyrolysis.

Furthermore, it can be inferred that by comparing the results obtained from different methods, a more accurate and reliable conclusion can be drawn about the suitability of

these materials as feedstocks for pyrolysis. These results indicate that LDPE and PET are more suitable as feedstock for the pyrolysis process as they have a lower activation energy requirement. When conversions with Ea values between 0.1 and 0.3 show a noticeable rise, the primary pyrolysis process begins. Ea values in the range of 0.3 to 0.8, on the other hand, indicate that the reaction has progressed to the charring stage, which is distinguished by similarly high Ea values. A detailed discussion has also been added in the table on how the activation energy (Ea) varies with the degree of conversion (α). The response mechanism is consistent across all conversion processes, as indicated by the best-fitting curves in Figs. 4.2, 4.3, and 4.4 for conversions between 0.2 and 0.8. The apparent activation energy values gradually increase as the conversion ratio increases, indicating that the apparent activation energy is dependent on both temperature and conversion ratio [23]. The lower Ea observed for LDPE and PET reflects their lower thermal stability and faster degradation kinetics, which contributes to higher liquid yields and enhanced hydrocarbon selectivity during co-pyrolysis. In contrast, the higher Ea of rice husk correlates with slower devolatilization and greater char formation due to its lignocellulosic composition. These kinetic differences also impact reactor design considerations, such as heating rate requirements and residence time optimization.

4.5 Error calculation

Standard error (SE) for different methods applied can be calculated using the following equation:

Standard error (SE) = Standard deviation (SD)/ $\sqrt{n}$

Where,

Standard deviation (SD) =$\sqrt{\frac{1}{(n-1)}} \sum_{i=1}^{n} (X_i - \mathrm{X})^2$

where X is the mean value of total inputs, n is the number of methods/ observation.

Table 4.11: Mean activation energy (Ea), standard deviation (SD), and standard error (SE) calculated for different kinetic methods applied in the analysis of thermal degradation. The standard error quantifies the variability of the mean activation energy estimate, based on eight conversion points (α = 0.1–0.8).

Method	Mean Ea (kJ/mol)	SD	SE
FWO	113	4.33	1.53
Friedman	123	5.1	1.8
KAS	120	4.2	1.48
Starink	117	4.15	1.47
Tang	121	2.54	0.9

Through Table 4.11 the standard deviation (SD) of activation energy provides insight into the consistency and reliability of a kinetic method across varying conversion levels. Among the methods evaluated, the Tang method exhibited the lowest standard deviation (2.54 kJ/mol), indicating a high level of consistency in the activation energy values across the conversion range (α = 0.1 to 0.8). In contrast, the Friedman method showed the highest SD (5.10 kJ/mol), suggesting more variability and potentially less robustness in capturing uniform kinetic behavior. A lower SD reflects greater stability and reliability of the method, making the Tang method more suitable for kinetic studies where consistent activation energy is critical. Therefore, based on statistical variation, the Tang method appears to offer a more accurate and reproducible estimation of activation energy in this study.

4.6 Pyrolysis Performance Index (CPI)

The comprehensive pyrolysis index (CPI) improved significantly with increasing heating rate; it was found that increasing heating rate is favorable for pyrolysis, it is given below in Table 4.11. The entire volatile release index (CPI) of RH, LDPE, and PET at 600 °C in N_2 atmospheres was 0.4 to 4.5 and 2.02 to 8.5 and 1.6 to 7.5 times that of the reactions in the whole process, respectively. In other words, it was more conducive to the pyrolysis of

all the samples at 600 °C. R_a (Average decomposition rate), R_m (maximum decomposition rate) and CPI values all significantly increased, indicating that the high heating rate improves pyrolysis performance. The CPI index is calculated by using equation [20]. CPI of RH, PET and LDPE has been discussed below in **Table 4.12**.

Table 4.12 CPI analysis of three different samples at four different heating rates.

Sample	β	Ti	Tp	Ra	Rm	$\Delta T_{1/2}$	CPI
RH	10	215.2	356.2	-1.12	-8.10	87.3	0.4
	20	272.9	369.4	-2.16	-15.3	81.7	1.5
	30	279.5	376.2	-3.19	-22.3	75.7	3.4
	40	292.6	381.5	-4.29	-28.08	78.9	4.5
PET	10	383.5	440.29	-1.48	-20.5	37.5	1.6
	20	405.5	454.04	-2.91	-41.09	38.2	2.4
	30	412.3	466.17	-4.26	-63.7	37.2	5.5
	40	424.8	469.59	-5.66	-84.7	38.11	7.5
LDPE	10	414.02	480.7	-1.518	-26.32	38.2	2.02
	20	431.5	492.7	-2.120	-27.7	51.8	3.61
	30	439.1	498.01	-3.067	-46.07	48.02	5.1
	40	448.7	505.2	-4.203	-64.9	45.9	8.5

4.7 Analysis of Thermodynamic Parameters

The thermodynamic parameters and their interaction may be a good way to characterize different stages of biomass breakdown. For each model-free iso-conversional strategy, the thermodynamic parameters were obtained using the equations presented in Chapter 3.

For each model, the variance of the change in the values of enthalpy (ΔH) and Gibbs free energy (ΔG) has been computed. In a chemical process, the change in enthalpy (ΔH) represents the energy difference between the reactants and products. It also shows if the process is endothermic or exothermic. The activation energy and the change in enthalpy in this study have a relatively modest energy difference (~ 5 kJ/mol), which indicates that the chemical reaction is happening quickly. The modest discrepancy between activation energy (Ea) and enthalpy (H), which suggests that the products may be synthesized with minimal additional energy, facilitates the synthesis of activated complexes [24]. The highest amount of work is found using the change in Gibbs free energy (G) of any system at a given temperature and pressure. The amount of energy that a biomass sample may produce is shown by a thermodynamic "state function" [25]. Table 9, given below, illustrates the frequency factor and thermodynamic triplets of the selected samples.

A closed analysis of parameters which was given in **Table 4.13**, it indicated that a change in entropy (ΔS) value indicates that the material has crossed the energy barrier and is approaching equilibrium. The material is less reactive in this state, and product formation takes a long time. Conversely, a high (S) value denotes a fast-reacting substance that yields a product faster [26]. It is shown that the breakdown process tends to become more chaotic when ΔS tends to take on positive values. Most of this can be attributed to the devolatilization phase, which requires progressively more energy input until all volatiles separate from the solid. The reaction experiences reduced resistance because of lower degrees of disorderliness, as evidenced by the negative ΔS values at lower conversions, which are in keeping with earlier findings [27]. The minimum entropy indicated less disorder during the reaction. The results for distinct thermodynamic parameters that were calculated using five different iso-conversional model-free approaches were very similar, which supports the validity of the thermodynamic study and the findings. These data and results, which relate modifications in thermodynamic parameters to many stages of the breakdown process, allow a detailed investigation of the pyrolysis reaction. The DTG analysis of the thermodynamics characterization is shown in **Table 4.12** below.

Table 4.13 Thermodynamic parameters of all three samples with five different methods.

Methods	The conversion used during the analysis was from 0.1 to 0.8											
	RICE				LDPE				PET			
	A	ΔH	ΔG	ΔS	A	ΔH	ΔG	ΔS	A	ΔH	ΔG	ΔS
KAS	3.7E+15	114	130	-0.062	3.6E+11	100	116	-0.038	2.6E+8	111	126	-0.052
FWO	2.9E+17	107	124	-0.066	1.7E+10	103	119	-0.047	2.8E+10	105	116	-0.049
FRIED-MAN	5.5E+16	118	137	-0.074	1.2E+16	98	117	-0.040	2.7E+11	100	118	-0.055
STARINK	7.6E+15	111	129	-0.070	1.5E+19	101	115	-0.042	2.5E+10	98	114	-0.065
TANG	6.4E+15	115	135	-0.078	2.4E+13	95	105	-0.050	2.1E+9	109	126	-0.057

ΔH-kJ/mol; ΔG-kJ/mol; ΔS-kJ/mol K.

4.8 Conclusions

This study provides valuable insights into the thermal breakdown characteristics of various wastes at different heating rates by utilizing both differential and integral techniques to quantify the kinetic parameters, such as activation energy and pre-exponential factor. For RH, LDPE, and PET, the average activation energy values were determined using the five different methods. The resulting ranges of values were, in order, 113-123 kJ/mol, 101-109 kJ/mol, and 105-117 kJ/mol. In light of their lower activation energy consumption, our findings indicate that PET and LDPE provide superior feedstock options for the pyrolysis process. The ranges of 99.4–113 kJ/mol, 105–131 kJ/mol, and -0.043–-0.07 are reported for the average value of thermodynamic triplets, ΔH, ΔG, and ΔS, respectively. This suggests that the reaction is non-spontaneous and endothermic. Additionally, the parameters of thermodynamic parameters and pyrolysis performance index of all three samples were thoroughly analysed by kinetics. This kinetic analysis of all materials used in this work is significant and helpful for designing a contemporary pyrolysis reactor.

4.9 References

1. Khan, M. Z. H., Sultana, M., Al-Mamun, M. R., & Hasan, M. R. (2016). Pyrolytic waste plastic oil and its diesel blend: fuel characterization. *Journal of environmental and public health*, *2016*(1), 7869080.

2. Bridgwater A V, (2003), Renewable fuels and chemicals by thermal processing of biomass, Chemical Engineering Journal, vol. 91, no. 2-3, pp. 87-102,https://doi.org/10.1016/S1385-8947(02)00142-0.

3. Zhang L, Xu C, and Champagne P, "Overview of recent advances in thermo-chemical conversion of biomass (2010), Energy Conversion and Management, vol. 51, no. 5, pp. 969 982, https://doi.org/10.1016/J.ENCONMAN.2009.11.038

4. NPTEL, Thermogravimetric analysis," http://nptel.ac.in/courses/115103030/21 accessed on 29th April 2018, 2016

5. Mishra, R.K., and Mohanty, K., 2020. Kinetic analysis and pyrolysis behavior of waste biomass towards its bioenergy potential. Bioresour. Technol. 311, 123480 https:// doi.org/10.1016/j.biortech.2020.123480.

6. Choudhary, M., Kumar Jain, S., Singh, ., Srivastava, K., Patel, A.K., Mahlknecht, J., Giri, B.S., Kumar, M., (2023). Determination of thermal degradation behavior and kinetics parameters of chemically modified sun hemp biomass. Bioresource Technology 380, 129065. https://doi.org/10.1016/j.biortech.2023.129065

7. Wang, Y., Ge, Z., Shang, F., Zhou, C., Guo, S., and Ren, C. (2023). Kinetic analysis of CO2 gasification of corn straw. *Renewable Energy*, *203*, 219-227.

8.Pal, D.B., Tiwari, A.K., Prasad, N., Srivastava, N., Almalki, A.H., Haque, S., and Gupta, V.K., (2022). Thermo-chemical potential of solid waste seed biomass obtained from plant Phoenix dactylifera and Aegle marmelos L. Fruit core cell. Bioresour. Technol. 345, 126441 https://doi.org/10.1016/j.biortech.2021.126441.

9.Barr, M.R., Volpe, M., Messineo, A., Volpe, R., (2020). On the suitability of thermogravimetric balances for the study of biomass pyrolysis. Fuel 276, 118069. https://doi.org/10.1016/j.fuel.2020.118069.

10. Sukarni, S., Prasetiyo, A., Fidiah, L., Permanasari, A. A., and Puspitasari, P. (2021, September). Kinetics and thermodynamics study of organic waste combustion using thermogravimetric analysis. In *IOP Conference Series: Earth and Environmental Science* (Vol. 847, No. 1, p. 012015). IOP Publishing.

11. Keattch, C. J. (1996). Studies in the history and development of thermogravimetry. *Journal of Thermal Analysis and Calorimetry*, *46*(5), 1501-1505.

12. Acquah, G. E., Via, B. K., Fasina, O. O., Adhikari, S., Billor, N., and Eckhardt, L. G. (2017). Chemometric modeling of thermogravimetric data for the compositional analysis of forest biomass. *PloS one*, *12*(3), e0172999.

13. Cai, J., Xu, D., Dong, Z., Yu, X., Yang, Y., Banks, S. W., and Bridgwater, A. V. (2018). Processing thermogravimetric analysis data for isoconversional kinetic analysis of lignocellulosic biomass pyrolysis: Case study of corn stalk. *Renewable and Sustainable Energy Reviews*, *82*, 2705-2715.

14. Kumar, M., Sabbarwal, S., Mishra, P. K., & Upadhyay, S. N. (2019). Thermal degradation kinetics of sugarcane leaves (Saccharum officinarum L) using thermo-gravimetric and differential scanning calorimetric studies. *Bioresource technology*, *279*, 262-270.

15. Ozawa T, (1965), A new method of analyzing thermogravimetric data. Bull Chem Soc Jpn , 38:1881–1886, https://doi.org/10.1246/bcsj.38.1881

16. Akahira T, and Sunose T, (1971) Method of determining activation deterioration constant of electrical insulating materials. Res Report Chiba Inst Technol,, 16:22–23, https://doi.org/10.1016/j.softx.2019.100359

17. Singh, R. K., and Ruj, B. (2016). Time and temperature depended fuel gas generation from pyrolysis of real world municipal plastic waste. *Fuel*, *174*, 164-171.

18. Zhang, J., Liu, J., Evrendilek, F., Zhang, X., & Buyukada, M. (2019). TG-FTIR and Py-GC/MS analyses of pyrolysis behaviors and products of cattle manure in CO2 and N2 atmospheres: Kinetic, thermodynamic, and machine-learning models. *Energy Conversion and Management*, *195*, 346-359.

19. Chen, W., Escalante, J., Chen, W., Tabatabaei, M., & Tuan, A. (2022). Pyrolysis of lignocellulosic , algal , plastic , and other biomass wastes for biofuel production and circular bioeconomy : *Renewable and Sustainable Energy Reviews*, *169*(September), 112914. https://doi.org/10.1016/j.rser.2022.112914

20.Olszak-Humienik, M., & Mozejko, J. (2000). Thermodynamic functions of activated complexes created in thermal decomposition processes of sulphates. *Thermochimica acta*, *344*(1-2), 73-79.

21. Agnihotri, N., Gupta, G.K., Mondal, M.K., 2022. Thermo-kinetic analysis, thermodynamic parameters and comprehensive pyrolysis index of Melia azedarach sawdust as a genesis of bioenergy. Biorefinery Biomass Convers. https://doi.org/ 10.1007/s13399-022-02524-y.

22. Singh, R.K., Patil, T., Sawarkar, A.N., 2020b. Pyrolysis of garlic husk biomass: physicochemical characterization, thermodynamic and kinetic analyses. Bioresour. Technol. Reports 12, 100558. https://doi.org/10.1016/j.biteb.2020.100558.

23. Nawaz, A., Kumar, P., 2022. Pyrolysis behavior of low value biomass (Sesbania bispinosa) to elucidate its bioenergy potential: Kinetic, thermodynamic and prediction modelling using artificial neural network. Renew. Energy 200, 257–270. https://doi. org/10.1016/j.renene.2022.09.110.

24. Vyazovkin, S., Burnham, A.K., Favergeon, L., Koga, N., Moukhina, E., P´erez-Maqueda, L. A., Sbirrazzuoli, N., 2020. ICTAC Kinetics Committee recommendations for

analysis of multi-step kinetics. Thermochimica Acta 689, 178597. https://doi.org/10.1016/j. tca.2020.178597.

25. Kumar, M., Shukla, S. K., Upadhyay, S. N., & Mishra, P. K. (2020). Analysis of thermal degradation of banana (Musa balbisiana) trunk biomass waste using iso-conversional models. *Bioresource technology*, *310*, 123393.

26. Ruvolo-Filho, A., & Curti, P. S. (2006). Chemical kinetic model and thermodynamic compensation effect of alkaline hydrolysis of waste poly (ethylene terephthalate) in nonaqueous ethylene glycol solution. *Industrial & engineering chemistry research*, *45*(24), 7985-7996.

27. Kumar, M., Upadhyay, S. N., and Mishra, P. K. (2020). Effect of Montmorillonite clay on pyrolysis of paper mill waste. *Bioresource technology*, *307*, 123161.

28. Sakthivel, R., Chidambaresh S, Sundarrajan H , Balakrishnan S , Sirohi R , Cao D N and, Hoang A T, 2023, Investigation of thermodynamic and kinetic parameters of Albizia lebbeck seed pods using thermogravimetric analysis, Bioresource Technology 384, 129333.

CHAPTER -5

Thermogravimetric Analysis of Rice Husk and Low-Density Polyethylene Co-Pyrolysis: Kinetic and Thermodynamic Parameters

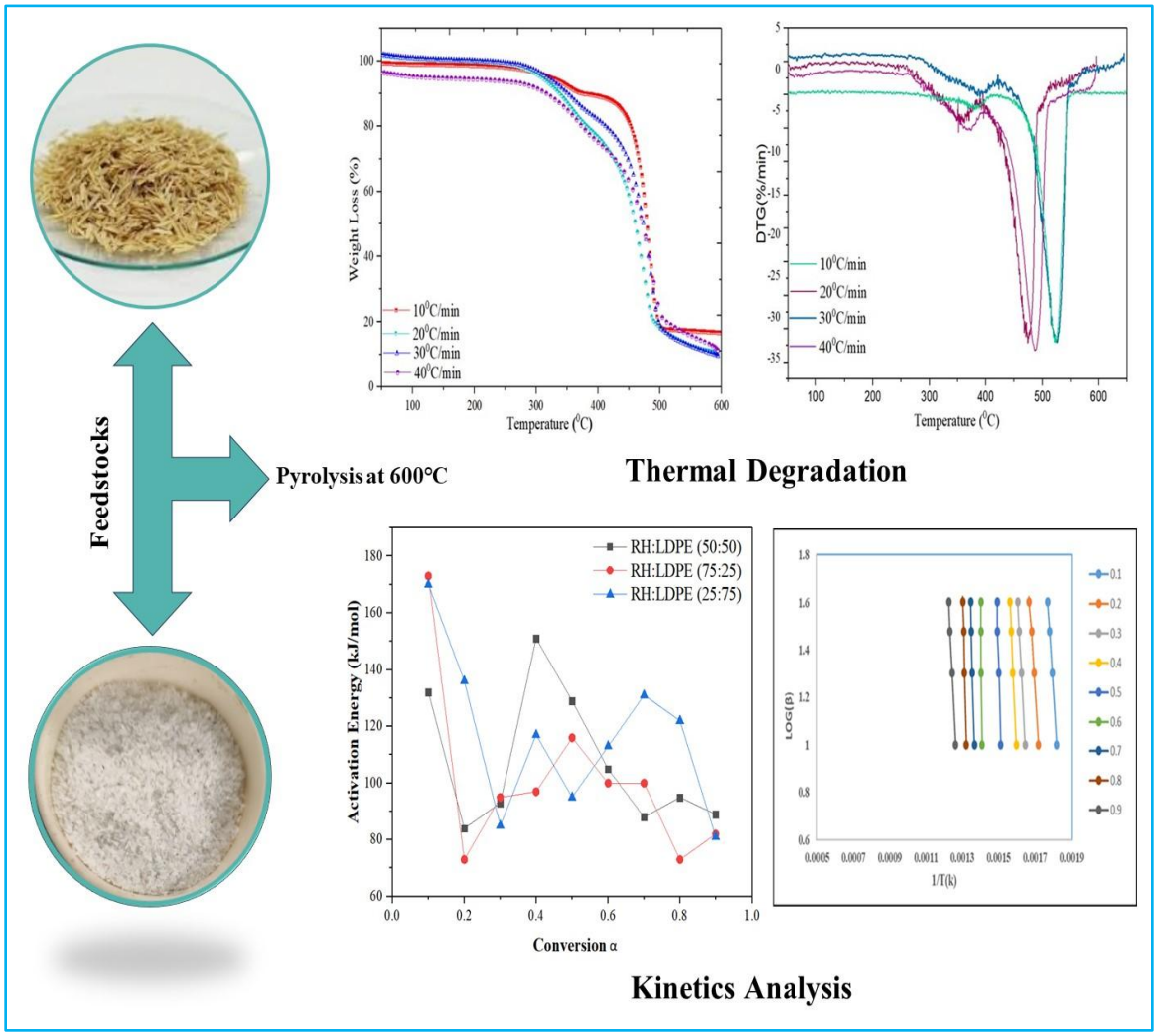

5.1 Introduction

Fossil fuels are employed as a source of energy these days, and due to their dependency on several economic sectors and urbanisation, they now hold a dominant position in the global

energy market [1]. To overcome these issues, researchers from all around the world are creating new renewable resources that will be used as energy fuels [2]. Biomass is a renewable energy source that is both safe and good for the environment [3, 4].

The use of biomass sources as an energy source is the main objective of this effort. Because of the significant yearly production rate of rice husk in Punjab and Haryana, which comes from rice mills in metric tons, rice husk has been selected for this study. The bulk is incinerated or landfilled, with a tiny amount going towards animal feed. We also use plastic waste as a way to lower the environmental carbon footprint. They may be more important in our daily lives than other conventional materials like plastics and biomass (agricultural waste), and their affordability, versatility, and low cost of production make their increasing use acceptable [5]. Since plastic is non-biodegradable and burning it in the open is bad for the environment and people, and illegal plastic dumping concerns the ecosystem. However, in a controlled heating environment, researchers used a thermogravimetric analysis in an inert atmosphere to explore the co-pyrolysis characteristics of blending rice husk with LDPE to learn more about the interactions between the two. Numerous writers have investigated plastic pyrolysis and demonstrated how the technology might be used to try to address plastic waste [6]. The several pyrolysis process types, reactor designs, and operating parameters that impact product quality were all covered in detail by Zamanet al. 2017 [7]. The IAE annual report (2006) covers the larger process of decomposition product creation from agricultural biomass [8]. Thermogravimetric measurements indicate that biomass starts to disintegrate at lower temperatures [9]. However, depending on the kind of plastic, items created with it decompose between 400 and 500°C [10]. In the last several years, thermal gravimetric analysis has been widely employed to control the temperature and time-dependent weight loss in the sample as well as to investigate the thermal outcomes and kinetics related to the breakdown of carbon-based materials.

A thorough grasp of thermogravimetric analysis and de-volatilization kinetics will make planning, building, and managing industrial pyrolysis systems easier [11,12]. One of the easiest methods for assessing the kinetics and thermal breakdowns of the pyrolysis process for solid raw natural resources like plastic and biomass is a thermo-gravimetric

examination [13,14]. Many researchers have investigated the kinetics of pyrolysis processes by calculating certain mass degradation slopes using the Arrhenius equation [15,16]. For analysis and comparison, a thorough investigation of the co-pyrolysis process and the kinetic behaviour of biomass and plastic waste under the same experimental circumstances is therefore essential. an extremely effective technique for examining the dynamics and pyrolytic characteristics of plastics-biomass utilising thermogravimetric (TG) measurement. To properly build and run thermochemical conversion units, one needs to have a solid understanding of the chemistry, pyrolytic characteristics, and kinetics of the basic pyrolysis process [17]. Co-pyrolyzing solid waste with plastic garbage has the potential to improve the quality of the final product [18]. In plastic trash, the H/C ratio is high while the O/C ratio is relatively low. Because co-pyrolysis does not need waste separation, it can ease the co-pyrolysis of solid biomass, which by nature has a high O/C ratio and a low H/C ratio, improving product quality and uniformity and minimizing coke deposition from the pyrolysis of plastic waste [19]. The heating value of oil is greatly increased when LDPE and biomass pyrolysis are combined. The combined pyrolysis of biomass (sugarcane bagasse) and plastic waste resulted in significant HHV (around 40 MJ/Kg) by reducing the quantity of oxygenated molecules. In order to promote liquid formation during co-pyrolysis, low-density polyethylene can act as an H-donor medium [20]. In order to predict the pyrolysis behaviour of a material, design an appropriate reactor, and numerically simulate the reactor for process optimization, it is frequently required to comprehend the pyrolysis kinetics of the primary thermal breakdown process. Process parameters, mass and heat transfer limitations, sample physical and chemical properties, systematic errors, and other variables can all have an impact on the kinetic parameters [21]. The features of co-pyrolysis can be ascertained by kinetic research and thermogravimetric examination. Numerous kinetic models may be used to calculate the kinetic parameters. Burra and Gupta (2018) used the distributed activation energy model (DAEM) to find synergy in the co-pyrolysis of PP and PET with biomass [22]. Oyedun et al. 2018 [9] investigated the co-pyrolysis kinetics of polymers and their blends with biomass. This study demonstrates that the E_a values in the first and second breakdown phases increase

and decrease, respectively, based on the number of plastics in the mixture. Researchers have also used various conversion methods, like the FWO technique and the KAS strategy to forecast the kinetic variables associated with the pyrolysis process [23,24]. To ascertain the distribution of activation energy across the reaction/process, iso-conversational approaches make use of thermal degradation data at various temperatures. Huang evaluated the heat degradation of soybean straw under non-isothermal circumstances using a thermogravimetric analyzer [25]. The kinetic parameters were investigated using three different methodologies: OFW, KAS, and CR. The average Ea was determined to be 154.15 kJ mol-1 using the FWO and KAS procedures [26]. Sugarcane bagasse (SB) physicochemical characteristics and pyrolysis kinetics were investigated in a TGA by Varma and Mondal (2016) using the KAS and FWO systems. The average Ea of SB was reported to be 91.64 and 104.43 kJ mol^{-1}. The kinetic parameters at active heating rates of Prosopis Juli flora fuel wood were studied by Chandrasekaran through thermogravimetric analysis. Several techniques were used to compute the energy needed to activate the pyrolysis, including the Friedman, OFW, Kissinger, and KAS models. The findings revealed that the activation energies were 164.6, 203.2, 204, and 219.3 kJ mol^{-1}, in that order [27]. The intricacy of thermal deterioration at different conversion phases can be explained by a variable activation energy. Despite several studies on biomass kinetics, no effort has been made to determine the kinetics of the co-pyrolysis reaction between LDPE and RH feedstocks to produce useful chemicals and green fuels. Understanding the thermal deterioration and physicochemical properties of RH and LDPE blends was the primary goal of this investigation. The current work employed a thermo-gravimetric analyser to evaluate the physicochemical composition and kinetic properties of a combination of LDPE and RH in an inert environment. Figure 1 shows the entire process.

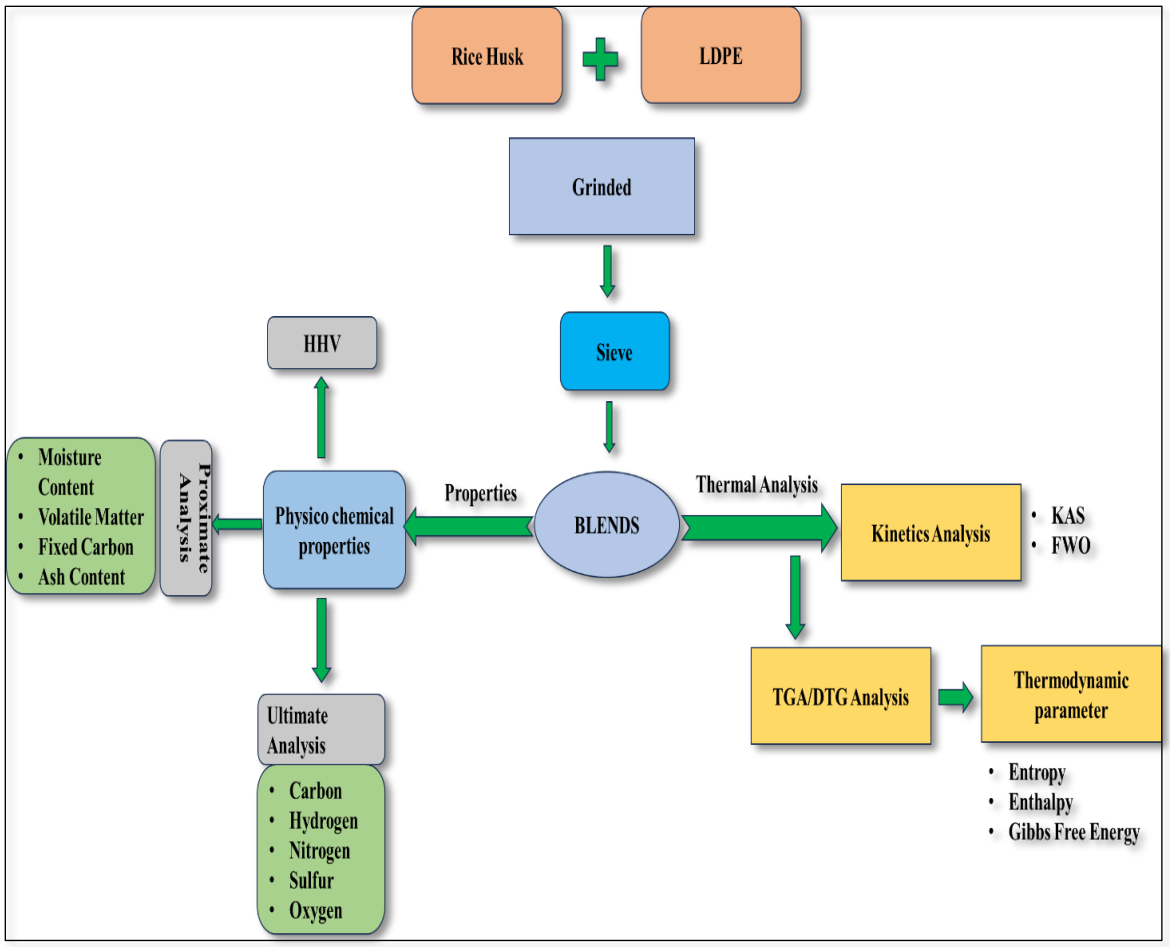

Fig. 5.1 Process flowchart of rice husk and LDPE co-pyrolysis.

The feasibility and benefits of combining LDPE with RH are examined in this study as presented in **Figure 5.1**. After the kinetics parameters were determined by fitting the TGA data at various heating rates, the kinetic parameter (E) was found using two separate techniques: the KAS and FWO methods. To examine whether these samples are suitable as energy feedstock, their activation energy is compared to samples of blended feedstock. Moreover, an extensive investigation was conducted to determine the thermodynamic parameters of blended samples, including variations in enthalpy (ΔH), entropy (ΔS), and Gibbs free energy (ΔG), and how these changes affected the samples' pyrolysis behavior.

5.2 Thermal analysis of the sample

Tables 5.1,5.2 and 5.3 provide information on the weight loss process in three stages of the blended samples RH: LDPE (50:50), RH: LDPE (75:25), and RH: LDPE (25:75) and the amount of weight loss that started initially and increased due to the water content of the biomass components in the mix. Nonetheless, only 1.42% to 4.40% of the sample's initial weight was lost during this initial phase as presented in Fig. 5.2 (a-c). The range temperature 200 to 500°C is the maximum weight loss that the mixture can experience during the 2nd stage of the volatile region degradation process, which occurs when the temperature is higher by 50% to 70%. In the last stage, only 4 to 5% weight loss occurs because of adding LDPE, so the ash content will be low.

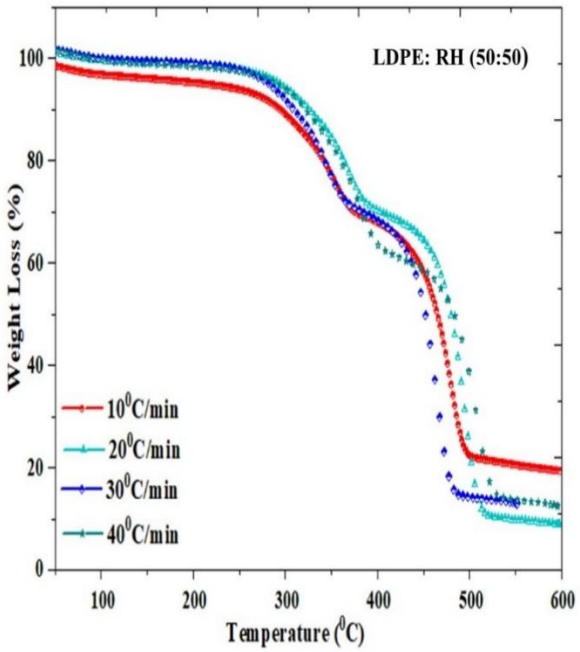

(a)

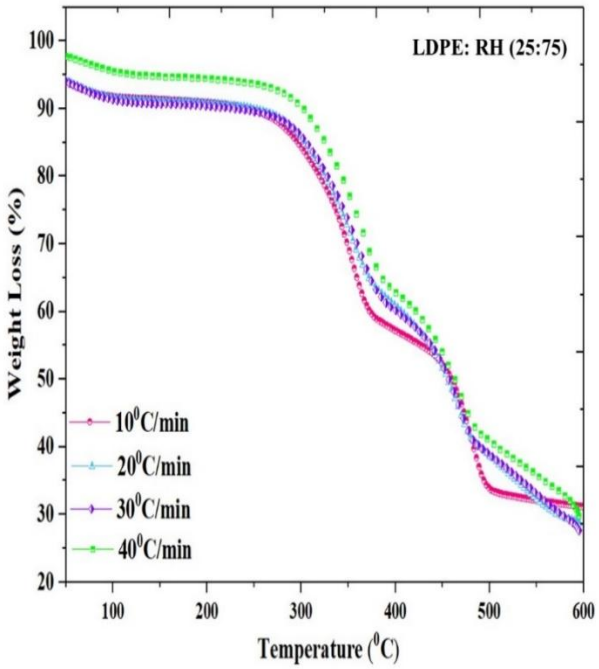

(b)

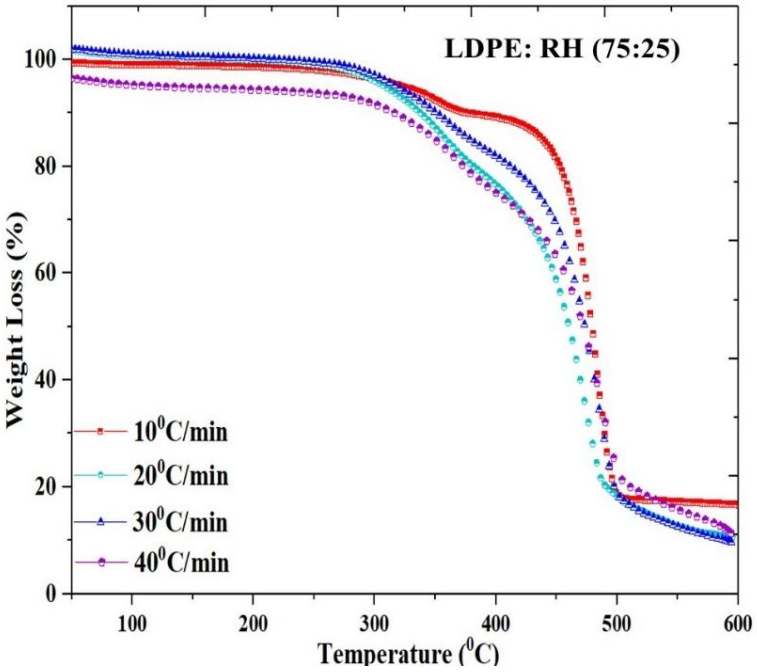

(c)

Figure. 5.2. Thermal analysis of all three graphs (a) LDPE: RH (50:50) (b)LDPE: RH (25:75), (c) LDPE: RH (75:25).

Table 5.1. Thermal process in different temperature ranges of LDPE: RH (50:50)

	First phase			**Second phase**			**Third phase**		
Heating rate (℃/min)	Initial temp	Final temp	Loss in weight (%)	Initial temp	Final temp	Loss in weight (%)	Initial temp	Final temp	Loss in weight (%)
10	30.2	111.3	3.2	271	497	70	499	598	3.11
20	30.8	192	3.0	254	503	56.2	514	600	2.3
30	30.15	210	2.8	261	520	55.4	527	600	1.8
40	31.8	232	2.1	266	522	54.2	525	600	1.53

The start is the initial temperature of a decomposition process that has been indicated. The end is used to describe the final temperature of a decomposition phase.

Table 5.2 Thermal process in different temperature ranges of LDPE: RH (25:75)

	First phase			Second phase			Third phase		
Heating rate (℃/min)	Initial temp	Final temp	Loss in weight (%)	Initial temp	Final temp	Loss in weight (%)	Initial temp	Final temp	Loss in weight (%)
10	30.2	96	3.7	256	500	70	502	599	4
20	31.8	104	3.2	249	510	77	510	600	3.1
30	30.15	107	2.8	266	530	75	530	606	2.4
40	30.19	111	2.1	273	560	76	560	600	2.3

The start is the initial temperature of a decomposition process that has been indicated. The end is used to describe the final temperature of a decomposition phase.

Table 5.3 Thermal process in different temperature ranges of LDPE: RH (75:25)

	First phase			Second phase			Third phase		
Heating rate (℃/min)	Initial temp	Final temp	Loss in weight (%)	Initial temp	Final temp	Loss in weight (%)	Initial temp	Final temp	Loss in weight (%)
10	30.2	91.2	2.1	243	483	56	483	599	4
20	31.8	92.1	1.8	248	485	60	485	598	3.3
30	30.15	99	1.5	266	497	62	497	599	3.1
40	30.19	105	1.2	273	472	68	472	600	2.3

The start is the initial temperature of a decomposition process that has been indicated. The end is used to describe the final temperature of a decomposition phase.

5.3 Kinetic analysis

When co-pyrolyzing plastic and solid biomass, TGA is a commonly employed method to study reaction kinetics and synergistic effects. Understanding how plastic and solid biomass are converted into fuel, as well as optimizing process parameters and designing effective gasification and pyrolysis reactors, all depend on thermal and kinetic analyses of the materials. Additionally, for quantitative kinetic analysis, Ea, A, and n can play a significant role. These findings can subsequently be used in mathematical modeling to create improved reactors [22]. By estimating E_a and A using two distinct techniques, such

as KAS and FWO methods, the kinetic parameter for the pyrolysis process is determined and for kinetic analysis of all three samples, the pyrolysis range is between 200- 600°C. The value of $E_a$in LDPE: RH (50:50) is determined to be 107 kJ/mol from the slope of the KAS plot and 102 kJ/mol from the FWO plot. For the second sample, the LDPE: RH (25:75) has a value of activation energy is 100kJ/mol from KAS and 101kJ/mol from the OFW plot, and the third sample LDPE: RH (75:25) value of Ea is 110kJ/mol for the KAS plot and 117kJ/mol for the FWO plot shown in Figure 5.3 (a-c). Future research ought to take into account the co-degradation of waste plastic, LDPE blends with solid biomass RH as feedstocks, in contrast to current studies, which only look at binary mixtures. It takes time to extract a single recyclable plastic or a single solid biomass fragment from trash, mix the chosen feedstock to create the ideal circumstances for achieving the required co-pyrolysis outcomes, and then leave the resulting combination alone. Therefore, it is necessary to look at multicomponent feedstocks that are comparable to actual garbage mixtures. Consequently, the pyrolysis features of rice husk combined with plastic waste are improved in terms of Ea, heating value, volatile content, and carbon content. Conversely, ashes, nitrogen, sulphur, and moisture show a decline. Low-density polyethylene significantly raises the activation energy, calorific value, and decreased char residues of LDPE: RH (50:50), LDPE: RH (25:75), and LDPE: RH (75:25). The pyrolysis findings of rice husk and plastic waste showed that the thermal characteristics enhanced the performance of the material, resulting in a significant energy release and decreased ash residue. The results of low-density polyethylene pyrolysis and rice husk pyrolysis show that these alternative energy sources may be used as fuel.

Table 5.4 Thermal kinetic Insights: E_a(kJ/mol) and Regression Factors for LDPE: RH (50:50) Using KAS and FWO methods.

	KAS			FWO		
α	**Equation**	**R^2**	**Ea**	**Equation**	**R^2**	**Ea**
0.1	Y=-19962x+43.09	0.99	132	Y = -4074x+25.50	0.99	74
0.2	Y = -10145x+9.84	0.99	84	Y=-3318.2x+11.76	0.99	60

0.3	Y=-11192x+11.53	0.99	93	Y=-5574x+10.22	0.99	101
0.4	Y=-18227x+30.45	0.99	151	Y=- 7148x+39.26	0.99	130
0.5	Y=-15528x+15.57	0.99	129	Y=-8919x+15.68	0.99	162
0.6	Y=-12630x+15.29	0.99	105	Y=-4550x+12.11	0.99	82
0.7	Y=-10602x+5.70	0.99	88	Y=-6312.9x+9.49	0.99	114
0.8	Y=-11435x+9.28	0.99	95	Y= -5928.4x+10.27	0.99	107
0.9	Y=-10739x+11.89	0.99	89	Y=-4743.1x+9.85	0.99	86
Average			**107**			**102**

Table 5.5 Thermal kinetic Insights: E_a(kJ/mol) and Regression Factors for LDPE: RH (25:75) Using KAS and FWO methods.

	KAS			**FWO**		
α	**Equation**	**R^2**	**Ea**	**Equation**	**R^2**	**Ea**
0.1	y=-9361x+23.4	0.99	130	y=-13000x+41.9	0.97	108
0.2	y=-7490x+20.7	0.99	136	y=-13125x+37.2	0.98	109
0.3	y=-4694x+25.1	0.99	95	y=-13602x+48.1	0.99	113
0.4	y =-6445x+28.8	0.99	117	y=-13310x+67.1	0.99	110
0.5	y=-5238x+43.6	0.97	95	y=-14041x+109.5	0.97	116
0.6	y=-6230x+55.2	0.99	113	y=-13238x+31.4	0.96	110
0.7	y=-7253x+38.6	0.98	131	y=-13084x+80.2	0.99	108
0.8	y=-6712x+21.4	0.99	122	y=-13356x+86.6	0.98	111
0.9	y=-4491x+ 42.8	0.98	81	y=-12613x+30.4	0.99	104
Average			**117**			**110**

Table 5.6 Thermal kinetic Insights: Activation Energies (kJ/mol) and Regression Factors for LDPE: RH (75:25) Using KAS and FWO methods.

	KAS			FWO		
α	**Equation**	**R^2**	**Ea**	**Equation**	**R^2**	**Ea**
0.1	y=-9512x+34.49	0.98	173	y = -10893x+66.4	0.99	90
0.2	y=-4049.2x+16.6	0.99	73	y=-10892x+26.99	0.98	90.5
0.3	y=-5273x+21.3	0.99	95	y=-11750x+38.18	0.99	97
0.4	y=-5373x+27.18	0.99	97	y = -11971x+59.07	0.98	99
0.5	y=-6411x+42.8	0.98	116	y=-14881x+105.89	0.99	121
0.6	y=-5509x+56.08	0.99	100	y=-12325x+126.7	0.99	102
0.7	y=-5500x+49.9	0.98	100	y=-13851x+106.4	0.99	114
0.8	y=-4016x+58.5	0.99	73	y= -12893x+121.3	0.99	107
0.9	y=-4532x+17.29	0.98	82	y=-11683x+20.07	0.98	97
Average			**101**			**100**

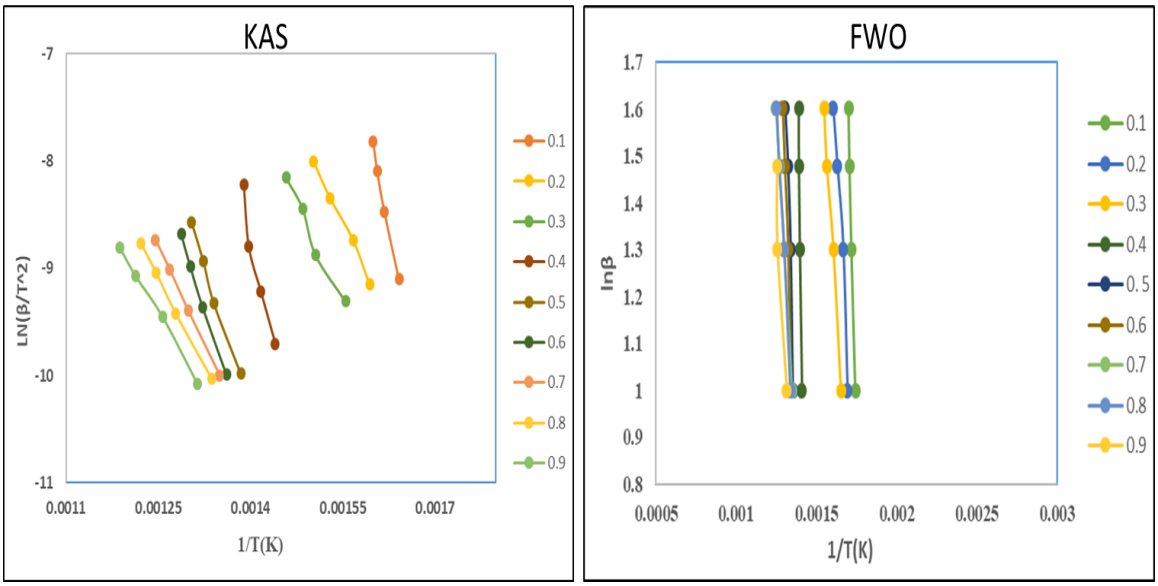

Figure 5.3. (a) Kinetic curves in the different conversions of LDPE: RH (50:50)

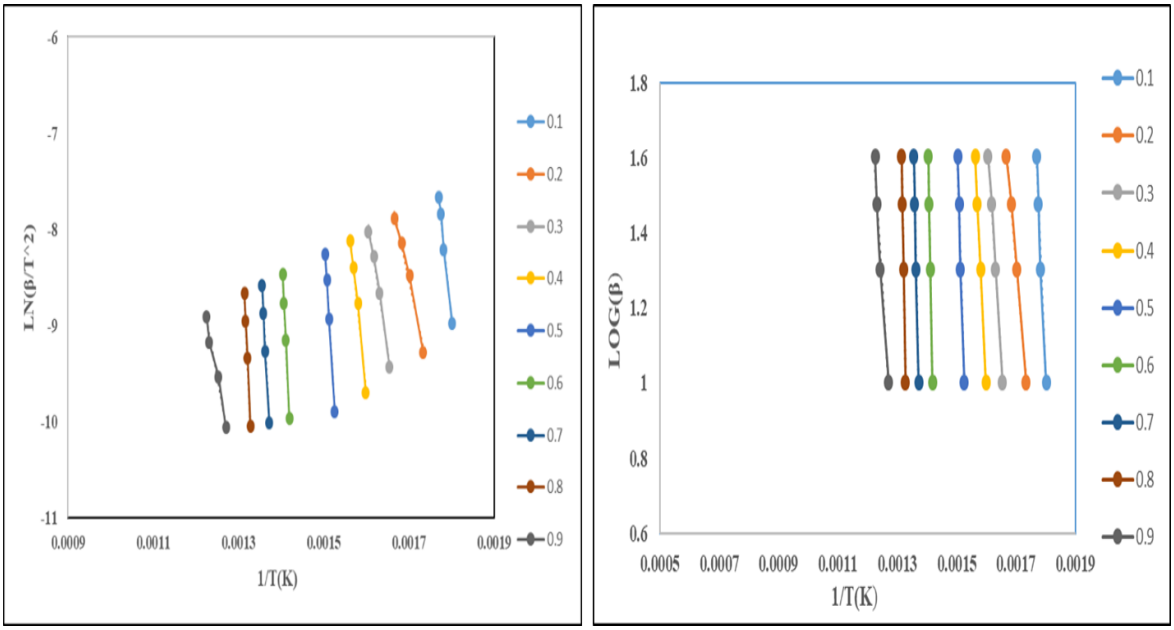

(b) Kinetic curves in the different conversions of LDPE: RH (25:75)

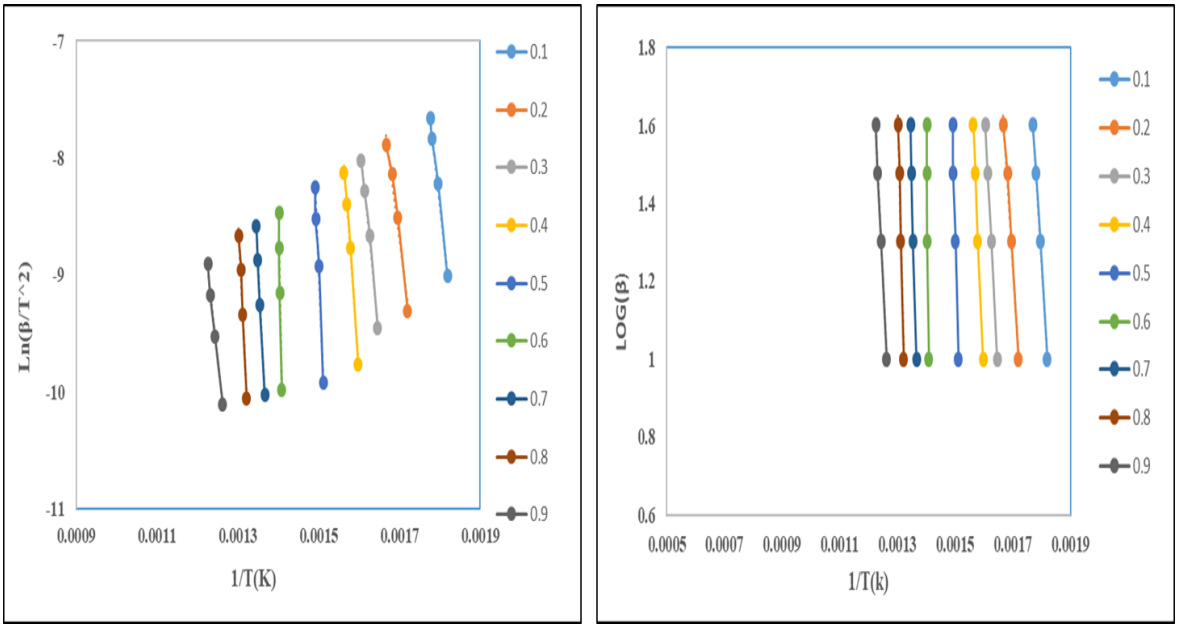

(c) Kinetic curves in the different conversion of LDPE: RH (75:25)

Tables 5.4, 5.5, and 5.6 show the activation energies, regression coefficient, and associated fitted calculations for conversion values between 0.1, 0.2, ….. 0.9 computed by using these 2 different methods. The pyrolysis kinetic parameters of the RH and LDPE combination were determined using TGA data based on KAS and OFW procedures for the final activation energy. The nonlinear process of pyrolysis entails a slow process known as thermal degradation, which is contingent upon the kind of biomass and heating rate. The general rate equation for pyrolysis of blended samples LDPE: RH (50:50), LDPE: RH (25:75), and LDPE: RH (75:25) as a function of conversion. Additionally, it is demonstrated in Fig. 5.4 that the KAS method has higher activation energy than the OFW method, and the kinetic parameter from both models rises with the conversion rate from 0.4 to 0.9**.** The variety in reaction mechanisms for the pyrolysis process is what causes the difference in Ea with a conversion factor. The lowest amount of energy needed to start a reaction, according to the definition of Ea, is lower and indicates a quicker reaction [30].

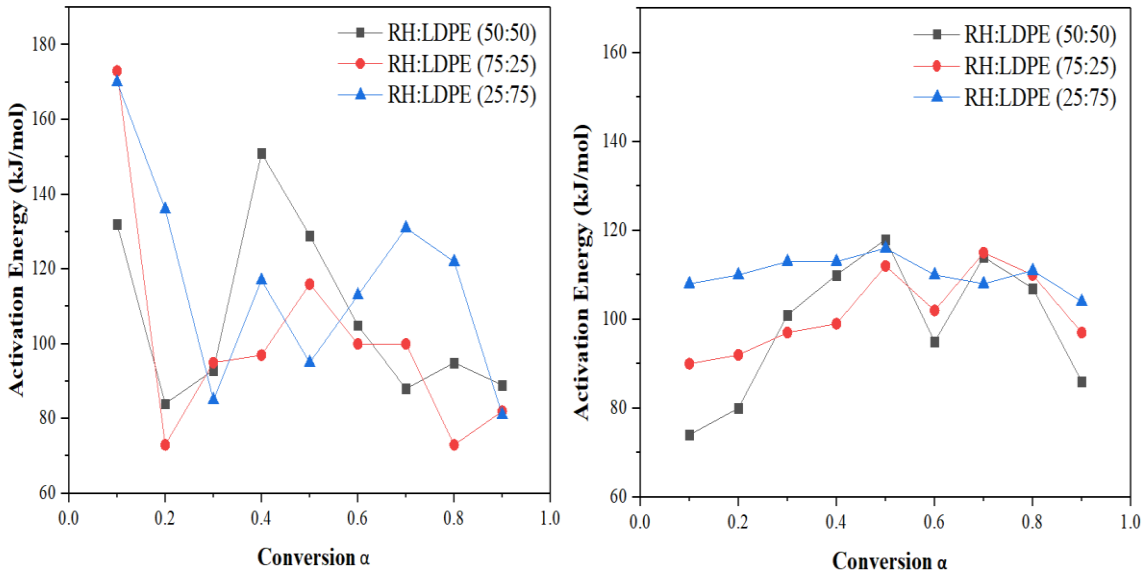

(a) (b)

Figure 5.4 (a) Comparison analysis of KAS Method **(b)** Comparison analysis of FWO Method

5.4 Synergistic effects of co-pyrolysis

The most crucial component in raising the yield and quality of pyrolysis is the synergistic impact, which might have a complicated mechanism due to feedstock interactions and co-pyrolysis process parameters. The pyrolysis feedstock's kind and connection, together with operational factors like temperature, heating rate, and catalyst count, might affect the final product's quality [31]. The initial stage in the breakdown of RH and LDPE was the thermal breakdown of rice husk, which happened at a lower temperature than that of LDPE. The solids from the biomass degradation process were employed as radical donors at a pyrolysis temperature of 400°C. The generated radicals gave the biomass particles hydrogen donors, which triggered plastic polymer chain scission. The fraction of biomass blending did not affect the initial scission of the polymer chain. A selection of recent studies showing synergistic effects during biomass and polymer co-pyrolysis is shown in **Table 5**.7. The observed synergistic effects were consistently supported through comparative trends in oil yield, gas composition, and hydrocarbon content across repeated experiments under controlled conditions.

Table 5.7 Insights into Activation Energy: Comparative Analysis of Different Feedstocks with Present Sample.

Samples	E_a(kJ/mol)	References
LDPE: RH (50:50)	102-107	Present study
LDPE: RH (25:75)	101-102	Present study
LDPE: RH (75:25)	110-117	Present study
Rice husk	51 – 100	[32]
Plastic bag	211	[33]
CS-PET	171.4	[34]
HS-PET	139.04	[34]

SFR-PET	261.38	[34]
ER-PET	316.7	[34]
PAW	189-190	[35]
50PAW:50PP	137-141	[35]
75PAW:25PP	136-140	[35]
25PAW:75PP	152-158	[35]
PP	149-153	[35]

PAW-Paulownia wood, PP –polypropylene, PET- polyethylene terephthalate, Cotton stalk, hazelnut shell, sunflower residue, and Euphorbia rigida.

5.5 Analysis of Thermodynamic parameters

Table 5.8 shows the thermodynamic parameters that were obtained using the Equations in Chapter 3. Throughout the reaction phase, the ΔH indicates the energy variation between the reactants and products. Additionally, it shows if the process is endothermic or exothermic. The study discovered a small energy variation (~ 5 kJ/mol) among the enthalpy change and E_a, suggesting that the chemical reaction started quickly. The synthesis of activated complexes is made easier by the minute difference between Ea and ΔH, which also shows that the products can be produced with very little additional energy (Kumara et al. 2020). The maximum amount of work is determined using the ΔG of a thermodynamic system at a particular T and P [35]. The magnitude of ΔS indicates that the substance has passed the energy barrier and is getting close to thermodynamic equilibrium. Production of products requires a long time owing to the less reactivity in this current state. On the other hand, a substance with a high entropy score interacts quickly and produces a product quickly. Table 5.8 shows the average values ΔH, ΔS and ΔG for the KAS model for the following samples: LDPE: RH (50:50), which has 113 kJ/mol, -0.063 J/molK, and 130 kJ/mol; LDPE: RH (25:75), which has 107 kJ/mol, -0.072 J/molK, and 129 kJ/mol; and sample LDPE: RH (75:25), which has 115 kJ/mol, -0.058 J/molK, and 136 kJ/mol.

Similarly, for the OFW model, the values of ΔS, ΔH, and ΔG were 150.63 kJ/mol, 6.34 J/molK, and 151.64 kJ/mol, respectively. The credibility of the thermodynamic analysis and the conclusions made from it are specified by the near-approximation of the findings for various thermodynamic parameters evaluated with three iso-conversional model-free approaches. For a comprehensive analysis of the pyrolysis reaction, these explanations and deductions linking disparity in thermodynamic triplets to distinct stages of the breakdown process are helpful.

Table 5.8 A Comparative Analysis of Thermodynamic Parameters in LDPE: RH (50:50), LDPE: RH (25:75) and LDPE: RH (75:25)

Thermodynamic parameter	LDPE: RH (50:50)	LDPE: RH (25:75)	LDPE: RH (75:25)
KAS Method			
ΔH(kJ/mol)	112	107	115
ΔG(kJ/mol)	130	129	136
ΔS(J/molK)	-0.063	-0.072	-0.058
FWO Method			
ΔH(kJ/mol)	107	106	122
ΔG(kJ/mol)	128	126	143
ΔS(J/molK)	-0.059	-0.076	-0.051

5.6 Conclusions

This chapter concluded that the comparative co-degradation kinetics of RH with LDPE ratios of 50:50, 25:75, and 75:25 were investigated in this work. Low-density polyethylene and rice husk together may be used as feedstocks for the thermochemical conversion processes, according to thermal characteristics. Using the Kissinger-Akahira-Sunose and Ozawa Flynn wall methods, a thermogravimetric analyzer calibrated to operate between 30°C and 600°C at varying heating rates of 10–40 °C/min in a nitrogen atmosphere was used to examine the co-pyrolysis behaviours of LDPE: RH (50:50), LDPE: RH (25:75), and LDPE: RH (75:25). This study results adding more plastic ratio into rice husk give more good results. The calculation of activation energy was made using the KAS and FWO

methods, yielding results of 107 and 102 kJ/mol with the LDPE: RH (50:50), 101 and 100 kJ/mol with the LDPE: RH (25:75), and 117 and 110 kJ/mol with the LDPE: RH (75:25). Additionally, higher heating levels were calculated experimentally with a bomb calorimeter and theoretically with the Dulong formula. Though the outcomes of these computations were remarkably similar, LDPE: RH (75:25) outperformed LDPE: RH (50:50) and LDPE: RH (75:25). The experimental heating value of LDPE: RH (75:25) was 20.61 MJ/kg, whereas the theoretical value recorded was 20.31 MJ/kg.

5.7 References

1. Alhumade, H., da Silva, J. C., Ahmad, M. S., Çakman, G., Yıldız, A., Ceylan, S., &Elkamel, A. (2019). Investigation of pyrolysis kinetics and thermal behavior of Invasive Reed Canary, bioenergy potential. Journal of Analytical and Applied Pyrolysis, 140, 385–392.
2. Danjanje, S. (2011). Fast pyrolysis of corn residues for energy production. Doctoral dissertation, Stellenbosch University.
3. Varma, A. K., & Mondal, P. (2016). Physicochemical characterization and kinetic study of pine needle for the pyrolysis process. Journal of Thermal Analysis and Calorimetry, 124, 487–497.
4. Garba, M. U., Inalegwu, A., Musa, U., Aboje, A. A., Kovo, A. S., & Adeniyi, D. O. (2016). Thermogravimetric characteristic and kinetics of catalytic co-pyrolysis of biomass with low- and high-density polyethylenes. Biomass Conversion and Biorefinery, 8, 143–150.
5. Al-Salem, S. M., Antelava, A., Constantinou, A., Manos, G., & Dutta, A. (2017). A review on thermal and catalytic pyrolysis of plastic solid waste (PSW). Journal of Environmental Management, 197, 177-198.
6. Zhou, L. M., Wang, Y. P., Huang, Q. W., & Cai, J. Q. (2006). Thermogravimetric characteristics and kinetic of plastic and biomass blend co-pyrolysis. Fuel Processing Technology, 87, 963–969.

7. Zaman, C. Z., Pal, K., Yehye, W. A., Sagadevan, S., Shah, S. T., Adebisi, G. A., ... & Johan, R. B. (2017). Pyrolysis: a sustainable way to generate energy from waste. Pyrolysis.
8. International Energy Agency. (2006). Annual report, 2006: IEA bioenergy: task 34, pyrolysis of biomass. International Energy Agency, Paris, France.
9. Oyedun, A. O., Gebreegziabher, T., & Hui, C. W. (2013). Mechanism and modeling of bamboo pyrolysis. Fuel Processing Technology, 106, 595–604.
10. Miskolczi, N., & Nagy, R. (2012). Hydrocarbons obtained by waste plastic pyrolysis: comparative analysis of decomposition described by different kinetic models. Fuel Processing Technology, 104, 96–104.
11. Grønli, M. G., Várhegyi, G., & Di Blasi, C. (2002). Thermogravimetric Analysis and Devolatilization Kinetics of Wood. Industrial & Engineering Chemistry Research, 41, 4201–4208.
12. Zhou, L., Luo, T., & Huang, Q. (2009). Co-pyrolysis characteristics and kinetics of coal and plastic blends. Energy Conversion and Management, 50, 705–710.
13. Koufopanos, C. A., Maschio, G., & Lucchesi, A. (1989). Kinetic model of the pyrolysis process of biomass and components. Canadian Journal of Chemical Engineering, 67, 75.
14. Hatakeyama, T., & Quinn, F. X. (1999). Thermal analysis - fundamentals and applications to polymer science. Wiley.
15. Nassar, M. N. (1999). Thermal analysis kinetic of rice husk and bagasse. Energy Sources, 21, 131.
16. Mansaray, K. G., & Ghaly, A. (1999). Determination of Reaction Kinetics of Rice Husks in Air Using Thermogravimetric Analysis. Energy Sources, 21, 899.
17. Zhao, H., Yan, H. X., Dong, S. S., Zhang, Y., Sun, B. B., Zhang, C. W., ... & Sui, T. T. (2013). Thermogravimetry study of the pyrolytic characteristics and kinetics of macro-algae Macrocystis pyrifera residue. Journal of Thermal Analysis and Calorimetry, 111, 1685–1690.

18. Oh, S.-Y., & Seo, Y.-D. (2016). Polymer/biomass-derived bio-char for use as a sorbent and electron transfer mediator in environmental applications. Bioresource Technology, 218, 77–83.
19. Chattopadhyay, J., Pathak, T. S., Srivastava, R., & Singh, A. C. (2016). Catalytic co-pyrolysis of paper biomass and plastic mixtures (HDPE (high density polyethylene), PP (polypropylene) and PET (polyethylene terephthalate)) and product analysis. *Energy*, *103*, 513-521.
20. Dewangan, A., Pradhan, D., & Singh, R. K. (2016). Co-pyrolysis of sugarcane bagasse and low-density polyethylene: influence of plastic on pyrolysis product yield. Fuel, 85, 508–516.
21. Prajapati, S. B., Gautam, A., Gautam, S., Yao, Z., Tesfaye, F., &Lü, X. (2023). Co-Pyrolysis Behavior, Kinetic and Mechanism of Waste-Printed Circuit Board with Biomass. Processes, 11(1), 229.
22. Burra, K. G., & Gupta, A. K. (2018). Kinetics of synergistic effects in co-pyrolysis of biomass with plastic wastes. Applied Energy, 220, 408–418.
23. Chee, A., Lim, R., Lai, B., Chin, F., Abbas, Z., & Ling, K. (2017). Kinetic Analysis of Rice Husk Pyrolysis Using Kissinger-Akahira-Sunose (KAS) Method. Procedia Engineering, 148, 1247–1251.
24. Li, D., Chen, L., Zhang, X., Ye, N., & Xing, F. (2011). Pyrolytic characteristics and kinetic studies of three kinds of red algae. Biomass and Bioenergy, 35, 1765–1772.
25. Huang, X., Cao, J. P., Zhao, X. Y., Wang, J. X., Fan, X., Zhao, Y. P., and Wei, X. Y. (2016). Pyrolysis kinetics of soybean straw using thermogravimetric analysis. *Fuel*, *169*, 93-98.
26. Vyazovkin, S., and Wight, C. A. (1998). Isothermal and non-isothermal kinetics of thermally stimulated reactions of solids. *International reviews in physical chemistry*, *17*(3), 407-433.
27. Chandrasekaran, A., Ramachandran, S., and Subbiah, S. (2018). Modeling, experimental validation and optimization of Prosopis juliflora fuelwood pyrolysis in fixed-bed tubular reactor. Bioresource Technology, 264, 66-77.
28. Sriram, A., & Swaminathan, G. (2018). Pyrolysis of Musa balbisiana flower petal using thermo-gravimetric studies. Bioresource Technology, 265, 236–246.

29. Kumar, M., Sabbarwal, S., Mishra, P. K., & Upadhyay, S. N. (2019). Thermal degradation kinetics of sugarcane leaves (Saccharum officinarum L) using thermo-gravimetric and differential scanning calorimetric studies. *Bioresource Technology*, *279*, 262-270.
30. Anshar, M., Tahir, D., & Ani, F. N. (2018). Pyrolysis characteristic of rice husk with plastic bag as fuel for power generation by using a thermo-gravimetric analysis. Earth and Environmental Science, 105, 012034.
31. Çepelioğullar, Ö., &Pütün, A. E. (2013). Thermal and kinetic behaviors of biomass and plastic wastes in co-pyrolysis. Energy Conversion and Management, 75, 263–270.
32. Chen, Y., Wang, F., Duan, L., Yang, H., & Gao, J. (2016). Tetracycline adsorption onto rice husk ash, an agricultural waste: Its kinetic and thermodynamic studies. *Journal of Molecular Liquids*, *222*, 487-494.
33. Olszak-Humienik, M., &Możejko, J. (2000). Thermodynamic functions of activated complexes created in thermal decomposition processes of sulphates. Thermochimica Acta, 344, 73–77.
34. Kumar, M., Shukla, S. K., Upadhyay, S. N., & Mishra, P. K. (2020). Analysis of thermal degradation of banana (Musa balbisiana) trunk biomass waste using iso-conversional models. *Bioresource technology*, *310*, 123393.
35. Ruvolo-Filho, A., & Curti, P. S. (2006). Chemical kinetic model and thermodynamic compensation effect of alkaline hydrolysis of waste (PET) in non-aqueous ethylene glycol solution. Industrial & Engineering Chemistry Research, 45, 7985–7996.

Chapter – 6

Thermal pyrolysis of Rice husk with plastic waste blends for Bio-oil Production

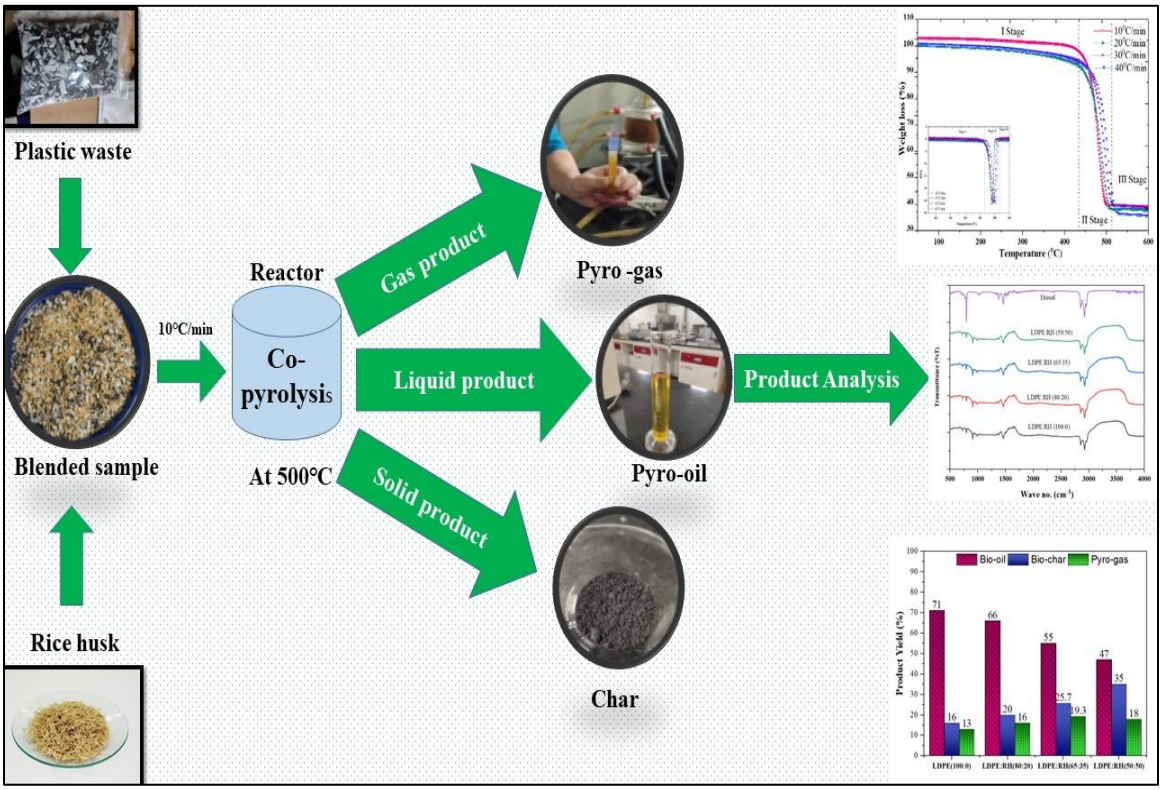

6.1 Introduction

Municipal solid waste poses a significant environmental encounter, primarily comprising biomass and plastic products. The widespread use of plastics adds to pollution in the environment, while the usage of fossil fuels makes energy shortages and environmental harm worse. Researchers have been looking for creative ways to solve these problems, and pyrolysis has emerged as a viable technique for producing alternative fuels and recycling trash [1-3]. Pyrolysis is a valuable process that may transform waste polymers including low- and high-density polyethylene, polyethylene terephthalate, polystyrene, and polyvinyl

chloride into chemicals that are useful. In addition to addressing plastic waste, this strategy provides a substitute energy source. Simultaneously, biomass which is rich in cellulose, hemicelluloses, and lignin, presents an opportunity for energy production through thermochemical transformations like gasification, combustion, and pyrolysis [4]. However, because of its unstable fuel properties, including greater oxygen and moisture content, biomass-based bio-oil has limits when used in car engines. Researchers suggested a co-pyrolysis method, in which polymers and biomass are combined in an appropriate ratio to produce fuels, to improve the fuel's qualities [5]. Research shows that co-pyrolysis, in which plastics act as hydrogen donors, produces bio-oil of higher quality and yield than single biomass pyrolysis. Prominent studies have shown that co-pyrolyzing low-density polyethylene with biomass, such sugarcane bagasse, improves liquid production, increases calorific value, and decreases undesired chemicals [6]. Further research explores the co-pyrolysis of LDPE with various biomasses, revealing higher oil yields, increased hydrocarbon content, and a composition akin to diesel fuel [7]. The resulting pyrolysis oil exhibits environmental advantages with reduced carbon residue and sulfur content, offering economic benefits at a lower production cost than conventional diesel fuel [8]. Additionally, the process of co-pyrolysis has been found to raise the production of aromatic compounds, prevent coke formation, and improve the H/C_{eff} ratio within the raw material system. This positively contributes to the quality of biofuel by promoting the dehydration of oxygen-containing compounds while impeding certain undesirable reactions [9]. Overall, the integration of plastic waste into biomass pyrolysis processes demonstrates a promising approach for addressing environmental challenges, creating alternative fuels, and promoting sustainable waste management [10]. Co-pyrolyzing biomass with plastic waste has been introduced and proven to be a potential way to boost the characteristics and output of the resulting bio-oil for fuel applications, as the bio-oil generated by the pyrolysis of biomass alone has limits. This study looks on the co-pyrolysis of rice husk combined with plastic waste. A common agricultural leftover that contains cellulose, hemicellulose, and lignin is rice husk. Conversely, LDPE and HDPE are typical plastics that have a low temperature of thermal degradation and a high hydrogen concentration. Plastic and biomass

may interact in a way that enhances the quality and stability of the bio-oil generated during co-pyrolysis. Plastic addition is thought to improve the co-pyrolysis bio-oil product's characteristics and quicken the rice husk pyrolysis reaction. Since biomass, like rice husk, typically decomposes at higher temperatures (approximately 500–800°C), low-density polyethylene (LDPE) typically decomposes at a lower temperature range (approximately 300–500°C). As a result, the LDPE and HDPE are likely to break down first and produce an oil phase that can help transfer heat to the rice husk particles. Due to this difference in thermal stability, LDPE decomposes earlier in the co-pyrolysis process, producing an oil phase. This early decomposition of LDPE generates hydrocarbons that can act as a medium for heat transfer, facilitating more uniform heating and more efficient thermal decomposition of the rice husk particles [11]. This, coupled with the hydrogen donating capacity of LDPE, HDPE could maximize bio-oil production and lead to a bio-oil fuel with optimized combustion properties, stability, and composition. The purpose of this work is to illustrate the benefits and technological viability of co-processing plastic waste and rice husk biomass thermochemically [12]. According to this work and related studies, co-pyrolysis of plastic and biomass has the potential to decrease material waste, make important chemical recycling easier, and provide energy substitutes for fossil fuels. Furthermore, co-pyrolysis technology could act as a catalyst for developing an efficient blend of traditional fossil energy sources and emerging renewable energies [13]. The current study demonstrated a thermochemical process to produce from rice husk and a mixture of waste plastics (LDPE, HDPE) with varying compositions, viz. 100:0, 80:20, 65:35, and 50:50 (wt./wt.) %. To provide a comprehensive understanding of the co-pyrolysis process, the precise ratios of 20:80, 35:65, and 50:50 were used. The objective is to maximise the yield and quality of pyrolysis oil while addressing the use of waste and renewable resources. According to the varied techniques suggested by the American Society for Testing and Materials (ASTM), it was discovered that the addition of LDPE and HDPE with distinct hydrocarbon chains generated from the co-pyrolysis considerably alters the fuel qualities. Additionally, other analytical methods including GC-MS, FTIR, elemental analyzer, ^{1}H, and ^{13}C NMR analysis, were used to validate the alterations in the

fuel's chemical characteristics including the determination of aromatic, paraffin, and olefin contents in the fuel.

6.2 Influence of the composition of the rice husk on adding plastic

After collecting the pyrolysis oil from the reactor, we employed a distillation process to remove moisture and impurities. This critical step not only refines the oil but also enhances its quality and usability. During distillation, the crude pyrolysis oil is heated, causing the moisture and light impurities to vaporize and separate from the main oil body. The vapors are then condensed and collected, effectively reducing the water content and eliminating undesirable impurities.

A 30% oil yield was achieved by pyrolysis when rice husk was utilised as the only feedstock. The greater tar content in rice husk, which is essential to the production of oil overall, is the cause of the increased output. The yield percentage of various products from the co-pyrolysis of low-density polyethylene (LDPE) and rice husk (RH) has been calculated using the formulas given in Chapter 3.

The liquid product (i.e. pyro-oil) of 71 wt.% with LDPE: RH (100:0) was achieved followed by 66 wt.% with LDPE: RH (80:20), 55 wt.% with LDPE: RH (65:35), and 47 wt.% with LDPE: RH (50:50). While for other composition of rice husk and high-density polyethylene the liquid product is 75 wt.% for HDPE: RH (100:0), 68 wt.% for HDPE: RH (80:20), 57 wt.% for HDPE: RH (65:35) and 50 wt.% for HDPE: RH (50:50). It was found that as the rice husk amount in the combination grows, so does the weight percentage of char. **Fig. 6.1** displays all of the product distribution's specific details.

Table 6.1 The output results from the thermochemical transformation of separate rice husks and combined waste plastic materials.

Sample	Pyro-oil (wt. %)	Solid-char (wt.%)	Pyro-Gas (wt. %)
RICE HUSK	30	47	33
LDPE: RH (100:0)	71	16	13

LDPE: RH (80:20)	66	20	14
LDPE: RH (65:35)	55	25.7	19.3
LDPE: RH (50:50)	47	35	18
HDPE: RH (100:0)	75	10	15
HDPE: RH (80:20)	68	15	17
HDPE: RH (65:25)	57	25	18
HDPE: RH (50:50)	50	30	20

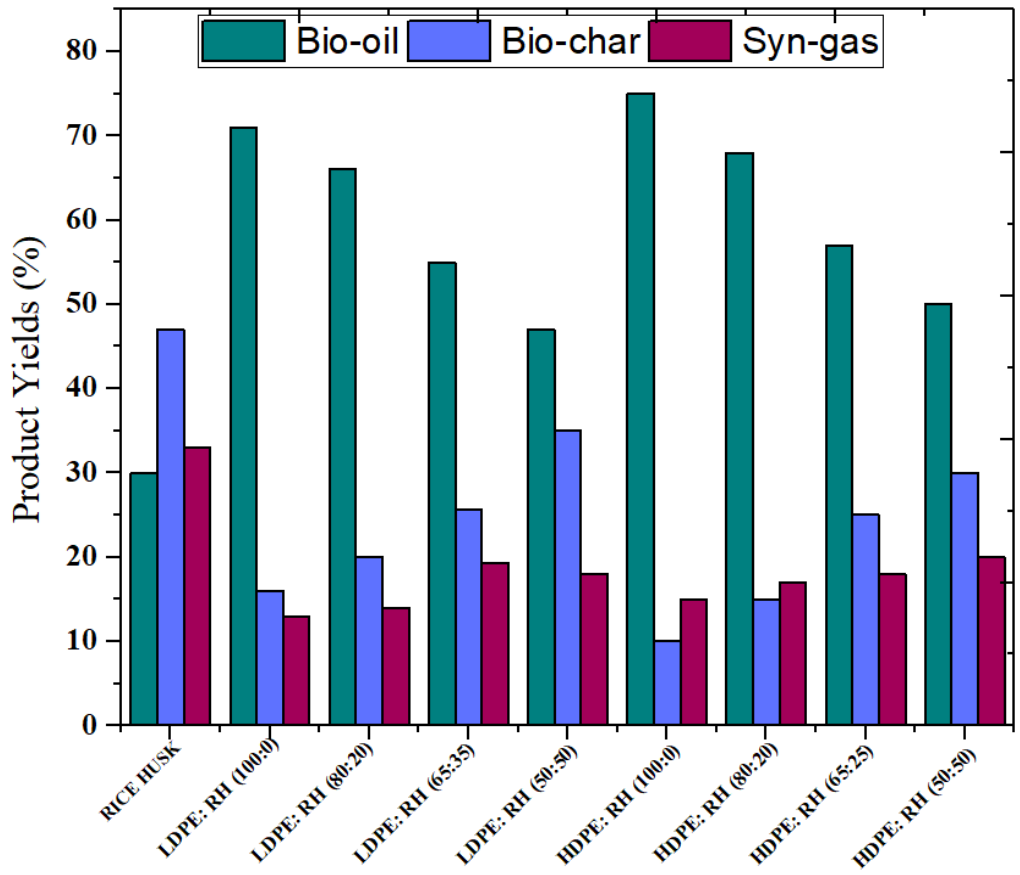

Figure 6.1 The weight percentages of products generated through the thermal conversion of plastic and rice husk blend via co-pyrolysis

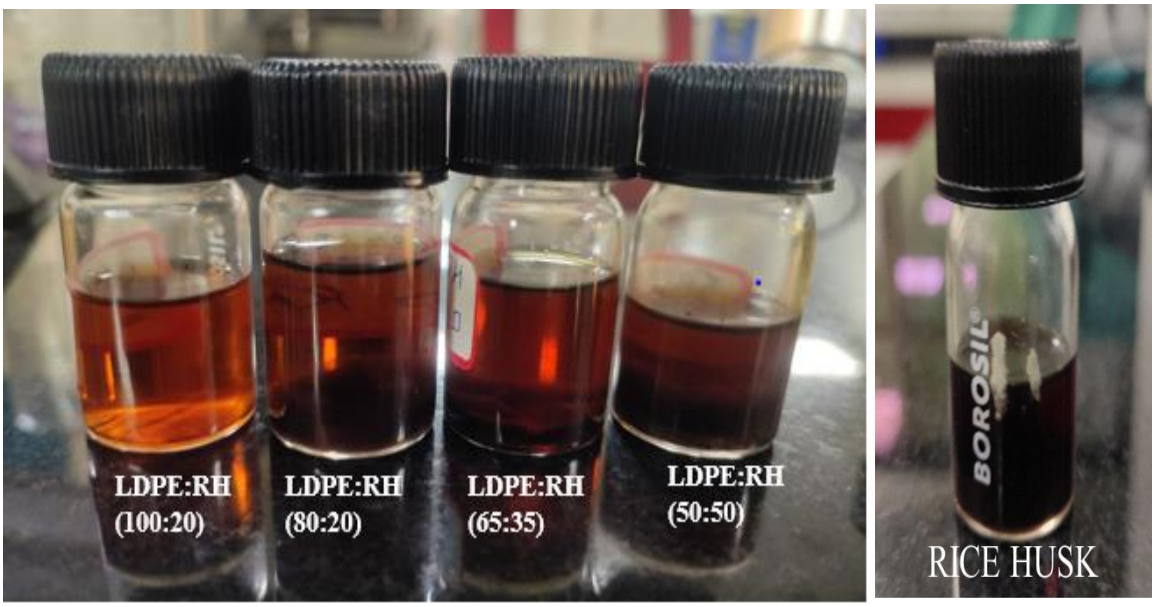

Figure 6.2 The appearances of pyrolysis oils in different ratio of LDPE and RH

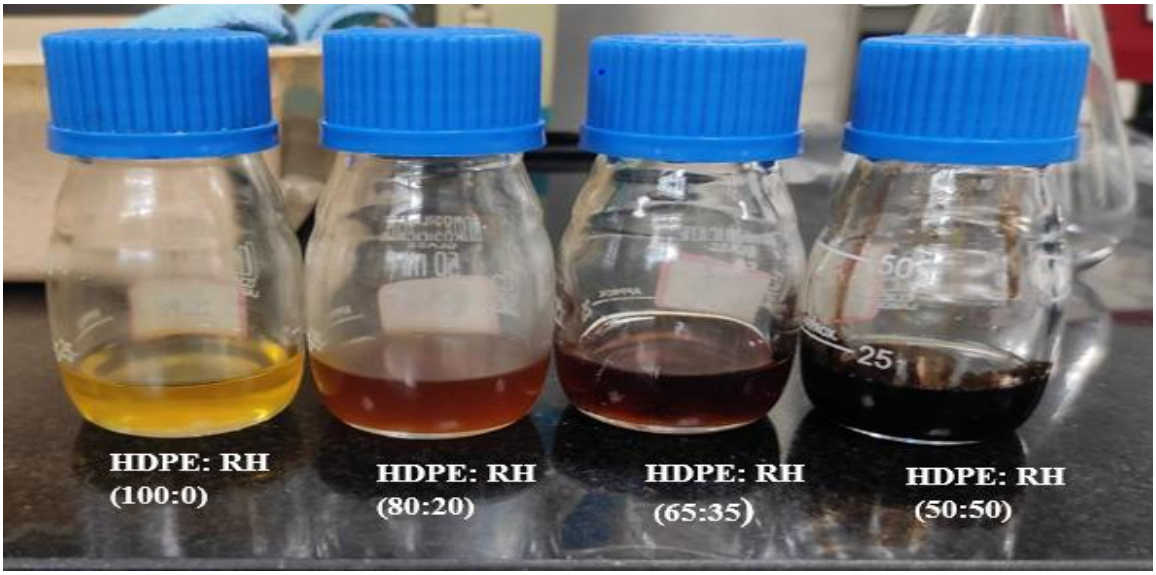

Figure 6.3 The appearances of pyrolysis oils in different ratios of HDPE and RH.

6.3 The physical and chemical characteristics of pyrolysis oil.

As was discussed in previous chapters, after collecting the pyrolysis oil from the reactor, we employed a distillation process to remove moisture and impurities. This critical step

not only refines the oil but also enhances its quality and usability. During distillation, the pyrolysis oil is heated, causing the moisture and light impurities to vaporize and separate from the main oil body. The vapors are then condensed and collected, effectively reducing the water content and eliminating undesirable impurities. To ensure experimental accuracy and reproducibility, all co-pyrolysis tests were performed in triplicate for each feedstock blending ratio and temperature configuration. The mentioned results for bio-oil, gas, and char yields are the average of three separate trials. Minor variations noted the physical and chemical characteristics of the pyro-oil produced from plastic waste and rice husk, as well as their various combinations, were investigated using a range of analytical techniques to assess the fuel's quality. We then compared these findings with those of commercial diesel fuel, as presented in Table 6.1. This study set out to determine how fuel properties are influenced by the mix of feedstock and thermo-chemical processes. In pursuit of this goal, a detailed assessment of several key fuel properties was carried out. The properties examined include cloud point (CP) and pour point (PP), kinematic viscosity, flash point (FP) and fire point, calorific value (CV), carbon residue (CR), and more. The subsequent sections contain a presentation of the results obtained.

Moreover, co-pyrolysis often produces a higher liquid yield and reduced solid (char) formation compared to the pyrolysis of biomass or plastic alone. Overall, co-pyrolysis offers a promising route for producing upgraded bio-oil while managing two major waste streams efficiently.

6.3.1 Analysis of Density, Specific Density, and API Gravity of Bio-oil

After the pyrolysis process, the densities of the pyrolysis oils obtained from rice husk are 1.3 g/cm^{3,} and adding plastic LPDE both separate and mixed compositions of LDPE: RH fell within the range of 0.813 to 1.12 g/cm^3, for other composition, the densities of all liquid fuels produced by all the samples HDPE, RH, and its mix composition were discovered to be between 0.814 and 0.991 g/cm^3, whereas the same for commercial diesel is 0.820 g/cm^3. Lower density in a fuel corresponds to a higher API gravity, representing better oil quality. The pyro-oil specific gravity measurements of RH are 1.0 while the composition of RH

and HDPE ranged from 0.787 to 0.864, for RH and LDPE the range is between 0.79 to 0.99 whereas the commercial diesel's specific gravity was 0.795. API gravity is a measure of oil density in water at 60°F (15.56°C), and it provides valuable information about the relative weight of the petroleum product associated with water. Fuels with an advanced API gravity possess a lesser density, indicating superior fuel quality. The API gravities of the RH-based bio-oil were 29.5, for LDPE pyrolysis oil were 43.8, and for HDPE-based oil were 48.2. The analysis of API gravity of the liquid oil samples obtained from various combinations of plastic and RH feedstocks ranged from 32.2 to 41.4.

6.3.2 Analysis of Cloud and Pour Points of Bio-oil

A fuel's cloud and pour points serve as indicators of its flow characteristics in cold conditions. In cold temperatures, most liquid fuels tend to undergo a phase change, transitioning into a semi-solid or solid state, which can result in the creation of wax crystals within the liquid [14]. Consequently, examining the cloud points and pour points is imperative to ascertain how well the oil can power the engine seamlessly without disruptions when operating in significantly low temperatures. In addition, to evaluate these qualities, the liquid oil's cloud point and pour point were found [15]. It was discovered that the pour and cloud points of the pyrolysis oils from different biomass rice husk were 16°C and 8°C, respectively, and that the plastics had pour and cloud points of 8°C and -9°C with HDPE sample and 9°C and 1°C with LDPE sample. It was observed that the cloud points and the pour points for the pyrolysis oils were examined to be for both pyrolysis oils obtained from blended LDPE and rice husk were identified at 10℃ and 2℃ for LDPE: RH (80:20),11℃ and 4℃, for the LDPE: RH (65:35), 13℃ and 5 ℃ for LDPE: RH (50:50) respectively. On the other hand, the cloud points and pour points of the liquid sample for the liquid sample that was obtained from the co-pyrolysis of HDPE and RH were as follows: For the combination compositions of HDPE: RH (80:20), HDPE: RH (65:35), and HDPE: RH (50:50), respectively, the temperatures are 10°C and -7°C, 13°C and -5°C, and 15°C and -1°C. We measured the diesel's cloud point and pour point for comparison, and

the results showed that they were similar to bio-oils. The cloud point of diesel was recorded at -3°C, while the pour point was measured at -13°C.

6.3.3 Analysis of Flashpoint and Fire point of liquid product

This test technique is frequently used to find flammable liquid products flash points around 70°C and -30°C. For a separate Rice husk sample, the flash points were measured at 80.1°C, while the fire points for the bio-oil derived from RH were 82.3°C. For waste plastic, the flash points were measured at 52.3°C for LDPE, while the fire points for the liquid sample derived from LDPE were 54.4°C. When assessing another plastic sample, the flash points for HDPE were found to be 58.5°C, Additionally, the fire points for the pyrolyzed oils derived were 63.2°C for HDPE respectively, when waste plastic and biomass were co-pyrolyzed at varying weight percentages of LDPE and RH, there was a noticeable change in both flash point and fire points. Specifically, the measured values were 64.2°C and 67.1°C, 70.1°C and 73.4°C and 77.2°C and 80.5°C for the compositions of LDPE: RH (80:20), LDPE: RH (65:35), and LDPE: RH (50:50). Diesel, on the other hand, has fire and flash points of 64°C and 57°C, respectively. The procedure outlined here is frequently used to determine the flash point of flammable liquid products that are between 70°C and -30°C in temperature. Regarding the oils produced by co-pyrolyzing HDPE and RH at different weight percentages, an intriguing finding was that there was a discernible variation in both the flash and fire points. The recorded values were as follows: 59.7°C, 60.8°C, 61.6°C, and 64.8°C, 66.1°C, 68.3°C for compositions of HDPE: RH (80:20), HDPE: RH (65:35) and HDPE: RH (50:50). Respectively, for diesel, the determined flash points and fire points were 57°C and 64°C [16].

6.3.4 Analysis of kinematic viscosity of the liquid product

Kinematic viscosity is a crucial factor in any fuel as it offers insights into how the fuel will spray and atomize when inserted into the combustion chamber. Lower-viscosity fuels are preferred for engine starters and general performance as they enable simple atomization, hence improving combustion [17]. Furthermore, high-viscosity fuels can pose significant

challenges during engine start-up, particularly in cold weather, as they can impede the proper operation of injectors by restricting the fluidity of fuel in the ignition chamber. Thus, the ASTM D-445 technique was used to test the kinematic viscosities of the liquid product at numerous temperatures. The results are shown in Figure 6.4.

The data reveals a consistent decrease in kinematic viscosity as the temperature rises, and this trend is consistent across all the samples. The viscosities of pyrolysis oils derived from separate plastic were determined to be 1.39 cSt for HDPE plastic, 1.92 cSt for LDPE plastic and 1.41 cSt for RH-based pyrolysis oil. The kinematic viscosity of the liquid sample falls within the range of 1.81 to 1.46 cSt at 40 °C, However, the viscosities of the liquid sample obtained from a blend of plastics and biomass (HDPE and RH) were examined as follows: 1.22 cSt, 1.19 cSt, and 1.12 cSt for the HDPE: RH mixtures in ratios of 80:20, 65:35 and 50:50 respectively, while adding rice husk to plastic waste the viscosity will reduce which is notably lower than that of diesel fuel, which measures 2.46 cSt at 40 °C. The liquid oil derived from plastic and rice husk-produced oil has the lowest viscosity. This lower viscosity of the liquid oil, whether from LDPE, Rice husk, or their combined composition, suggests that it would not pose any adverse effects on the fuel injector and would promote smooth engine operation. Temperature fluctuations can also affect the viscosity of the liquid oil, which can affect engine performance. Consequently, we looked into how temperature affected kinematic viscosity, and the findings are shown in Figure 6.4(a, b).

The fluctuations in the kinematic viscosity of liquid samples originating from plastic and RH may be attributed to factors such as process parameters, experimental settings, and potential contaminants. When comparing the current findings with earlier data, it becomes evident that the liquid sample obtained from the thermochemical conversion of biomass by adding plastic exhibits improved fluidity characteristics throughout the engine combustion process, mainly owing to its lower viscosity.

6.3.5 Calculation of calorific value

Another crucial parameter for evaluating liquid products is their calorific value (CV), which is directly linked to the energy released upon combustion. The projected CV for the liquid sample was 46.31 MJ/kg for HDPE and 16.34 MJ/kg for RH biomass and LDPE was 39.7 MJ/Kg. Notably, the pyro-oil derived from LDPE and Rice husk composition in an LDPE: RH (80:20), LDPE: RH (65:35), and LDPE: RH (50:50) displayed the calorific value at 34.6 MJ/Kg,29.3 MJ/Kg, and 27.1 MJ/Kg. In the instance of co-pyrolysis of HDPE plastic and RH, the calorific values for fuel samples were measured as 42.30 MJ/kg, 39.48 MJ/kg, and 36.68 MJ/kg, for HDPE: RH (80:20), HDPE: RH (65:35) and HDPE: RH (50:50), respectively. Estimating the quantity of heat energy that can be released during the burning of pyrolysis oil is the process of determining the calorific value. These results are in line with published findings on CVs, which range in value from 42 MJ/kg to 48.4 MJ/kg. Overall, the results show that the examined samples' calorific values (CV) are quite comparable to those found in the body of current research. The efficient method that helped produce the bio-oil with a high calorific content in **Table 6.1**.

6.3.6 Analysis of pH value of liquid sample

To assess how corrosive the bio-oil products are the pH of the liquid sample was gauged using a pH meter by Eutech Instruments, specifically the pH tutor model. This meter's electrode was calibrated using two buffer solutions and directly immersed into a 1-2 ml sample of bio-oil. The resulting value obtained from this process represents the final pH reading of the bio-oil [20]. Liquid samples made solely from biomass usually have a pH of 3.5, which is quite acidic. When plastic is added to the biomass during the pyrolysis process, the pH of the resulting bio-oil often rises. The addition of LDPE plastic, which contains less oxygenated compounds than biomass, might result in a bio-oil with a higher pH value, typically ranging from 4.4 to 5.2. This is in contrast to the oil samples from the pyrolysis of separate and blended samples of RH and HDPE, which varied in pH from 4.2 to 5.4. The PH value is rising when HDPE is added to RH. This increase in pH makes the bio-oil less acidic and can contribute to improved stability. The production of NH3 from

protein pyrolysis, which dissolves in the pyro oil, is thought to be the cause of the drop in pH in the co-pyrolytic oil [21]. The commercial diesel's pH was found to be 5.5.

6.3.7 Analysis of Carbon Residue

A higher presence of carbon residue is an indicator of poorer fuel quality. Thus, it's strongly recommended to use low-carbon residue fuel for sustainability purposes [22]. The oil generated by pyrolysis tended to create carbonaceous deposits, as determined by the Ramsbottom carbon residue (CR) equipment (ASTM D524). During pyrolysis of rice husk, the residue of carbon was 0.25 and LDPE produced a carbon residue at 0.34 wt%, followed by LDPE: RH (80:20) measured at 0.38 wt%, LDPE: RH (65:35) at 0.36 wt%, and LDPE: RH (50:50) at 0.25 wt%. for another sample the carbon residues for the pyro-oil derived from waste HDPE and RH and its composition HDPE: RH (100:0), HDPE: RH (80:20), HDPE: RH (65:35), and HDPE: RH (50:50) were measured at 0.44, 0.38, 0.34, and 0.36 weight percent, while the carbon residue present in diesel at 0.54 wt%, respectively. For the plastic and rice husk composition, the low weight percentage of carbon residue in all cases suggests their suitability for use as fuel. In Figure 6.5 (a, b), you can observe the variations in carbon residues for the pyrolysis oils derived from plastic (LDPE, HDPE) and biomass (RH), and their blend compositions.

6.3.8 Aniline point of Bio-oil

The aniline point serves as an indicator of the aromatic content in oil samples. A lower aniline point suggests a higher aromatic content, while a higher aniline point indicates a lower aromatic content. For individual samples, RH, HDPE, and LDPE measured aniline points were 69.5℃, 61.3 ℃, and 61.2 ℃, respectively. Similarly, while adding LDPE to rice husk the aniline points decreased so for mixed plastic with RH were determined to be 64.5 ℃, 66.3 ℃, and 67.8 ℃ for fuel derived from the following mixtures: LDPE: RH (80:20), LDPE: RH (65:35), and LDPE: RH (50:50), respectively [23]. Likewise, the aniline point for adding HDPE with RH was determined to be 62.5 ℃, 65.4 ℃, and 66.6 ℃ for fuel derived from the following mixtures: HDPE: RH (80:20), HDPE: RH (65:35),

and HDPE: RH (50:50), respectively [23]. Additionally, the diesel and cetane index were determined based on aniline point data.

6.4 Elemental Composition Analysis

Utilizing an elemental analyzer, the liquid sample composition that was produced by converting waste plastic and biomass was analyzed in order to regulate the carbon and hydrogen content. In the pyrolysis oil made from a mixture of plastic waste (LDPE, HDPE) and rice husk (RH) feedstock, a greater proportion of hydrocarbons was discovered, suggesting that the oil had a higher energy content and could be utilized as fuel. The percentage of carbon and hydrogen in oil samples determines their heating value. Moreover, it is clear that the presence of low-density and high-density polyethylene during the pyrolysis of rice husk (RH) modifies the properties of the fuel that is produced. The energy potential of hydrocarbon fuels is significantly influenced by their carbon content, while the inclusion of higher hydrogen elements further enhances the fuel's calorific value **[24]. Table 6.2.** showcases the findings of the CHNS analysis conducted on fuels derived from the separate pyrolysis of HDPE, RH, and LDPE and their combination with both the plastic. The outcomes indicate that the oil samples exhibit a hydrocarbon content ranging from 60-70%.

Table 6.2 The physicochemical characteristics of the pyrolysis oil generated from both separate and combined sources of rice husk (RH) and low-density polyethylene (LDPE).

Fuel Properties	**LDPE: RH (0:100)**	**LDPE: RH (100:0)**	**LDPE: RH (80:20)**	**LDPE: RH (65:35)**	**LDPE: RH (50:50)**
Density (g/cm^3)	1.3	0.813	0.876	0.946	1.12
Specific density	1.0	0.790	0.832	0.920	0.992
Cloud point (°C)	16	9	10	11	13
Pour point (°C)	8	1	2	4	5
Flashpoint (°C)	80.1	52.3	64.2	70.1	77.2

Fire point (°C)	82.3	54.4	67.1	73.4	80.5
Kinematic viscosity (@ 40 ◦C in cSt)	1.41	1.92	1.81	1.62	1.46
Aniline point (g/cm^3)	69.5	61.2	64.5	66.3	67.8
Calorific value (MJ/kg)	23.4	39.7	34.6	29.3	27.1
Carbon Residue(wt.%.)	0.74	0.62	0.38	0.36	0.30
API gravity	28.5	40.1	37.7	34.2	31.77
pH Value	3.5	5.2	4.8	4.7	4.1
Carbon content (wt.%)	58.1	76	72.16	68.3	62.5
Hydrogen content (wt.%)	7.22	13.6	12.13	10.41	9.13
Nitrogen content(wt.%)	3.33	0.44	0.54	1.45	2.11
Sulfur content (wt.%)	0.1	0	0.07	0.11	0.23
Oxygen content (wt.%)	35	9.96	12.56	17.8	20.1

Table 6.3 The physicochemical characteristics of the pyrolysis oil generated from separate and combined rice husk (RH) sources and High-density polyethylene (HDPE).

Fuel Properties	**HDPE: RH (100:0)**	**HDPE: RH (80:20)**	**HDPE: RH (65:35)**	**HDPE: RH (50:50)**	**Diesel**
Density (g/cm^3)	0.814	0.889	0.931	0.99	0.820
Specific density	0.787	0.818	0.845	0.864	0.794
Cloud point (°C)	8	10	13	15	-3
Pour point (°C)	-9	-7	-5	-1	-13
Flashpoint (°C)	58.5	59.7	60.8	61.6	57
Fire point (°C)	63.2	64.8	66.1	68.3	64
Kinematic viscosity (@ 40 ◦C in cst)	1.39	1.22	1.19	1.12	2.46

Aniline point (g/cm^3)	61.3	62.5	65.4	66.6	56.8
Calorific value (MJ/kg)	46.2	44.1	40.3	38.6	46.18
Carbon Residue (wt%.)	0.44	0.38	0.38	0.25	0.57
API gravity	48.2	41.4	35.9	32.2	46.77
Diesel Index	67.5	59.8	53.7	48.9	62.76
Cetane index	58.5	53.05	48.6	45.2	55.19
PH Value	5.4	5.2	4.8	4.2	5.5
Carbon content (wt.%)	79.21	70.1	65.3	61.5	86.6
Hydrogen content (wt.%).	15.15	12.19	10.41	9.13	13.4
Nitrogen content (wt.%)	0.38	0.97	1.32	2.32	-
Sulfur content (wt.%)	0	0.04	0.09	0.21	-
Oxygen content (wt.%)	5.26	9.56	12.8	15.1	-

Kinetic viscosity and carbon Residue of all the samples

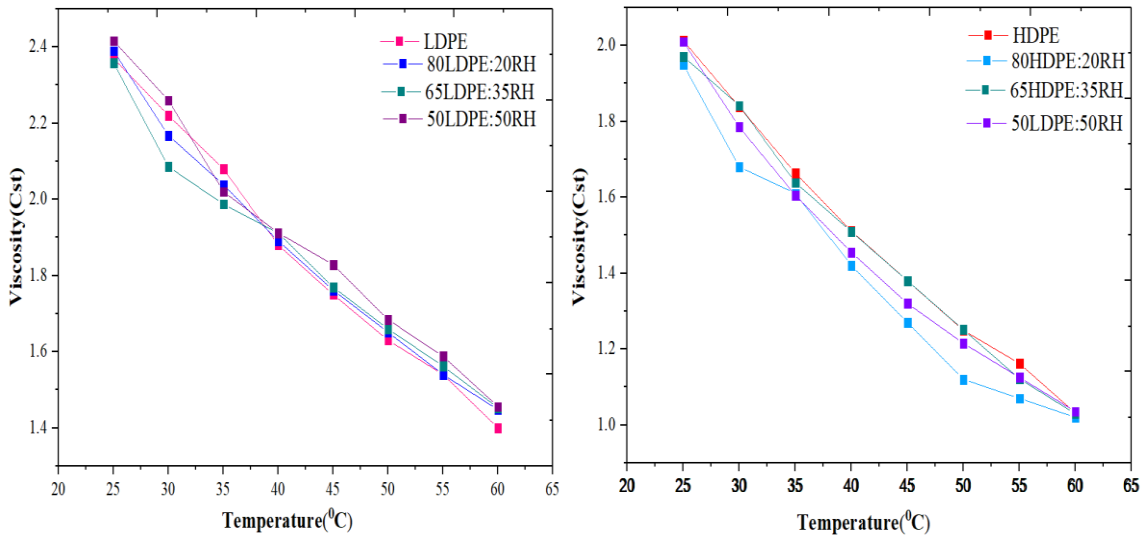

(a) (b)

Figure 6.4 (a) A comparative investigation of how temperature impacts the kinematic viscosities of diesel fuel and pyrolysis oil derived from LDPE, rice husk, and their

mixtures. (b) A comparative investigation of how temperature impacts the kinematic viscosities of diesel fuel and pyrolysis oil derived from HDPE, rice husk, and their mixtures

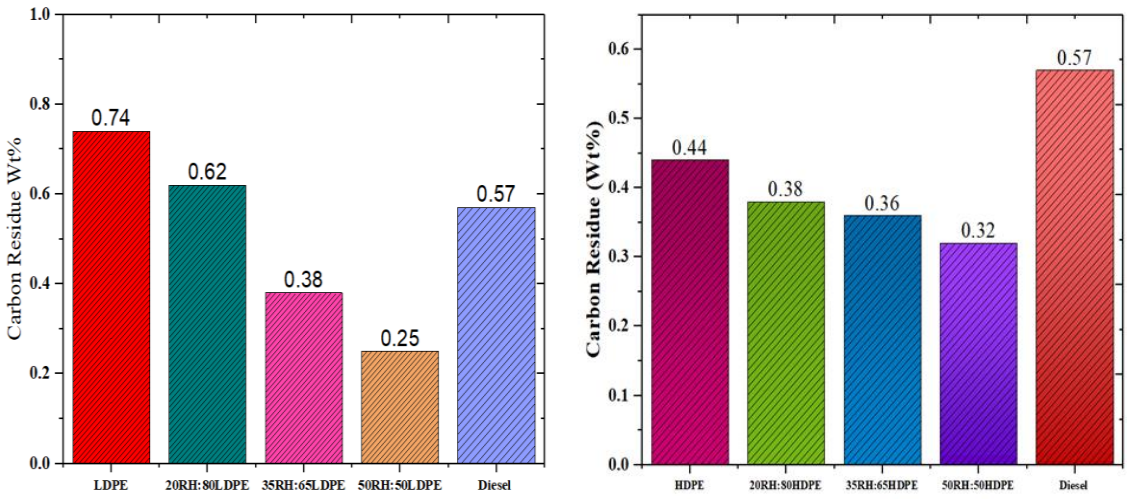

(a) **(b)**

Figure 6.5. (a) Difference in carbon residue of liquid fuel got from LDPE, Rice husk and their blends (b) Distinction in carbon residue (CR) of liquid fuel got from HDPE, Rice husk and their blends.

6.5 Hydrocarbon classification and identification

To classify the chemical components, contained in the liquid product formed from the pyrolysis process of LDPE, HDPE, and rice husk, and their combinations, numerous analytical methods, including the NMR technique, FTIR technique, and GC-MS technique, were applied. The findings of these analyses are shown below.

6.5.1 FTIR investigation of liquid product

Fourier-transform infrared spectroscopy (FTIR) was used to analyze the pyrolysis oil's composition; the findings are displayed in Figure 6.6. In the spectrum area of 3000–2850 $cm^{-}1$, asymmetric and symmetric vibrations linked to the methyl (-CH3) and methylene (>CH2) sets in hydrocarbons were detected [42, 43]. A peak at 2952 cm^{-1} corresponded to

methyl (-CH_3), associated with methyl C-H asymmetric/symmetric stretching. Peaks at 2920 cm^{-1} and 2849 cm^{-1} represented the C-H asymmetric or symmetric functional groups, indicating the presence of alkane series in the oil [35,44]. The alkene C-H stretching band was identified as the band at 3024 cm^{-1}, showing the existence of olefin content [42]. The absorption of the peak signal suggested the existence of aliphatic groups in the region of 1680–1600 cm^{-1}. Furthermore, the -CH3 groups were represented by the peak at 1375 cm^{-1}. The "fingerprint region" is the term used to describe the spectral band between 1500 and 400 cm^{-1} [23,35]. The rice husk and LDPE co-pyrolysis yields liquid products with prominent peaks at 2956.87, 2924.09, and 2856.65 cm^{-1}. When it comes to pyrolysis products, the R-CH=CH2 group is visible at 910 cm^{-1} [42]. The liquid sample derived from separate plastic materials, specifically LDPE and RH, prominently features paraffin and olefin compounds, consistent with the findings from $_1$H NMR and $_{13}$C NMR spectroscopy analyses. Additionally, the other samples of rice husk and HDPE composition will be displayed in a table for better understanding and the FTIR spectra of these products reveal prominent peaks in the 2800 to 3000 cm^{-1} range, corresponding to the characteristic vibrational frequencies of C-H bonds in alkanes and alkenes.

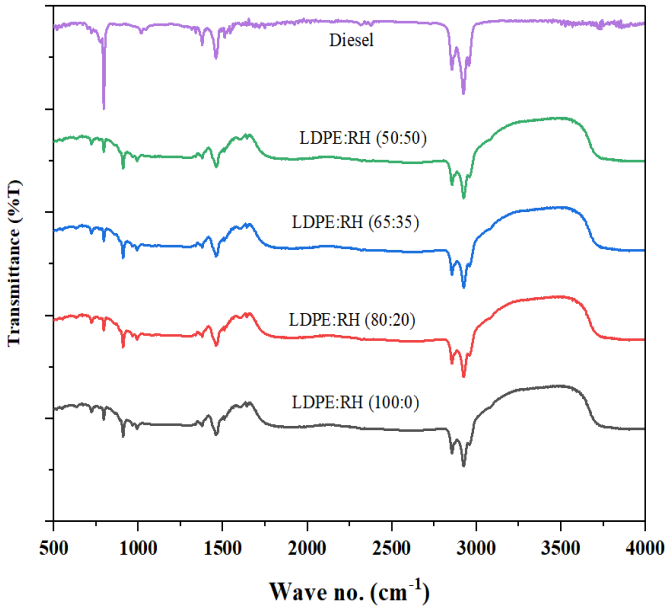

Figure 6.6 FTIR spectra of mixed samples with different ratios of LDPE and RH, as well as oil products obtained from the co-pyrolysis of plastic and biomass.

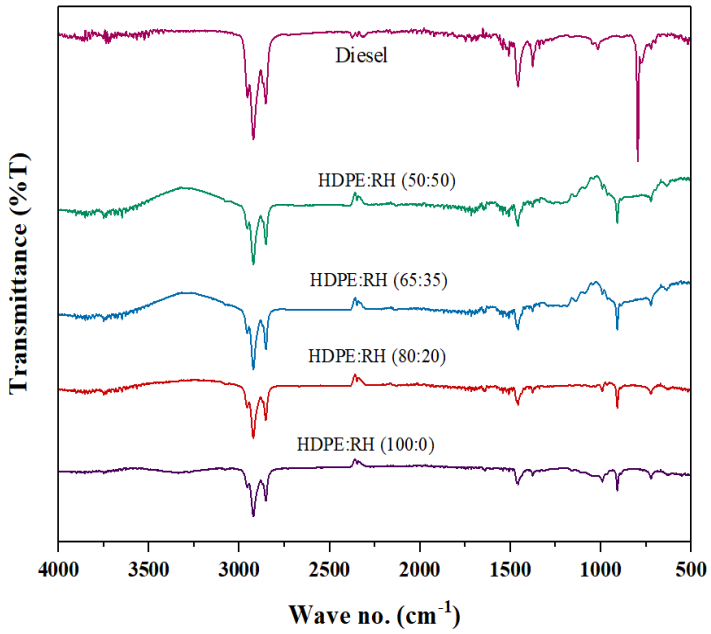

Figure 6.7 FTIR spectrum of the oil products derived from the co-pyrolysis of plastic and biomass (HDPE and RH) as well as mixed samples with varying HDPE and RH compositions

Table 6.4 FT-IR analysis of pyro-oils made by thermos-chemically converting various blends of RH and HDPE.

Wave No. (cm^{-1})	HDPE:RH (100:0)	HDPE:RH (80:20)	HDPE:RH (65:35)	HDPE:RH (50:50)	Diesel	Bond identification	Functional group
3074.65	×	×	×	×	×	C-H vinyl stretch	Alkenes
2956.21	✓	✓	✓	✓	✓	C-H methyl asymmetric stretch	R-CH3
2924.87	×	✓	✓	✓	✓	C-H methylene asymmetric stretch	Methylene (>CH2)

2869.79	✓	✓	✓	✓	✓	Methyl C–H symmetric Stretch	>CH-, Methyne
2853.80	×	×	×	×	×	Methylene C–H symmetric Stretch	Methylene (>CH2)
1649.22	×	×	×	×	×	Alkenyl C—C stretching	olefinic (alkene)
1458.13	✓	✓	✓	✓	✓	C=C-C Aromatic ring stretching	Aromatic ring
1374.80	×	×	×	×	✓	Methyl C–H symmetric bend	-CH3
1155.07	×	×	×	×	×	C-O stretch	Cyclic ethers
968.56	×	×	×	×	×	trans-C-H out-of-plane bend	olefinic (alkene)
887.63	✓	✓	✓	✓	✓	Vinylidene C–H out-of-plane bend	olefinic (alkene)
670.54	×	×	×	×	×	Alkyne C–H bend	Acetylenic(alkyne)

6.5.2 NMR Analysis:

The ^{1}H-NMR method has been used to assess the fractional composition of the olefin, paraffin, and aromatic contents of the pyrolysis oil, as described [34, 35]. Utilizing a volume ratio of 1:20 at 500MHz, the deuterated ($CDCl_3$) was employed as a solvent. The liquid sample produced by LDPE alone and in combination with RH through co-pyrolysis oil demonstrates the predominating peak of R-CH3, R2-CH2, and R3-CH hydrocarbon types in the 0.7–1.5 ppm chemical peak territory. Olefinic hydrocarbons may be detected in the 1.5–2.5 ppm peak area, whereas vinylic compounds were detected in the 4–6.2 ppm peak range [36,37].

The involvement of RH biomass during the co-pyrolysis changes the content of olefin, paraffin, and aromatics as shown in Fig. 6.8 (a) Similar observation where paraffin content enhances with increasing PP content was also reported for the co-pyrolysis of LDPE and

PP [34]. While the presence of a catalyst during co-pyrolysis impacts the hydrocarbon contents, viz. lower carbon chain is expected [38,39]. It has been noted that increasing the RH concentration during co-pyrolysis increases the aromatics concentrations and decreases the paraffin contents. It was also noteworthy that biomass concentration of 20 to 50 wt. % during co-pyrolysis also reduces the olefin contents by 12.73% as indicated. The 1H-NMR results indicate that the LDPE pyro-oil has paraffin, olefin, and aromatic concentrations of 64.75, 21.11, and 14.75 v/v%, respectively. Conversely, the paraffin, olefin, and aromatic content of the co-pyrolysis oil derived from LDPE and RH at varying ratios were initially within the range of 36.92-42.77, 42.97-49.24, and 7.99-20.11 v/v%, therefore. The example of LDPE had the greatest paraffin concentration, and the addition of RH biomass considerably lowered the paraffin level.

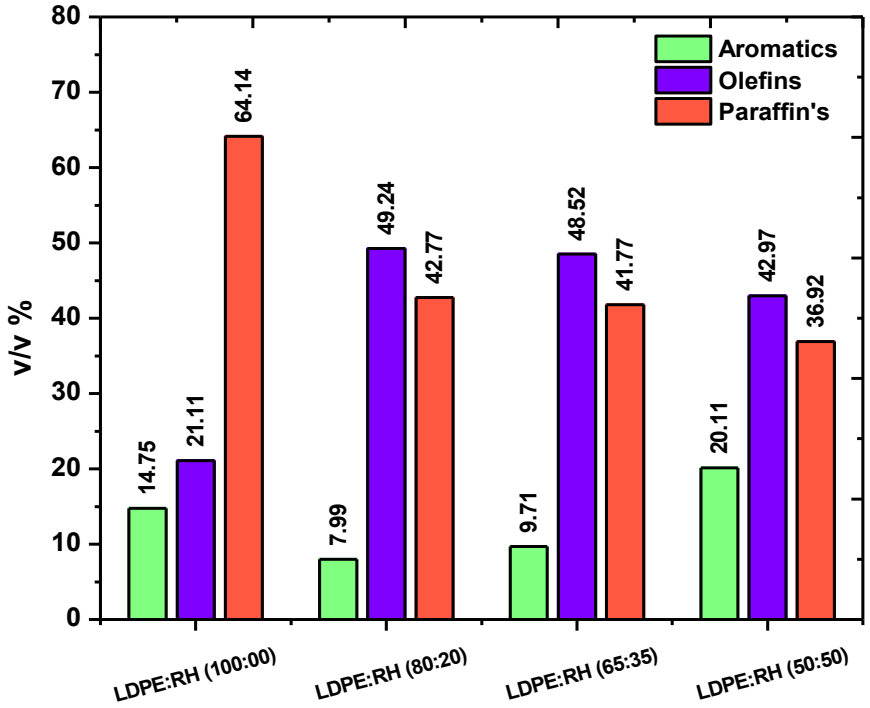

(a)

Figure 6.8 (a) Fractional composition of the co-pyrolysis oil obtained through co-pyrolysis of co-pyrolysis of Low-density Polyethylene (LDPE) and Rice Husk (RH) at various ratio.

It has been noted that when RH is increased during co-pyrolysis, aromatic concentrations are increased and paraffin content is decreased. It is also worth noting that biomass concentrations ranging from 20 to 50 wt.% during co-pyrolysis reduce olefin levels by 12.73%, as shown. According to the ^{1}H-NMR data, HDPE pyro-oil contains paraffin, olefin, and aromatic at 62.14, 20.11, and 11.95 v/v%, respectively. LDPE pyro-oil's paraffin, olefin, and aromatic concentrations are 64.75, 21.11, and 14.75 v/v%, respectively, according to the 1H-NMR results. Yet, the paraffin, olefin, and aromatic content of the co-pyrolysis oil derived from LDPE and RH at various ratios occurred in the range of 36.92-42.77, 42.97-49.24, and 7.99-20.11 v/v%, correspondingly. The highest amount of paraffin content was discovered in HDPE, and the addition of RH biomass greatly decreases the paraffin content as shown in Fig. 6.8 (b).

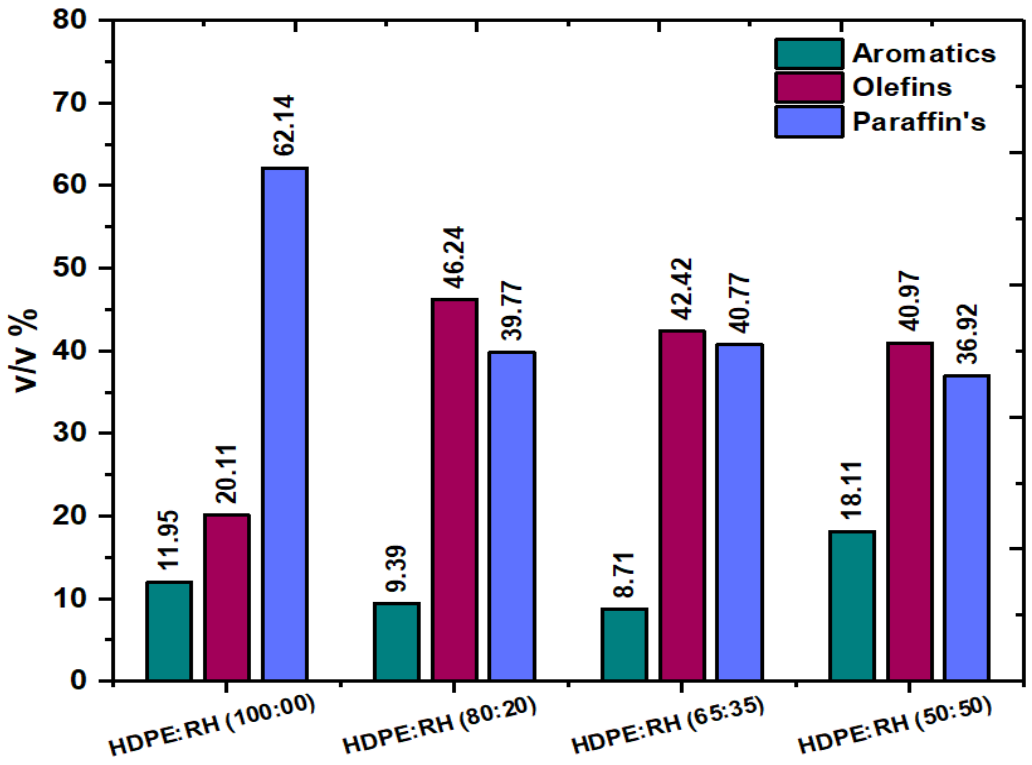

(b)

Figure 6.8 (b) The liquid product generated from HDPE, RH, and its blend ratio, together with the volume fractional composition of aromatics, olefins, and paraffin content.

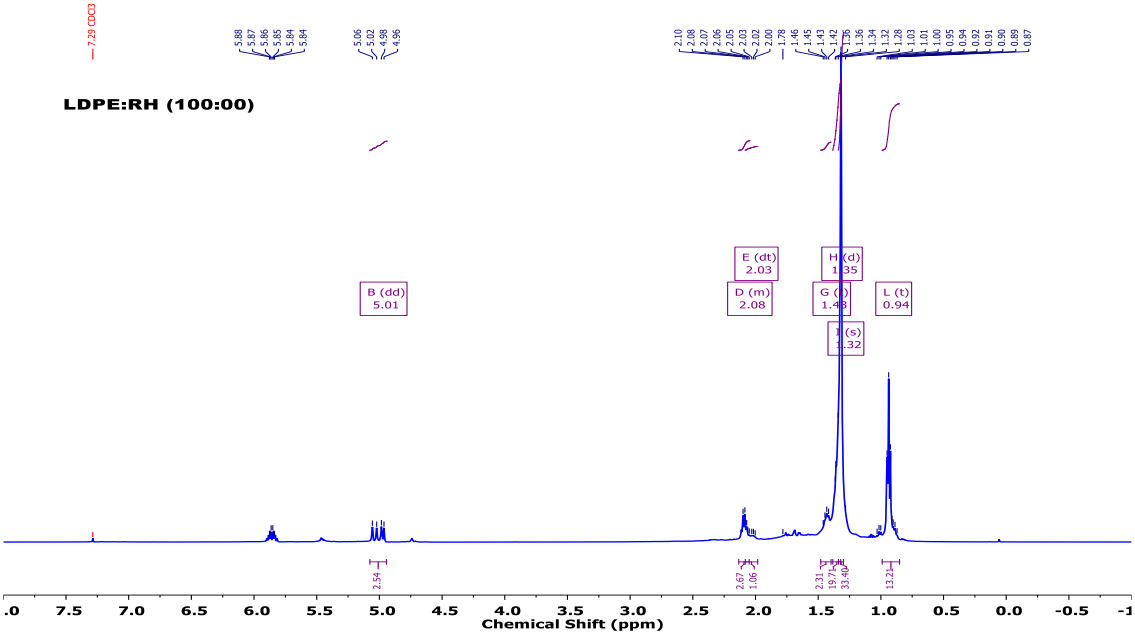

Figure 6.9 (a) [1]H-NMR examination of pyrolysis oil produced by co-pyrolyzing of LDPE and RH (100:00).

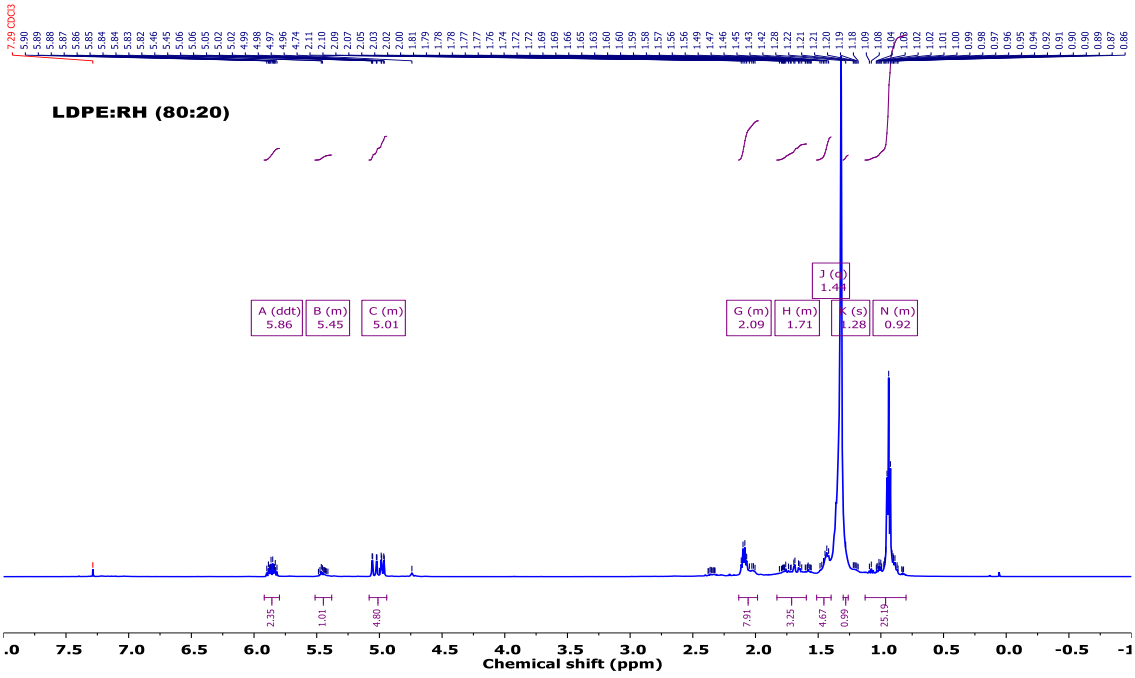

Figure 6.9 (b) ^{1}H-NMR examination of the pyrolysis oil produced by co-pyrolysis of LDPE and RH (80:20)

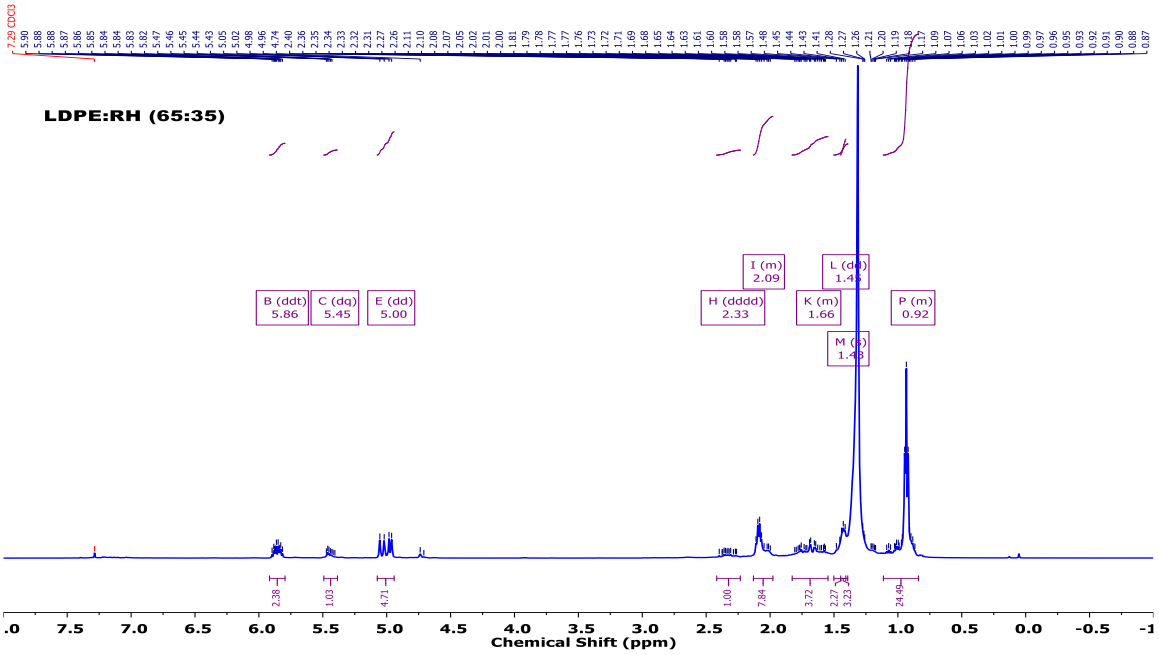

Figure 6.9 (c) ^{1}H-NMR examination of pyrolysis oil produced by co-pyrolysis of LDPE and RH (65:35).

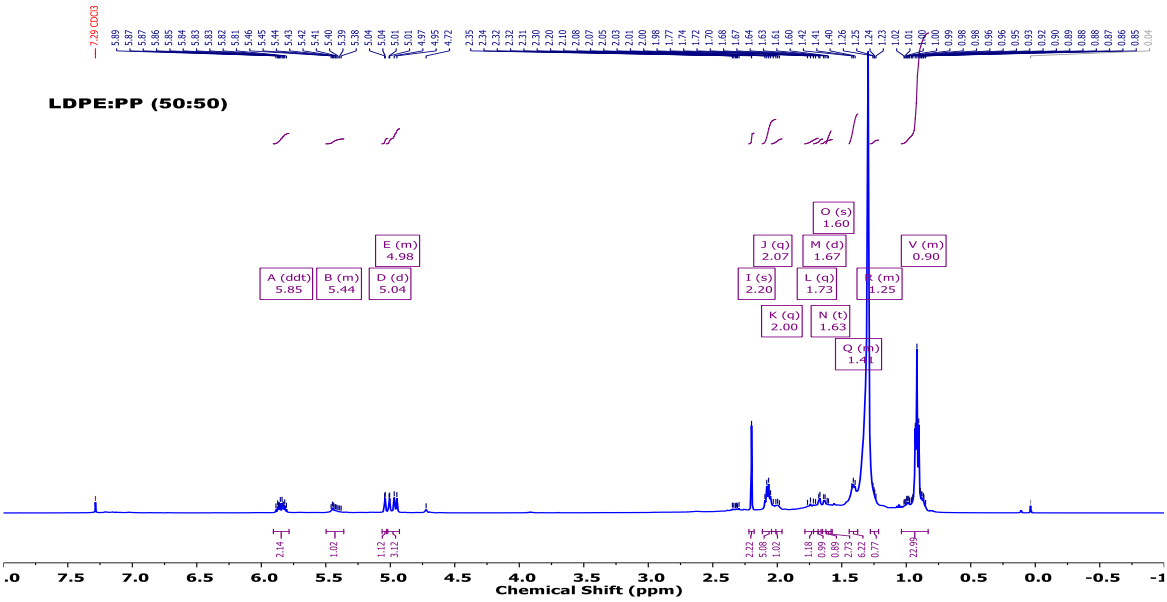

Figure 6.9 (d) [1]H-NMR examination of pyrolysis oil produced by co-pyrolyzing LDPE and RH (50:50).

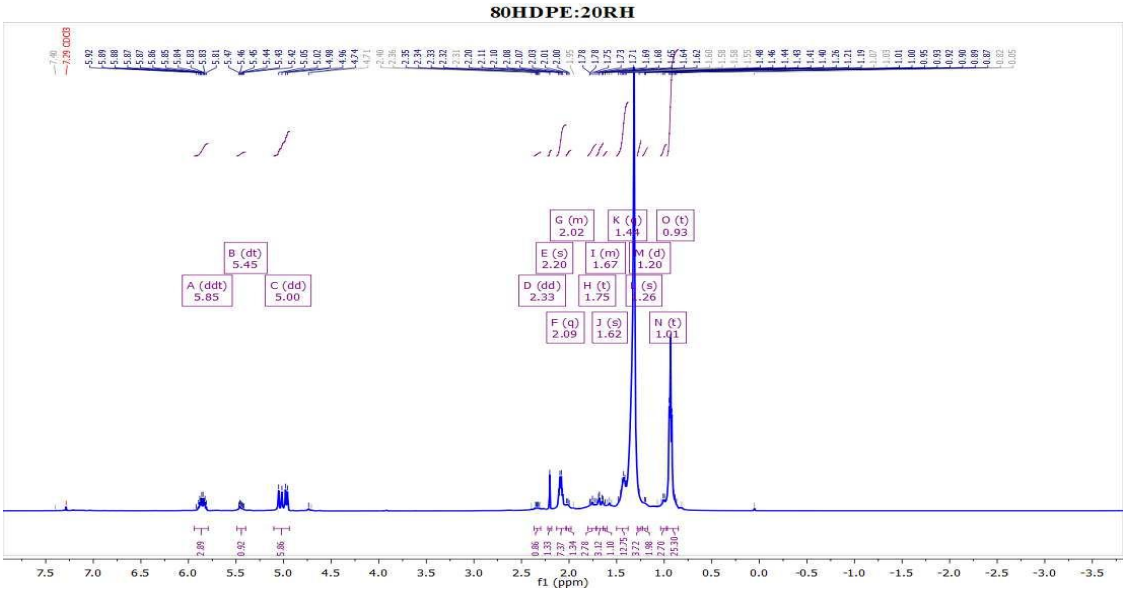

Figure 6.9 (e) [1] H NMR spectrum of the liquid sample produced by co-pyrolyzing HDPE and RH (80:20) under ideal circumstances.

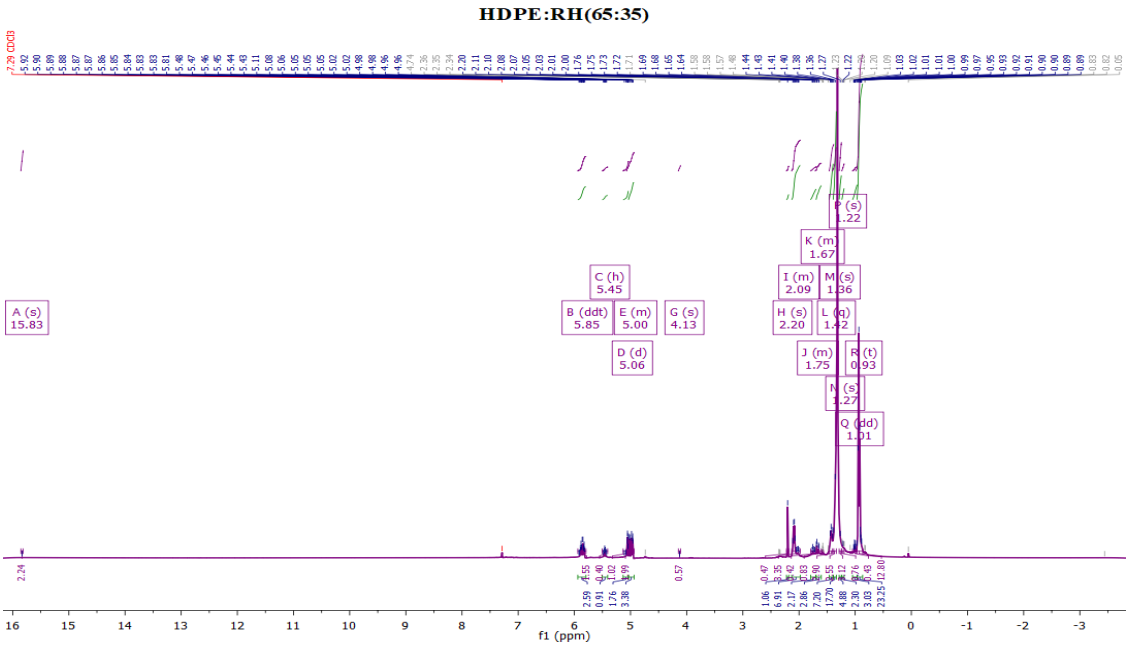

Figure 6.9 (f): [1]H-NMR analysis of pyrolysis oil obtained through co-pyrolysis of HDPE: RH (65:35).

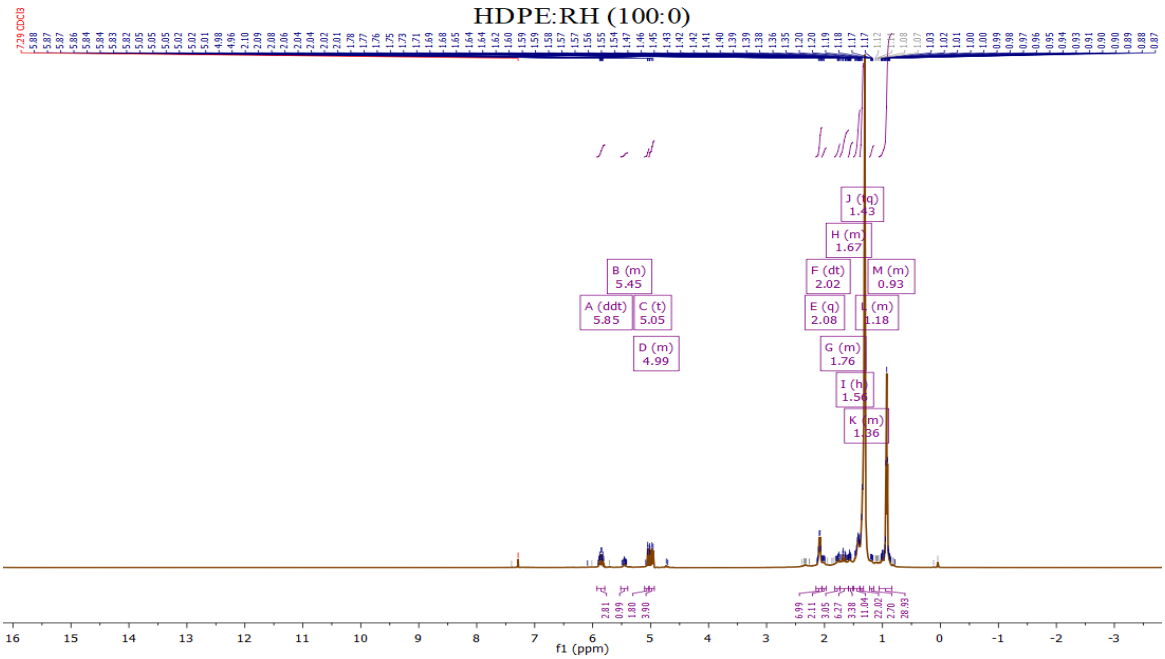

Figure 6.9 (g): [1]H-NMR analysis of pyrolysis oil obtained through co-pyrolysis of HDPE: RH (100:0).

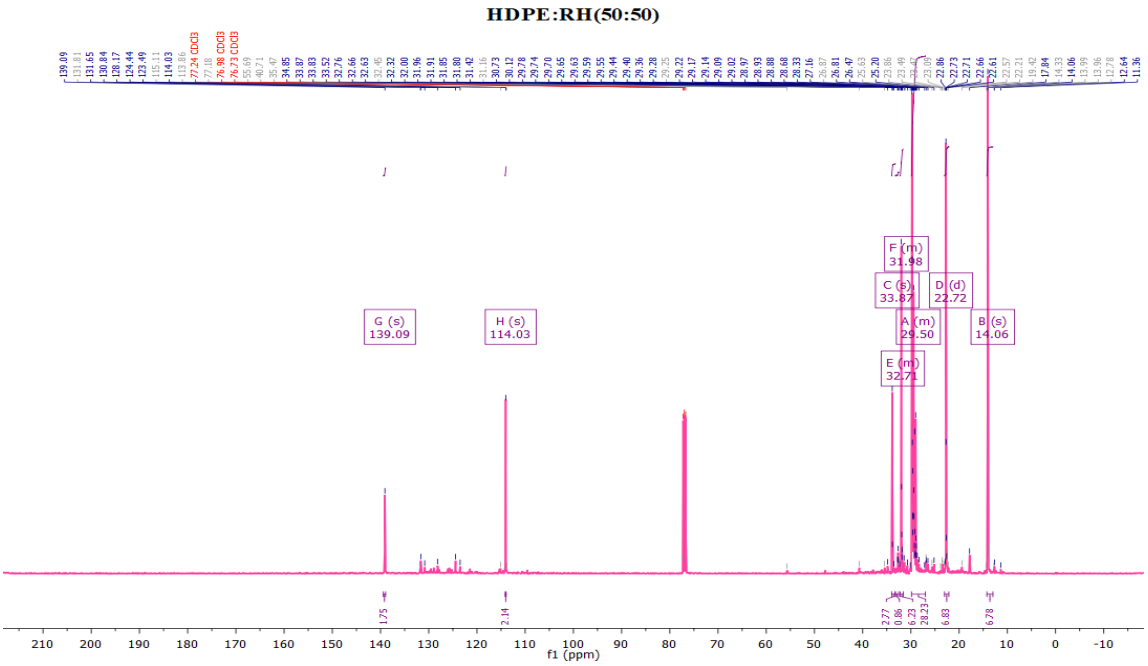

Figure 6.9 (h): ^{1}H-NMR analysis of pyrolysis oil originates through co-pyrolysis of HDPE: RH (50:50).

6.5.2.1 ^{13}C-NMR analysis:

The 13C-NMR spectrum of the LDPE-based pyro-oil of the LDPE and RH liquid samples has been observed to analyze the different types of carbon atoms present in the liquid samples, the degree of branching, and the length of H-C chains. Figure 6.10 displays the 13C-NMR spectra of each co-pyrolysis sample (a-d). Paraffinic hydrocarbons are present in all samples within the 14.10–36.31 ppm chemical shift area. The co-pyrolysis oils show various chemical shifts due to various mixtures of carbons at various chemical shifts. The liquid samples produced by co-pyrolyzing LDPE and RH show the presence of olefinic hydrocarbons, as shown by the chemical shifts of 114.04 ppm and 139.22 ppm. The GCMS results, which are also confirmed by the ^{13}C-NMR data, are in good agreement with the ^{1}H-NMR findings, as seen in Fig. 6.11 (a, b).

The 13C-NMR spectra of the co-pyrolysis oil from HDPE and RH oil samples were recorded to determine the length of H-C chains, assess the degree of branching, and identify the different carbon atom types in the pyro-oil samples. The 13C-NMR spectra of each co-pyrolysis sample are shown in Figure 7. Across all samples, paraffinic hydrocarbons are evident in the chemical shift range of 14.10-36.31 ppm. The co-pyrolysis oils exhibit distinct chemical shifts, reflecting various combinations of carbons at different positions. Notably, chemical shifts at 114.04 ppm and 139.22 ppm indicate the existence of olefinic hydrocarbons in the oil samples obtained through the co-pyrolysis of HDPE and RH. The ^{13}C-NMR results align well with the ^{1}H-NMR findings and are further supported by the GCMS results illustrated in Figure 6.11. samples obtained through co-pyrolysis of HDPE and RH. The ^{13}C-NMR has a good agreement with the ^{1}H-NMR findings as also supported by the GCMS results shown in Figure 6.10 (e-h).

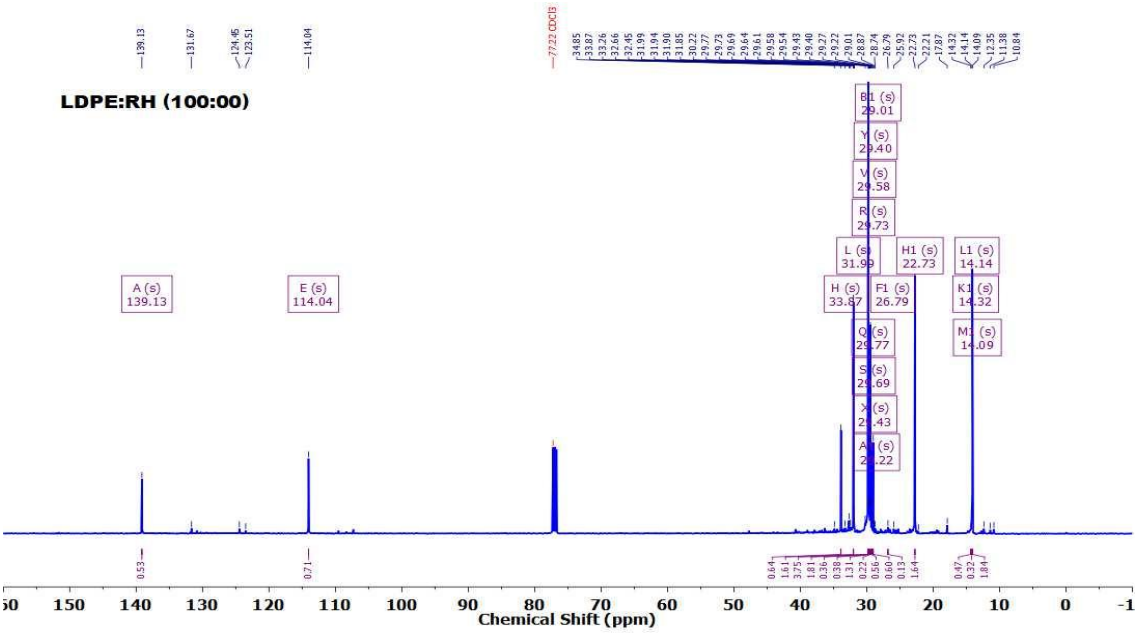

Figure 6.10 (a): ^{13}C-NMR analysis of pyrolysis oil produced by co-pyrolzing of LDPE: RH (100:00).

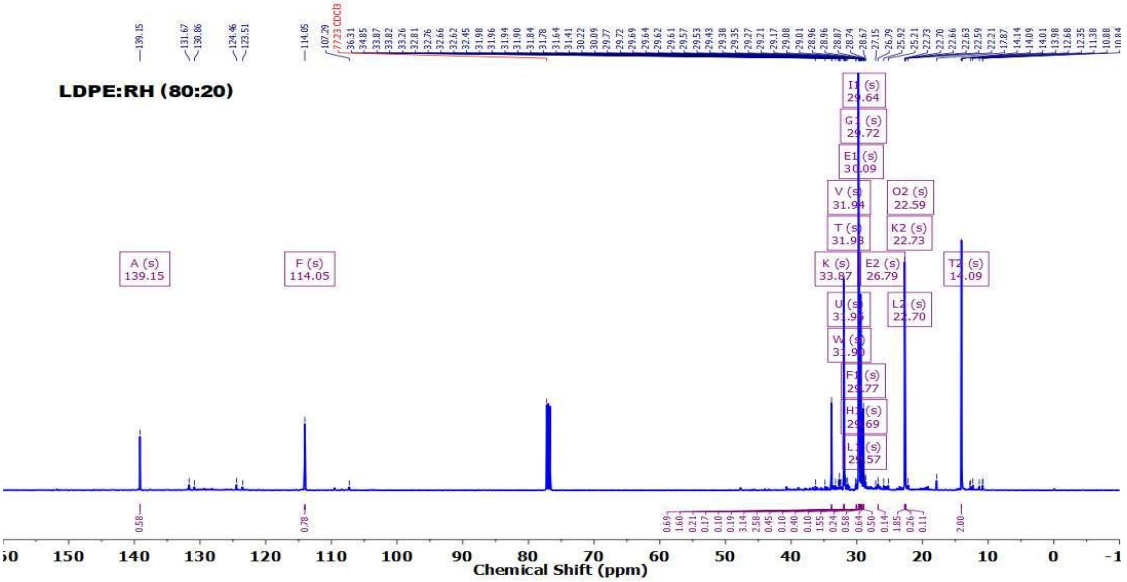

Figure 6.10 (b): ^{13}C-NMR analysis of pyrolysis oil originate by co-pyrolysis of LDPE: RH (80:20).

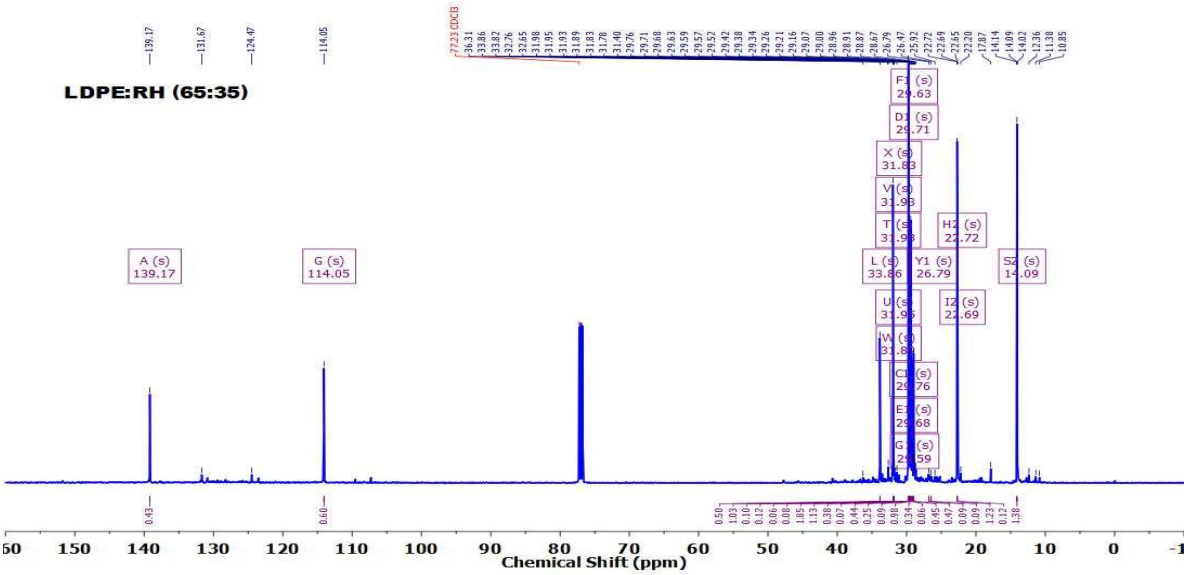

^{13}C NMR (126 MHz, CDCl$_3$) δ 139.17, 131.67, 124.47, 114.05, 77.23, 36.31, 33.86, 33.82, 32.76, 32.65, 31.98, 31.95, 31.93, 31.89, 31.83, 31.78, 31.40, 29.76, 29.71, 29.68, 29.63, 29.59, 29.57, 29.52, 29.42, 29.38, 29.34, 29.26, 29.21, 29.16, 29.07, 29.00, 28.96, 28.91, 28.87, 28.67, 26.79, 26.47, 25.92, 22.72, 22.69, 22.65, 22.20, 17.87, 14.14, 14.09, 14.02, 12.36, 11.38, 10.85.

Figure 6.10 (c): ^{13}C-NMR analysis of pyrolysis oil originate by co-pyrolysis of LDPE: RH (65:35).

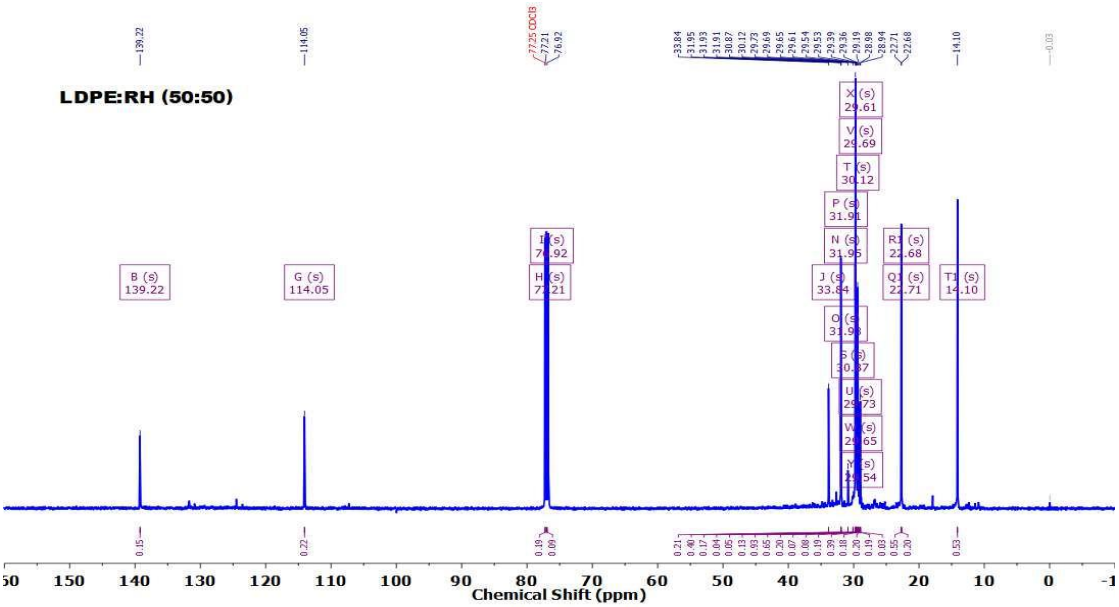

^{13}C NMR (126 MHz, CDCl$_3$) δ 139.22, 114.05, 77.25, 77.21, 76.92, 33.84, 31.95, 31.93, 31.91, 30.87, 30.12, 29.73, 29.69, 29.65, 29.61, 29.54, 29.53, 29.39, 29.36, 29.19, 28.98, 28.94, 22.71, 22.68, 14.10, -0.03.

Figure 6.10 (d) ^{13}C-NMR analysis of pyrolysis oil originate by co-pyrolysis of LDPE: RH (50:50).

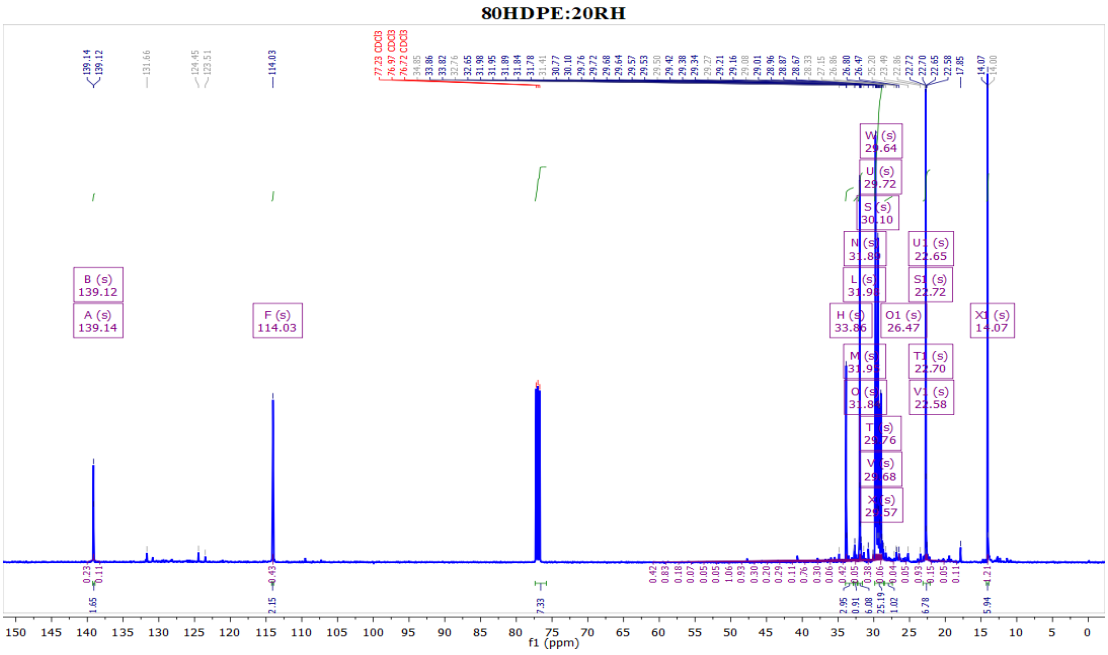

Figure 6.10 (e): ^{13}C NMR spectrum of pyrolysis oil obtained by optimal co-pyrolysis of HDPE and RH (80:20).

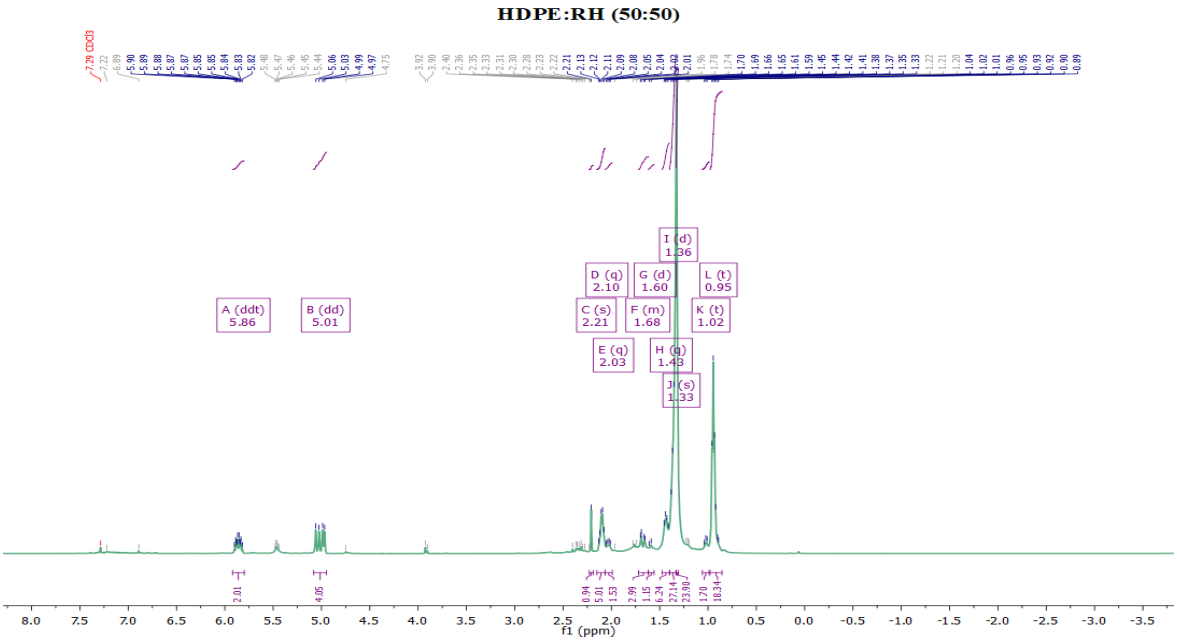

Figure 6.10 (f) ^{13}C-NMR analysis of pyrolysis oil obtained by co-pyrolysis of HDPE: RH (50:50).

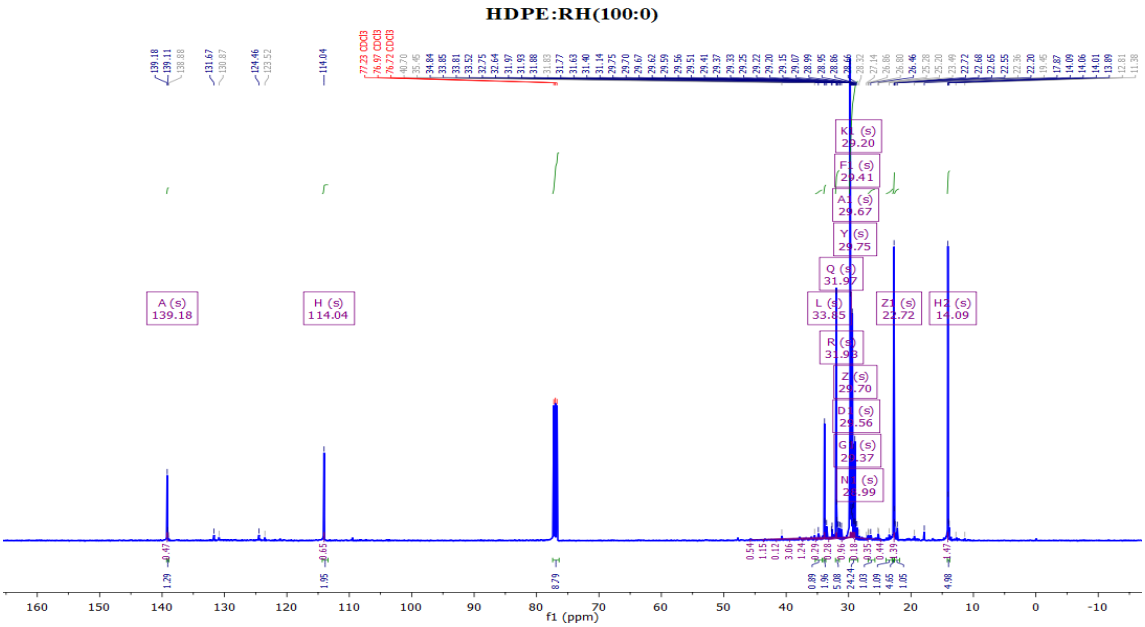

Figure 6.10 (g): ^{13}C-NMR analysis of pyrolysis oil obtained by co-pyrolysis of HDPE: RH (100:00).

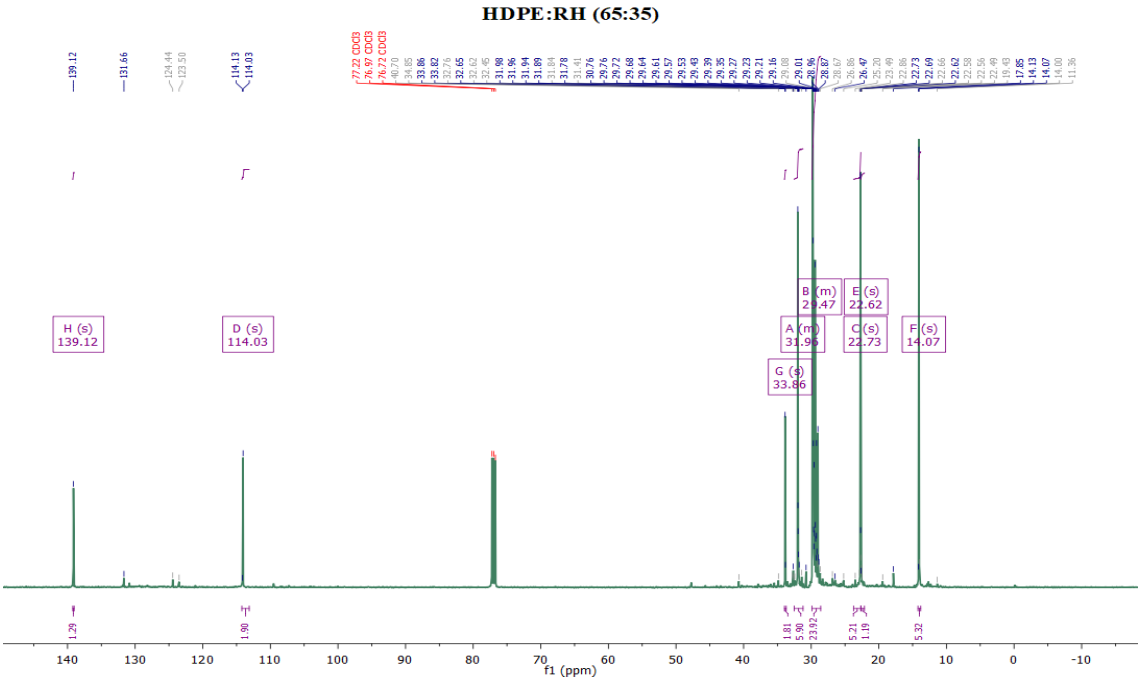

Figure 6.10 (h) ^{13}C-NMR analysis of pyrolysis oil obtained by co-pyrolysis of HDPE: RH (65:35).

6.5.3 GC-MS Analysis:

The chemicals found in the pyro-oils produced by co-pyrolyzing LDPE and RH were examined using GC-MS analysis in accordance with the methodology employed in our earlier studies [40]. The results are shown in **Table 6.5-6.8** and **Figure 6.11**. The results showed that co-pyrolysis oils contain different kinds of hydrocarbons (alcohols, and esters along with alkanes, alkenes, and alkynes) in the range of C_7-C_{24}. The hydrocarbon carbon chain was characterized in the series of $<C_9$, C_9-C_{12}, C_{13}-C_{24}, and $>C_{24}$. Furthermore, the selectivity % of alcohol, esters, and other hydrocarbons was also represented as shown in **Figure 6.11.** The co-pyrolysis oil obtained through LDPE: RH (80:20) gives higher selectivity (88.93%) in the carbon range of C_{13}-C_{24} which dominates the diesel fractions [41,42]. However, this fuel oil has a higher content of oxygenated compounds (49.85%), which influences the fuel properties as indicated in **Table 6.8.** The selectivity % of hydrocarbons in the range of C_{13}-C_{24} were found to be 68.47, 88.93, 67.54 and 49.13% respectively in the case of LDPE: RH (100:00), LDPE: RH (80:20), LDPE: RH (65:35), and LDPE: RH (50:50) pyro-oil.

Similarly, the selectivity % of the carbon chain of C9-C12 were found to be 26.43, 5.30, 32.46, and 41.37 respectively for LDPE: RH (100:00), LDPE: RH (80:20), LDPE: RH (65:35), and LDPE: RH (50:50) pyro-oil. The involvement of RH biomass during co-pyrolysis increases the lower carbon chain (below C_{12}) significantly as shown in **Figure 6.11** supported by the reported results [43]. It is noteworthy that the RH increases the C_{12}-C_{24} fraction up to 20% during co-pyrolysis, further increment in RH ratio increases the content of C_9-C_{12}. Also, the involvement of RH increases the oxygenated compounds due to the input of lignocellulosic material that has high oxygen content. Furthermore, the co-pyrolysis oil obtained through LDPE: RH (50:50) found high selectivity (9.5%) of lower range hydrocarbon (below C_9) as compared to other pyro-oils. This investigation implies that the suitable % ratio (20% in the current investigations) will be suitable to tune the overall properties of the alternate fuels as represented in **Figure 6.11.**

The hydrocarbon selectivity percentages within the C_{13}-C_{24} range were determined to be 80.47%, 76.93%, 69.54%, and 53.13% for HDPE: RH (100:00), HDPE: RH (80:20), HDPE: RH (65:35), and HDPE: RH (50:50) pyro-oils, respectively. Similarly, the selectivity percentages for the carbon chain of C_9-C_{12} were discovered to be 26.43%, 26.30%, 31.45%, and 36.36% for HDPE: RH (100:00), HDPE: RH (80:20), HDPE: RH (65:35), and HDPE: RH (50:50) pyro-oils, respectively. The RH biomass addition during co-pyrolysis greatly enhances the lower carbon chain content (below C_{12}), as seen in **Figure 6.12,** which is corroborated by previous observations (Ferdous et al., 2024). Notably, RH raises the C_{12}-C_{24} proportion by up to 20% during co-pyrolysis, and higher RH ratios add to C_9-C_{12} content. Furthermore, the participation of RH causes a rise in oxygenated compounds due to the entrance of lignocellulosic material with a high oxygen concentration. Furthermore, as compared to other pyro-oils, the co-pyrolysis oil produced by HDPE: RH (50:50) demonstrates a high selectivity (8.50%) of lower-range hydrocarbons (below C_9). This study reveals that a reasonable percentage ratio (20% in this case) is beneficial in modifying the overall qualities of alternative fuels, as shown in Figure 6.12.

The molecular makeup of pyro-oil produced by copyrolyzing rice husk (RH) and high-density polyethylene (HDPE) at an 80:20 ratio. Alkanes and alkenes with carbon numbers between C9 and C25 make up the majority of the components that have been found. The presence of specific compounds has been highlighted, and a comparison with previous studies [44]. indicates similar observations. The components carried out from HDPE and RH (80:20) are 1-decanol, 2-hexyl, 1-hexadecanol, 2-methyl, Oxalic acid, isobutyl hexadecyl ester, The whole list of substances included oil sample made from leftover HDPE and RH is recorded in Tables 6.9 and 6.12. The molecular makeup of oil derived from the 80:20 copyrolysis of rice husk (RH) and high-density polyethylene (HDPE). The analysis was conducted using Gas Chromatography-Mass Spectrometry. A few of the spotted chemicals in the HDPE and RH (80:20) co-pyrolysis are 1-decanol, 2-hexyl, 1-hexadecanol, 2-methyl, Oxalic acid, isobutyl hexadecyl ester, cis-1,2-Cyclododecanediol, Heptadecane, 2,3-dimethyl, cis-1,2-Cyclododecanediol, cis-1,2-Cyclododecanediol, 1-Octanol, 2-butyl,

Tables 6.9 to 6.13 include a comprehensive list of all the chemical components found in the liquid sample made from HDPE and RH and their combination. The supplementary information includes a comprehensive GC-MS analysis and pyrolysis oil composition from LDPE and RH feedstocks.

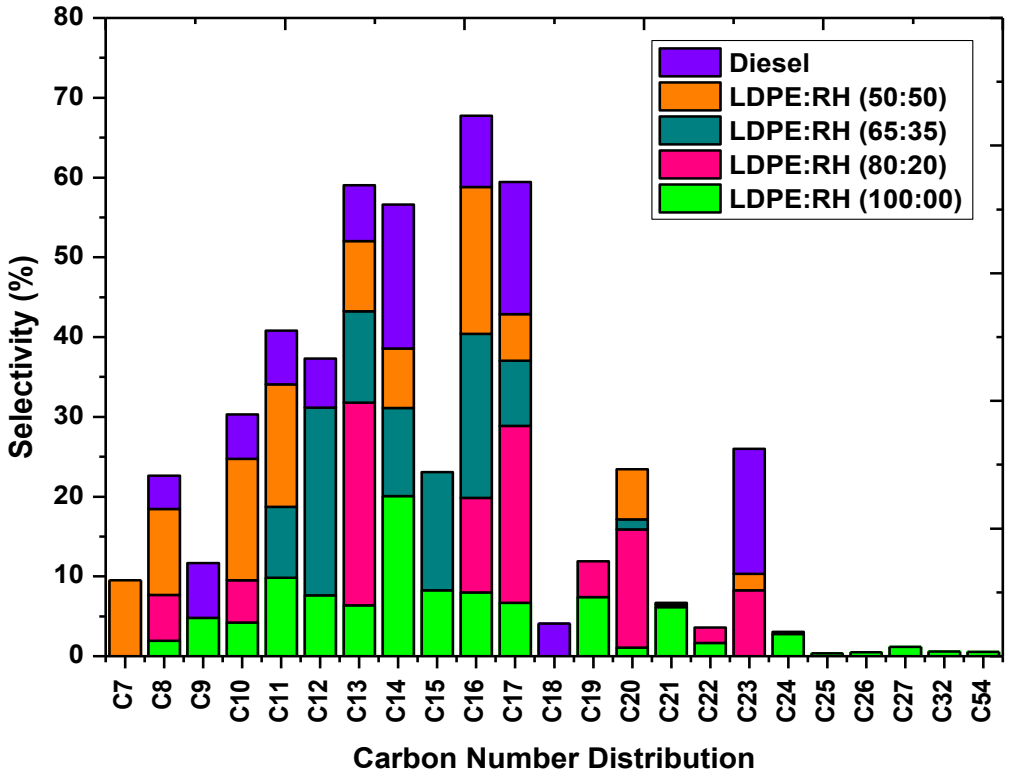

Figure 6.11 Carbon number distribution of pyro-oil produced by co-pyrolyzing of LDPE and RH at various ratios (100:00, 80:20, 65:35, and 50;50).

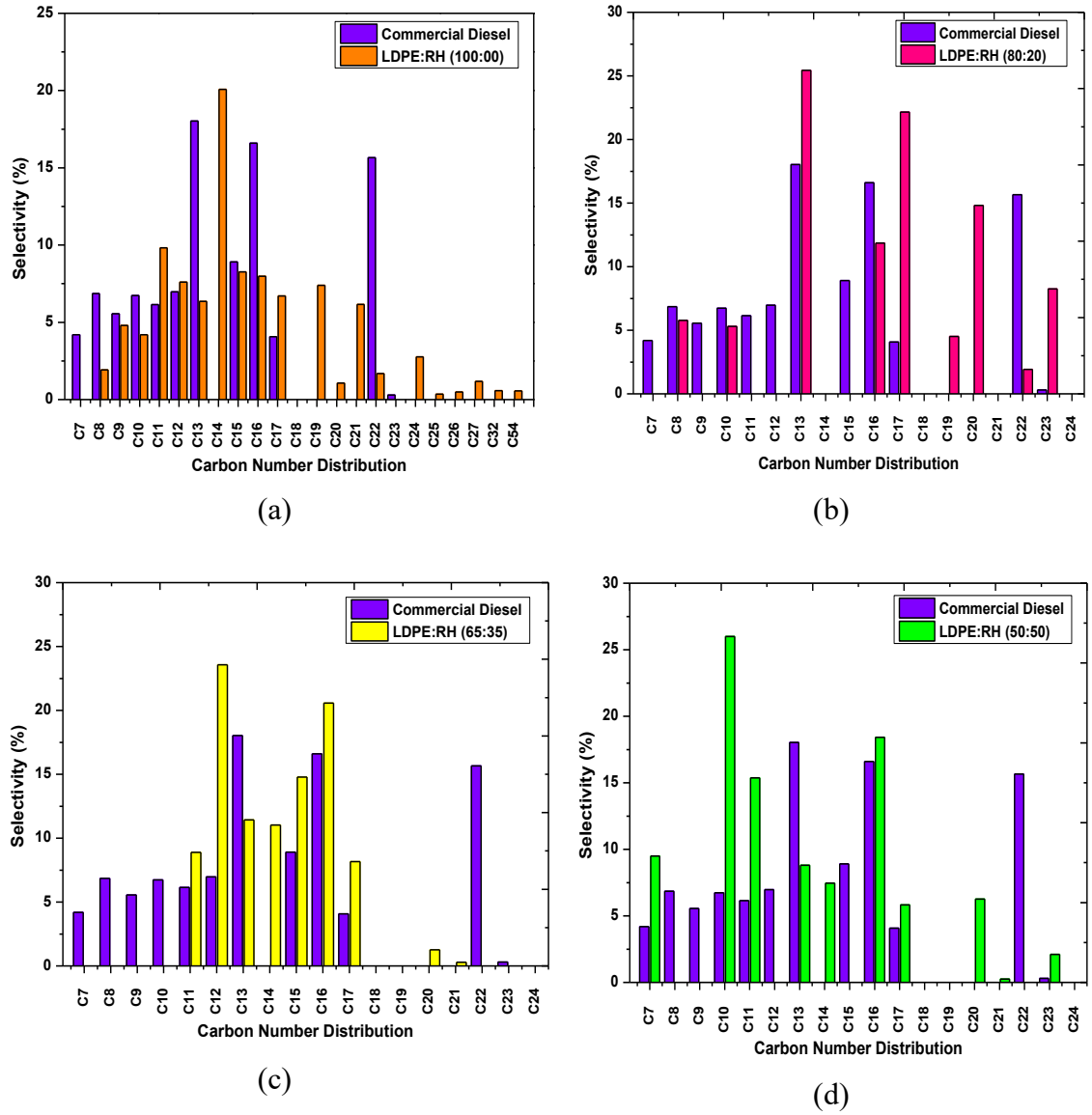

Figure 6.12: Carbon number distribution and selectivity of the pyro-oil produced from co-pyrolysis of LDPE and RH at various feed ratios (a) LDPE: RH (100:00), (b) LDPE: RH (80:20), (c) LDPE: RH (65:35), and (d) LDPE: RH (50:50).

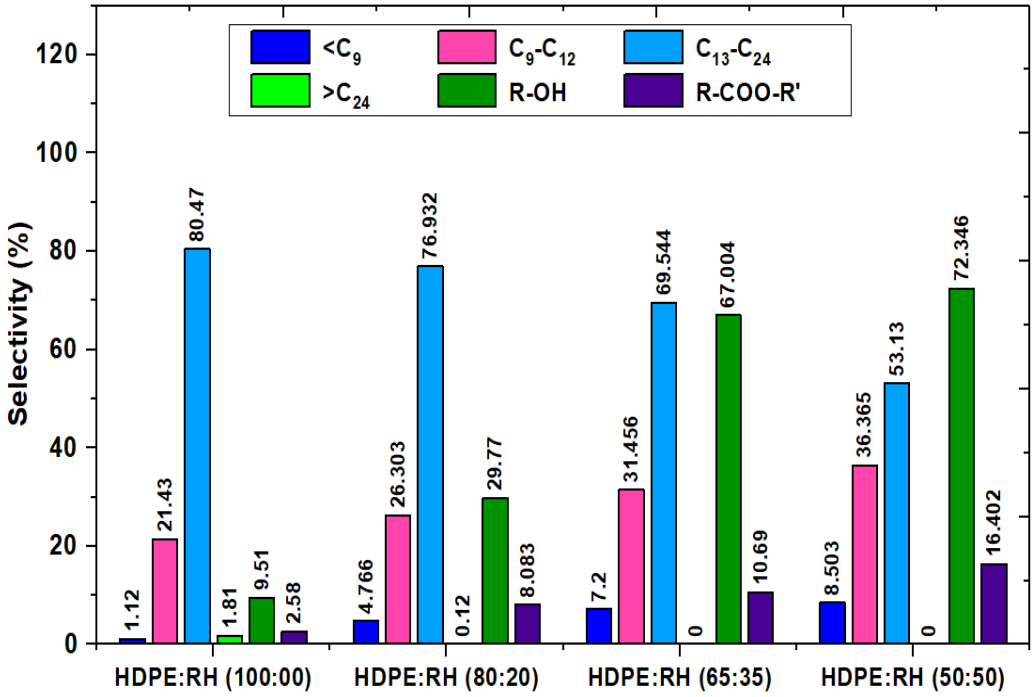

Figure 6.13. Carbon number distribution and selectivity of the pyro-oil formed from co-pyrolysis of HDPE and RH at various feed ratios.

Table 6.5 Identified compounds present in pyro-oil produced through pyrolysis of waste LDPE at optimum condition.

S. No.	R. Time	Compound Name	Mol. Formula	Mol. Weight	Area(%)
1	4.128	Octane	C_8H_{18}	114	1.42
2	4.994	Cyclohexane, ethyl-	C_8H_{16}	112	0.22
3	5.805	Cyclohexane, ethylidene-	C_8H_{14}	110	0.28
4	6.318	1-Nonene	C_9H_{18}	126	2.23
5	6.524	Nonane	C_9H_{18}	126	2.4
6	7.895	Mesitylene	C_9H_{12}	120	0.17
7	8.531	1-Decene	$C_{10}H_{20}$	140	4.2

8	8.71	Undecane	$C_{11}H_{24}$	156	3.51
9	10.28	1,10-Undecadiene	$C_{11}H_{20}$	152	1.01
10	10.44	1-Undecene	$C_{11}H_{22}$	154	5.3
11	11.989	1,9-Tetradecadiene	$C_{14}H_{26}$	194	1.09
12	12.119	1-Tridecene	$C_{13}H_{26}$	182	6.36
13	12.254	Dodecane	$C_{12}H_{26}$	170	6.55
14	12.324	Cyclododecane	$C_{12}H_{24}$	168	0.54
15	14.942	1,15-Pentadecanediol	$C_{15}H_{32}O_2$	244	1.44
16	15.047	1-Tetradecene	$C_{14}H_{28}$	196	7.06
17	15.155	Tetradecane	$C_{14}H_{30}$	198	6.6
18	16.084	2-Methyltetracosane	$C_{25}H_{52}$	352	0.35
19	16.264	1,19-Eicosadiene	$C_{20}H_{38}$	278	1.06
20	16.36	1-Pentadecene	$C_{15}H_{30}$	210	6.16
21	16.459	Hexadecane	$C_{16}H_{34}$	226	6.9
22	16.509	1-Dodecanol	$C_{12}H_{26}O$	186	0.52
23	17.509	(Z)-Tetradec-11-en-1-yl 2,2,2-trifluoroacetate	$C_{16}H_{27}F_{32}$	308	1.08
24	17.597	1-Tetradecanol	$C_{14}H_{30}O$	214	5.33
25	17.687	Heneicosane	$C_{21}H_{44}$	296	6.16
26	18.685	(R)-(-)-(Z)-14-Methyl-8-hexadecen-1-ol	$C_{17}H_{34}O$	254	0.75
27	18.767	n-Nonadecanol-1	$C_{19}H_{40}O$	284	4.24
28	18.848	Heptadecane	$C_{17}H_{36}$	240	5.31
29	18.89	n-Pentadecanol	$C_{15}H_{32}O$	228	0.67
30	19.802	(R)-(-)-(Z)-14-Methyl-8 hexadecen-1-ol	$C_{17}H_{34}O$	254	0.65

31	19.877	1-Nonadecene	$C_{19}H_{38}$	266	3.16
32	21.942	Behenic alcohol	$C_{22}H_{46}O$	326	1.68
33	22.904	1-Heptacosanol	$C_{27}H_{56}O$	396	1.18
34	24.754	Tetracosane	$C_{24}H_{50}$	338	1.71
35	25.55	1-Hexacosanol	$C_{26}H_{54}O$	382	0.49
36	26.684	Bis(2-ethylhexyl) phthalate	$C_{24}H_{38}O_4$	390	1.06
37	27.186	Dotriacontane	$C_{32}H_{66}$	450	0.58
38	30.161	Tetrapentacontane	$C_{54}H_{110}$	759	0.56

Table 6.6 Identified of compounds present in pyro-oil produced through co-pyrolysis of LDPE and RH (LDPE: RH; 80:20) at optimum condition.

S No.	R. Time	Compound name	Mol. Formula	Mol. Weight	Area(%)
1	4.715	5-Octen-1-ol, (Z)-	$C_8H_{16}O$	128	5.766
2	8.194	8-Methyl-6-nonenoic acid	$C_{10}H_{18}O_2$	170	5.303
3	11.744	2-Tridecene, (Z)-	$C_{13}H_{26}$	182	7.813
4	15.089	2-Tridecene, (Z)-	$C_{13}H_{26}$	182	8.903
5	18.138	8-Hexadecenal, 14-methyl-, (Z)-	$C_{17}H_{32}O$	252	8.614
6	20.959	4-Tridecene, (Z)-	$C_{13}H_{26}$	182	8.73
7	23.604	3-Eicosene, (E)-	$C_{20}H_{40}$	280	9.736
8	26.077	E-2-Hexadecacen-1-o	$C_{16}H_{32}O$	240	8.43
9	28.394	1-Hexadecanol, 2-methyl	$C_{17}H_{36}O$	256	6.799
10	30.585	1-Hexadecanol, 2-methyl	$C_{17}H_{36}O$	256	6.744
11	32.637	1-Tricosene	$C_{23}H_{46}$	322	5.63
12	34.595	Z-5-Nonadecene	$C_{19}H_{38}$	266	4.508

13	36.468	1-Decanol, 2-hexyl	$C_{16}H_{34}O$	242	3.417
14	38.248	1-Tricosene	$C_{23}H_{46}$	322	2.613
15	39.958	Heneicosane, 10-methyl	$C_{22}H_{46}$	310	1.916
16	41.595	Ethanol, 2-(octadecyloxy)-	$C_{20}H_{42}O_2$	314	1.43
17	43.169	Ethanol, 2-(octadecyloxy)-	$C_{20}H_{42}O_2$	314	1.025
18	44.69	Ethanol, 2-(octadecyloxy)-	$C_{20}H_{42}O_2$	314	0.756
19	46.159	Ethanol, 2-(octadecyloxy)-	$C_{20}H_{42}O_2$	314	0.508
20	47.579	Ethanol, 2-(octadecyloxy)-	$C_{20}H_{42}O_2$	314	0.407
21	48.957	10-Methylnonadecane	$C_{20}H_{42}$	282	0.299
22	50.289	Ethanol, 2-(octadecyloxy)-	$C_{20}H_{42}O_2$	314	0.246
23	51.61	Ethanol, 2-(octadecyloxy)-	$C_{20}H_{42}O_2$	314	0.153
24	53.102	Ethanol, 2-(octadecyloxy)-	$C_{20}H_{42}O_2$	314	0.151
25	54.878	Ethanol, 2-(octadecyloxy)-	$C_{20}H_{42}O_2$	314	0.104

Table 6.7 Identified the compounds present in pyro-oil produced through co-pyrolysis of LDPE and RH (LDPE: RH; 65:35) at optimum condition.

S.No.	R. Time	Compound Name	Mol. Formula	Mol. Weight	Area (%)
1	4.983	2-Pentadecyn-1-o	$C_{15}H_{28}O$	224	7.532
2	8.24	2,4-Undecadien-1-ol	$C_{11}H_{20}O$	168	8.888
3	11.817	2-Dodecenal, (E)-	$C_{12}H_{22}O$	182	11.499

4	15.163	2-Dodecenal, (E)-	$C_{12}H_{22}O$	182	12.069
5	18.213	13-Tetradecenal	$C_{14}H_{26}O$	210	11.028
6	21.023	4-Tridecene, (Z)-	$C_{13}H_{26}$	182	11.437
7	23.637	cis-9-Hexadecenal	$C_{16}H_{30}O$	238	10.3
8	26.044	Z-8-Methyl-9-tetradecenoic acid	$C_{15}H_{28}O$	240	7.253
9	28.295	1-Decanol, 2-hexyl	$C_{16}H_{34}O$	242	4.831
10	30.436	1-Decanol, 2-hexyl	$C_{16}H_{34}O$	242	3.645
11	32.487	1-Hexadecanol, 2-methyl	$C_{17}H_{36}O$	256	3.152
12	34.436	1-Hexadecanol, 2-methyl	$C_{17}H_{36}O$	256	2.278
13	34.319	1-Hexadecanol, 2-methyl	$C_{17}H_{36}O$	256	1.607
14	38.107	1-Hexadecanol, 2-methyl	$C_{17}H_{36}O$	256	1.12
15	39.834	1-Decanol, 2-hexyl	$C_{16}H_{34}O$	242	0.833
16	41.49	1-Decanol, 2-hexyl	$C_{16}H_{34}O$	242	0.623
17	43.081	Ethanol, 2-(octadecyloxy)-	$C_{20}H_{42}O_2$	314	0.345
18	44.621	1-Decanol, 2-hexyl	$C_{16}H_{34}O$	242	0.346
19	46.107	Ethanol, 2-(octadecyloxy)-	$C_{20}H_{42}O_2$	314	0.287
20	47.537	Ethanol, 2-(octadecyloxy)-	$C_{20}H_{42}O_2$	314	0.232
21	48.929	Ethanol, 2-(octadecyloxy)-	$C_{20}H_{42}O2$	314	0.179
22	50.267	Ethanol, 2-(octadecyloxy)-	$C_{20}H_{42}O_2$	314	0.149
23	51.588	Eicosane, 10-methyl	$C_{21}H_{44}$	296	0.123
24	53.083	Pentadecane, 8-hexyl	$C_{21}H_{44}$	296	0.167
25	54.857	Ethanol, 2-(octadecyloxy)-	$C_{20}H_{42}O_2$	314	0.077

Table 6.8 Identified of compounds present in pyro-oil produced through co-pyrolysis of LDPE and RH (LDPE: RH; 50:50) at optimum condition.

S.No.	R. Time	Compound Name	Mol. Formula	Mol. Weight	Area(%)
1	5.019	1-Cyclohexene-1-methanol	$C_7H_{12}O$	112	9.503
2	8.304	2,4-Decadien-1-ol	$C_{10}H_{18}O$	154	10.751
3	11.897	2-Decyn-1-ol	$C_{10}H_{18}O$	154	15.243
4	15.243	(2,2,6-Trimethyl-bicyclo[4.1.0]hept-1-yl)-methanol	$C_{11}H_{20}O$	168	15.371
5	18.247	cis-9-Hexadecenal	$C_{16}H_{30}O$	238	12.62
6	20.97	Tridecanedial	$C_{13}H_{24}O_2$	212	8.808
7	23.514	9-Hexadecenoic acid	$C_{16}H_{30}O_2$	254	5.794
8	25.919	1-Hexadecanol, 2-methyl	$C_{17}H_{36}O$	256	3.97
9	28.19	2-Ethyl-1-dodecanol	$C_{14}H_{30}O$	214	2.985
10	30.358	2-Hexyl-1-octanol	$C_{14}H_{30}O$	214	2.327
11	32.425	2-Hexyl-1-octanol	$C_{14}H_{30}O$	214	2.146
12	34.399	1-Hexadecanol, 2-methyl	$C_{17}H_{36}O$	256	1.861
13	36.294	Octadecane, 1-(ethenyloxy)-	$C_{20}H_{40}O$	296	1.569
14	38.101	Ethanol, 2-(octadecyloxy)-	$C_{20}H_{42}O_2$	314	1.304
15	39.843	Ethanol, 2-(octadecyloxy)-	$C_{20}H_{42}O_2$	314	1.322
16	41.51	Carbonic acid, isobutyl octadecyl ester	$C_{23}H_{46}O_3$	370	0.801
17	43.113	Carbonic acid, isobutyl octadecyl ester	$C_{23}H_{46}O_3$	370	0.827
18	44.656	Ethanol, 2-(octadecyloxy)-	$C_{20}H_{42}O_2$	314	0.548
19	46.145	Ethanol, 2-(octadecyloxy)-	$C_{20}H_{42}O_2$	314	0.53
20	47.577	Carbonic acid, isobutyl octadecyl ester	$C_{23}H_{46}O_3$	370	0.47
21	48.968	Ethanol, 2-(octadecyloxy)-	$C_{20}H_{42}O_2$	314	0.466
22	50.298	Ethanol, 2-(octadecyloxy)-	$C_{20}H_{42}O_2$	314	0.312
23	51.63	Ethanol, 2-(octadecyloxy)-	$C_{20}H_{42}O_2$	314	0.22
24	53.13	Eicosane, 2-methyl	$C_{21}H_{44}$	296	0.25

Table 6.9 Identified of compounds present in pyro-oil produced through pyrolysis of HDPE at optimum condition.

SI. No	Ret. Time	Compound Name	Mol. formula	Mol. Weight	Area (%)
1	6.124	2,4-Dimethyl-1- heptene	C_9H_{18}	126	0.778
2	7.812	1-Nonane	C_9H_{20}	128	0.935
3	8.049	Nonane	$C_{10}H_{22}$	142	0.9
4	11.544	Decane	$C_{10}H_{22}$	142	1.981
5	14.88	Undecane	$C_{11}H_{24}$	156	3.531
6	17.693	2-Dodecene, (E)-	$C_{12}H_{24}$	168	4.51
7	17.937	Dodecane	$C_{12}H_{26}$	170	4.828
8	20.758	Tridecane	$C_{13}H_{28}$	184	5.07
9	20.866	3-Tetradecene, (Z)	$C_{14}H_{28}$	196	1.444
10	23.379	7-Hexadecene, (Z)	$C_{16}H_{32}$	224	5.255
11	25.65	Decane, 2,3,5,8- tetramethyl	$C_{14}H_{30}$	198	5.114
12	25.843	3-Hexadecene, (Z)	$C_{16}H_{32}$	224	5.647
13	27.977	Tetradecane, 6,9- dimethyl	$C_{16}H_{34}$	226	4.504
14	28.165	3-Octadecene, (E)-	$C_{18}H_{36}$	252	5.529
15	30.357	7-Hexadecene, (Z)	$C_{16}H_{32}$	224	5.066
16	32.434	3-Eicosene, (E)-	$C_{20}H_{40}$	280	4.288
17	32.252	Heptadecane, 2,6,10,14-tetramethyl	$C_{21}H_{44}$	296	1.981
18	34.415	3-Eicosene, (E)-	$C_{20}H_{40}$	280	3.444
19	36.298	5-Eicosene, (E)-	$C_{20}H_{40}$	280	2.606
20	37.973	Heptadecane, 2,6,10,14-tetramethyl	$C_{21}H_{44}$	296	0.938
21	38.107	10-Heneicosene (c,t)	$C_{21}H_{42}$	294	1.819
22	39.728	Heptadecane, 2,6,10,14-tetramethyl	$C_{21}H_{44}$	296	0.51

23	39.839	1-Decanol, 2-hexyl	$C_{16}H_{34}O$	242	1.339
24	41.504	1-Decanol, 2-hexyl	$C_{16}H_{34}O$	242	1.513
25	43.102	Methoxyacetic acid, 2-tridecyl ester	$C_{16}H_{32}O_3$	272	1.192
26	44.653	Oxalic acid, isobutyl hexadecyl ester	$C_{22}H_{42}O_4$	370	0.768
27	46.159	Oxalic acid, isobutyl hexadecyl ester	$C_{22}H_{42}O_4$	370	0.564
28	47.6	Oxalic acid, isobutyl hexadecyl ester	$C_{22}H_{42}O_4$	370	0.353

Table 6.10 Identified of compounds present in pyro-oil produced through co-pyrolysis of HDPE and RH (HDPE: RH; 80:20) at optimum condition.

Peaks	**Ret Time**	**Compound Name**	**Mol. formula**	**Mol weight**	**Area (%)**
1	5.014	5-Octen-1-ol, (Z)	$C_8H_{16}O$	128	7.649
2	8.257	4,4-Dimethyl-cyclohex-2-en-1-o	$C_8H_{14}O$	126	9.809
3	11.806	3-Tetradecyn-1-ol	$C_{14}H_{26}O$	210	14.931
4	15.135	2-Dodecenal, (E)	$C_{12}H_{22}O$	182	15.294
5	18.173	8-Hexadecenal, 14-methyl-, (Z)-	$C_{17}H_{32}O$	252	13.431
6	20.98	9-Octadecenal, (Z)-	$C_{18}H_{34}O$	266	10.744
7	23.603	1-Decanol, 2-hexyl	$C_{16}H_{34}O$	242	8.339
8	26.052	1-Hexadecanol, 2-methyl	$C_{17}H_{36}O$	256	6.591
9	28.343	3-Heptadecene, (Z)	$C_{17}H_{34}$	238	3.794
10	30.518	2-Ethyl-1-dodecanol	$C_{14}H_{30}O$	214	2.763
11	32.593	Ethanol, 2-(octadecyloxy)-	$C_{20}H_{42}O_2$	314	1.706
12	34.559	Ethanol, 2-(tetradecyloxy)-	$C_{16}H_{34}O_2$	258	1.200
13	36.446	1-Tricosene	$C_{23}H_{46}$	322	0.904

14	38.242	1-Decanol, 2-hexyl	$C_{16}H_{34}O$	242	0.649
15	39.966	Tritetracontane	$C_{43}H_{88}$	604	0.509
16	41.615	Ethanol, 2-(octadecyloxy)	$C_{20}H_{42}O_2$	314	0.447
17	43.192	Ethanol, 2-(octadecyloxy)-	$C_{20}H_{42}O_2$	314	0.282
18	44.723	Ethanol, 2-(octadecyloxy)-	$C_{20}H_{42}O_2$	314	0.190
19	46.19	1-Chloroeicosane	$C_{20}H_{41}Cl$	316	0.183
20	47.611	Oxalic acid, isobutyl hexadecyl ester	$C_{22}H_{42}O_4$	370	0.145
21	48.977	Oxalic acid, isobutyl hexadecyl ester	$C_{22}H_{42}O_4$	370	0.120
22	50.305	Heptadecane, 2,3-dimethyl	$C_{19}H_{40}$	268	0.103
23	51.616	Eicosane, 7-hexyl	$C_{26}H_{54}$	366	0.076
24	53.106	Pentadecane, 8-hexyl	$C_{21}H_{44}$	296	0.083
25	54.864	Oxalic acid, isobutyl hexadecyl ester	$C_{22}H_{42}O_4$	370	0.056

Table 6.11. Identified compounds present in pyro-oil produced by co-pyrolysis of HDPE and RH (HDPE: RH (65:35) at optimum condition.

Peaks	**Ret Time**	**Compound Name**	**Mol formula**	**Mol weight**	**Area (%)**
1	5.007	2-Pentadecyn-1-ol	$C_{15}H_{28}O$	224	7.649
2	8.297	5-Octen-1-ol, (Z)-	$C_8H_{16}O$	128	9.809
3	11.897	2-Tridecene, (Z)-	$C_{13}H_{26}$	182	14.931
4	15.253	9-Octadecenal	$C_{18}H_{34}O$	266	15.294
5	18.299	2-Tridecenal, (E)	$C_{13}H_{24}O$	196	13.431
6	21.086	2-Dodecenal	$C_{12}H_{22}O$	182	10.744
7	23.668	Ethanol, 2-(octadecyloxy)-	$C_{20}H_{42}O_2$	314	8.339

8	26.074	1-Decanol, 2-hexyl	$C_{16}H_{34}O$	242	6.591
9	28.328	1-Hexadecanol, 2-methyl	$C_{17}H_{36}O$	256	3.794
10	30.478	2-Hexyl-1-octanol	C14H30O	214	2.763
11	32.527	2-Ethyl-1-dodecanol	C14H30O	214	1.706
12	34.484	3-Heptadecene, (Z)-	$C_{17}H_{34}$	238	1.200
13	36.355	2-Ethyl-1-dodecanol	$C_{14}H_{30}O$	214	1.706
14	38.144	Ethanol, 2-(tetradecyloxy)-	$C_{16}H_{34}O_2$	258	0.649
15	39.865	Ethanol, 2-(tetradecyloxy)-	$C_{16}H_{34}O_2$	258	0.509
16	41.514	2-Hexyl-1-octanol	$C_{14}H_{30}O$	214	0.447
17	43.106	Ethanol, 2-(octadecyloxy)-	$C_{20}H_{42}O_2$	314	0.282
18	44.639	1-Decanol, 2-hexyl	$C_{16}H_{34}O$	242	0.190
19	46.115	1-Decanol, 2-hexyl	$C_{16}H_{34}O$	242	0.183
20	47.542	Ethanol, 2-(tetradecyloxy)-	$C_{16}H_{34}O_2$	258	0.145
21	48.927	Ethanol, 2-(octadecyloxy)-	$C_{20}H_{42}O_2$	314	0.120
22	50.261	Ethanol, 2-(octadecyloxy)-	$C_{20}H_{42}O_2$	314	0.103
23	51.581	1-Decanol, 2-hexyl	$C_{16}H_{34}O$	242	0.076
24	53.075	Ethanol, 2-(octadecyloxy)-	$C_{20}H_{42}O_2$	314	0.083
25	54.844	Ethanol, 2-(octadecyloxy)-	$C_{20}H_{42}O_2$	314	0.056

Table 6.12. Identified of compounds present in pyro-oil produced by co-pyrolysis of waste HDPE and RH (HDPE: RH (50:50) at optimum condition.

Peaks	**Ret Time**	**Compound Name**	**Mol formula**	**Mol weight**	**Area (%)**
1	5.043	2-Pentadecyn-1-ol	$C_{15}H_{28}O$	224	7.649

2	8.413	Z-10-Pentadecen-1-ol	$C_{15}H_{30}O$	226	9.809
3	11.772	3-Tetradecyn-1-ol	$C_{14}H_{26}O$	210	14.931
4	15.344	3-Decyn-2-ol	$C_{10}H_{18}O$	154	15.294
5	18.264	9-Octadecenal	$C_{18}H_{34}O$	266	13.431
6	20.953	E-2-Octadecadecen-1-ol	$C_{18}H_{36}O$	268	10.744
7	23.49	cis-11-Hexadecenal	$C_{16}H_{30}O$	238	8.339
8	25.895	2-Dodecenal, (E)-	$C_{12}H_{22}O$	182	6.591
9	28.179	2-Tridecenal, (E)-	$C_{13}H_{24}O$	196	3.794
10	30.355	1-Hexadecanol, 2-methyl	$C_{17}H_{36}O$	256	2.763
11	32.433	1-Hexadecanol, 2-methyl	$C_{17}H_{36}O$	256	1.706
12	34.416	1-Decanol, 2-hexyl	$C_{16}H_{34}O$	242	1.200
13	36.314	4-Octadecenal	$C_{18}H_{34}O$	266	0.904
14	38.123	1-Hexadecanol, 2-methyl	$C_{17}H_{36}O$	256	0.649
15	39.864	1-Decanol, 2-hexyl	$C_{16}H_{34}O$	242	0.509
16	41.528	2-Hexyl-1-octanol	$C_{14}H_{30}O$	214	0.447
17	43.136	2-Ethyl-1-dodecanol	$C_{14}H_{30}O$	214	0.282
18	44.677	1-Decanol, 2-hexyl	$C_{16}H_{34}O$	242	0.190
19	46.167	Carbonic acid, isobutyl octadecyl ester	$C_{23}H_{46}O_3$	370	0.183
20	47.602	Carbonic acid, isobutyl octadecyl ester	$C_{23}H_{46}O_3$	370	0.145
21	48.989	Ethanol, 2-(octadecyloxy)-	$C_{20}H_{42}O_2$	314	0.120
22	50.323	Ethanol, 2-(octadecyloxy)-	$C_{20}H_{42}O_2$	314	0.103
23	51.647	Ethanol, 2-(octadecyloxy)-	$C_{20}H_{42}O_2$	314	0.076
24	53.148	Carbonic acid, isobutyl octadecyl ester	$C_{23}H_{46}O_3$	370	0.47

25	54.923	9-Hexadecenoic acid	$C_{16}H_{30}O_2$	254	0.056

Table 6.13 Identified compounds present in Bio-oil produced by pyrolysis of Rice husk (RH) at optimum conditions.

Peak	R. Time	Compound Name	Molecular formula	Molecular weight	Area (%)
1	3.171	Phenol	C_6H_5OH	94	3.98
2	3.28	2,5-Dimethylfuran	C_6H_8O	96	0.68
3	3.23	2-Butanone	C_4H_8O	72	2.20
4	3.32	1-Acetoxy-2- propanone	$C_5H_8O_8$	116	1.06
5	3.40	Decane	$C_{10}H_{22}$	142	0.27
6		1-Methyltetrazole	$C_2H_4N_4$	84	0.68
7	4.33	2-Hydroxy-2-cyclopenten-1-one	$C_5H_6O_2$	98	0.54
8	4.45	4-octyne	C_8H_{14}	110	1.07
9	4.51	1-Hydroxy-3-methyl-2-butanone	$C_5H_{10}O_2$	102	2.08
10	4.56	3-Methyl-1,2-cyclopentanedione	$C_6H_8O_2$	112	3.16
11	4.67	1-Acetyl-2-methylcyclopentene	$C_8H_{12}O$	124	0.69
12	5.08	Phenol,3-methyl-	C_4H_8O	108	2.58
13	6.16	3-octadecene (E)-	$C_{11}H_{16}O_2$	180	0.39
14	7.51	1-Tridecene	C13H26.	144	0.71
15	7.61	2-Isopropyl phenol	$C_9H_{12}O_2$	182	0.64
16	8.87	3-Methyl-3-cyclohexene-1-carbaldehyde	$C_8H_{12}O$	124	0.46
17	8.95	2,6-Dimethoxyphenol	$C_8H_{10}O_3$	154	0.80
18	9.51	2,3-Dimethylcyclohexanol	$C_8H_{16}O$	128	0.99
19	10.25	1-Heptanol,2,4-diethyl-	$C_{11}H_{24}O$	172	0.41

20	10.75	2-Decanoic acid	$C_{10}H_{18}O_2$	170	1.42
21	11.6	Tetradecane	$C_{14}H_{30}$	198	0.55
22	11.72	4-Hydroxy-3-methoxyphenyl acetone	$C_{10}H_{12}O_3$	180	0.26
23	12.65	2-Propentyl diacetate	$C_7H_{10}O_4$	158	0.83
24	12.73	Nonadecane	$C_{19}H_{40}$	180	0.90
26	13.66	Hexadecane	$C_{16}H_{34}$	210	0.40
25	15.70	Naphthalene,2-phenyl	C_6H_{12}	204	1.47

6.6 Bio-oil from PET

In an initial investigation, pyrolysis of PET (Polyethylene terephthalate) was carried out to examine the potential products it could generate. A transparent acrylic condenser was employed within the same setup to facilitate observation during the experiment. The results revealed that a yellowish liquid was produced and collected in the condenser, as depicted in Figure 6.14. Over a few minutes, this yellowish liquid transformed into a solid state and adhered to the inner walls of the condenser. This yellowish substance caused blockages in the piping from the reactor to the condenser, leading to issues with collecting the product and maintaining system sterility.

According to the findings of Cepeliogullar and Putun [45], this yellowish substance was identified as benzoic acid, known for its propensity to obstruct pipes and heat exchangers. As a result, this issue requires serious consideration when operating at an industrial scale. These findings suggest that the pyrolysis of PET proved to be inefficient in terms of both time and cost due to the need for frequent maintenance.

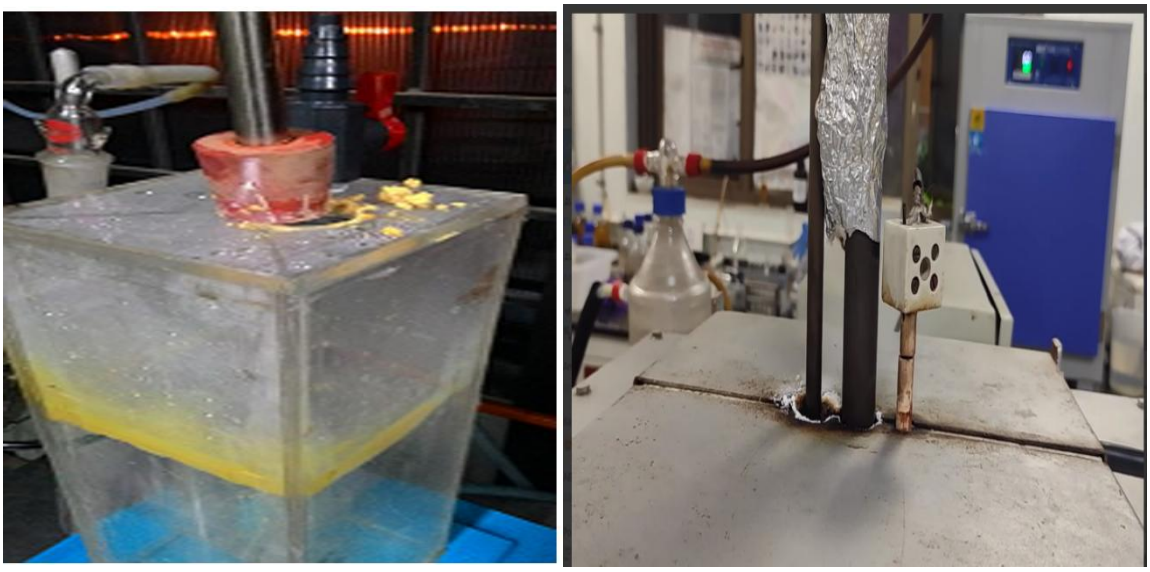

Figure 6.14 Real view image of PET pyrolysis after effect reactor blockage.

6.7 Conclusion

The growing global energy demand and the serious environmental dangers associated with the usage of fossil fuels have made sustainable and renewable energy sources urgently necessary. Biomass-derived bio-oil has come to light as a viable option due to its potential as a renewable energy source and its ability to help reduce greenhouse gas emissions. Pyrolysis, a heat process that breaks down biomass, produces bio-oil, a liquid byproduct. However, the traditional pyrolysis process has certain limitations, including low bio-oil yield and poor quality. To overcome these limitations, co-pyrolysis, a promising technique that involves the simultaneous thermal decomposition of multiple feedstocks, has garnered significant attention. By enabling the use of various biomass feedstocks, such as lignocellulosic materials, algae, and waste materials, the co-pyrolysis process offers a special benefit in producing bio-oil with enhanced yield, quality, & energy content. The combination of various feedstocks in co-pyrolysis not only enhances the energy output but also provides an opportunity to manage waste and reduce the environmental impact. Additionally, co-pyrolysis can help mitigate the challenges associated with feedstock availability and variability, making it a versatile and sustainable approach for bio-oil

production. The usability of the produced pyrolytic oil as a transportation fuel can be better evaluated by comparing its physicochemical properties with standard specifications of conventional fuels like diesel and gasoline. Parameters, including calorific value, viscosity, density, flash point, and water content, were evaluated against these benchmarks. While the bio-oil demonstrated promising energy content and comparable density, deviations in viscosity and oxygenated compounds suggest that further upgrading or blending may be required to meet commercial fuel specifications.

6.8 References

1. Saynik, P.B., Moholkar, V.S. (2021). Investigations in the influence of different pretreatments on A. donax pyrolysis: trends in product yield, distribution, and chemical composition. Journal of Analytical and Applied Pyrolysis, 158, 105276. https://doi.org/10.1016/j.jaap.2021.105276.

2. Raja, R. B., Sarathi, R., & Vinu, R. (2022). Selective production of hydrogen and solid carbon via methane pyrolysis using a swirl-induced point–plane non-thermal plasma reactor. *Energy & Fuels*, *36*(2), 826-836.

3. Mishra, R.K., Kumar, P. (2022). Studies of physicochemical properties, kinetic behavior, and thermal degradation profile of waste bio-crude derived from slow pyrolysis in a nitrogen atmosphere. Bioresource Technology Reports, 17, 100984. https://doi.org/10.1016/j.biteb.2022.100984.

4. Eagle L, Hamann M, Low DR (2016) The role of social marketing, marine turtles and sustainable tourism in reducing plastic pollution. Marine Pollution Bulletin, 107(1), 324–332.

5. Sudhir B. Desai, & Chetan K. Galage. (2015). Production and Analysis of Pyrolysis oil from waste plastic in Kolhapur City. International Journal of Engineering Research and General Science, 3(1), 590-595.

6. Dewangan, A., Pradhan, D., & Singh, R. K. (2016). Co-pyrolysis of sugarcane bagasse and low-density polyethylene: Influence of plastic on pyrolysis product yield. Fuel,

185, 508–516. https://doi.org/10.1016/j.fuel.2016.08.011

7. X. Yang, D. Jiang, X. Cheng, F. Marrakchi, C. Yuan, Z. He, S. Wang, A. Zheng. (2022). Nitrogen transfer mechanism research on the co-pyrolysis macroalgae with polyethylene. Sustainable Energy Technology and Assessments, 51, 101886. https://doi.org/10.1016/j.seta.2021.101886.

8. Wang, Z., Burra, K.G., Lei, T., & Gupta, A.K. (2021). Co-pyrolysis of waste plastic and solid biomass for synergistic production of biofuels and chemicals-A review. Progress in Energy and Combustion Science, 84, 1–84. https://doi.org/10.1016/j.pecs.2020.100899.

9. Alam, M., Bhavanam, A., Jana, A., Peela, N.R. (2020). Co-pyrolysis of bamboo sawdust and plastic: synergistic effects and kinetics. Renewable Energy, 149, 1133–1145.

10. Ding, Z., Liu, J., Chen, H., Huang, S., Evrendilek, F., He, Y., Zheng, L. (2021). Co-pyrolysis performances, synergistic mechanisms, and products of textile dyeing sludge and medical plastic wastes. Science of The Total Environment, 799, 149397.

11. Oyedun, A.O., Gebreegziabher, T., Hui, C.W. (2013). Co-pyrolysis of Biomass and Plastics Waste: a Modelling Approach. Chemical Engineering Transaction, 35, 883-888.

12. Arabiourrutia, M., Elordi, G., Lopez, G., Borsella, E., Bilbao, J., & Olazar, M. (2012). Characterization of the waxes obtained by the pyrolysis of polyolefin plastics in a conical spouted bed reactor. Journal of Analytical and Applied Pyrolysis, 94, 230–237. https://doi.org/10.1016/j.jaap.2011.12.012

13. Zhang, B., San, X., Wei, X., Wu, B., Zheng, S., Zhou, Y., Shao, X., Jin, Q., Yang, L., Oguzie, E., Ma, X. (2018). Quasi-in-situ observing the growth of native oxide film on the FeCr15Ni15 austenitic alloy by TEM. Corrosion Science, 140, 1–7.

14. Peng, S., Zhou, M., Liu, F., Zhang, C., Liu, X., Liu, J., Zou, L., Chen, J. (2017). Flame-retardant polyvinyl alcohol membrane with high transparency based on a reactive

phosphorus-containing compound. Royal Society Open Science, 4, 170512. https://doi.org/10.1098/rsos.170512.

15. Miandad, R., Barakat, M.A., Aburiazaiza, A.S., Rehan, M., Ismail, I.M., Nizami, A.S. (2017). Effect of plastic waste types on pyrolysis liquid oil. International Biodeterioration & Biodegradation, 119, 239–252. https://doi.org/10.1016/j.ibiod.2016.09.017.

16. Kumar, R., Mishra, M.K., Singh, S.K., Kumar, A. (2016). Experimental evaluation of waste plastic oil and its blends on a single cylinder diesel engine. Journal of Mechanical Science and Technology, 30(10), 4781–4789. https://doi.org/10.1007/s12206-016-0950-7.

17. Peng, S., Zhou, M., Liu, F., Zhang, C., Liu, X., Liu, J., Zou, L., Chen, J. (2017). Flame-retardant polyvinyl alcohol membrane with high transparency based on a reactive phosphorus-containing compound. Royal Society Open Science, 4, 170512. https://doi.org/10.1098/rsos.170512.

18. Miandad, R., Barakat, M.A., Aburiazaiza, A.S., Rehan, M., Ismail, I.M., Nizami, A.S. (2017). Effect of plastic waste types on pyrolysis liquid oil. International Biodeterioration & Biodegradation, 119, 239–252. https://doi.org/10.1016/j.ibiod.2016.09.017

19. Gaurh, P., Pramanik, H. (2018). A novel approach of solid waste management via aromatization using multiphase catalytic pyrolysis of waste polyethylene. Waste Management, 71, 86–96. https://doi.org/10.1016/j.wasman.2017.10.053.

20. Adegoke, I. A., Ogunsanwo, O., & Ige, A. R. (2021). Bio-Fuel Properties and Elemental Analysis of Bio-Oil Produced from Pyrolysis of Gmelina Arborea. Acta Chemica Malaysia, 5(1), 38–41. https://doi.org/10.2478/acmy-2021-0006.

21. Tang, Z., Chen, W., Chen, Y., Yang, H., and Chen, H. (2019). Co-pyrolysis of microalgae and plastic: Characteristics and interaction effects. Bioresource Technology, 274, 145-152.

22. Khan, M.Z.H., Sultana, M., Al-Mamun, M.R., Hasan, M.R. (2016). Pyrolytic waste plastic oil and its diesel blend: fuel characterization. Journal of Environmental Public Health, 2016, 7869080. https://doi.org/10.1155/2016/7869080.

23. Ahmad, I., Khan, M.I., Khan, H., Ishaq, M., Tariq, R., Gul, K., and Ahmad, W. (2015). Pyrolysis study of polypropylene and polyethylene into premium oil products. International Journal of Green Energy, 12(7), 663–671.

24. Singh, M.V., Kumar, S., and Sarker, M., 2018. Waste HD-PE plastic, deformation into liquid hydrocarbon fuel using pyrolysis-catalytic cracking with a CuCO3 catalyst. Sust. Energy Fuels 2 (5), 1057–1068.

25. Yan, G., Jing, X., Wen, H., and Xiang, S. (2015). Thermal cracking of virgin and waste plastics of PP and LDPE in a semi-batch reactor under atmospheric pressure. *Energy & Fuels*, *29*(4), 2289-2298.

26. Heydariaraghi, M., Ghorbanian, S., Hallajisani, A., Salehpour, A. (2016). Fuel properties of the oils produced from the pyrolysis of commonly-used polymers: effect of the fractionating column. Journal of Analytical and Applied Pyrolysis, 121, 307–317. https://doi.org/10.1016/j.jaap.2016.08.010.

27. Pavia, D.L., Lampman, G.M., Kriz, G.S., Vyvyan, J.A. (2014). Introduction to spectroscopy. Cengage Learning.

28. Nandiyanto, A. B. D., Oktiani, R., and Ragadhita, R. (2019). How to read and interpret FTIR spectroscope of organic material. *Indonesian Journal of Science and Technology*, *4*(1), 97-118.

29. Jing, X., Yan, G., Zhao, Y., Wen, H., & Xu, Z. (2014). Co-cracking kinetics of PE/PP and PE/hydrocarbon mixtures (I) PE/PP mixtures. *Energy & Fuels*, *28*(8), 5396-5405.

30. Yasar, A., Rana, S., Moniruzzaman, M., Nazar, M., Tabinda, A. B., Haider, R., and Ullah, S. (2021). Quality and environmental impacts of oil production through pyrolysis of waste tyres. *Environmental Technology & Innovation*, *23*, 101565.

31. Alawa, B. and Chakma, S., 2022. Synergism and production of hydrocarbon-rich fuel

from mixed-feedstock through co-pyrolysis of LDPE and PP: an assessment of fuel properties, engine performance, and gas emission. Journal of Analytical and Applied Pyrolysis, 168, p.105736.

32. Alawa, B. and Chakma, S., 2023a. Upgradation, product analysis and engine performance of hydrocarbon fuels produced through pyrolysis of thermoplastic polymers with Si and ZSM-5 modified catalysts. Fuel Processing Technology, 250, p.107918.

33. Pavia, D.L., Lampman, G.M., Kriz, G.S. and Vyvyan, J.A., 2014. Introduction to.

spectroscopy. Cengage learning.

34. Clayden, J., Greeves, N. and Warren, S., 2012. Organic chemistry. Oxford University Press, USA.

35. Dwivedi, U., Pant, K.K. and Naik, S.N., 2021. Controlling liquid hydrocarbon composition in valorization of plastic waste via tuning zeolite framework and SiO2/Al2O3 ratio. Journal of Environmental Management, 297, p.113288.

36. Alawa, B. and Chakma, S., 2023b. Insight into the engine performance of pyro-oil synthesized through catalytic co-pyrolysis of mixed waste plastics in the presence of dolomite modified with silica and ZSM-5. Fuel, 354, p.129190.

37. Ferdous, J., Hossain, M.S., Rahman, M.S., Kader, M.A. and Islam, M.R., 2024. Experimental investigation of optimum bio-oil production parameters through co-pyrolysis of three organic wastes. Journal of Analytical and Applied Pyrolysis, 177, p.106308.

38. Anaga, E.S., Oji, A.A. and Okwonna, O.O., 2023. Bio-oil production from co-pyrolysis of rice husk and plastic waste. EQA-International Journal of Environmental Quality, 54, pp.27-35.

39. Cai, W., Wang, X., Zhu, Z., Kumar, R., Amaniampong, P.N., Zhao, J. and Hu, Z.T., (2023). Synergetic effects in the co-pyrolysis of lignocellulosic biomass and plastic waste for renewable fuels and chemicals. Fuel, 353, p.129210.

40. Alawa, B. and Chakma, S., 2023a. Upgradation, product analysis and engine performance of hydrocarbon fuels produced through pyrolysis of thermoplastic polymers with Si and ZSM-5 modified catalysts. Fuel Processing Technology, 250, p.107918.

41. Alawa, B. and Chakma, S., 2022. Synergism and production of hydrocarbon-rich fuel from mixed-feedstock through co-pyrolysis of LDPE and PP: an assessment of fuel properties, engine performance, and gas emission. Journal of Analytical and Applied Pyrolysis, 168, p.105736.

42. Anaga, E.S., Oji, A.A. and Okwonna, O.O., 2023. Bio-oil production from co-pyrolysis of rice husk and plastic waste. EQA-International Journal of Environmental Quality, 54, pp.27-35

43. Ferdous, J., Hossain, M.S., Rahman, M.S., Kader, M.A. and Islam, M.R., 2024. Experimental investigation of optimum bio-oil production parameters through co-pyrolysis of three organic wastes. Journal of Analytical and Applied Pyrolysis, 177, p.106308

44. Cepeliogullar O, Putun AE. Utilization of two different types of plastic wastes from daily and industrial life. In: Ozdemir C, Sahinkaya S, Kalipci E, Oden MK, editors. ICOEST Cappadocia 2013. Turkey: ICOEST Cappadocia; 2013. p. 1–1.

CHAPTER -7

Upgradation of Bio-oil through catalytic cracking by using Dolomite and DOLZSM catalyst

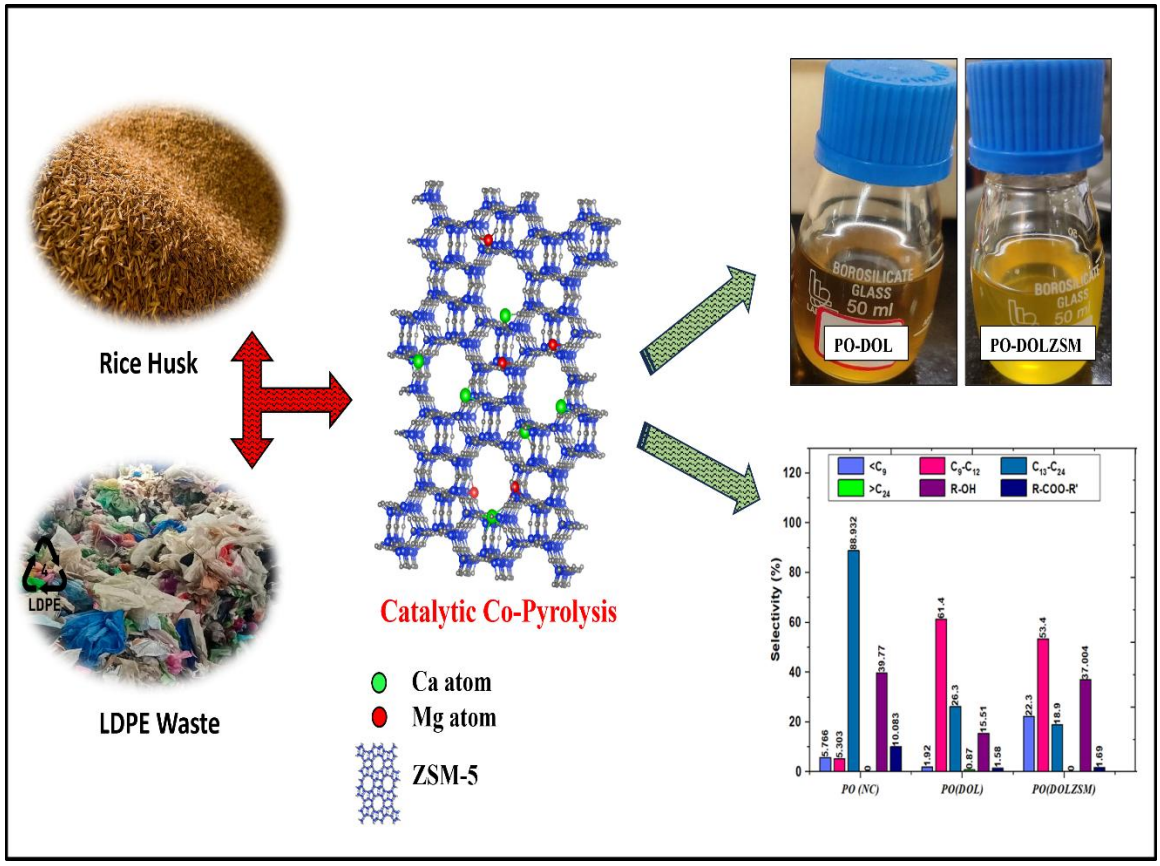

7.1. Introduction

Solid waste management is a key worry for authorities in both small and large cities, since the growing volume of solid garbage created in developing nations puts strain on municipal finances. The financial burden is compounded by a lack of understanding of various factors impacting the entire solid waste handling system [1]. Moreover, the increase in population, rapid urbanization, a thriving economy, and improved living standards in developing

countries collectively accelerate the pace, volume, and quality of municipal solid waste generation [2]. As a global concern, the rising consumption of plastics contributes significantly to the growth of plastic waste within municipal solid waste. Effectively managing this challenge requires implementing various methods based on local regulations and social acceptability. These methods encompass recycling, reusing, land disposal, and the innovative approach of converting waste plastic to energy through pyrolysis [3]. Moreover, biomass is thought to be an abundant renewable energy source on Earth and has a great deal of potential for use as a fossil fuel substitute if it can be transformed into valuable commodities [4]. Pyrolysis is a unique method of managing trash that produces solid char and gases as useful byproducts while also producing liquid oil for energy [5,6,7]. Rice husk, a common agricultural waste that may be found in the environment, is regarded to be a sustainable energy source to produce bio-oil through the process of pyrolysis [8]. However, the oil from the bio-oil cannot be utilized directly in the engines that are now in use due to its high oxygen concentration (high O/C ratio) and low hydrogen content (low H/C ratio) [9]. However, further improvement procedures, including the use of a catalyst or a hydrogen doner, are necessary for the bio-oil generated by pyrolysis [10]. Therefore, the catalytic co-pyrolysis process holds immense potential to transform into a quality fuel by increasing the hydrogen content (high H/C ratio) and decreasing the oxygen content (low O/C ratio).

It has been investigated to add plastic waste to biomass to increase the energy content and quality of the produced biofuels [4]. In order to improve the blended fuel's heating value and combustion properties, plastic components might be mixed in during the pyrolysis process. Compared to biomass, plastics have a higher carbon and hydrogen content but a lower oxygen concentration [11]. Co-processing plastic with rice husk provides more well-rounded fuel characteristics in the resulting pyro-oil. The plastic polymers break down and react with the organic components of rice husk to produce an optimized fuel composition. Research has shown mixing specific plastics with biomass can increase higher heating value to over 30 MJ/kg compared to 16 MJ/kg for biomass [12,13,14]. Overall, adding certain plastic waste feeds can enhance both the fuel's physical properties as well as the net

calorific value [12]. Consequently, numerous strategies have been proposed to convert raw bio-oil into a high-quality and stable oil, making subsequent catalytic processing more feasible. In catalytic co-pyrolysis, catalysts are vital, their primary functions include minimizing coke deposits and increasing the yield of aromatics particularly for processing plastic and biomass blends during co-pyrolysis [15]. Moreover, these catalysts aid in decreasing oxygen content, improving the quality of biofuels, and significantly reducing both the energy required and tar formation [16]. The use of different catalysts, during the pyrolysis of biomass and polymers has been the subject of several investigations such as bentonite clay [17, 18], Ni/dolomite [19], NiO/dolomite [20,21], dolomite [22,23,24] calcined dolomite [25,26], HZSM-5 [27], SiO_2/Al_2O_3 [28,29], $CaO/MgO/Fe_3O_4$ [30], mordenite [31], Y-zeolite [32], ZSM-5 zeolites [33,34], Ni/ZSM-5 [35], and modified CaO and Ga/ZSM-5 [36]. However, studies are reporting the synergistic effects during pyrolysis if catalysts such as dolomite and ZSM-5 are combined to get a versatile acid-base catalyst for enhancing the catalytic performance [37,38]. Thus, these studies have shown that these catalysts could increase selectivity and raise the caliber of the final product. It's crucial to recognize that incorporating a versatile catalyst modifies both the physicochemical traits and chemical properties of the resulting pyrolysis oil. Therefore, selecting catalysts that are easily accessible and cost-effective is vital for minimizing production expenses and ensuring economic viability.

In our investigation, catalytic co-pyrolysis was performed using dolomite (DOL) and zeolite (ZSM) as catalysts, selected for their natural availability and cost-effectiveness compared to other catalysts commonly utilized in pyrolysis processes. Dolomite, a naturally occurring mineral composed of calcium magnesium carbonate, can serve as a basic catalyst, when combined with ZSM-5, a synthetic zeolite rich in acidic sites, it forms a versatile catalytic system, and this catalytic system offers advantages in the shape selectivity functionality due to presence of ZSM-5 and also dolomite addition helps mitigating coke formation. Additionally, the modified catalyst, DOLZSM, was employed to enhance the efficiency of catalytic co-pyrolysis for generating valuable chemicals from mixed biomass and plastic waste, particularly rice husk (RH) and low-density polyethylene

and high-density polyethylene (LDPE, HDPE). Further, the biorefinery approach was utilized by integrating an additional distillation process during the co-pyrolysis to obtain the refined pyro-oil. The resulting liquid products, referred to as pyro-oils, were thoroughly analysed using ASTM methods to assess their chemical composition and physical characteristics. FTIR, NMR, GC–MS, and CHNS analytical techniques were among the several analytical techniques used to carefully characterize the liquid sample. We call attention to the growing importance of the biorefinery technique for bio-oil upgrading technologies in R&D, considering that bio-oil has to be upgraded for use in automobiles, power plants, combustion engines, and biochemical fractionation.

7.2. Characterization of catalysts

7.2.1. Catalyst Structural Evaluation

The calcined dolomite catalyst was analyzed using X-ray diffraction (XRD) to determine its characteristics as depicted in **Figure 7.1**. Consistent with the findings of reported literature, the presence of diffraction peaks at 31° (006), 37° (110), 42° (202), 63° (122), and 67° (300) suggests that $CaMg(CO_3)_2$ constitutes the predominant phase in the calcined dolomite. The characteristic peaks of dolomite (DOL) are discerned at 34.46°, 39.38°, 42.89°, 43.06°, 62.55°, and 79.290°, as observed in prior research [39]. Utilizing the Scherrer equation, the crystal sizes of CaO and MgO were determined based on the peaks at $2\theta = 37.6°$ and 43.06°, respectively. The calculated average particle sizes for CaO and MgO were found to be 77.8 nm and 43.7 nm, respectively, underscoring the nanocrystalline nature of these phases. Remarkably, elevated calcination temperatures induce surface segregation of Mg, facilitating the dispersion of MgO nanocrystals across CaO particles [40]. The distinctive peaks of ZSM were observed at 7.86° (010), 8.82° (020), 23.1° (051), 23.8° (303), and 24.26° (313) according to the JCPDC (ID: 42–0024) [37]. The combined DOLZSM catalyst exhibited distinctive peaks associated with both ZSM and calcined DOL as shown in **Figure 7.1**. Peaks observed at 7.8° (011), 8.8° (020), 22° (051), 23.02° (303), and 24.33° (313) were attributed to ZSM, whereas peaks at 31° (006), 37° (110), 63° (122) and 67° (300) corresponded to the distinctive peaks of calcined DOL [40,34] .

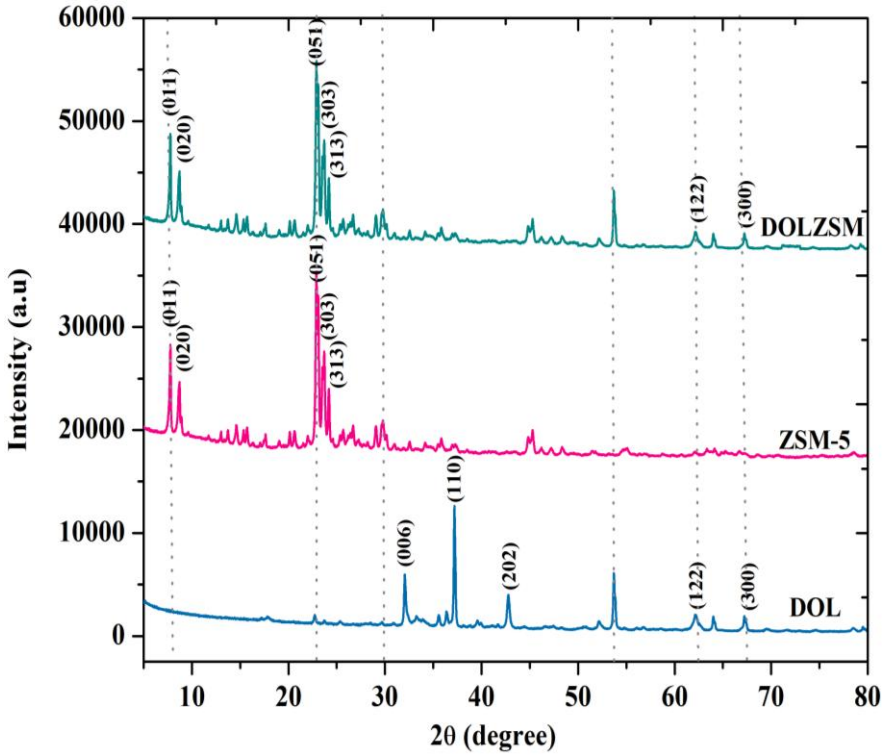

Figure 7.1. XRD spectra of calcined dolomite, ZSM, and DOLZSM catalysts.

7.2.2 FTIR analysis

Different catalysts' FTIR spectra are shown in Figure 7.2. Interestingly, when comparing the FTIR spectra of DOL and ZSM-5 together, they differ from those of DOL and ZSM-5 alone. Furthermore, the presence of a trace amount of adsorbed surface water is verified by the wide OH stretching associated with hydrated carbonate, which is seen in the 2500–3500 cm^{-1} range [41]. Notable characteristics may be seen in the FTIR spectra of calcined dolomite (DOL) at 900°C. In particular, the carbonate bending mode, which is typical of carbonate compounds, is indicated by the existence of a peak at 881 cm^{-1}. Moreover, the peaks observed at 1489.03 cm^{-1} signify the presence of carbonate ions within the sample and it exhibited a novel hydroxyl band peak at 3654 cm^{-1}, suggesting the existence of the -OH functional group and indicating the existence of calcium oxide [42] .

The ZSM-5 catalyst exhibited prominent peaks at specific wavenumbers, providing insights into its structural characteristics. Notably, peaks were observed at 421.44, 448.67,

and 542.71 cm^{-1}. The silicon-oxygen bonds inside the ZSM-5 structure are shown by the Si-O bending mode, which has a peak at 448.67 cm^{-1}. Similarly, the presence of Si-O-H functional groups, which are indicative of ZSM-5's double five-ring structure, especially in its asymmetric stretching mode, is shown by the peak located at 542.71 cm^{-1}. Furthermore, the peak that reaches its highest intensity at 1630 cm^{-1} is credited to the physically adsorbed water bending approach, suggesting that moisture is present in the catalyst. Furthermore, pentasil framework disparity and crystalline substance are indicated by the signal at 550 cm^{-1}, which helps to characterize the ZSM-5 structure further. Moreover, the signal detected at 3621.35 cm^{-1} indicates the vibrational stretching of the hydroxyl group Al-OH, providing further proof of the makeup of the ZSM-5 catalyst. ZSM-5 and dolomite components were both present in the ZSM-5/dolomite (ZSMDOL) catalyst, as Figure 7.2 shows. This indicates the successful preparation of the hybrid catalyst, which incorporates both ZSM-5 and dolomite materials, potentially enhancing the catalytic properties for the pyrolysis process [43].

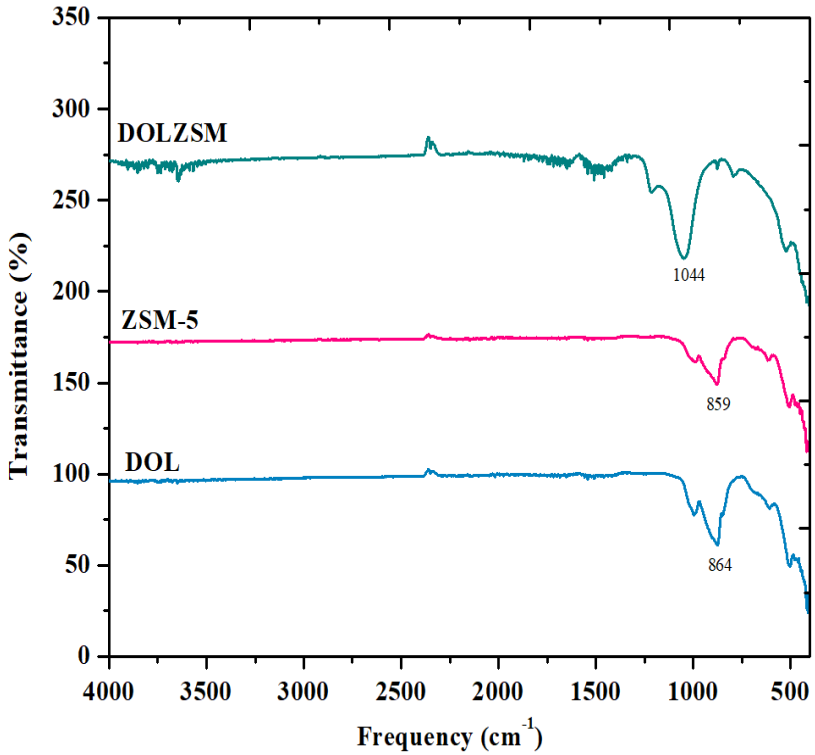

Figure 7.2. FTIR spectra of calcined dolomite, ZSM, and DOLZSM catalysts.

7.2.3 FE-SEM analysis

Field emission scanning electron microscopy (FE-SEM) was used to investigate the catalyst's internal microstructure, particle size, and surface morphology. **Figure 7.3(a), (b), and (c)** shows the FE-SEM images that were obtained. The photos demonstrated the high porosity of the catalyst particles, indicating a large specific surface area that increases the catalyst's activity by providing a high number of active sites for catalytic reactions. This facilitates effective mass transport and reactant molecular diffusion. Furthermore, the synthesized catalysts underwent an energy dispersive X-ray (EDX) analysis, the results of which are shown in Figure **7.3(d), (e), and (f).** The FE-SEM results showed that calcined DOL catalyst consisted of CaO and MgO having uniform particle size, high porosity and homogenous nature which can be also validated from the EDX analysis (**Figure 7.4(a), and (d)**). The calcined dolomite possesses a greater surface area due to the formation of porous grains, rough surface structure, and a cluster of tidy irregular particles [38]. Yang et al. also observed uneven textures on the calcined dolomite catalyst which resulted in CO_2 decomposition occurring over the catalyst's surface [44].

The ZSM-5 catalysts had smooth quasi-rhombohedral particles (with an average size of approximately 100 nm) into surfaces exhibiting unevenness and irregular edges, attributed to the presence of the surrounding matrix enveloping the zeolite crystals (**Figure 7.3(b)**). Additionally, the ZSM catalyst exhibited a crystalline structure with a surface morphology resembling layers or sheets, consistent with findings previously documented [44]. Further, the EDX analysis confirmed the acidic nature of the ZSM catalyst due to the presence of Aluminum (Al) in the ZSM-5 (**Figure 7.3(e)**). Finally, the FE-SEM results of DOLZSM catalysts showed the uniform distribution of dolomite and ZSM-5 particles, a uniform distribution of Mg, Ca, O, Si, and Al which was also confirmed by the EDX results as shown in **Figure 7.3(c), and (f)**.

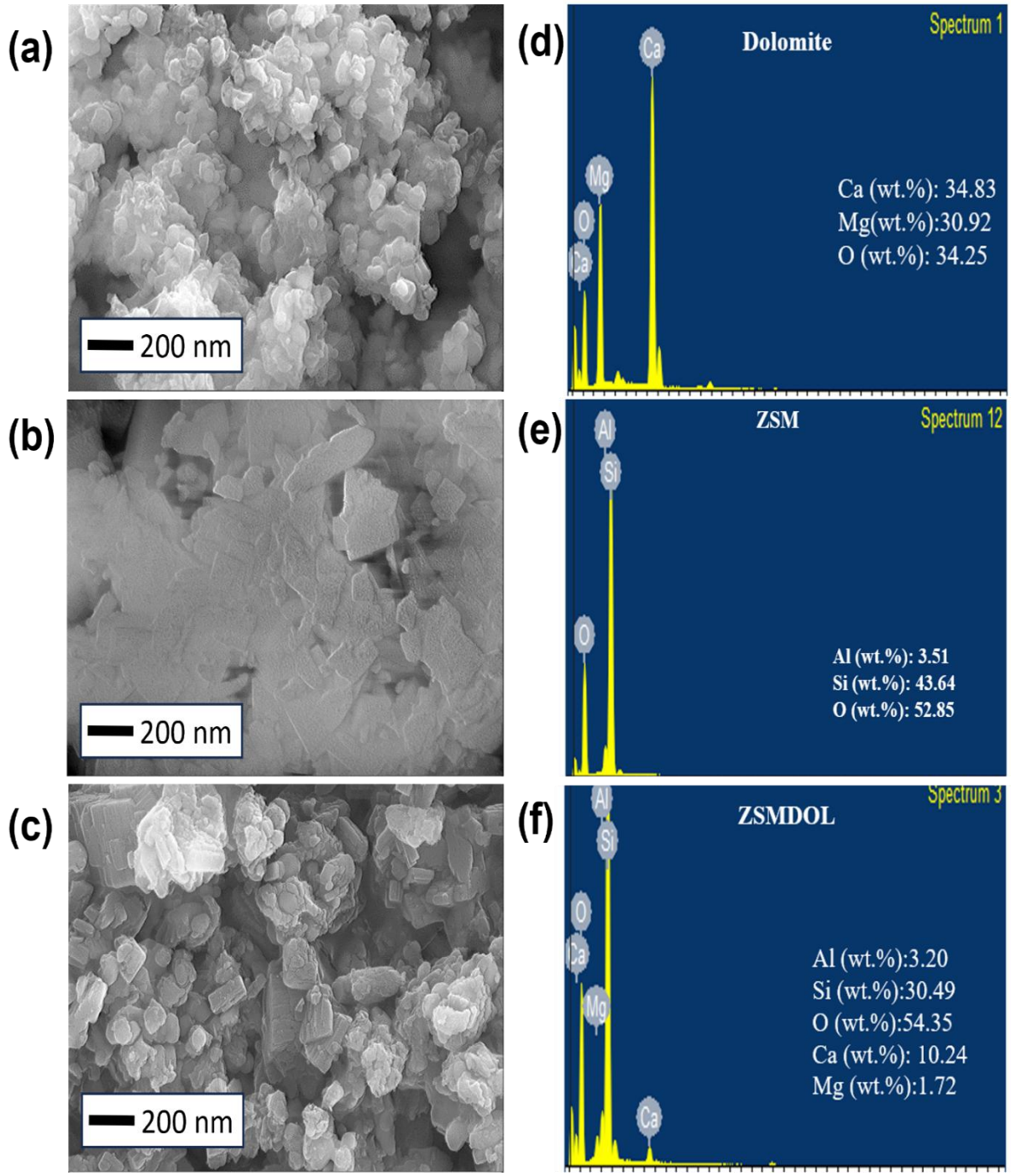

Figure 7.3. FE-SEM images and EDX analysis of the (a), (d) Calcined Dolomite (b), (e) ZSM-5, and (c), (f) DOLZSM catalysts.

7.2.4 BET Surface Area Analysis

BET analysis was used to estimate the catalyst's specific surface area; the results are shown in Table 7.1 and Figure 7.4(a-c). This analysis consisted of quantifying the amounts of nitrogen gas that were absorbed and desorbed on the catalyst surface at a constant temperature of 77 K. The BET results provided information on the catalyst's total pore volume, specific surface area, pore volume, and average pore diameter, among other metrics. The catalyst's pore volume and surface area have an impact on the thermo-catalytic process's catalytic performance [37]. Therefore, to assess the catalytic efficiency of three catalysts dolomite powder (DOL), ZSM-5 powder, and the hybrid catalyst dolomite/ZSM-5 (DOLZSM) an examination of the precise BET surface area and pore size distribution was essential. The surface areas of calcined DOL (calcination at 900°C), ZSM-5, and DOLZSM were found to be 12.70, 343.3, and 138 m^2/g, respectively, based on the results. Significantly, the reduced surface area of ZSMDOL in contrast to ZSM-5 can be explained by the inclusion of dolomite, which fills the pores within the ZSM-5 framework. This result is in line with other studies [46,47] that found that adding metal nanoparticles to the HZSM-5 catalyst reduced its surface area. The influence of secondary components on the porous structure of the catalyst was further demonstrated by the decrease in specific surface area that resulted from the addition of dolomite to the ZSM-5 structure. All things considered, the BET analysis offered insightful information about the catalysts' surface characteristics, which helped to clarify their catalytic behavior and suggest possible uses in thermo-catalytic processes.

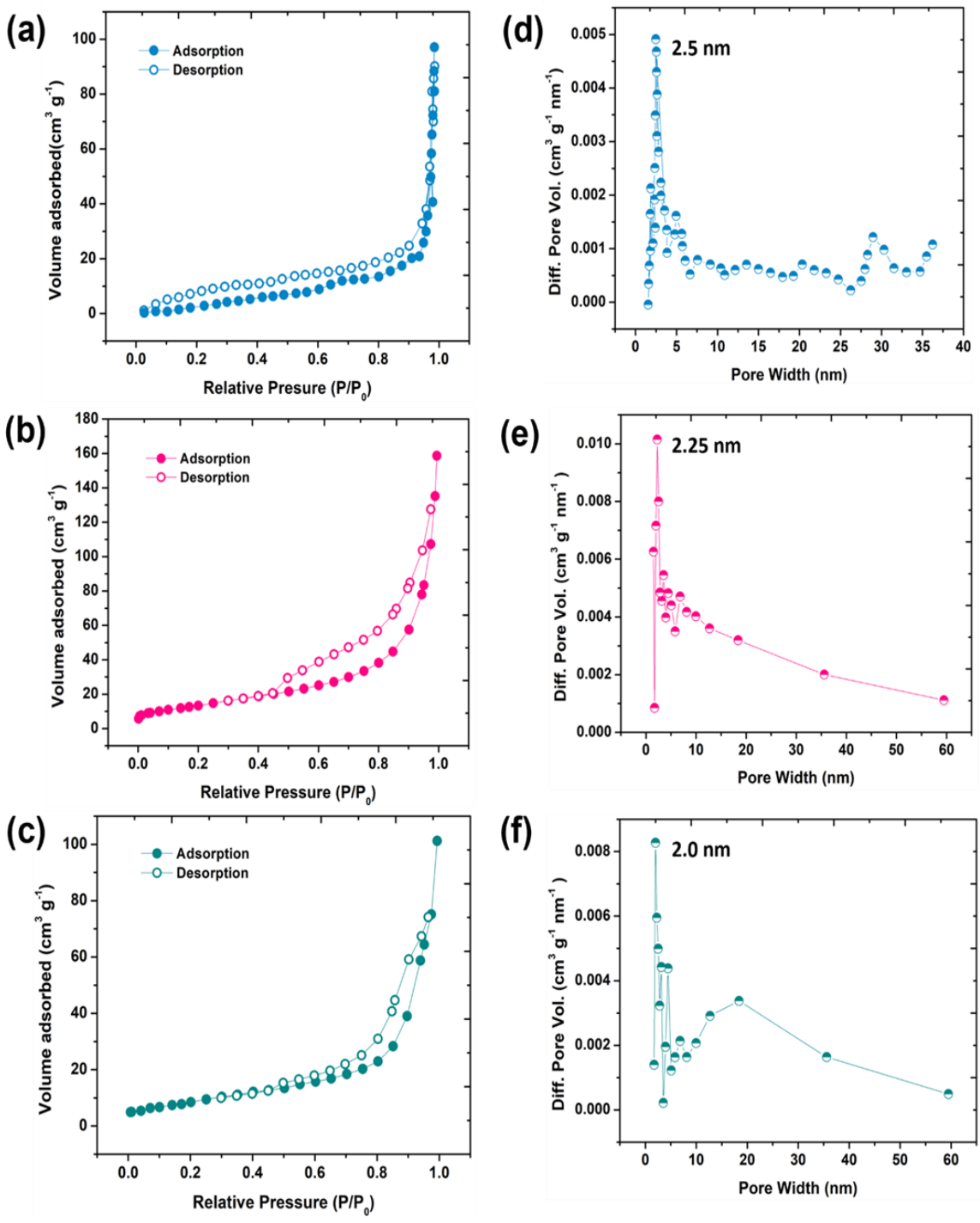

Figure 7.4. BET surface area analysis (a) DOL, (b) ZSM-5, (c) DOLZSM and pore diameter for (d) DOL, (e) ZSM-5, (f) DOLZSM catalysts

Table 7.1. Analysis of Calcined Dolomite, ZSM, and ZSMDOL

Sample	Surface area ($m^2 g^{-1}$)	Volume ($cm^3 g^{-1}$)	Pore size (nm)
Calcined DOL (at 900°C)	12.70	0.78	9.87
ZSM	343.3	0.21	1.27
ZSMDOL	138	0.91	7.3

7.2.5 Dynamic Light Scattering (DLS) Data Analysis

The ZSM-5 and dolomite powder catalysts' particle size distributions were examined using dynamic light scattering (DLS). The study's conclusions provide crucial details on the catalyst particles' size distribution. The dolomite powder's average particle size, according to the DLS Analysis, was 962.2 nm. It was also observed that most of the catalyst particles were distributed within the nanometer range. This finding indicates that the dolomite powder consists of very fine particles, contributing to its high surface area. In contrast, the DLS analysis showed that the ZSM-5 catalyst had a larger average particle size of 3895.7 nm. Despite this larger particle size, the ZSM-5 catalyst exhibited a higher surface area of 20.26 m^2/g. This discrepancy between particle size and surface area suggests that other factors, such as pore structure and morphology, contribute to determining the catalyst's surface area.

7.3 Process yields and fuel property characterization

Figure 7.5 displays the product yields that were achieved by catalytic co-pyrolysis of LDPE and rice husk. The product yield varies between 58–60 wt. % as a liquid product, 8–10 wt. % as a solid-char, and 33–38 wt. % as a gas product when using the DOL catalyst. However, the DOLZSM catalyst produced the most gaseous product (35-37 wt.%) with 10-12 wt. % and 53-54 wt.% of solid char and pyro-oil, respectively. In comparison to catalytic co-pyrolysis without a catalyst, thermal pyrolysis yielded the highest pyro-oil

(liquid product) ~ 65-66 wt. % with 19-20 wt. % and 14-15 wt. % of solid char and pyro-gas, respectively as shown in **Figure 7.5** (a) The order of pyro-oil (liquid) products was found to be without catalyst (~66%) > DOL (~60%) > DOLZSM (54%). Because of the catalyst's wide surface area and enhanced cracking, which produced fewer hydrocarbon products and more gaseous products, the liquid yields under the catalytic co-pyrolysis process fell and gas products rose [37]. However, the solid-char formation was reduced by ~40 wt.% for both DOL and DOLZSM when compared with without a catalyst due to fast kinetics during the co-pyrolysis reaction. The order of solid-char product was found to be DOLZSM (8%) < DOL (~10%) < without catalyst (~20%). **Figure 7.5** (b) displays the product yields that were achieved by catalytic co-pyrolysis of rice husk and HDPE. When employing the DOL catalyst, the product yield ranges from 62% as a liquid product, 12% as a solid char, and 26% as a gas product. However, the DOLZSM catalyst yielded the most gaseous product 26 weight percent along with 10 weight percent and 61 weight percent of solid char and pyro-oil, respectively. As seen in Figure 5, thermal pyrolysis produced the maximum pyro-oil (liquid product) ~ 65-66 wt% with 10-18 wt% and 16-17 wt% of solid char and pyro-gas, respectively, in contrast to catalytic co-pyrolysis without a catalyst. It was discovered that the pyro-oil (liquid) products were arranged as follows: DOL (~62%) > DOLZSM (60%), > catalyst-free (~65%).

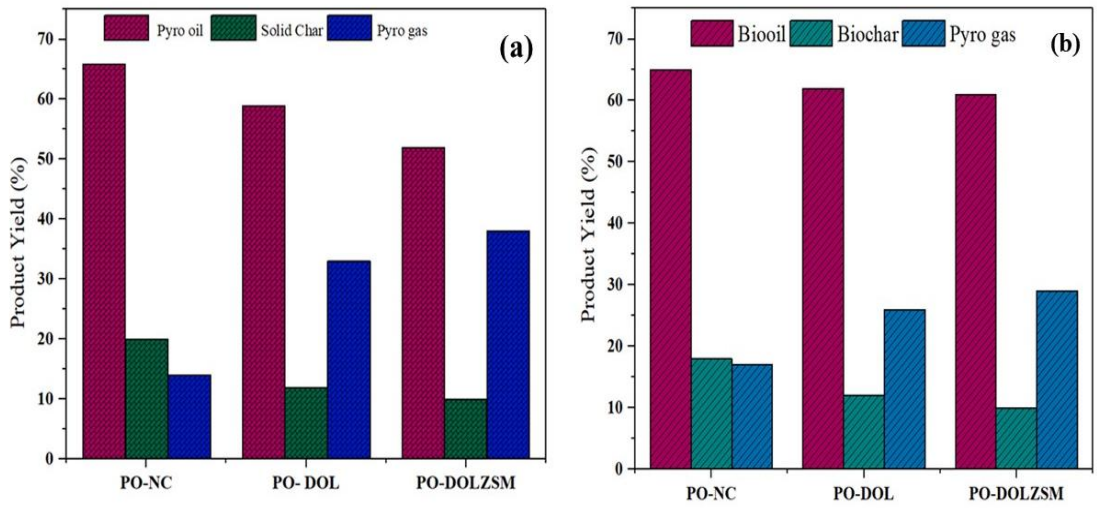

Figure 7.5. (a) Variation of product yields without catalyst, DOL, and DOLZSM catalysts during the catalytic co-pyrolysis of rice husk and LDPE. (b) Variation of product yields without catalyst, DOL, and DOLZSM catalysts during the catalytic co-pyrolysis of rice husk and HDPE.

7.4 Physical and chemical characteristics of refined pyro-oil

Table 7.2 lists the physical and chemical properties of the liquid pyro-oil that was produced when rice husk, LDPE, and HDPE were co-pyrolyzed at a ratio of 80:20, using different catalyst settings. The fuel attributes of pure diesel and non-catalytic pyro-oil (PO-NC) are contrasted with those of the catalytically processed liquid fuel dolomite-based sample (PO-DOL) and ZSM mixed Dolomite Powder (DOLZSM). The physical properties of the liquid samples generated by the catalytic and non-catalytic co-pyrolysis techniques varied significantly.

7.4.1 Analysis of Density, Specific gravity, and API gravity:

In the liquid sample derived from HDPE and RH combination with and without catalyst, the densities of oil from PO-NC, PO-DOL, and PO-DOLZSM were 0.889g/cm³, 0.858 g/cm³, and 853 g/cm³ aligning closely with the density of commercial diesel at 0.820 g/cm³. Additionally, the pyro-oil's specific gravity measurements for these samples, without a catalyst, were 0.818, and with catalyst PO-DOL, and PO-DOLZSM were 0.795 and 0.782, respectively, compared to 0.794 for commercial diesel. API gravity, inversely related to fuel density in comparison to water at 60°F (15.56°C), serves as a crucial metric to gauge the heaviness or lightness of petroleum products. Higher API gravity indicates lower density and thus higher fuel quality. HDPE: RH (80:20) non-catalytic pyrolysis oil had an API gravity of 41.4 and with catalyst PO-DOL, and PO-DOLZSM had 44.9, and 48.3, respectively. Which is nearly close to pure diesel.

Notably, the liquid sample derived from catalytic pyrolysis from LDPE and RH exhibited a density of 0.858 g/cm^3 for PO-DOL and 0.830 g/cm^3 for PO-DOLZSM, contrasting with the density of non-catalytic pyro-oil (PO-NC) at 0.876 g/cm^3. This discrepancy in density

arises due to the increased cracking intensity during catalytic co-pyrolysis, leading to a higher abundance of lower fraction hydrocarbons and reduced density in the resulting pyro-oil. Moreover, catalytic co-pyrolysis with DOLZSM typically yielded pyro-oil with a lower density (~0.830 g/cm^3) which was very close to the commercial diesel (~0.820 g/cm^3). Additionally, it was shown that ignition properties, encompassing carbon residue, diesel index, cetane index, flashpoints, and fire point, calorific value, & diesel index value, were influenced by catalytic co-pyrolysis as shown in **Table 7.3**.

7.4.2 Flash and Fire points

The ignition properties, including flash and fire points, were calculated to be 64.2℃ and 67.1℃, respectively for non-catalytic (NC) liquid fuel. For catalytic pyrolysis, the flash and fire points were measured at 52.3℃ and 58.6℃ for PO-DOL and 48.7℃ and -55.3℃ for PO-DOLZSM. For the other feedstocks of HDPE: RH mixture pyro oil derived from catalytic pyrolysis. In non-catalytic pyrolysis, the pyrolysis oil of ignition properties (flash and fire points) was measured at 59.7°C and 64.8°C respectively. Conversely, in catalytic pyrolysis, these points were recorded as 50.2°C and 58.3°C for PO-DOL, 40.3℃ and 51.1℃ and PO-DOLZSM, 40.1℃ respectively, the catalytic pyrolysis produces pyro oil with lower flash and fire points, indicating more volatility and lower hydrocarbon content compared to non-catalytic pyrolysis processes and for diesel, the determined flash points and fire points were 57°C and 64°C.

7.4.3 Calorific Value

The liquid fuel of LDPE: RH exceeded the pyro-oil calorific value of 34.6 MJ/kg obtained through non-catalytic co-pyrolysis produced employing the catalysts DOL and DOLZSM had estimated calorific values of 35.5 and 37.2 MJ/kg, sequentially. For another composition ratio of HDPE: RH Pyro-oil derived from non-catalytic pyrolysis exhibited a calorific value of 42.3 MJ/kg, whereas catalytic pyrolysis yielded a higher value of 43.5 MJ/kg for PO-DOL and 44.8 MJ/kg. for PO-DOLZSM. At the same time, analysis indicates that most samples exhibit calorific values close to that of commercial diesel,

which was calculated at 46.17 MJ/kg. Overall, the findings indicate that the calorific values of the analyzed samples are near those reported in existing literature [22].

7.4.4 Carbon residue

An essential criterion for any fuel is its carbon residue, which can impede its engine utility if it's higher. **Figure 7.6(a)** shows the ratio of LDPE: RH produced the liquid fuel without catalyst (PO-NC) showcased a carbon residue of 0.38 wt. %, PO-DOL, and PO-ZSMDOL demonstrated remarkably low carbon residues of 0.32 and 0.28 wt. %, respectively as shown in **Figure 7.6 (b)** For the other feedstock ratio of HDPE: RH produced the pyro-oil (PO) carbon residues derived from the non-catalytic pyrolysis process are 0.38, and through catalytic pyro-oil, carbon residues are 0.25 for PO-DOL and 0.19 for PO-DOLZSM. While diesel was measured at 0.57 weight percent, Carbon residue is a significant characteristic of any fuel. A higher presence of carbon residue is an indicator of poorer fuel quality. Thus, it's strongly recommended to use low-carbon residue fuel for sustainability purposes [22]. respectively. Nevertheless, the low weight percentage of carbon residue in all cases suggests their suitability for use as fuel which is shown in Figure 7.6 (a), (b).

7.4.5 Kinematic viscosity

The kinematic viscosity values were calculated as well, and as Figure 7.7(a) and (b) illustrate, the values were originated to be lower for the liquid sample generated via catalytic co-pyrolysis with DOL and DOLZSM. Consequently, the quality of pyro-oil may be enhanced using catalysts throughout the co-pyrolysis process. Lower-viscosity fuels are preferred for engine starters and general performance as they enable simple atomization, hence improving combustion. Furthermore, high-viscosity fuels can pose significant challenges during engine start-up, particularly in cold weather, as they can impede the proper operation of injectors by restricting the flow of fuel into the combustion chamber.

7.4.6 Aniline point

In fuel analysis, the aniline point is a significant indicator of the level of aromatics present. A decreased aniline point corresponds to a higher aromatic content, while a higher aniline point suggests a lower aromatic content. For LDPE: RH composition produced liquid fuel for non-catalytic analysis the aniline point is 64.5℃ and for catalytic pyro oil for PO-DOL are 56.3℃ and for PO-DOLZSM are 52.3℃ and for other feedstock HDPE: RH ratio the aniline points of non-catalytic oil were measured at 62.5℃ and for catalytic pyro oil 63.4℃ for PO-DOL, and 64.5℃ for PO-DOLZSM, respectively. While for pure diesel the aniline point is 56.8℃.

As the biomass mix percentage increased, the bio-oil's pH level decreased. This pH decrease is brought on by the synthesis of NH3, which is the end result of protein pyrolysis and dissolves in the bio-oil. The calculated PH value for commercial diesel was 5.5, while the PH for liquid samples from the thermal pyrolysis of non-catalytic pyro oil PH value was 5.2, and for catalytic samples, the PO-DOL PH value was 5.3, and for DOLZSM 5.6. while adding catalyst on HDPE: RH the PH value increases. For another sample LDPE: RH non-catalytic pyro oil PH value is 4.8 and catalytic pyro oil for PO-DOL are 5.3 and for PO-DOLZSM are 5.1 are nearly comparable to diesel fuel.

The examination of the other properties, such as the cetane index and diesel index, is also included in **Table 7.2.** The cetane index of the pyro-oil produced by catalytic co-pyrolysis was found to be greater than that of commercial diesel. This implies that, in comparison to pure diesel, the process of combustion in the diesel engines of POs obtained through catalytic co-pyrolysis will be more efficient and faster.

Table 7.2. Physicochemical properties of pyro-oil from RH: LDPE with different catalysts.

Fuel Properties	**PO-NC**	**PO-DOL**	**PO-DOLZSM**	**Commercial Diesel**
Density (g/cm^3)	0.876	0.858	0.830	0.820

Specific density	0.832	0.823	0.818	0.794
Cloud point (°C)	10	7	5	-3
Pour point (°C)	2	-1	-2	-13
Flashpoint (°C)	64.2	52.3	48.7	57
Fire point (°C)	67.1	58.6	55.3	64
Kinematic viscosity (40◦Cin cst)	1.32	1.18	1.04	2.46
Aniline point (g/cm^3)	64.5	56.3	52.3	56.8
Calorific value (MJ/kg)	34.6	35.5	37.2	46.18
Carbon Residue (wt.%.)	0.38	0.32	0.28	0.57
API gravity	41.4	42.5	44.3	46.77
Diesel Index	66.8	63.6	61.5	62.76
Cetane index	53.05	58.4	56.2	55.19
PH Value	4.8	5.3	5.0	5.5

PO- Pyrolysis oil, DOL- Dolomite, ZSM - zeolite Socony mobil-5, DOLZSM- Blends of dolomite and ZSM-5.

Table 7.3- Properties of liquid fuel from with and without catalyst rice husk and HDPE feedstock.

Fuel Properties	**NC-PO**	**PO-DOL**	**PO- DOLZSM**	**Pure Diesel**
Density (g/cm^3)	0.889	0.858	0.853	0.820
Specific density	0.818	0.795	0.782	0.794
Cloud point (°C)	10	3	1	-3
Pour point (°C)	-7	-10	-18	-13
Flashpoint (°C)	59.7	50.2	40.3	57
Fire point (°C)	64.8	58.3	51.1	64
Kinematic viscosity (40◦Cin Cst)	1.22	1.15	1.11	2.46
Aniline point (g/cm^3)	62.5	63.4	64.5	56.8
Calorific value (MJ/kg)	42.31	43.5	44.8	46.18

Carbon Residue (wt.%.)	0.38	0.25	0.19	0.57
API gravity	41.4	44.9	48.3	46.77
Diesel Index	59.8	58.2	56.5	62.76
Cetane index	53.05	55.7	57.4	55.19
PH Value	5.2	5.3	5.6	5.5

NC- Without a catalyst, PO- Pyro oil, Dol- Calcined Dolomite Powder, ZSM-5- Zeolite Socony Mobil-5, DOLZSM- a blend of Dolomite and ZSM-5

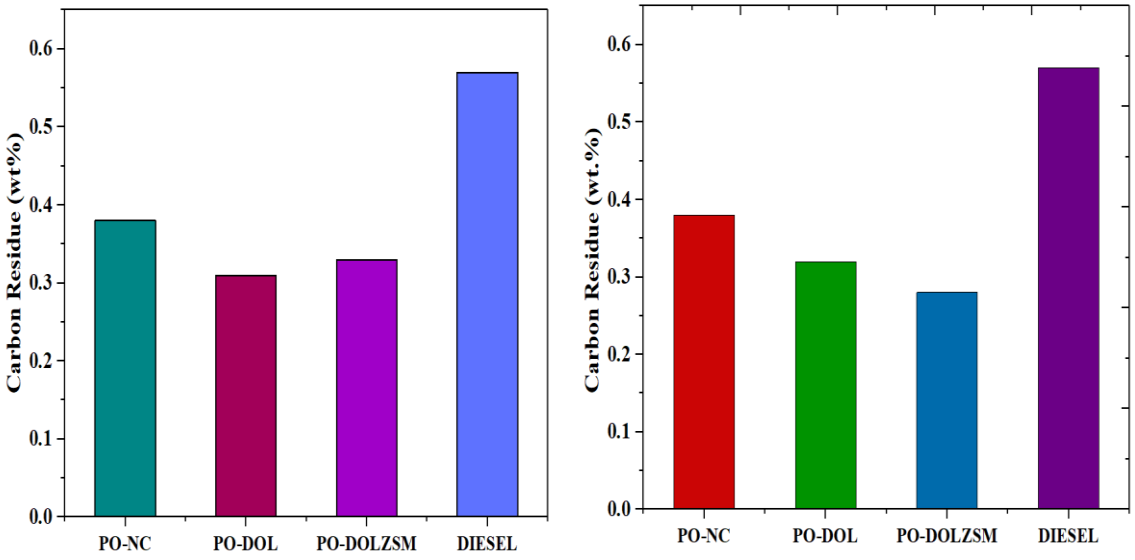

(a) (b)

Figure 7.6. Variation of carbon residue of pyro-oil obtained without catalyst, DOL, and DOLZSM catalysts during the catalytic (a) co-pyrolysis of rice husk and HDPE (b) co-pyrolysis of rice husk and LDPE.

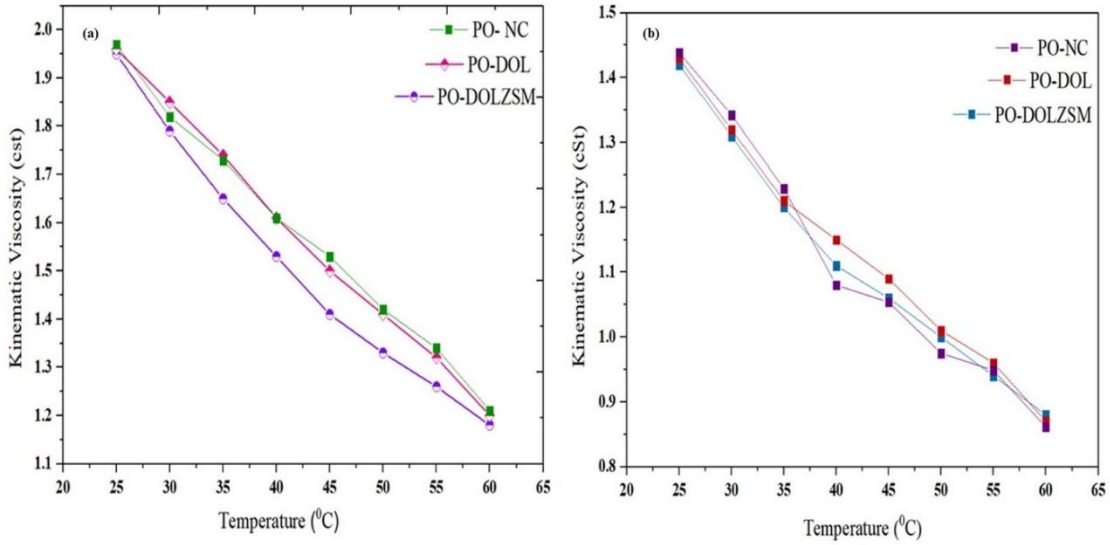

Figure 7.7 Variation of kinematic viscosity of pyro-oil obtained without catalyst, DOL, and DOLZSM catalysts during the catalytic co-pyrolysis. (a) Rice husk and LDPE (b) Rice husk and HDPE

7.5 Elemental Analysis of Pyro-oil

Hydrogen and carbon levels were measured in pyrolysis oil that was produced by the thermochemical conversion of LDPE and rice husk materials, both with and without catalysts, using the CHNS analyzer. To analyze the H/C ratio in liquid oil samples, an elemental examination of liquid samples produced by thermal and catalytic pyrolysis of waste plastic and rice husk under various catalyst settings was required. The H/C ratio is a gauge of how feasible liquid fuels are as a substitute energy source; lower heating values are associated with lower H/C values, which in turn affect viscosity, density, and calorific values. The findings demonstrated that pyro-oil produced with a catalyst had a greater hydrocarbon content than pyro-oil produced without a catalyst, indicating that the fuels had a higher calorific value as shown in Table **7.3**.

Table 7.4. Elemental investigation of liquid fuel resulting from thermal and catalytic pyrolysis processes of LDPE and RH.

Sample	Carbon	Hydrogen	Nitrogen	sulfur	Oxygen	H/C
PO – NC	72.16	9.5	0.54	0.07	17.73	1.57
PO-DOL	76.3	10.3	0.66	0	12.74	1.62
PO- DOLZSM	77.9	12.6	0.72	0	8.78	1.94
DIESEL (CD)	81.17	13.34	0.14	0	5.34	1.96

Table 7.5 Elemental investigation of liquid fuel resulting from thermal and catalytic pyrolysis processes of HDPE and RH.

Sample	Carbon	Hydrogen	Nitrogen	sulfur	Oxygen	H/C	O/C
PO – NC	76	13.6	0.44	0	9.96	2.13	0.098
PO-DOL	78	12.8	0.52	0	8.68	1.95	0.083
PO-DOLZSM	79	13.1	0.66	0	7.24	1.97	0.068
DIESEL (CD)	81.17	13.34	0.14	0	5.34	1.96	0.04

7.6 Catalytic cracking of plastic waste and rice husk

LDPE was used in a co-pyrolysis process with rice husk. The interaction between the feedstock components exhibited favorable synergistic effects and HDPE, particularly in the volatile reaction that took place within the char bed. With increasing temperatures, plastic melts and forms a protective layer over biomass particles. The decomposition of biomass occurs first due to variations in thermal stability, resulting in the formation of radicals that subsequently react with LDPE and HDPE to generate volatile compounds at elevated temperatures. The proportion of plastics to biomass influences the liquid's

chemical composition and the intended product's yields. Co-pyrolysis of plastic waste (LDPE, HDPE) and biomass (Rice husk) without a catalyst led to a brown-colored oil, while catalytic co-pyrolysis of the feedstocks had little effect on the color of the oil (yellow-gold color) as observed in **Figure 7.8**.

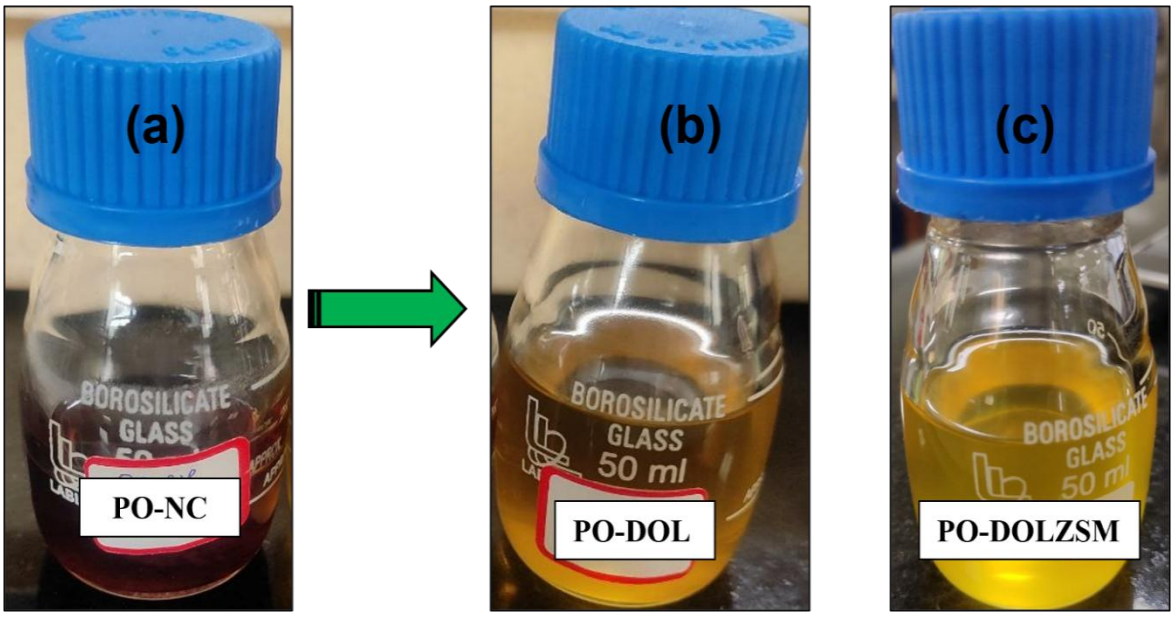

Figure 7.8. The visual appearance of the obtained pyro-oil through a combination of Rice husk and plastic waste (a) no catalyst, (b) DOL, and (C) DOLZSM catalytic co-pyrolysis.

7.7 Estimation of the chemical composition

7.7.1 ^{1}H and ^{13}C NMR Spectral Analysis

The fractional composition of the aromatic, paraffin, and olefin content of the co-pyrolysis oil has been estimated using ^{1}H-NMR and ^{13}C-NMR analysis. The deuterated ($CDCl_3$) was used as a solvent with a 1:20 volume ratio at 500MHz frequency. The ^{1}H-NMR spectra captured in Figure 7.9 were subjected to NMR spectroscopy for hydrocarbon identification within the pyro-oil samples. Through ^{1}H NMR analysis, the volume percentages of paraffin, olefin, and aromatic compounds were determined employing experimental equations established in prior research. Notably, findings revealed that in non-catalytic pyro oil, aromatic, olefin, and paraffin complexes constituted 7.89, 49.24%, and 42.77%

v/v, sequentially. In contrast, catalytic pyrolysis oil exhibited variations in hydrocarbon composition, with aromatic, olefin, and paraffin compounds content for PO-DOL at 10.27%,42.16%, and 40.11% v/v. while for PO-DOLZSM the content is 9.66%,52.8%and 38.3%, sequentially. Among the catalytic processes, the highest olefin content was observed in PO-DOLZSM (52.8% v/v), followed by PO-DOL (42.16% v/v) as shown in **Figure 7.9(a)**. Although the DOL catalyst was used, the hydrocarbon composition did not alter significantly; rather, as was previously said, it made it easier to produce lower hydrocarbon chains. While combined LDPE and rice husk were being pyrolysis, however, the modified DOL catalyst and ZSMDOL tended to produce olefins. These observations highlight the importance of catalyst type in determining the hydrocarbon distribution of pyro-oil, suggesting the feasibility of tailored catalyst design to regulate product yields in catalytic pyrolysis processes.

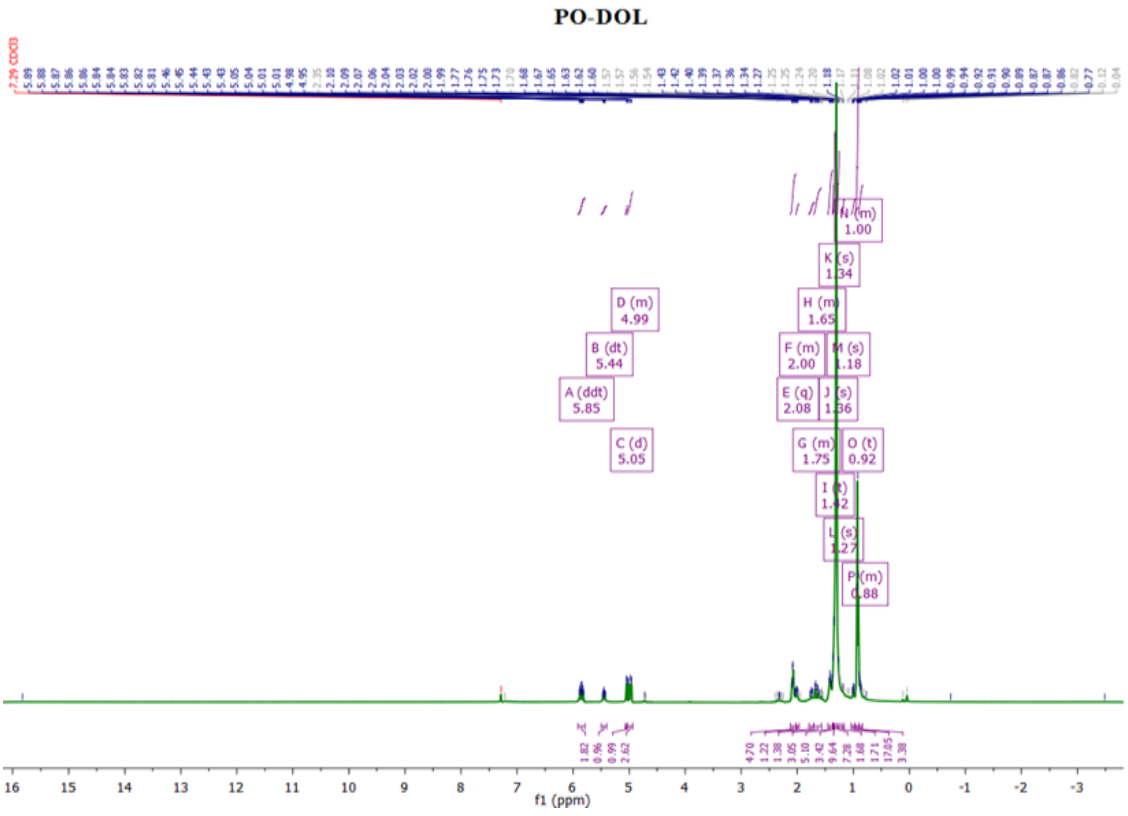

(a)

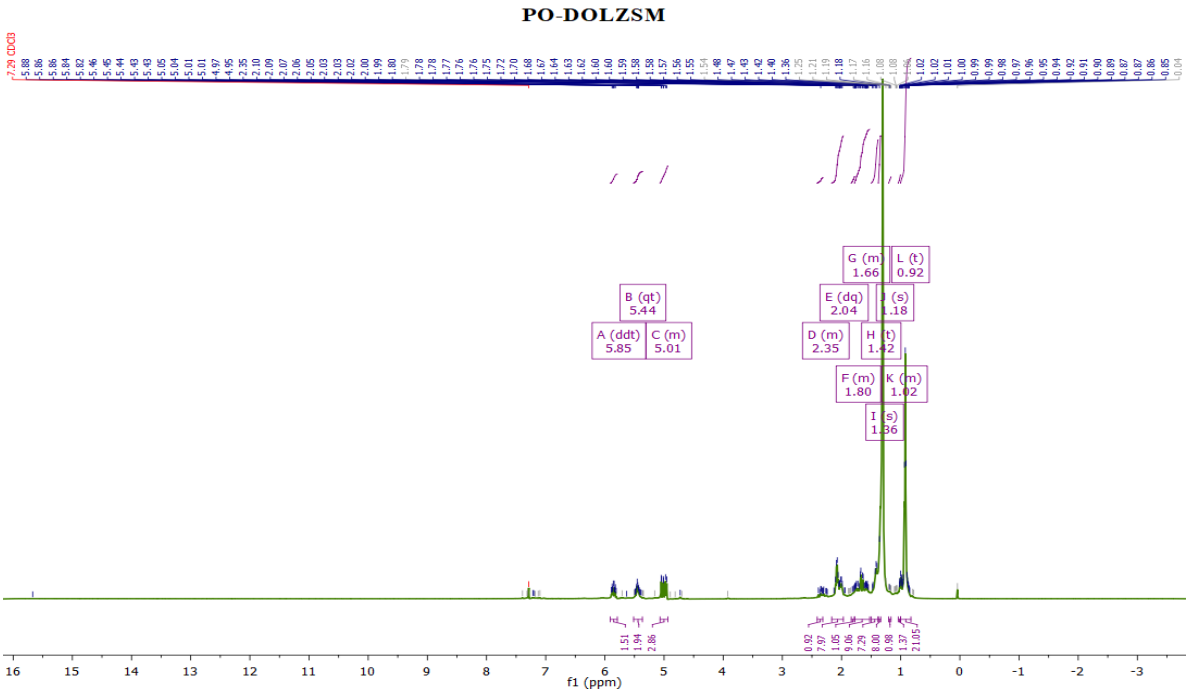
PO-DOLZSM
G (m) 1.66
L (t) 0.92
B (qt) 5.44
E (dq) 2.04
J (s) 1.18
A (ddt) 5.85
C (m) 5.01
D (m) 2.35
H (t) 1.42
F (m) 1.80
K (m) 1.02
I (s) 1.36
f1 (ppm)

(b)

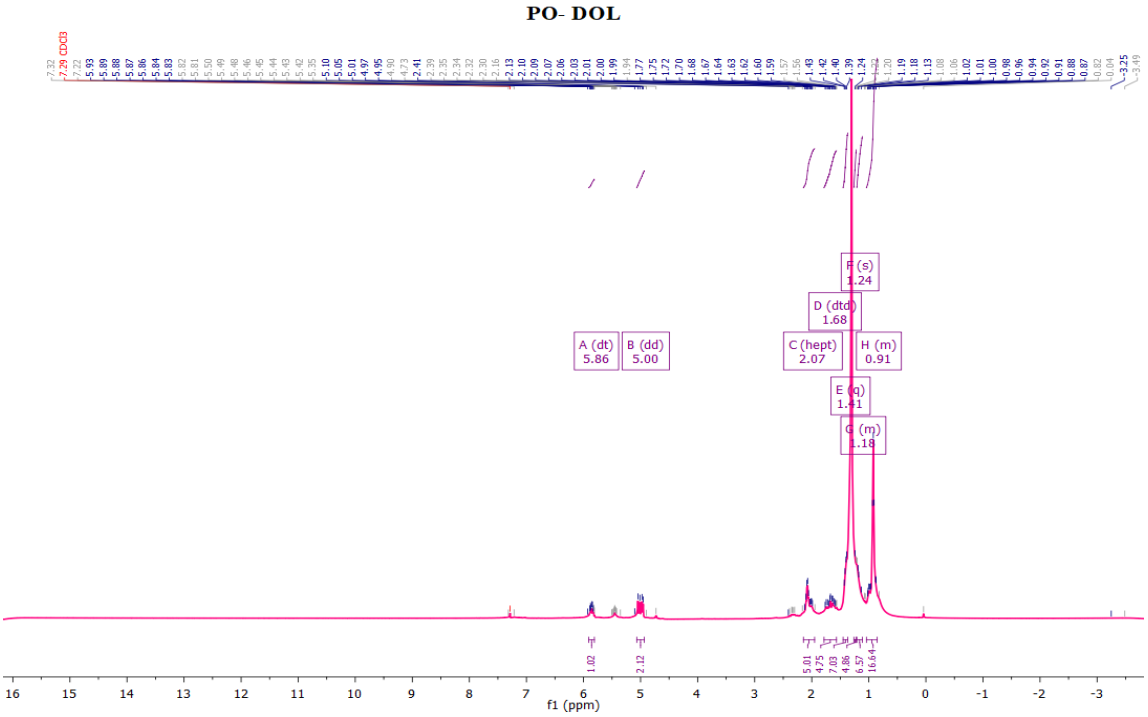
PO- DOL
F (s) 1.24
D (dtd) 1.68
A (dt) 5.86
B (dd) 5.00
C (hept) 2.07
H (m) 0.91
E (q) 1.41
G (m) 1.18
f1 (ppm)

(c)

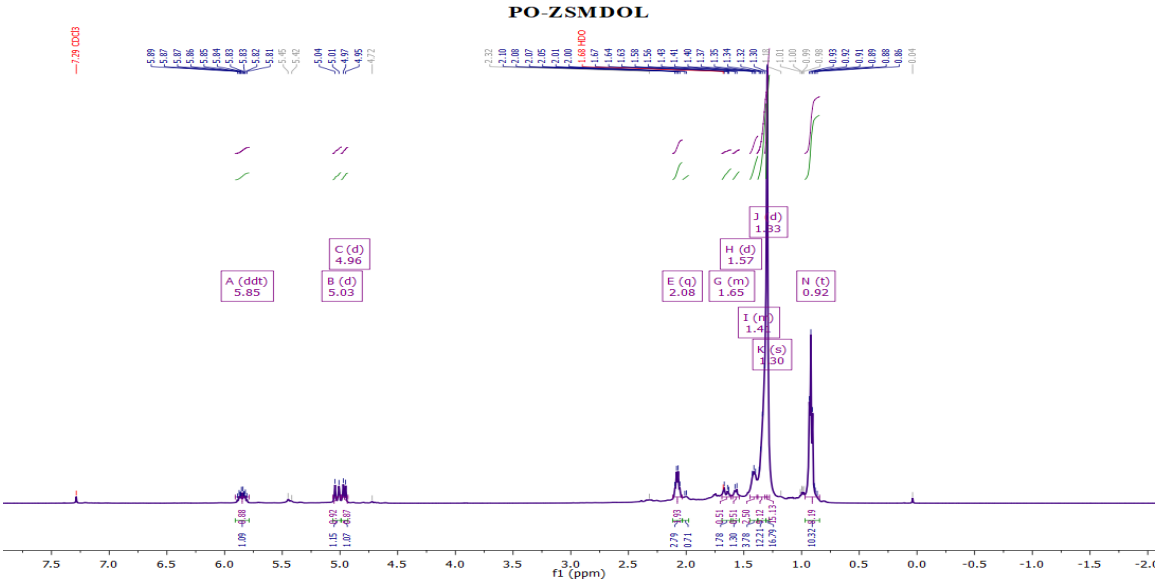

(d)

Figure 7.9. [1]H-NMR analysis of pyro-oil obtained through plastic waste and biomass (a) DOL-PO from HDPE and RH (b) DOLZSM -PO from HDPE and RH (c) DOL-PO from LDPE and RH (d) DOLZSM-PO from LDPE and RH.

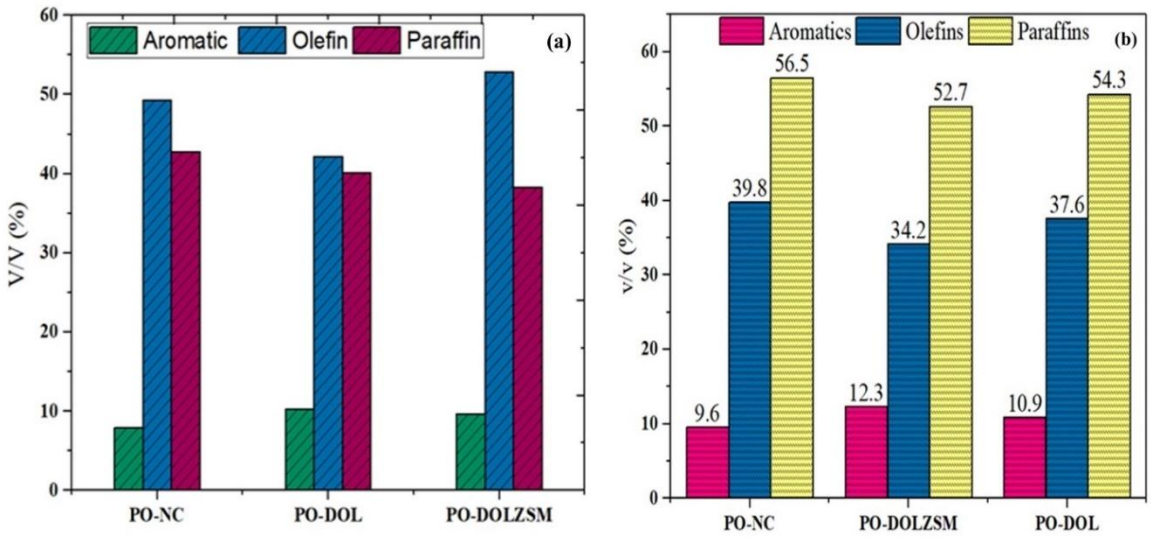

Figure 7.10. Variation of paraffin, olefins, and aromatic hydrocarbon components in the obtained non-catalytic and catalytic derived pyrolysis oil. (a) LDPE and RH (b) HDPE and RH

To elucidate the composition of carbon atoms and the structural properties exhibited by the pyro-oil samples, including the degree of branching and dimension of the H-C chains, ^{13}C-NMR spectrum of the co-pyrolysis oil derived from LDPE and Rice husk samples were recorded. In Figure 7.11, it is evident that distinct attributes are observed in the ^{13}C-NMR spectra of all co-pyrolysis samples. Paraffinic hydrocarbons are observed across all samples within the chemical shift range of 14.10–36.31 ppm. The varied chemical shifts observed in the co-pyrolysis oils indicate diverse combinations of carbons present in the samples. Additionally, the occurrence of olefinic hydrocarbons can be observed in the liquid fuel samples resulting from plastic waste and Rice husk co-pyrolysis, both with and without catalyst, with chemical shifts detected at 114.04 ppm and 139.22 ppm. These observations from the ^{13}C-NMR spectra are consistent with findings from the ^{1}H-NMR analysis, as corroborated by the GCMS results shown in Figure 7.11. Utilizing ^{13}C-NMR analysis proves invaluable in unravelling the structure of molecules and the makeup of the pyro-oil samples. By supplementing data collected from other ways, this analytical methodology advances our grasp of the chemical characteristics of the liquid products created by co-pyrolysis procedures and fosters a thorough comprehension of them.

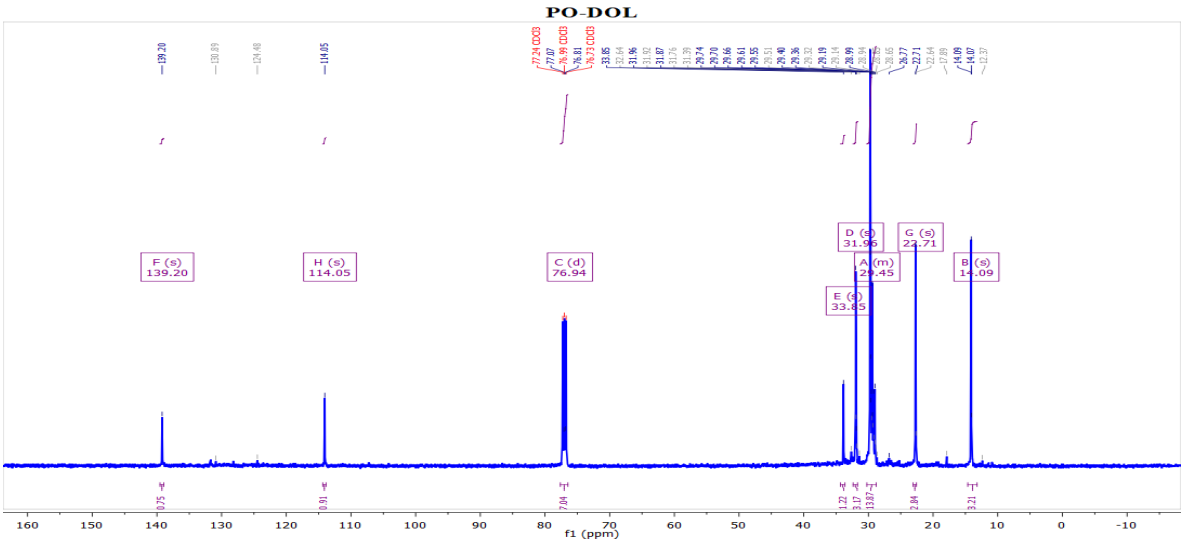

(a)

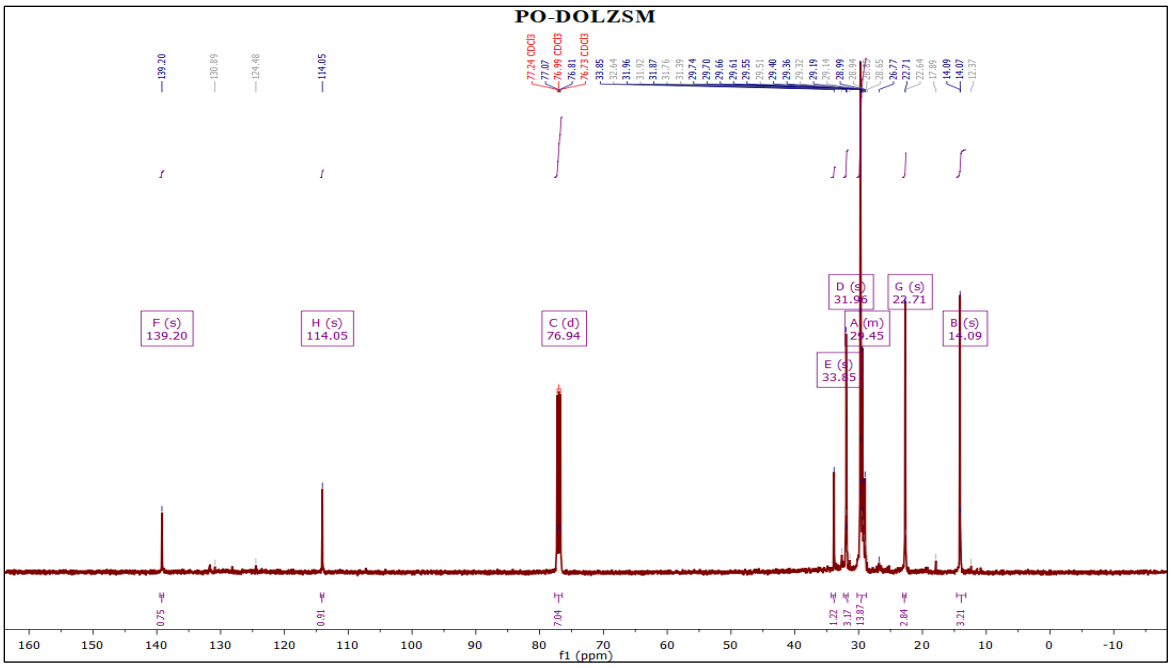
PO-DOLZSM
F (s)
139.20
H (s)
114.05
C (d)
76.94
D (s)
31.96
A (m)
29.45
E (s)
33.85
G (s)
22.71
B (s)
14.09
f1 (ppm)

(b)

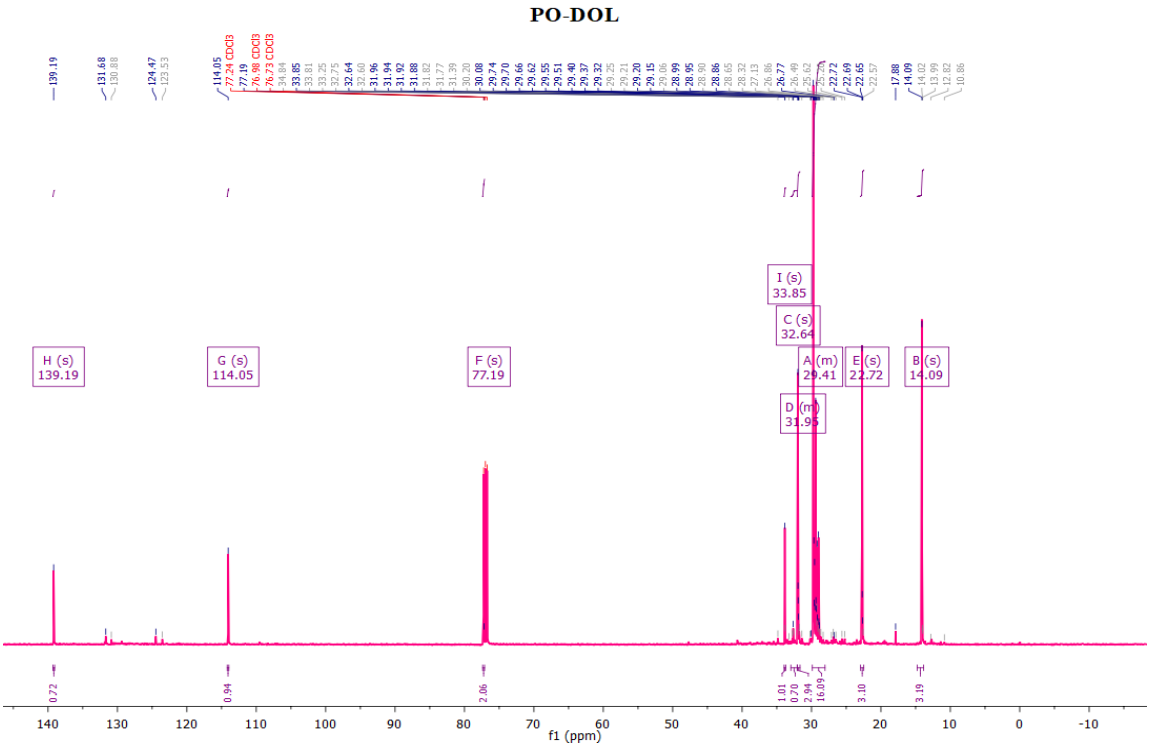
PO-DOL
H (s)
139.19
G (s)
114.05
F (s)
77.19
I (s)
33.85
C (s)
32.64
A (m)
29.41
E (s)
22.72
B (s)
14.09
D (m)
31.96
f1 (ppm)

(c)

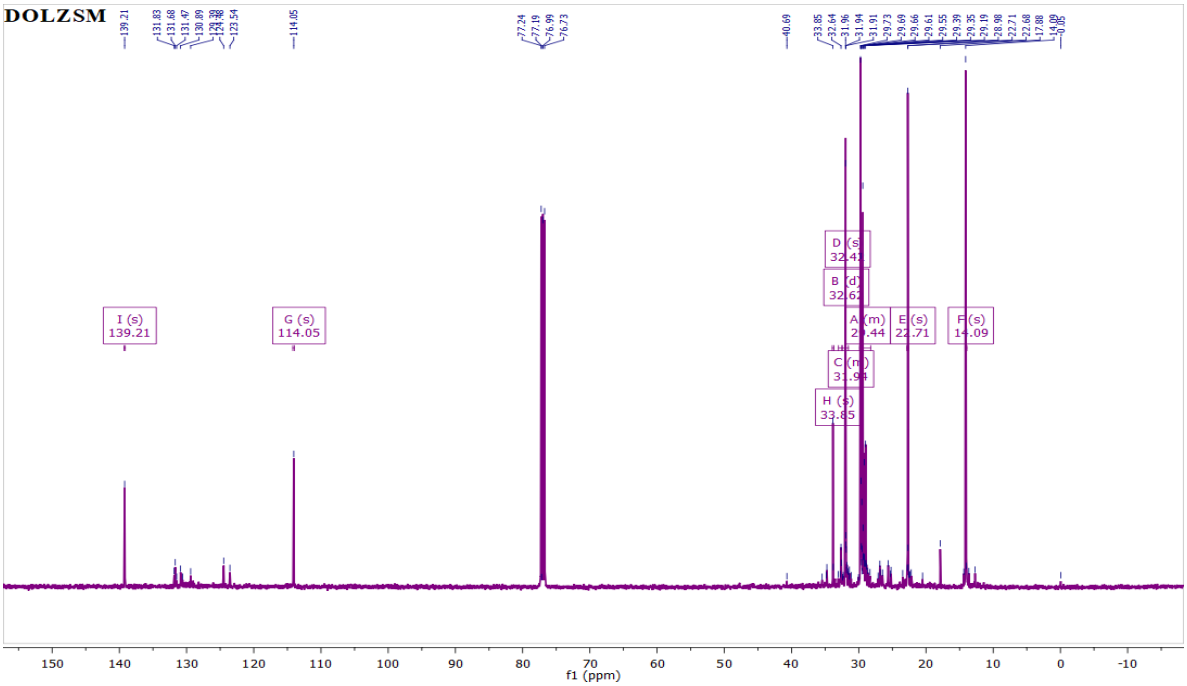

(d)

Figure 7.11. ^{13}C-NMR analysis of pyro-oil obtained through plastic waste and RH (a) DOL-PO from LDPE and RH (b) DOLZSM -PO from LDPE and RH (c) DOL-PO from HDPE and RH (d) DOLZSM-PO from HDPE and RH.

7.7.2 GC-MS Analysis of liquid product (pyro-oil)

The hydrocarbon content and carbon number distribution in the liquid products resulting from the non-catalytic and catalytic cracking of waste plastic and rice husk were analyzed using gas chromatography-mass spectrometry (GC-MS). There was a precise temperature regime that the GC-MS algorithm followed. This involved stabilizing the temperature at 50°C for five minutes before progressively increasing it to 280°C at a rate of 5°C per minute. The oven then maintained the temperature at 300°C for five minutes. Figure 7.12 displays the chromatogram spectrum. **Tables 7.6** and **7.7** reveal that the liquid result comprises a diverse range of hydrocarbon types, such as alcohols, esters, alkanes, and alkenes.

The length of their carbon chains, which varied from less than C9 to less than C24, was used to characterize the hydrocarbon compounds found by GC-MS. According to the results, non-catalytic pyro-oil was found to have higher selectivity (88.93%) in the carbon range of C_{13}-C_{24} which dominates the pyro-oil fractions. However, this fuel oil has a higher content of oxygenated compounds (49.85%), which influences the properties of the fuel. For catalytic puro-oil, the hydrocarbon content was in the range C_{13}–C_{24} and selectivity were found to be 26.3% and 18.9% in the pyro-oils using PO-DOL and PO-ZSMDOL catalysts, respectively, Additionally, it was revealed that when employing ZSM-5 in conjunction with a calcined dolomite catalyst (DOLZSM), the carbon ranges below C_{12} constituted approximately 70% of the product distribution. Conversely, the utilization of a calcined dolomite catalyst (DOL) resulted in a notable reduction in the selectivity range for carbon chains within the C_{13}-C_{24} range, decreasing from 25.66% to 17.43%. These findings underscore the significant influence of catalyst composition on product distribution during pyrolysis processes, highlighting the potential for tailored catalyst design to optimize desired hydrocarbon product yields [37]. Furthermore, the co-pyrolysis oil obtained through a catalytic process found high selectivity to lower range hydrocarbon (below C_9) as compared to non-catalytic obtained pyro-oil. This investigation implies that the DOL and DOLZSM catalysts both will be suitable to tune the overall properties of the obtained pyro-oil as represented in **Figure 7.13.**

Gas chromatography-mass spectrometry (GC-MS) was used to examine the liquid sample obtained from the co-pyrolysis of rice husk (RH) and high-density polyethylene (HDPE) and to compare catalytic and non-catalytic procedures. This comprehensive analytical approach enables detailed characterization of the pyrolysis products, facilitating insights into the chemical composition and structural features of the resulting oils, which is crucial for optimizing pyrolysis processes and harnessing their potential in various industrial applications. The categorization of hydrocarbon compounds acknowledged through GC-MS analysis was conducted according to their carbon chain lengths, dividing them into four main groups: $<C_9$, C_9-C_{12}, C_{13}-C_{24}, and $>C_{24}$. The pyro-oil that was generated contained a wide range of carbon and hydrogen-based substances, including both

oxygenated and non-oxygenated hydrocarbons. In both the catalytic & non-catalytic co-pyrolysis procedures, the pyro-oil composition showed that alkanes and alkenes in the C9–C25 carbon range dominated. The presence of specific compounds was highlighted, and a comparison with previous studies indicated similar observations are present in Tables 7.8 and 7.9.

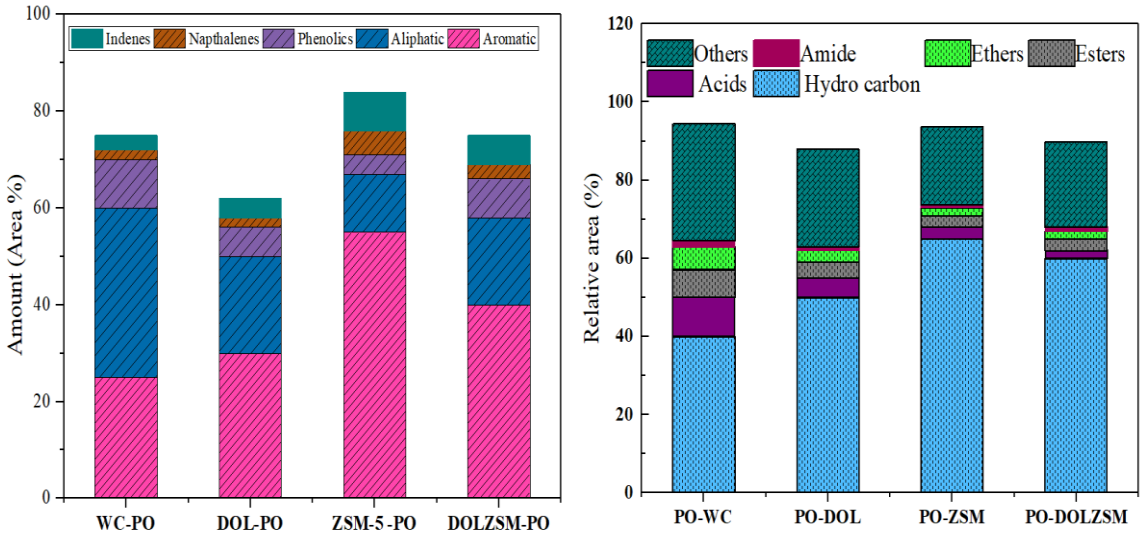

(a) **(b)**

Figure 7.12 Pictorial presentation of GC–MS analysis without catalyst and with catalyst Pyro-oil from RH and HDPE blends.

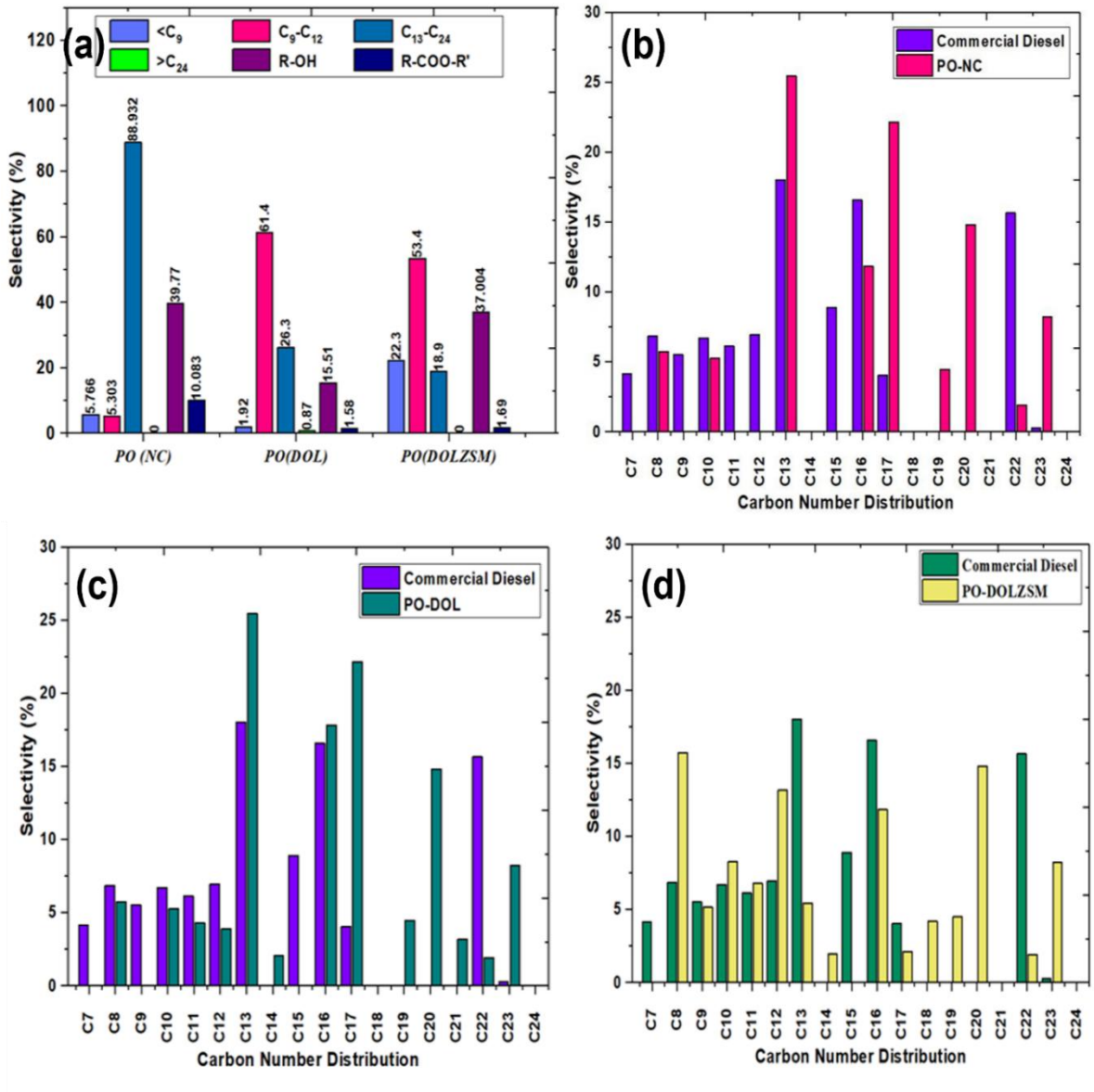

Figure 7.13. (a) Variation in the selectivity of hydrocarbons in RH: LDPE liquid oil obtained from non-catalytic and various catalytic conditions. (b) Examining the hydrocarbon content of pyro-oil in non-catalytic and (c) DOL, (d) DOLZSM catalytic conditions and contrasting it with diesel.

Table 7.6. GCMS analysis of pyro-oil obtained through RH: LDPE with dolomite (DOL) catalyst.

Peak	Compound	Mol. Formula	Mo. Weight	Retention Time	Area (%)
1	3-Decyn-2-ol	$C_{10}H_{18}O$	154	5.076	8.628
2	2-Octyn-1-ol	$C_8H_{14}O$	126	8.613	12.636
3	2,4-Undecadien-1-ol	$C_{11}H_{20}O$	168	12.293	14.822
4	2-Tridecene, (Z)-	$C_{13}H_{26}$	182	15.569	12.066
5	3-Tetradecene, (E)	$C_{14}H_{28}$	196	18.747	10.316
6	4-Tetradecene, (E)-	$C_{14}H_{28}$	196	21.207	5.451
7	1-Decanol, 2-hexyl	$C_{16}H_{34}O$	242	23.954	5.239
8	2-Hexyl-1-octanol	$C_{14}H_{30}O$	214	26.324	4.725
9	1-Octanol, 2-butyl	$C_{12}H_{26}O$	186	28.593	3.632
10	1-Dodecanol, 2-methyl-, (S)-	$C_{13}H_{28}O$	200	30.74	2.781
11	Ethanol, 2-(tetradecyl oxy)-	$C_{16}H_{34}O_2$	258	32.791	2.460
12	Ethanol, 2-(octadecyl oxy)-	$C_{20}H_{42}O_2$	314	34.77	1.893
13	Ethanol, 2-(tetradecyl oxy)-	$C_{16}H_{34}O_2$	258	36.645	1.799
14	Ethanol, 2-(octadecyl oxy)-	$C_{20}H_{42}O_2$	314	38.459	1.667
15	Ethanol, 2-(octadecyl oxy)-	$C_{20}H_{42}O_2$	314	40.209	1.338
16	Docosane, 9-octyl	$C_{30}H_{62}$	422	41.889	1.305
17	Docosane, 7-hexyl	$C_{28}H_{58}$	394	43.515	1.367
18	Tetracosane	$C_{24}H_{50}$	388	45.074	1.617
19	Tetracosane, 11-decyl	$C_{34}H_{70}$	478	46.575	1.433
20	Tetracosane, 9-octyl	$C_{32}H_{66}$	450	47.999	1.138
21	Ethanol, 2-(octadecyl oxy)-	$C_{20}H_{42}O_2$	314	49.373	1.016

22	Nonacosane	$C_{29}H_{60}$	408	50.706	0.924
23	Hexacosane, 9-octyl	$C_{34}H_{70}$	478	52.052	0.713
24	Hexacosane, 13-dodecyl	$C_{38}H_{78}$	534	53.606	0.665
25	Tetratriacontane	$C_{34}H_{70}$	478	55.439	0.369

Table 7.7 GCMS analysis of pyro-oil obtained through RH: LDPE with DOLZSM catalyst.

Peak	**Compound**	**Mol. Formula**	**Mo. Weight**	**Ret. Time**	**Area (%)**
1	3-Octene, (Z)-	C_8H_{16}	112	4.848	1.530
2	1-Heptene, 3-methyl	C_8H_{16}	112	8.128	3.758
3	4-Tridecene, (Z)-	$C_{13}H_{26}$	182	11.995	9.979
4	2-Decene, (Z)-	$C_{10}H_{20}$	140	15.514	13.761
5	2-Dodecenal, (E)-	$C_{12}H_{22}O$	182	18.874	14.420
6	2-Tridecenal, (E)-	$C_{13}H_{24}O$	196	21.641	11.442
7	3-Undecene, (Z)-	$C_{11}H_{22}$	154	24.185	8.968
8	8-Hexadecenal, 14-methyl-, (Z)-	$C_{17}H_{32}O$	252	26.548	7.080
9	9-Octadecenal	$C_{18}H_{34}O$	266	28.757	5.193
10	1-Decanol, 2-hexyl	$C_{16}H_{34}O$	242	30.880	4.262
11	2-Hexyl-1-octanol	$C_{14}H_{30}O$	214	32.896	3.326
12	2-Ethyl-1-dodecanol	$C_{14}H_{30}O$	214	34.838	2.880
13	1-Octanol, 2-butyl	$C_{12}H_{26}O$	186	36.694	2.132
14	2-Hexyl-1-octanol	$C_{14}H_{30}O$	214	38.479	1.982
15	1-Dodecanol, 2-methyl-, (S)-	$C_{13}H_{28}O$	200	40.193	1.483
16	2-Hexyl-1-octanol	$C_{14}H_{30}O$	214	41.853	1.243

17	2-Ethyl-1-dodecanol	$C_{14}H_{30}O$	214	43.449	1.137
18	1-Hexadecene	$C_{16}H_{32}$	224	44.975	1.138
19	1-Decanol, 2-hexyl	$C_{16}H_{34}O$	242	46.458	0.771
20	Ethanol, 2-(tetradecyloxy)-	$C_{16}H_{34}O_2$	258	47.881	0.884
21	Z-5-Nonadecene	$C_{19}H_{38}$	266	49.248	0.645
22	Ethanol, 2-(octadecyloxy)-	$C_{20}H_{42}O_2$	314	50.586	0.786
23	Ethanol, 2-(octadecyloxy)-	$C_{20}H_{42}O_2$	314	51.920	0.576
24	Docosane, 7-hexyl	$C_{28}H_{58}$	394	53.464	0.356
25	Ethanol, 2-(octadecyloxy)-	$C_{20}H_{42}O_2$	314	55.291	0.268

Table 7.8. Identified substances found in pyro-oil produced by co-pyrolyzing waste HDPE and RH with dolomite powder.

Peaks	**Ret Time**	**Compound**	**Mol formula**	**Mol weight**	**Area (%)**
1	5.227	1-Nonyne	C_9H_{16}	124	11.354
2	8.789	6-Hepten-1-ol, 3-methyl	$C_8H_{16}O$	128	14.673
3	12.495	3-Decyn-2-ol	$C_{10}H_{18}O$	154	17.022
4	15.717	3-Nonen-1-ol, (E)	$C_9H_{18}O$	142	12.990
5	18.824	3-Octen-1-ol, (E)-	$C_8H_{16}O$	128	8.962
6	21.453	4-Tridecene, (Z)-	$C_{13}H_{26}$	182	6.123
7	23.932	2-Decene, (Z)-	$C_{10}H_{20}$	140	4.778
8	26.321	1-Nonene	C_9H_{18}	126	3.148
9	28.567	2-Dodecenal, (E)	$C_{12}H_{22}O$	182	2.955
10	30.715	9-Octadecynoic acid	$C_{18}H_{32}O_2$	280	2.432
11	32.775	1,12-Tridecadiene	$C_{13}H_{24}$	180	1.873
12	34.754	1-Hexadecanol, 2-methyl	$C_{17}H_{36}O$	256	1.633
13	36.650	2,4-Undecadien-1-ol	$C_{11}H_{20}O$	168	1.518

14	38.451	2-Ethyl-1-dodecanol	$C_{14}H_{30}O$	214	1.462
15	40.207	1-Octanol, 2-butyl	$C_{12}H_{26}O$	186	1.311
16	41.880	1-Decanol, 2-hexyl	$C_{16}H_{34}O$	242	1.182
17	43.488	Ethanol, 2-(octadecyloxy)-	$C_{20}H_{42}O_2$	314	1.061
18	45.036	Ethanol, 2-(tetradecyloxy)	$C_{16}H_{34}O_2$	258	1.051
19	46.494	Ethanol, 2-(octadecyloxy)-	$C_{20}H_{42}O_2$	314	0.975
20	47.948	Ethanol, 2-(octadecyloxy)-	$C_{20}H_{42}O_2$	314	0.919
21	49.323	Ethanol, 2-(eicosyloxy)	$C_{22}H_{46}O_2$	342	0.717
22	50.650	1-Hexacosene	$C_{26}H_{52}$	364	0.583
23	51.983	1-Tricosene	$C_{23}H_{46}$	322	0.588
24	53.530	1-Decanol, 2-hexyl	$C_{16}H_{34}O$	242	0.399
25	55.361	Ethanol, 2-(octadecyloxy)-	$C_{20}H_{42}O_2$	314	0.290

Table 7.9. Identified substances found in pyro-oil produced by co-pyrolyzing leftover HDPE and RH with DOLZSM.

Peaks	**Ret Time**	**Compound**	**Mol formula**	**Mol weight**	**Area (%)**
1	4.918	3-Decyn-2-ol	$C_{10}H_{18}O$	154	3.300
2	8.742	trans-2-Ethyl-2-hexen-1-ol	$C_8H_{16}O$	128	7.782
3	12.662	4-Octene, (Z)-	C_8H_{16}	112	17.906
4	16.071	3-Tetradecyn-1-ol	$C_{14}H_{26}O$	210	20.146
5	19.230	1-Nonene	C_9H_{18}	126	15.631
6	21.849	3-Decyn-2-ol	$C_{10}H_{18}O$	154	10.492
7	24.279	Z-10-Pentadecen-1-ol	$C_{15}H_{30}O$	226	7.424
8	26.564	4-Tridecene, (Z)-	$C_{13}H_{26}$	182	5.465
9	28.714	Dodecanal	$C_{12}H_{24}O$	184	3.457
10	30.785	1-Dodecanol,2-methyl-, (S)-	$C_{13}H2_8O$	200	2.236

11	32.785	Ethanol, 2-(octadecyloxy)-	$C_{20}H_{42}O_2$	314	1.583
12	34.695	Z-5-Nonadecene	$C_{19}H_{38}$	266	1.032
13	36.540	1-Decanol, 2-hexyl	$C_{16}H_{34}O$	242	0.759
14	38.321	1-Decanol, 2-hexyl	$C_{16}H_{34}O$	242	0.546
15	40.026	Ethanol, 2-(octadecyloxy)-	$C_{20}H_{42}O_2$	314	0.353
16	41.674	Ethanol, 2-(octadecyloxy)-	$C_{20}H_{42}O_2$	314	0.340
17	43.260	1-Tricosene	$C_{23}H_{46}$	322	0.258
18	44.801	Hexacosane, 9-octyl	$C_{34}H_{70}$	478	0.263
19	46.277	Ethanol, 2-(octadecyloxy)-	$C_{20}H_{42}O_2$	314	0.251
20	47.708	Ethanol, 2-(octadecyloxy)-	$C_{20}H_{42}O_2$	314	0.190
21	49.084	Nonacosane	$C_{29}H_{60}$	408	0.145
22	50.430	Tetracosane, 11-decyl	$C_{34}H_{70}$	478	0.309
23	51.764	1-Hexacosene	$C_{26}H_{52}$	364	0.131

7.7.3 FTIR Analysis of the pyro-oil

The functional groups in the oil samples resulting from the thermal and catalytic pyrolysis processes were described using FTIR analysis. The FTIR spectra of the pyro-oil samples are shown beside those of pure diesel in Figure 7.14. Different functional groups may be seen in the pyro-oil produced by thermal and catalytic pyrolysis, depending on the catalyst employed in the process. A notable peak at 3074.65 cm^{-1}, indicative of C–H vinyl stretching, suggesting the presence of alkenes, was missing in the catalytic pyrolysis oil produced using dolomite & ZSMDOL catalysts. The C-H methyl asymmetric stretch at 2950.21 cm^{-1}, on the other hand, consistently revealed the existence of the R-CH3 (alkanes) functional group in all of the pyro-oil samples. The peaks at 2914.87 cm^{-1} and 2866.79 cm^{-1}, respectively, were further corroborated by the typical C–H symmetric stretch for methyl and asymmetric stretch for methylene, which matched to the functional groups (>CH2). Furthermore, the presence of C=C-C aromatic ring stretch bonds was shown in all liquid samples by the identification of aromatic compounds with ring structures at the peak

signal of 1458.13 cm^{-1}. The presence of cyclic ethers was indicated by the peak at 1154.07 cm^{-1} in catalytic samples of pyro-oil (i.e., PO-DOL and PO-DOLZSM), which was absent in non-catalytic pyro-oil, confirming the identification of C–O stretch bonds. Additionally, signals at 968.56 cm^{-1} and 881.23 cm^{-1} represented olefinic hydrocarbons with trans-C-H out-of-plane bend and vinylidene C–H out-of-plane bend characteristics, in the respective order. Moreover, alkyne hydrocarbons were found in pyro-oil samples, as evidenced by alkyne C–H bend bonds, specifically in the catalytic pyro-oil produced with the DOLZSM catalyst. Moreover, the FTIR spectra of pyro-oils showed similar functional groups by showing same peaks as seen in commercially available diesel. These findings highlight the distinct functional group compositions influenced by the catalytic pyrolysis process, offering valuable insights into the chemical nature of the resulting liquid products.

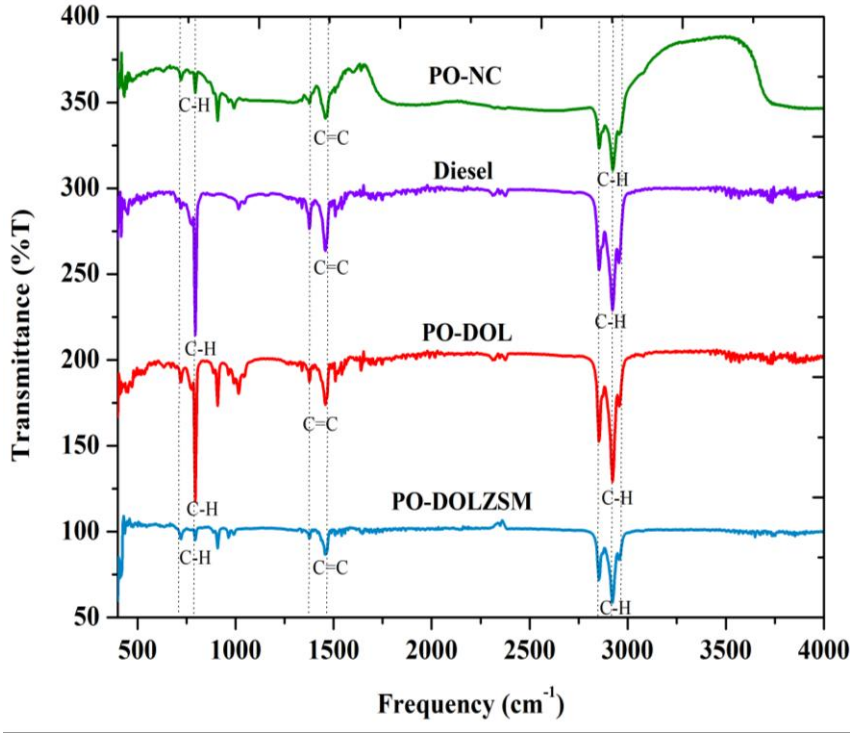

Figure 7.14 (a) FTIR spectrum of pyro-oil obtained without catalyst, DOL, and DOLZSM catalyst in comparison with the commercially available diesel.

Fourier-transform infrared spectroscopy, or FTIR spectroscopy, is a commonly used non-destructive analytical method. It functions by measuring the amount of energy absorbed in the infrared region of the electromagnetic spectrum by the functional groups present in liquid fuel. The oil absorbs infrared radiation within a certain wavelength range when infrared light interacts with the molecules, causing the chemical bonds to expand and contract. This absorption occurs regardless of the overall structure of the surrounding molecules. The functional groups in the pyrolytic oil were found using FTIR analysis. Figure 7.14 shows the transmittance versus wavenumber curves shown. The -OH vibration found in the adsorption band between 3000 cm^{-1} and 3750 cm^{-1} showed the presence of water, phenols, alcohol, aromatics, and protein [45]. The peak at 2925 cm^{-1} shows the axial deformation of the C-H group. The C-H and =C-H stretching vibrations, which peaked at 2612 cm^{-1}, were used to distinguish between alkanes and alkenes [215]. A carbonyl group-like ester (C=O) was found at peak 1730 cm^{-1}, indicating the existence of carboxylic acid and ether. The presence of an asymmetric stretch of methyl C-H was suggested by the signal between 1400 cm^{-1} and 1595 cm^{-1}. Alcohol and saturated aliphatic molecules were indicated to be present by the signal between 1275 cm^{-1} and 1378 cm^{-1} [216]. The presence of alkenes and monocyclic aromatic compounds was suggested by the signal between 606 cm^{-1} and 880 cm^{-1} [45].

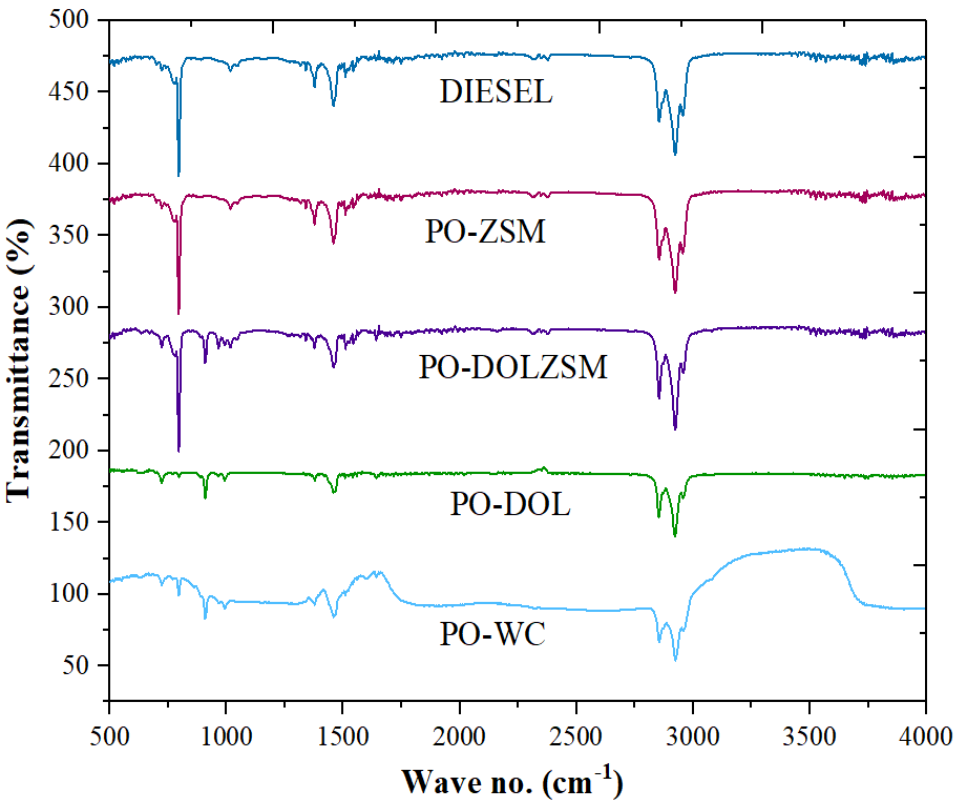

Figure 7.14 (b) FTIR spectrum of pyro-oil obtained from RH: HDPE without catalyst and DOL, and DOLZSM catalyst in comparison with the commercially available diesel.

7.8 Comparative analyses of catalysts used in the co-pyrolysis of plastic and biomass

The results of a comparative analysis investigating synergies between biomass and plastic co-pyrolysis, utilizing calcined dolomite catalyst and other catalysts across diverse reaction conditions, are summarized in **Table 7.** The utilization of a dolomite catalyst led to a decrease in oxygenated compounds in the bio-oil, bringing the percentage down to 14.68% and exhibited enhanced deoxygenation catalytic activity during co-pyrolysis, yielding 85.32% hydrocarbons. Zheng et al. (2018) have demonstrated that the ZSM-5 catalyst exhibits selectivity towards aromatic compounds, hence improving the reaction

and resulting in a significant decrease in reaction activation energy. According to research by Dyer et al. (2021), catalytic zeolite upgrading catalytic zeolite upgrading resulted in bio-oil enriched with hydrocarbons number fuel range and a low fraction of oxygenated molecules. Harith et al. (2022) noted a transformation in pore structure from macropores to mesopores upon incorporating Ni metal onto dolomite catalysts, leading to synergistic effects due to the bi-functional NiO-CaO/MgO (acid-base) properties. Porosity and surface acidity were underscored by Xu et al. (2022) as key factors influencing product composition, particularly concerning aromatic hydrocarbons. In their investigation of various metal-doped mesoporous graphite-like catalysts, Ni/C emerged with the highest mesoporous surface area and mesoporosity, potentially bolstering catalytic efficiency by enhancing the concentration of hydrocarbons, notably aromatics

Table 7.10: Comparing previous studies employing heterogeneous catalysts for the co-pyrolysis of biomass and plastic reveals significant insights.

Feedstocks	**Catalyst**	**Condition**			**Oil Yield(wt. %)**	**Hydrocarbon (%)**	**Oxygenated compound(%)**	**References**
		Feedstock Catalyst	Temp. (°C)	Reactor type				
Pine sawdust & LDPE	HZSM-5	1:1	450	Fixed-bed reactor	42.87	82.17	17.90	49
Sawdust pellets: HDPE	ZSM-5 catalyst	1:1	500	2-stage Fixed-bed reactor	53.10	88.30	11.70	50

Sugarcane bagasse & HDPE	Faujasite -type zeolite	1:6	500	Fixed-bed reactor	68.56	74.55	1.24	51
Corn stover: Plastic Waste (1:1)	Ni/C	1:1	500	Thermogravi metric analyzer	47.70	50.00	50.00	52
Empty fruit bunch: HDPE	NiO/Dol omite	1:10	500	Fluidized bed reactor	6.4	85.32	14.68	53

7.9 Conclusion

In conclusion, catalytic co-pyrolysis using a biorefinery approach stands out as a viable strategy for enhancing the deoxygenation reaction while concurrently maximizing bio-oil yield in the thermochemical conversion of mixed plastic and RH samples. The utilization of inexpensive and easily accessible dolomite as a catalyst has demonstrated significant potential in this regard. Specifically, the integration of calcined dolomite alongside the ZSM catalyst yielded superior catalytic efficiency when compared to each process being used independently, leading to notable enhancements in the characteristics of pyro-oil. The presence of a catalyst resulted in reduced pour points, elevated calorific values, and decreased densities and viscosities of the pyro-oil, indicating enhanced fuel characteristics. Moreover, analysis via NMR, GC–MS, and FTIR revealed lower hydrocarbon fractions such as long-chain waxy residues and tar-like substances. The catalytic action facilitated the breakdown of oxygenated compounds and heavy fractions into lighter, more volatile hydrocarbons, thereby improving the oil's overall quality in catalytic pyro-oils compared to non-catalytic counterparts. These findings underscore the promising role of low-cost catalysts in catalytic pyrolysis processes, offering avenues for further exploration in converting diverse waste materials into valuable products. Moving forward, future studies can leverage these insights to advance the scalability and efficiency of catalytic pyrolysis operations, contributing to sustainable waste management and resource utilization efforts.

In terms of cost-effectiveness and scalability, catalytic pyrolysis using low-cost catalysts such as dolomite and modified zeolites presents a promising solution. These materials are abundant, inexpensive, and exhibit moderate activity, making them suitable for pilot and industrial-scale applications.

7.9 References

1. Guerrero, L. A., Maas, G., & Hogland, W. (2013). Solid waste management challenges for cities in developing countries. *Waste Management*, *33*(1), 220–232. https://doi.org/10.1016/j.wasman.2012.09.008

2. Minghua, Z., Xiumin, F., Rovetta, A., Qichang, H., Vicentini, F., Bingkai, L., Giusti, A., & Yi, L. (2009). Municipal solid waste management in Pudong New Area, China. *Waste Management*, *29*(3), 1227–1233. https://doi.org/10.1016/j.wasman.2008.07.016

3. Awasthi, A. K., Shivashankar, M., & Majumder, S. (2017). Plastic solid waste utilization technologies: A Review. *IOP Conference Series: Materials Science and Engineering*, *263*(2), 022024. https://doi.org/10.1088/1757-899X/263/2/022024

4. Kumar Mishra, R., & Mohanty, K. (2020). Co-pyrolysis of waste biomass and waste plastics (polystyrene and waste nitrile gloves) into renewable fuel and value-added chemicals. *Carbon Resources Conversion*, *3*, 145–155. https://doi.org/10.1016/j.crcon.2020.11.001

5. Alawa, B., Choudhary, J., & Chakma, S. (2023). Discernment of synergism in co-pyrolysis of HDPE and PP waste plastics for production of pyro-oil: Mechanistic investigation with economic analysis and health risk assessment. *Process Safety and Environmental Protection*, *169*, 107–131. https://doi.org/10.1016/j.psep.2022.10.077

6. Choudhary, J., Alawa, B., & Chakma, S. (2023). Insight into the kinetics and thermodynamic analyses of co-pyrolysis using advanced isoconversional method and thermogravimetric analysis: A multi-model study of optimization for enhanced

fuel properties. *Process Safety and Environmental Protection*, *173*, 507–528. https://doi.org/10.1016/j.psep.2023.03.033

7. Fivga, A., & Dimitriou, I. (2018). Pyrolysis of plastic waste for production of heavy fuel substitute: A techno-economic assessment. *Energy*, *149*, 865–874. https://doi.org/10.1016/j.energy.2018.02.094

8. Ji-lu, Z. (2007). Bio-oil from fast pyrolysis of rice husk: Yields and related properties and improvement of the pyrolysis system. *Journal of Analytical and Applied Pyrolysis*, *80*(1), 30–35. https://doi.org/10.1016/j.jaap.2006.12.030

9. Ansari, K. B., Hassan, S. Z., Bhoi, R., & Ahmad, E. (2021). Co-pyrolysis of biomass and plastic wastes: A review on reactants synergy, catalyst impact, process parameter, hydrocarbon fuel potential, COVID-19. *Journal of Environmental Chemical Engineering*, *9*(6), 106436. https://doi.org/10.1016/j.jece.2021.106436

10. Choudhary, J., Kumar, A., Alawa, B., & Chakma, S. (2024). Optimization and prediction of thermodynamic parameters in co-pyrolysis of banana peel and waste plastics using AIC model and ANN modeling. *Energy Nexus*, *14*, 100302. https://doi.org/10.1016/j.nexus.2024.100302

11. Kumar, S., Panda, A. K., & Singh, R. K. (2011). A review on tertiary recycling of high-density polyethylene to fuel. *Resources, Conservation and Recycling*, *55*(11), 893–910. https://doi.org/10.1016/j.resconrec.2011.05.005

12. Adeniyi, A. G., Iwuozor, K. O., Emenike, E. C., Ajala, O. J., Ogunniyi, S., & Muritala, K. B. (2024). Thermochemical co-conversion of biomass-plastic waste to biochar: A review. *Green Chemical Engineering*, *5*(1), 31–49. https://doi.org/10.1016/j.gce.2023.03.002

13. Cupertino, G. F. M., Silva, Á. M. da, Pereira, A. K. S., Delatorre, F. M., Ucella-Filho, J. G. M., Souza, E. C. de, Profeti, D., Profeti, L. P. R., Oliveira, M. P., Saloni, D., Luque, R., & Dias Júnior, A. F. (2024). Co-pyrolysis of biomass and

polyethylene terephthalate (PET) as an alternative for energy production from waste valorization. *Fuel*, *362*, 130761. https://doi.org/10.1016/j.fuel.2023.130761

14. Han, J., Yao, X., Zhan, Y., Oh, S.-Y., Kim, L.-H., & Kim, H.-J. (2017). A method for estimating higher heating value of biomass-plastic fuel. *Journal of the Energy Institute*, *90*(2), 331–335. https://doi.org/10.1016/j.joei.2016.01.001

15. Uzoejinwa, B. B., He, X., Wang, S., El-Fatah Abomohra, A., Hu, Y., & Wang, Q. (2018). Co-pyrolysis of biomass and waste plastics as a thermochemical conversion technology for high-grade biofuel production: Recent progress and future directions elsewhere worldwide. *Energy Conversion and Management*, *163*, 468–492. https://doi.org/10.1016/j.enconman.2018.02.004

16. Ryu, H. W., Kim, D. H., Jae, J., Lam, S. S., Park, E. D., & Park, Y.-K. (2020). Recent advances in catalytic co-pyrolysis of biomass and plastic waste for the production of petroleum-like hydrocarbons. *Bioresource Technology*, *310*, 123473. https://doi.org/10.1016/j.biortech.2020.123473

17. Budsaereechai, S., Hunt, A. J., & Ngernyen, Y. (2019). Catalytic pyrolysis of plastic waste for the production of liquid fuels for engines. *RSC Advances*, *9*(10), 5844–5857. https://doi.org/10.1039/C8RA10058F

18. Mo, F., Ullah, H., Zada, N., & Shahab, A. (2023). A Review on Catalytic Co-Pyrolysis of Biomass and Plastics Waste as a Thermochemical Conversion to Produce Valuable Products. *Energies*, *16*(14), Article 14. https://doi.org/10.3390/en16145403

19. Elbaba, I. F., & Williams, P. T. (2014). Deactivation of Nickel Catalysts by Sulfur and Carbon for the Pyrolysis–Catalytic Gasification/Reforming of Waste Tires for Hydrogen Production. *Energy & Fuels*, *28*(3), 2104–2113. https://doi.org/10.1021/ef4023477

20. Friengfung, P., Jamkrajang, E., Sunphorka, S., Kuchonthara, P., & Mekasut, L. (2014). NiO/Dolomite Catalyzed Steam/O2 Gasification of Different Plastics and

Their Mixtures. *Industrial & Engineering Chemistry Research*, *53*(5), 1909–1915. https://doi.org/10.1021/ie401893s

21. Praserttaweeporn, K., Vitidsant, T., & Charusiri, W. (2022). Ni-modified dolomite for the catalytic deoxygenation of pyrolyzed softwood and non-wood to produce bio-oil. *Results in Engineering*, *14*, 100461. https://doi.org/10.1016/j.rineng.2022.100461

22. Al-Obaidi, M. M. A., Ishak, N. S., Ali, S., Arifin, N. A., Raja Shahruzzaman, R. M. H., Wan Abdul Karim Ghani, W. A., Yun Hin, T.-Y., & Shamsuddin, A. H. (2021). H2-Rich and Tar-Free Downstream Gasification Reaction of EFB by Using the Malaysian Dolomite as a Secondary Catalyst. *Catalysts*, *11*(4), Article 4. https://doi.org/10.3390/catal11040447

23. Gandidi, I. M., Suryadi, E., Mardawati, E., Kendarto, D. R., & Pambudi, N. A. (2022). Two stage co-pyrolysis improvement to produce synthetic oil and gas simultaneously from mixed municipal solid waste using natural dolomite-based catalyst. *Results in Engineering*, *16*, 100753. https://doi.org/10.1016/j.rineng.2022.100753

24. Shahruzzaman, R. M. H. R., Ali, S., Yunus, R., & Yun-Hin, T. Y. (2018). Green Biofuel Production via Catalytic Pyrolysis of Waste Cooking Oil using Malaysian Dolomite Catalyst. *Bulletin of Chemical Reaction Engineering & Catalysis*, *13*(3), 489–501. https://doi.org/10.9767/bcrec.13.3.1956.489-501

25. Chen, X., Liu, Z., Li, S., Xia, S., Cai, N., Chen, W., Chen, Y., Yang, H., Wang, X., & Chen, H. (2021). Catalytic Pyrolysis of Biomass to Produce Aromatic Hydrocarbons over Calcined Dolomite and ZSM-5. *Energy & Fuels*, *35*(20), 16629–16636. https://doi.org/10.1021/acs.energyfuels.1c02318

26. Wang, P., & Shen, Y. (2021). *Catalytic Pyrolysis of Cellulose and Chitin with Calcined Dolomite—Pyrolysis Kinetics and Products Analysis* (SSRN Scholarly Paper 3962022). https://doi.org/10.2139/ssrn.3962022

27. Shahdan, N. A., Balasundram, V., Ibrahim, N., Isha, R., & Manan, Z. A. (2022). Catalytic Co-pyrolysis of empty fruit bunch and high-density polyethylene mixtures over rice husk ash: Thermogravimetric, kinetic and thermodynamic analyses. *Cleaner Engineering and Technology*, *9*, 100538. https://doi.org/10.1016/j.clet.2022.100538

28. Dwivedi, U., Pant, K. K., & Naik, S. N. (2021). Controlling liquid hydrocarbon composition in valorization of plastic waste via tuning zeolite framework and SiO2/Al2O3 ratio. *Journal of Environmental Management*, *297*, 113288. https://doi.org/10.1016/j.jenvman.2021.113288

29. Zulkafli, A. H., Hassan, H., Ahmad, M. A., Mohd Din, A. T., & Wasli, S. M. (2023). Co-pyrolysis of biomass and waste plastics for production of chemicals and liquid fuel: A review on the role of plastics and catalyst types. *Arabian Journal of Chemistry*, *16*(1), 104389. https://doi.org/10.1016/j.arabjc.2022.104389

30. Wu, C., & Williams, P. T. (2010). A novel Ni–Mg–Al–CaO catalyst with the dual functions of catalysis and CO2 sorption for H2 production from the pyrolysis–gasification of polypropylene. *Fuel*, *89*(7), 1435–1441. https://doi.org/10.1016/j.fuel.2009.10.020

31. Paula, T. P., Marques, M. de F. V., Marques, M. R. da C., Oliveira, M. S., & Monteiro, S. N. (2022). Thermal and Catalytic Pyrolysis of Urban Plastic Waste: Modified Mordenite and ZSM-5 Zeolites. *Chemistry*, *4*(2), Article 2. https://doi.org/10.3390/chemistry4020023

32. Eze, W. U., Madufor, I. C., Onyeagoro, G. N., & Obasi, H. C. (2020). The effect of Kankara zeolite-Y-based catalyst on some physical properties of liquid fuel from mixed waste plastics (MWPs) pyrolysis. *Polymer Bulletin*, *77*(3), 1399–1415. https://doi.org/10.1007/s00289-019-02806-y

33. Binnal, P., Mali, V. S., Karjekannavar, S. P., & Mogaveera, S. R. (2020). Enhancing Gasoline Range Hydrocarbons by Catalytic Co-pyrolysis of Rice Husk

with Low Density Polyethylene (LDPE) Using Zeolite Socony Mobil#5(ZSM-5). *Periodica Polytechnica Chemical Engineering*, *64*(2), Article 2. https://doi.org/10.3311/PPch.13850

34. Sivagami, K., Kumar, K. V., Tamizhdurai, P., Govindarajan, D., Kumar, M., & Nambi, I. (2022). Conversion of plastic waste into fuel oil using zeolite catalysts in a bench-scale pyrolysis reactor. *RSC Advances*, *12*(13), 7612–7620. https://doi.org/10.1039/D1RA08673A

35. Al-asadi, M., & Miskolczi, N. (2021). Hydrogen rich products from waste HDPE/LDPE/PP/PET over Me/Ni-ZSM-5 catalysts combined with dolomite. *Journal of the Energy Institute*, *96*, 251–259. https://doi.org/10.1016/j.joei.2021.03.004

36. Fu, L., Xiong, Q., Wang, Q., Cai, L., Chen, Z., & Zhou, Y. (2022). Catalytic Pyrolysis of Waste Polyethylene Using Combined CaO and Ga/ZSM-5 Catalysts for High Value-Added Aromatics Production. *ACS Sustainable Chemistry & Engineering*, *10*(29), 9612–9623. https://doi.org/10.1021/acssuschemeng.2c02881

37. Alawa, B., & Chakma, S. (2023a). Insight into the engine performance of pyro-oil synthesized through catalytic co-pyrolysis of mixed waste plastics in the presence of dolomite modified with silica and ZSM-5. *Fuel*, *354*, 129190. https://doi.org/10.1016/j.fuel.2023.129190

38. Alawa, B., & Chakma, S. (2023b). Upgradation, product analysis and engine performance of hydrocarbon fuels produced through pyrolysis of thermoplastic polymers with Si and ZSM-5 modified catalysts. *Fuel Processing Technology*, *250*, 107918. https://doi.org/10.1016/j.fuproc.2023.107918.

39. Wang, P., & Shen, Y. (2021). *Catalytic Pyrolysis of Cellulose and Chitin with Calcined Dolomite—Pyrolysis Kinetics and Products Analysis* (SSRN Scholarly Paper 3962022). https://doi.org/10.2139/ssrn.3962022

40. Lee, A. F., & Wilson, K. (2015). Recent developments in heterogeneous catalysis for the sustainable production of biodiesel. *Catalysis Today*, *242*, 3–18. https://doi.org/10.1016/j.cattod.2014.03.072

41. Shahruzzaman, R. M. H. R., Ali, S., Yunus, R., & Yun-Hin, T. Y. (2018). Green Biofuel Production via Catalytic Pyrolysis of Waste Cooking Oil using Malaysian Dolomite Catalyst. *Bulletin of Chemical Reaction Engineering & Catalysis*, *13*(3), 489–501. https://doi.org/10.9767/bcrec.13.3.1956.489-501

42. Correia, L. M., de Sousa Campelo, N., Novaes, D. S., Cavalcante, C. L., Cecilia, J. A., Rodríguez-Castellón, E., & Vieira, R. S. (2015). Characterization and application of dolomite as catalytic precursor for canola and sunflower oils for biodiesel production. *Chemical Engineering Journal*, *269*, 35–43. https://doi.org/10.1016/j.cej.2015.01.097

43. Mohammed, M. a. A., Salmiaton, A., Wan Azlina, W. a. K. G., Mohamad Amran, M. S., & Taufiq-Yap, Y. H. (2013). Preparation and Characterization of Malaysian Dolomites as a Tar Cracking Catalyst in Biomass Gasification Process. *Journal of Energy*, *2013*(1), 791582. https://doi.org/10.1155/2013/791582

44. Tran, T. N., Pham, T. V. A., Le, M. L. P., Nguyen, T. P. T., & Tran, V. M. (2013). Synthesis of amorphous silica and sulfonic acid functionalized silica used as a reinforced phase for polymer electrolyte membrane. *Advances in Natural Sciences: Nanoscience and Nanotechnology*, *4*(4), 045007. https://doi.org/10.1088/2043-6262/4/4/045007

45. Asghari, A., Khorrami, M. K., & Kazemi, S. H. (2019). Hierarchical H-ZSM5 zeolites based on natural kaolinite as a high-performance catalyst for methanol to aromatic hydrocarbons conversion. *Scientific Reports*, *9*(1), 17526. https://doi.org/10.1038/s41598-019-54089-y

46. Akubo, K., Nahil, M. A., & Williams, P. T. (2019). Aromatic fuel oils produced from the pyrolysis-catalysis of polyethylene plastic with metal-impregnated zeolite

catalysts. *Journal of the Energy Institute*, *92*(1), 195–202. https://doi.org/10.1016/j.joei.2017.10.009

47. Xu, Y., Liu, J., Ma, G., Wang, J., Lin, J., Wang, H., Zhang, C., & Ding, M. (2018). Effect of iron loading on acidity and performance of Fe/HZSM-5 catalyst for direct synthesis of aromatics from syngas. *Fuel*, *228*, 1–9. https://doi.org/10.1016/j.fuel.2018.04.151

Chapter-8

Conclusion and Future Scope

The findings of this study are presented in this chapter within the framework of the main objective of the thesis: 'Investigation of Bio-oil Production through Co-pyrolysis Technique Using Rice Husk and Plastic Waste".′ The results indicate that low-density and high-density polyethylene plastic wastes, along with the selected biomass (rice husk), are suitable feedstocks for bio-oil production.

The co-pyrolysis of plastic and biomass waste presents a viable approach for enhancing bio-oil yield and improving its properties. Furthermore, the study highlights the synergistic interactions between biomass and plastics, offering a pathway to optimize fuel quality. These findings provide a strong foundation for scaling up the process, enhancing oil quality through catalysis, and ultimately integrating renewable fuels into industrial and transportation sectors supporting a circular economy and sustainable energy goals.

8.1 Based on the research conducted in this thesis, the following conclusions have been drawn:

[1] The selection of rice husk and plastic waste as feed materials for pyrolysis is crucial due to their significant impact on bio-oil output and their availability. Plastic trash, which is mostly made of hydrocarbons, and rice husk, which is high in cellulose, hemicellulose, and lignin, have an impact on the quantity and quality of bio-oil that is generated. When these materials are co-pyrolyzed, synergistic effects can be produced that improve conversion efficiency and thermal degradation.

[2] The pyrolysis process is highly influenced by operating parameters such as temperature, heating rate, sweep gas flow rate, particle size, and reactor residence time. Based on the literature review, feedstock materials were selected for the co-pyrolysis process, and an operating temperature of 500 °C with a heating rate of 10 °C/min. was employed. A fixed-

bed reactor was designed considering the internal characteristics of the selected feedstocks and kinetic parameters.

[3] TGA and DSC analyzers were used to estimate the kinetic parameters. The thermal behavior of rice husk, LDPE, and PET was investigated using iso-conversional kinetic techniques. The Flynn-Wall-Ozawa (FWO), Kissinger-Akahira-Sunose (KAS), Friedman, Starink, and Tang iso-conversional models were applied to analyze the TGA data at different heating rates ranging from 10 to 40 °C/min. The average activation energies were calculated using the five methods as follows: 113 kJ/mol by FWO with a standard deviation of 4.33 and a standard error of 1.53; 123 kJ/mol by the Friedman method with a standard deviation of 5.10 and a standard error of 1.8; 120 kJ/mol by KAS with a standard deviation of 4.2 and a standard error of 1.48; 117 kJ/mol by Starink with a standard deviation of 4.15 and a standard error of 1.47; and 121 kJ/mol by the Tang method with a standard deviation of 2.54 and a standard error of 0.9. All methods were found to be appropriate; however, the Tang method proved to be particularly effective for kinetic calculations.

[4] FTIR (Fourier-transform infrared) analysis of biomass and plastic samples indicates that these feedstocks are rich in functional groups such as aldehydes, carboxylic acids, nitrogenous compounds, alkanes, alkenes, and phenols. These substances are important because they enhance the potential of bio-oil. Therefore, the existence of these functional groups in liquid samples obtained from the co-pyrolysis of plastic waste and rice husk highlights the material's potential for use in fuel production. Efforts were also made to calculate enthalpy, entropy, and Gibbs free energy. These results were supported by a Differential Scanning Calorimetry (DSC) study, which revealed endothermic peaks associated with sample degradation and an exothermic peak related to moisture evolution. These insights are crucial for refining the pyrolysis process to enhance both the yield and quality of the resulting liquid oil.

[5] The optimum bio-oil yields from selected feedstocks were 30 wt.% from rice husk, 71 wt.% from LDPE, and 75 wt.% from HDPE under the operating conditions of 500 °C

pyrolysis temperature, 20 ml/min sweep gas flow rate, and a 10 °C/min heating rate. The blending ratio also played a significant role in bio-oil production. Blending ratios of RH with LDPE and HDPE (20:80, 35:65, and 50:50) demonstrated positive interactions, highlighting the effective synergy between biomass and plastic waste. Co-pyrolysis of RH with LDPE and HDPE resulted in increased liquid yields and enhanced fuel properties. The optimum bio-oil yields from blends were achieved at an 80:20 ratio of LDPE:RH (66 wt.%) and HDPE:RH (68 wt.%).

[6] Bio-oil upgradation was also performed using two catalysts, ZSM-5 and DOL. These selected catalysts were calcined at different temperature ranges and dried in a hot air oven at varying temperatures, then stored for use in pyrolysis experiments. Both catalysts were also used to prepare a mixed catalyst, DOLZSM, by combining them in a 50:50 ratio. The resulting mixture, known as ZSMDOL, was employed in the catalytic co-pyrolysis process. During the catalytic pyrolysis tests, a catalyst-to-feed ratio of 1:20 was maintained for both materials — calcined dolomite (DOL) and DOLZSM. The use of catalysts resulted in a decrease in bio-oil production but enhanced the fuel properties of the bio-oil. The catalysts increased the output gas yield (wt.%) while reducing the amount of bio-oil produced.

[7] The addition of plastic to biomass improved the fuel's characteristics, as demonstrated by increased concentrations of aromatics and paraffin in the NMR study and the presence of advantageous functional groups in the FTIR analysis. Alcohols and aldehydes increased whereas oxygenated compounds and acids decreased in pyrolytic oils, according to GC-MS study. These findings underscore the potential of co-pyrolysis as a sustainable method for generating fuels with improved characteristics, utilizing both biomass and plastic waste effectively.

[8] It was found that the yield of pyrolytic liquid dropped while the yield of gas rose in the catalytic pyrolysis of rice husk (RH) and plastic waste (both LDPE and HDPE) using dolomite and ZSM-5 updated catalyst (DOLZSM) at a feedstock ratio of 20:80 and a

catalyst ratio of 1:20. Even with the decrease in liquid production, the pyrolytic oil's characteristics were noticeably better. GC-MS analysis revealed that the optimized catalytic conditions significantly reduced the presence of oxygenated compounds and increased the proportion of alcohols and hydrocarbons in the bio-oil. The inclusion of catalysts like dolomite and DOLZSM improves the quality of the resultant bio-oil, perhaps making it more suited for high-quality fuel applications, even if there is a trade-off between quantity and quality of the pyrolytic liquid. The bio-oil's fraction of alcohols and hydrocarbons rose while the presence of oxygenated compounds was dramatically reduced under the improved catalytic conditions, according to GC-MS analysis.

[9] Two types of plastic waste, LDPE and HDPE, were used, and blending ratios were prepared and employed for pyrolysis. A blend of rice husk and LDPE was used for the upgradation of bio-oil. The produced bio-oil was characterized, revealing that its density and specific gravity were very similar to those of diesel fuel, especially in the raw bio-oil. The flash point and fire point were highest in the raw bio-oil but decreased after catalytic treatment using DOL and DOLZSM, becoming comparable to diesel. The calorific value increased after catalytic upgradation and was found to be very close to that of diesel. The diesel index and cetane value also improved significantly and were observed to be nearly equivalent to those of diesel fuel.

Similar results were also observed with blends of rice husk and HDPE.

8.2 Future Aspects and Scope

The use of plastic and biomass waste in the creation of liquid fuel is the main focus of the current investigation. The following recommendations for further research are made in light of the study's findings:

1. To evaluate the emissions, fuel efficiency, compatibility, and environmental impact of pyrolytic fuel in various engine types compared to conventional fuels.

2. To explore innovative methods for utilizing the char produced as a by-product in various industrial applications, and to investigate its potential in soil amendment, adsorption processes, and as a precursor for activated carbon production
3. To investigate and develop novel, cost-effective metal catalysts that enhance the yield and quality of pyrolytic liquid.
4. To maximize liquid production by designing and optimizing reactors that enhance the scalability of the pyrolysis process for industrial applications, with a focus on reactor modifications that improve heat transfer, feedstock mixing, and overall process efficiency.
5. To apply techno-economic analysis (TEA) to estimate capital and operational costs, return on investment, and environmental benefits. Incorporating these factors will help ensure that the process is not only scientifically robust but also commercially and environmentally sustainable.

Certifications and Workshops-

International Conference in NIT Jalandhar (CHEMBIO) – paper presented on the topic- Review on the Chemical and Physical Methods for Upgrading Bio-oil.

International Conference in NIT Jalandhar (ICHEC) - paper presented on the topic- Prediction of the heating value of biomass wastes by using linear regression method by using machine learning tool with R (rattle).

Internship in making bio-composites and lignin, cellulose preparation under Dr. V R Arun Prakash in the Department of **Material Physics**, Chennai

Conference of the international conclave on Material Energy and Climate (IAAM) – poster presentation on topic- thermal study and kinetic behavior of rice husk blended with polyethylene terephthalate for co-pyrolysis characteristic.

DST workshop in Doon University, Dehradun, under STUTI – a synergetic training program utilizing the scientific and technological infrastructure

Second rank in a conference of RAFAS 4th International Conference on "Recent Advances in Fundamental and Applied Sciences"2023- Comparative Study on thermal analysis in Differential scanning calorimetry of rice husk, polyethylene Terephthalate and Low-density polyethylene.

Workshop- on Nano transistors and Energy Devices Technology organized by **INUP-i2i, IIT Guwahati.**

Workshop- fabrication and characterization of nano-composites **by INUP-i2i , IIT-DELHI**

Hands on training on fabrication and characterization of nanomaterials and lab visit in **IIT Guwahati** by INUP-i2i ,2023

Hands-on training on fabrication and characterization of nanomaterials and lab visit in **IIT DELHI** by INUP-i2i,2023

Workshop on Nano transistors and Energy Devices Technology organized by **INUP-i2i, IIT Kharagpur.**

SEMINAR - "Two-Day National Seminar on **Microplastics: Current Scenario, Challenges, & Future Perspectives**

Workshop- Advanced Entrepreneurship-cum Skill Development Program (e-SDP) in nit Jalandhar

ICSEE Conference on MANIT BHOPAL – poster presentation in title Co-Pyrolysis of Rice Husk and HDPE with Dolomite Catalyst for Enhancement of Bio-oil Production and Quality.

Publications

Bisen, D., Chouhan, A. P. S., Pant, M., and Chakma, S. (2025). Advancement of thermochemical conversion and the potential of biomasses for production of clean energy: A review. *Renewable and Sustainable Energy Reviews*, *208*, 115016. https://doi.org/10.1016/j.rser.2024.115016.

Bisen, D., Chouhan, A. P. Singh and Sakthivel, R. M. (2024). A Comparative Study of Thermal Behavior and Kinetics of the Rice Husk, Low-Density Polyethylene (LDPE) and Polyethylene Terephthalate (PET) for Pyrolysis. *Journal of Renewable Energy and Environment*, *11*(2), 151-162. doi: 10.30501/jree.2024.416390.1688.

Bisen, D., Chouhan, A.P.S., Sarma, A.K. *et al.* Thermogravimetric analysis of rice husk and low-density polyethylene co-pyrolysis: kinetic and thermodynamic parameters. *Sci Rep* 14, 31798 (2024). https://doi.org/10.1038/s41598-024-82830-9

Bisen, D., Lanjewar, R., Chouhan, A.P.S. *et al.* Catalytic co-pyrolysis of rice husk and high-density polyethylene using dolomite for enhancement of bio-oil production and quality. *Environ Sci Pollut Res* (2025). https://doi.org/10.1007/s11356-025-36600-3

Bisen, D., Lanjewar, R., Alawa, B., Chouhan, A. P. S., and Chakma, S. (2025). Kinetic Analysis and Fuel Characterization with Hydrocarbon Distribution in Pyro-Oil Produced from Co-Pyrolysis of Rice Husk and Low-Density Polyethylene. *Journal of the Energy Institute*, 102175.

Conferences Paper

Sharma, V., Chouhan, A. P. S., & Bisen, D. (2022, May). Study of bio-oil production from (Eucalyptus and Plastic) wastes by using the Co-pyrolysis technique. In *Journal of Physics: Conference Series* (Vol. 2267, No. 1, p. 012021). IOP Publishing.

Bisen, D., Chouhan, A. P. S., & Sharma, V. (2022, May). Study of co-pyrolysis process of biomass and plastic polymers for bio-oil production and upgradation: A review. In *Journal of Physics: Conference Series* (Vol. 2267, No. 1, p. 012010). IOP Publishing.

Sharma, V., Chouhan, A. P. S., and Bisen, D. (2022). Prediction of activation energy of biomass wastes by using multilayer perceptron neural network with Weka. *Materials Today: Proceedings*, *57*, 1944-1949.

Book Chapter

Chouhan, A.P.S., Bisen, D., Mourya, V. (2025). Biocrude Production and Upgradation by Using an Emerging Biorefining Approach. In: Aslam, M., Mishra, S., Aburto Anell, J.A., Sarma, A.K. (eds) Biocrude Oil Biorefinery. Biofuel and Biorefinery Technologies, vol 14. Springer, Cham. https://doi.org/10.1007/978-3-031-85036-3_17.

Bio-refinery Approach for a Sustainable Eco-system and Circular Bio-economy. Divya Bisen, Ashish Pratap Singh Chouhan, and Manish Pant.

Under Revision

1. Co-Pyrolysis of High-Density Polyethylene and Rice Husk for Bio-Oil Production: Experimental and ANN Modeling Approach, Bisen, D., Chouhan, A. P. S., Jitendra Choudhary, **Journal of analytical and Applied pyrolysis**

2. Pyrolysis of LDPE and Rice husk with Dolomite and ZSM-5 Modified Catalysts: Fuel Quality Analysis, Bisen, D., Lanjewar, R., Chouhan, A. P. S., and Chakma, S. **Fuel**

3. Investigation of Kinetic and Thermodynamic Parameters of Raw and Torrefied Low-density polyethylene Blends with Rice husk: A Comparative Study. Bisen,. Chouhan, A. P. S., **Journal of Thermal Analysis and Calorimetry**

4. Investigating the influence of catalyst on hydrocarbon yield in co-pyrolysis of high-density polyethylene and Rice husk. Bisen, D., Chouhan, A. P. S., and Chakma, S.